



**Richard António
Martins Tavares**

**Libertação acidental de gases tóxicos: modelação e
avaliação do risco**

**Accidental release of hazardous gases: modelling
and assessing risk**



**Richard António
Martins Tavares**

**Libertação acidental de gases tóxicos: modelação e
avaliação do risco**

**Accidental release of hazardous gases: modelling
and assessing risk**

Dissertação apresentada à Universidade de Aveiro para cumprimento dos requisitos necessários à obtenção do grau de Doutor em Ciências Aplicadas ao Ambiente, realizada sob a orientação científica da Doutora Ana Isabel Miranda, Professora Associada com Agregação do Departamento de Ambiente e Ordenamento da Universidade de Aveiro.

Apoio financeiro da Fundação para a Ciência e Tecnologia (FCT) e do Fundo Social Europeu no âmbito do III Quadro Comunitário de Apoio pela Bolsa de Doutoramento Ref^a (SFRH/BD/22742/2005) Apoio financeiro da Comissão Europeia no âmbito do projecto BRIDGE - sustainaBle uRban plannIng Decision support accountinG for urban mEtabolism (Collaborative Project n.º 211345/EC).

Este trabalho é financiado por Fundos FEDER através do Programa Operacional Factores de Competitividade (COMPETE) e por Fundos Nacionais através da FCT no âmbito do projecto INSPIRAR (PTDC/AAC-AMB/103895/2008)

Para a minha Família.

o júri
presidente

Prof. Doutor Mário Guerreiro da Silva Ferreira
professor catedrático da Universidade de Aveiro

Prof. Doutor Carlos Alberto Diogo Soares Borrego
professor catedrático da Universidade de Aveiro

Prof. Doutora Ana Isabel Couto Neto Silva Miranda
professora associada com agregação da Universidade de Aveiro

Prof. Doutor Nelson Augusto Cruz de Azevedo Barros
professor associado da Faculdade de Ciências e Tecnologia da Universidade Fernando Pessoa

Prof. Doutor João Miguel Pires Ventura
Professor auxiliar do Instituto Superior Técnico da Universidade Técnica de Lisboa.

Prof. Doutora Maria Celeste Rodrigues Jacinto
professora auxiliar da Faculdade de Ciências e Tecnologia da Universidade Nova de Lisboa

Prof. Myriam Alexandra dos Santos Batalha Dias Nunes Lopes
professora auxiliar da Universidade de Aveiro

agradecimentos

A realização deste trabalho nunca seria possível sem o incentivo e orientação da Prof. Ana Isabel Miranda. Devo também um agradecimento especial ao Prof. Carlos Borrego, por me ter dado esta oportunidade e desafio, sabendo da minha pouca experiência 'científica'.

A conclusão deste trabalho apenas foi possível por integrar o grupo de trabalho GEMAC e acima de tudo aos meus colegas e amigos que fizeram e fazem parte desta 'segunda família, pelo que só posso dizer OBRIGADO! No entanto, existem uns agradecimentos mais particulares pois sem eles não conseguiria terminar esta tese. Ao Jorge, aos Pedros (Santos e Cascão), à Myriam, à Vera Rodrigues e às minhas colegas de gabinete (Xana, Helena, Cristinas e Isabel) com quem tenho partilhado interessantes discussões, momentos bem animados, bem como, o 'tradicional' silêncio do gab. 200.

A todos os professores do Departamento de Ambiente e Ordenamento que acompanharam este meu trabalho, em especial à Prof. Isabel Nunes pelas palavras de apoio e incentivo.

Não posso deixar de agradecer à Equipa da COST Action 732, com quem tive a oportunidade de partilhar interessantes discussões e aprender imenso, bem como ao Dr. Morten Nielsen e ao Prof. Jeroen van Beek pela ajuda e discussões interessantes ao longo do trabalho.

A todos os meus amigos pelo incentivo ao longo desta aventura.

Por último, e como diz o ditado 'last but not the least', à minha família, a quem devo um MUITO OBRIGADO pelo carinho, compreensão e partilha dos momentos bons e menos bons, pelo apoio e acima de tudo pela paciência que tiveram nestes últimos anos!

Sem correr o risco de me esquecer de alguém, até porque os agradecimentos devem ser feitos pessoalmente, um MUITO OBRIGADO a todos que de uma forma ou de outra me apoiaram ao longo deste trabalho.

palavras-chave

Análise de consequências, gases perigosos, gases pesados, libertação accidental, modelação atmosférica, qualidade do ar, risco tecnológico.

resumo

A renovada preocupação na avaliação dos riscos e consequências dos perigos tecnológicos em zonas industriais e urbanas continua a enfatizar o desenvolvimento de modelos de análise de consequências (AC) à escala local, capazes de simular episódios de poluição de curto prazo e seus efeitos na saúde humana e ambiente resultantes da exposição em situação de acidentes com substâncias perigosas.

Neste sentido, o principal objecto desta tese é o desenvolvimento e validação do modelo Effects of Released Hazardous gAses (EFRHA). Esta ferramenta foi desenvolvida para simular a libertação e dispersão atmosférica de gases perigosos pesados e passivos em ambientes de topografia complexa e edificadas, bem como, estimar as consequências da exposição a episódios de poluição de curta duração de acordo com limites de segurança e controlo.

O modelo é constituído por cinco módulos principais: meteorológico, fontes, terreno, dispersão e efeitos. Diferentes estados físicos e tipos de acidente podem ser analisados. Considerado o elemento principal da ferramenta, o módulo de dispersão é baseado na modelação 'shallow layer', que permite considerar a influência de obstáculos na dispersão de gases perigosos.

A validação do modelo inclui métodos de análise qualitativa e quantitativa através da comparação dos principais outputs com bases de dados medidos ou simulados. A análise preliminar dos módulos meteorológica e fontes baseada na comparação com resultados de modelos também validados demonstra a correcta descrição das condições ambientais e da variação das características da fonte ao longo da libertação. O módulo de dispersão é comparado com resultados de medições experimentais considerando diferentes condições de libertação e dispersão atmosférica. Em geral, os critérios de qualidade estimados encontram-se dentro dos limites de aceitação para modelos 'non-CFD', demonstrando a capacidade para simular razoavelmente a libertação e dispersão atmosférica de gases pesados perigosos em ambientes industriais e urbanos.

O modelo EFRHA também foi aplicado a um caso de estudo, o Complexo Químico de Estarreja (ECC), com base num conjunto de cenários de libertação accidental, no âmbito de um estudo de AC. Os resultados demonstram a potencial magnitude dos efeitos na área envolvente ao ECC, bem como a influência das condições meteorológicas e tipo de acidente. De um modo geral, a presente tese demonstra a aplicabilidade do modelo como ferramenta para estudos de CA, bem como no suporte à decisão e preparação de resposta de emergência em situação de libertação accidental em zonas urbanas e industriais.

keywords

Accidental release, air quality, atmospheric modeling, consequence analysis, hazardous gases, technological risk.

abstract

The renewed concern in assessing risks and consequences from technological hazards in industrial and urban areas continues emphasizing the development of local-scale consequence analysis (CA) modelling tools able to predict short-term pollution episodes and exposure effects on humans and the environment in case of accident with hazardous gases (hazmat).

In this context, the main objective of this thesis is the development and validation of the EEffects of Released Hazardous gAses (EFRHA) model. This modelling tool is designed to simulate the outflow and atmospheric dispersion of heavy and passive hazmat gases in complex and build-up areas, and to estimate the exposure consequences of short-term pollution episodes in accordance to regulatory/safety threshold limits.

Five main modules comprising up-to-date methods constitute the model: meteorological, terrain, source term, dispersion, and effects modules. Different initial physical states accident scenarios can be examined. Considered the main core of the developed tool, the dispersion module comprises a shallow layer modelling approach capable to account the main influence of obstacles during the hazmat gas dispersion phenomena.

Model validation includes qualitative and quantitative analyses of main outputs by the comparison of modelled results against measurements and/or modelled databases. The preliminary analysis of meteorological and source term modules against modelled outputs from extensively validated models shows the consistent description of ambient conditions and the variation of the hazmat gas release. Dispersion is compared against measurements observations in obstructed and unobstructed areas for different release and dispersion scenarios. From the performance validation exercise, acceptable agreement was obtained, showing the reasonable numerical representation of measured features. In general, quality metrics are within or close to the acceptance limits recommended for 'non-CFD models', demonstrating its capability to reasonably predict hazmat gases accidental release and atmospheric dispersion in industrial and urban areas.

EFRHA model was also applied to a particular case study, the Estarreja Chemical Complex (ECC), for a set of accidental release scenarios within a CA scope. The results show the magnitude of potential effects on the surrounding populated area and influence of the type of accident and the environment on the main outputs. Overall the present thesis shows that EFRHA model can be used as a straightforward tool to support CA studies in the scope of training and planning, but also, to support decision and emergency response in case of hazmat gases accidental release in industrial and built-up areas.

Although we cannot eliminate the risk of industrial accidents in modern societies, we can strive to minimise the risks of such accidents happening and to mitigate their consequences.

Stavros Dimas

TABLE OF CONTENTS

TABLE OF CONTENTS	I
LIST OF FIGURES	III
LIST OF TABLES	VII
ACRONYMS	IX
NOTATION	XVII
1. INTRODUCTION	3
1.1 Industrial accidents involving hazardous materials.....	3
1.1.1 Concepts	4
1.1.2 Historical overview of major industrial accidents	5
1.1.3 Available information of major industrial accidents	15
1.2 European regulatory instruments on industrial accidents	24
1.2.1 The ‘Seveso Directives Regime’	25
1.2.2 Seveso establishments EU-wide	28
1.2.3 Other relevant European regulatory instruments	30
1.3 Research objectives and structure of the thesis	32
2. QUANTITATIVE RISK AND CONSEQUENCE ANALYSIS: SCIENTIFIC BACKGROUND	37
2.1 Quantitative risk analysis of industrial accidents	37
2.2 Consequence analysis of industrial accidents	42
2.3 Consequence analysis modelling.....	44
2.3.1 Source term modelling	45
2.3.2 Atmospheric dispersion modelling	50
2.3.3 Meteorological modelling.....	69
2.3.4 Effects modelling	70
2.4 Synthesis	72
3. DEVELOPMENT OF THE EFFECTS OF RELEASED HAZARDOUS GASES MODEL.....	77
3.1 General structure of the EFRHA model	77
3.2 EMM – EFRHA Meteorological Module	80
3.3 ETM – EFRHA Terrain Module	88
3.4 ESTM – EFRHA Source Term Module.....	90
3.4.1 ESTM1 – Compressed gas	93
3.4.2 ESTM2 – Non-boiling liquid	97
3.4.3 ESTM3 – Pressurized liquefied gas	98

3.4.4	ESTM4 – Liquid pool evaporation.....	103
3.5	EDM – EFRHA Dispersion module.....	105
3.6	EEM – EFRHA Effects Module	110
3.7	Main input and output data of EFRHA model	111
3.8	Synthesis	112
4.	VALIDATION OF EFRHA MODEL	117
4.1	Overview of the methodology.....	117
4.2	Stage 1: Meteorology	121
4.3	Stage 2: Source term.....	127
4.4	Stage 3: Dispersion in obstructed areas	132
4.4.1	The Mock Urban Setting Test experiment.....	132
4.4.2	EFRHA modelling set up and validation for the -45 ^o MUST case	135
4.5	Stage 4: Dense gas accidental release and dispersion	143
4.5.1	Experimental test trials.....	145
4.5.2	EFRHA modelling set up and validation for the set of DGD test cases.....	148
4.6	Synthesis	156
5.	APPLICATION OF EFRHA TO A CONSEQUENCE ANALYSIS STUDY.....	161
5.1	Selection of the case study	161
5.2	Estarreja Chemical Complex	164
5.2.1	Overview of the ECC.....	164
5.2.2	Hazmat production and transportation.....	166
5.2.3	Safety and accident prevention measures	171
5.3	Estarreja municipality characterization.....	172
5.3.1	Physical characterization	172
5.3.2	Demographic and economical characterization	175
5.4	Accident scenarios	178
5.5	Results.....	184
5.6	Synthesis	199
6.	CONCLUSIONS.....	203
	REFERENCES.....	213
	APPENDIX A: MAJOR INDUSTRIAL ACCIDENTS.....	249
	APPENDIX B: EFFECTS OF RELEASED HAZARDOUS GAS MODEL DEVELOPMENT	253
	APPENDIX C: VALIDATION OF EFRHA MODEL	257
	APPENDIX D. CASE STUDY: ESTARREJA.....	269

LIST OF FIGURES

Figure 1.1 – Time evolution of technological disasters reported between 1900 and 2009 [URL1.2].	6
Figure 1.2 – Aerial (a) and local (b) views over Flixborough explosion Ground Zero area [HMSO, 1975].	8
Figure 1.3 – Time magazine front cover reporting Bhopal accident [URL1.4].	10
Figure 1.4 – Time magazine front cover reporting Bhopal accident [URL1.5].	10
Figure 1.5 – Aerial view over the nuclear reactor after the explosion at Chernobyl plant [URL1.7].	11
Figure 1.6 – Ground deposition of ¹³⁷ Cs radionuclide in Europe after the Chernobyl accident [EEA, 2003].	11
Figure 1.7 – View over crater formed during the explosion of AZF plant in Toulouse [URL1.9].	12
Figure 1.8 – View of the AZF fertilizer plant structure after the explosion [URL1.10].	12
Figure 1.9 – Aerial photographs of Buncefield explosion and resulting fire [URL1.11].	13
Figure 1.10 – Aerial photographs of Viareggio trains station explosion and resulting fire [URL1.12].	14
Figure 1.11 – EM-DAT reported technological accidents summary for the period 1900-2010 [URL1.2].	18
Figure 1.12 – MIA (light blue) between 1996 and 2009 and related fatalities (dark blue) between 1998 and 2009 reported in MARS database [EEA, 2010; URL1.11].	19
Figure 1.13 – Percentage of MIA reported in MARS database per type of industry in the period 1985-2003 [Nivolianitou <i>et al.</i> , 2006].	20
Figure 1.14 – Causes of major accidents in the process industries [Rasmussen, 1996].	21
Figure 1.15 –MIA in Europe reported between 1998 and 2009 in MARS database [EEA, 2010]. ...	23
Figure 1.16 – Scheme of chronological evolution of EU regulation and relevant MIA EU-wide.	26
Figure 1.17 – Seveso establishments by EU member state and tier class in 2009 [COM(2010)781-SEC(2010)1591].	29
Figure 1.18 – Upper-tier establishments per EU member state: 2002, 2005 and 2009 [2009 [COM(2010)781-SEC(2010)1591].	29
Figure 2.1 – Scheme of quantitative risk analysis methodology [based on Mannan, 2005].	38
Figure 2.2 – Scheme of consequence analysis methodology [based on CCPS, 1999].	43
Figure 2.3 – Illustration of some conceivable release mechanisms according to (a) initial condition, (b) container, (c) aperture, (d) enclosure, (e) height, and (f) fluid momentum [Mannan, 2005].	46
Figure 2.4 – Phases in the dispersion of a dense gas cloud [based on Britter and McQuaid, 1988].	53
Figure 2.5 – Slumping phase of dense gas cloud dispersion [based on Casal, 2008].	54
Figure 2.6 – Photographs taken during Burro series: (a) LNG gas plume in Burro test 8 after 30 s; (b) LNG gas plume in Burro test 6 at quasi-steady state [Ermak, <i>et al.</i> , 1982].	58
Figure 2.7 – Photographs of collapsing cloud observed in Thorney Island Test 8 [Prince <i>et al.</i> , 1987].	60
Figure 2.8 – Idealised cloud shape assumed in box models for instantaneous releases [based on Cox and Carpenter, 1980].	63
Figure 2.9 – Idealised cloud shapes assumed in uniform models for continuous steady state grounded releases [based on Cox and Carpenter, 1980].	64
Figure 2.10 – Schematic representation of a Generalized plume model [based on Havens, 1988].	65

Figure 3.1 – EFRHA model: (a) organization of the steps modules, and (b) basic structure with data flow along the simulation process.	78
Figure 3.2 – Schematic representation of EMM structure and data flow.	80
Figure 3.3 – General calculation equations flowchart of EMM.	82
Figure 3.4 – ETM basic structure with the different stages of process.....	88
Figure 3.5 – Schematic representation of terrain, receptors and source gridded data used in EFRHA.....	88
Figure 3.6 – ESTM basic structure with data flow.....	90
Figure 3.7 – EDM basic structure with the different stages of process.	106
Figure 3.8 – EEM basic structure with the different stages of process.....	110
Figure 4.1 – Schematic summary of stages of EFRHA model validation exercise.....	120
Figure 4.2 – Scatter plots of EMM modelled ABL scaling parameters for the MET1 test case period.	123
Figure 4.3 – Scatter plots of EMM modelled ABL scaling parameters for the MET2 test cases period.....	124
Figure 4.4 – Time evolution of source term parameters of EFRHA (red) and EFFECTS 7.5 (blue) models for: (a) SRC1, (b) SRC2, (c) SRC3 and (d) SRC4 test cases.	130
Figure 4.5 – 3D perspective of MUST case obstacles array with identification of VIP car.....	133
Figure 4.6 –The MUST wind tunnel model set up in WOTAN facility [Bezpalcova and Harms, 2005].	134
Figure 4.7 – MUST test set-up reference coordinate system for the -45° MUST case.....	134
Figure 4.8 – Location of point source (orange spot) and concentration sensors (black spots) considered for the -45° MUST case validation study.	135
Figure 4.9 – Q-q plots of the IOMC modelled against measured concentrations for the -45° MUST case.	137
Figure 4.10 – Estimated maximum concentrations using Gaussian fitting, with distance x from the source (with obstacles IOMC1 – IOMC3; without obstacles: IOMC4 – IOMC6).	139
Figure 4.11 – Estimated plume width, using Gaussian fitting, with distance x from the source for the IOMCs.	140
Figure 4.12 – Schematic representations of Thorney Island trials site layout [Hansen <i>et al.</i> , 2010].	145
Figure 4.13 – Scheme of Burro test series measurement array. The closed circles represent masts with concentration sensors and the open circles indicate poles with meteorological sensors [Nielsen and Ott, 1996]......	146
Figure 4.14 – Scheme of Desert Tortoise test series measuring array. The closed circles represent masts with concentration sensors and the open circles indicate poles with concentration sensors [Nielsen and Ott, 1996]......	147
Figure 4.15 – Scheme of Lathen test series measuring array. The open spots represent 2 m poles with concentration sensors and dashed line represents the fence [Nielsen and Ott, 1996].	148
Figure 4.16 –Comparison of the time evolution of measured and modelled peak concentrations [%vol/vol] at plume centreline for (a) DGD1, (b) DGD2 (c) DGD3, (d) DGD4, (e) DGD5, (f) DGD6, (g) DGD7 and (h) DGD8 test cases runs during the initial instants after the release. .	149
Figure 4.17 – Quantile-quantile plots of modelled results against measurements concentrations [% vol/vol] for set of DGD test cases.	153
Figure 5.1 – Spatial distribution of MIA hazards estimated based on the density of chemical and petrochemical establishments per km ² per NUT3 EU-wide [Schmidt-Thomé and Kallio, 2006].	162
Figure 5.2 – Location of ECC and Estarreja Municipality areas [URL5.3].	164
Figure 5.3 – Chronogram of relevant dates of ECC development.....	165
Figure 5.4 – Scheme of relevant products chain in ECC [based on Teixeira, 2010; URL5.6]......	167

Figure 5.5 – Climate normal values of temperature in Aveiro District (1971-2000) [IM and AEMET, 2010].	173
Figure 5.6 – Climate normal values of precipitation in Aveiro (1971-2000) [IM and AEMET, 2010].	173
Figure 5.7 – Prevailing wind direction measured in S. Jacinto meteorological station at (a) winter and (b) summer periods (1954-1980) [SMPC, 2006a; Castro, 2010].	174
Figure 5.8 – Distribution of resident population of Estarreja municipality by ages in 2001 and 2009 [INE, 2001, 2010].	176
Figure 5.9 – Main road and railway networks in Estarreja municipality area [URL5.3].	177
Figure 5.10 – Spatial distribution of vulnerable spots and communication ways in Estarreja Municipality area [URL5.3].	178
Figure 5.11 – Location of accident points (red spots) considered in the ECC CA study.	179
Figure 5.12 – Dimensions of domains D1 and D2 used in CA study of ECC.	182
Figure 5.13 – Location of vulnerable spots in domains D1 and D2.	184
Figure 5.14 – Modelled chlorine maximum concentration time evolution and ERPG limits for CE1 scenario conditions during the initial 3600 s.	186
Figure 5.15 – Modelled phosgene maximum concentration time evolution and ERPG limits for CE2 scenario conditions during the initial 3600 s.	186
Figure 5.16 – Modelled vinyl chloride maximum concentration time evolution and ERPG limits for CE3 scenario conditions during the initial 3600 s.	187
Figure 5.17 – Modelled benzene maximum concentration time evolution and ERPG limits for CE4 scenario conditions during the initial 1800 s.	187
Figure 5.18 – Snapshots of modelled chlorine concentration fields [ppm] at 5 (a), 15 (b), 30 (c) and 60 (d) minutes after the vessel piping rupture for the set of ME of CE1 scenario.	191
Figure 5.19 – Snapshots of modelled phosgene concentration fields [ppm] at 5 (a), 15 (b), 30 (c) and 60 (d) minutes after the vessel piping rupture for the set of ME of CE2 scenario.	192
Figure 5.20 – Snapshots of modelled vinyl chloride concentration fields [ppm] at 5 (a), 15 (b), 30 (c) and 60 (d) minutes after the vessel piping rupture for the set of ME of CE3 scenario.	193
Figure 5.21 – Snapshots of modelled benzene concentration fields [ppm] at 2 (a), 5 (b) and 8 minutes after the cistern truck accident and crash for the set of ME conditions of CE4 scenario.	194
Figure A.1 – Number of people reported (a) killed and (b) affected by technological disasters 1900 – 2009 [URL1.1].	249
Figure A.1 – Basic fluxogram of EFRHA model data transfer and modelled outputs.	253
Figure C.1 – Time evolution plots of AERMET (green) and EMM (red) estimated ABL scaling parameters for MET1 test case.	257
Figure C.2 – Time evolution plots of AERMET (green) and EMM (red) estimated ABL scaling parameters for MET2 test case.	259
Figure C.3 – Scatter plots of IOMCs modelled results against wind tunnel mean concentration measurements for the -45° MUST case – IOMC runs (a) with and (b) without obstacles definition.	263
Figure C.4 – Scatter plots: non-CFD model results against wind tunnel measurements for the -45° MUST case [Schatzmann <i>et al.</i> , 2010].	265
Figure C.5 – Comparison of plume shape based on residuals concentrations modelled/measurements for the -45° MUST test case (with obstacles: IOMC1-3; without obstacles: IOMC4-6).	266
Figure D.1 – Spatial distribution of natural and technological risk at Portuguese national level [Gaspar, 2005].	270

LIST OF TABLES

Table 1.1 – Some noteworthy reported major industrial accidents worldwide. ^(a)	7
Table 1.2 – Examples of available databases of MIA reports.	15
Table 2.1 – Examples of QRA techniques as a function of the approach methodology [based on Tixier <i>et al.</i> , 2002; Casal, 2008].	40
Table 2.2 – Classification of accidental release situations [based on Mannan, 2005; VROM, 2005a].	47
Table 2.3 – Summary of well known experimental tests.	57
Table 2.4 – Classes of CA atmospheric dispersion models.	62
Table 3.1 – Thermodynamic states [VROM, 2005a].	91
Table 3.2 – ESTM sub-modules and integrated release scenarios.	92
Table 4.1 – Statistical parameters for the assessment of modelling performance. S_i is the i^{th} simulated value, M_i is the i th measured value, and x is the quantity under analysis [Abramowitz and Stegun, 1972; ASTM International, 2005; Chang and Hanna, 2005].	119
Table 4.2 – Summary of MET test cases used in EFRHA validation Stage 1.	122
Table 4.3 – Summary of quality metrics for modelled ABL scaling parameters for MET test cases (parameters not satisfying guidance acceptability limits are in bold).	126
Table 4.4 – Summary of test case scenarios defined for the ESTM validation study.	128
Table 4.5 – Summary of quality metrics of ESTM modelled source term parameters for the set of SRC test cases.	131
Table 4.6 – Overview of the IOMC runs and input parameters for the -45 ^o MUST case.	136
Table 4.7 – Summary of quality metrics estimated for IOMC runs modelled concentrations of -45 ^o MUST case (with: IOMC1 – IOMC3; without: IOMC4-IOMC6).	141
Table 4.8 – Overview of experimental data sets used for the validation of EFRHA model. [Nielsen and Ott, 1996; Mannan, 2005]	144
Table 4.9 – Summary of quality metrics for the set of DGD test cases.	155
Table 5.1 – Summary of criteria considered for the selection of the demonstrative case study. .	161
Table 5.2 – Relevant hazmat storage/process capacity present in ECC in 2004 [SMPC, 2006a]. ...	168
Table 5.3 – Summary of transportation modes and nominal capacity of hazmat in ECC [SMPC, 2006a].	170
Table 5.4 – Averaged monthly relative humidity and number of days with rain in the District of Aveiro [SMPC, 2006a].	174
Table 5.5 – Population distribution in the municipality of Estarreja divided by parish [INE, 2011].	175
Table 5.6 – ECC plausible and worst-case scenarios involving the release of hazmat.	179
Table 5.7 – Meteorological conditions considered for the ECC accident scenarios EFRHA runs. ...	181
Table 5.8 – Identification of vulnerable spots considered in the application of EFRHA model to ECC accident scenarios.	183
Table 5.9 – Reference ERPG threshold limits considered for the analyzed hazmat [AIHA, 2008].	185
Table 5.10 – Comparison of maximum concentrations estimated in vulnerable spots against reference ERPG values for CE1 accident scenario.	196
Table 5.11 – Comparison of maximum concentrations estimated in vulnerable spots against reference ERPG values for CE2 accident scenario.	196
Table 5.12 – Comparison of vinyl chloride maximum concentrations estimated in vulnerable spots against reference ERPG values for CE3 accident scenario.	197

Table 5.13 – Comparison of maximum concentrations estimated in vulnerable spots against reference ERPG values for CE4 accident scenario.	197
Table A. 1. Number of ‘Seveso establishments by Member State [EEA, 2010].	250
Table A. 2. Distribution of Number of ‘Seveso establishments by activity [EEA, 2010].	251
Table B.1 – Input parameters used by the EFRHA model.	254
Table B.2 – Interpretation of the L with respect to PG Stability Class [Seinfeld and Pandis, 2006].	255
Table B.3 – Output parameters estimated by the EFRHA model.....	255
Table C.1 – Summary of input parameters of SRC1 test case [VROM,2005a].	261
Table C.2 – Summary of input parameters of SRC2 test case [VROM,2005a].	261
Table C.3 – Summary of input parameters of SRC9 test case [VROM,2005a].	262
Table C.4 – Summary of input parameters of SRC4 test case [VROM,2005a].	262
Table D.1 – Types of vulnerable spots considered in the municipality of Estarreja [SMPC, 2006; URL5.3].....	271

Acronyms

ABL	Atmospheric Boundary Layer
AEGL	Acute Exposure to gas level
AEMET	Agencia Estatal de Meteorologia
AIChE/CCPS	American Institute of Chemical Engineers/Centre for Chemical Process Safety.
AIHA	American Industry Hygiene Association
AIS	Accident Inquiry System
AIST	Japanese National Institute of Advanced Industrial Science and Technology
ANPC	Autoridade Nacional da Protecção Cível [in Portuguese]
APEC	Associação Portuguesa de Empresas Químicas
APELL	Awareness and Preparedness for Emergencies at Local Level
API	American Petroleum Institute
AQP	Aliada Química de Portugal
ARIA	Analyse, Recherche et Information sur les Accidents
AZF	Azote de France
BAT	Best Available Techniques
BCC	Barreiro Chemical Complex
BLEVE	Boiling liquid expansion vapour explosion
BMIIB	Buncefield Major Incident Investigation Board
CA	Consequence analysis
CAC	Chemical Accident Case database
CBL	Convective Bouldary Layer
CCPS	Centre for Chemical Process Safety
CCSA	China Chemical Safety Association

CEC	Council of European Commission
CEDVAL	Compilation of Experimental Data for Validation of Microscale Dispersion Models
CEU	Council of the European Union
CFD	Computational Fluid Dynamics
CIRES	Companhia Industrial de Resinas Sintéticas
CLP	Classification, Labelling and Packaging
CRED	Centre for Research on the Epidemiology of Disasters
CUF-QI	Companhia União Fabril – Químicos Industriais
DAI	Daily Accident Information
DIERS	Design Institute for Emergency Relief Systems
DNS	Direct Numerical Simulation models
DNV	Det Norske Veritas [Norwegian: The Norwegian Veritas]
DOT	US Department of Transportation
DTA	Deterministic Test Case Analysis
EC	European Commission
ECC	Estarreja Chemical Complex
ECE	Economic Commission for Europe
ECHA	European Chemicals Agency
EC-MTH	European Commission Major Technological Hazards Program
ECPMS	Estarreja Civil Protection Municipal Service
EDM	EFRHA Dispersion Module
EEA	European Environmental Agency
EEEP	Estarreja External Emergency Plan
EEM	EFRHA Effects Module
EFRHA	Effects of Released Hazardous gAses

EM-DAT	Emergency Events Disasters Database
EMM	EFRHA Meteorological Module
EPA	Environmental Protection Agency
ERCOFTAC	European Research Community on Flow, Turbulence and Combustion
ERNS	Emergency Response Notification System
ERPG	emergency response planning gas limit
ESPON	European Spatial Planning Observation Network
ESSO	Esso Research and Engineering Company
ESTM	EFRHA Source Term Module
ETM	EFRHA Terrain Module
EU	European Union
EWTL	Environmental Wind Tunnel Laboratory of Hamburg University
FAC2	Geometric factor within a factor of 2
FACTS	Failure and accidents technical information system
FAO	Food and Agriculture Organization
FB	Fractional bias
GHS	Globally Harmonised System of Classification and Labelling of Chemicals
GIS	Geographical information system
hazmat	hazardous materials/substances
HAZOP	Hazard and Operability Studies
HEM	Homogeneous Equilibrium Model
HF	Hydrogen Fluoride
HMSO	Her Majesty's Stationery Office
HSE	Health and Safety Executive
HSMO	Her Majesty's Stationery Office

IAEA	Atomic Energy Agency
ICMESA	Industrie Chimiche Meda Società Azionaria
IEC/ISO	International Electrotechnical Commission and International Organization for Standardization
IEP	Internal Emergency Plan
IEP	Internal Emergency Plan
IIT	Indian Institute of Technology
IM	Instituto de Meteorologia
IOMC	Input Obstructions Modelling Configuration
IPPC	Integrated Pollution Prevention and Control
IRIS	Incident Reporting Information System
ISO	International Organization for Standardization
JRC	Joint Research Centre
JST	Japan Science and Technology Agency
LES	Large Eddy Simulation models
LFL	Lower Flammability Limit
LNG	Liquefied Natural Gas
LNLL	Lawrence National Livermore Laboratory
LP	Liquefied petroleum
LPG	Liquefied Pressurized Gas
MAHB	Major Accident Hazards Bureau
MARS	Major Accidents Reporting System
MDI	Methyl-di-isocyanate
MEESD	French Ministry for Ecology, Energy, Sustainable Development and the Sea
MEG	Model Evaluation Group
MEGPD	Model Evaluation Guidance Protocol Document

MEP	Chinese Ministry of Environmental Pollution
MG	Geometric mean bias
MHIDAS	Major Hazard Incident Data Service
MIA	Major Industrial Accidents
MIC	Methyl isocyanate
MOST	Monin-Obukhov Similarity Theory
MTH	Major Technological Hazards Program
MT-TNO	TNO Division of Technology for Society
MUST	Mock Urban Setting Test
NMSE	Normalized means square error
Non-CFD	Non Computational Fluid Dynamics Models
NRC	National Response Centre or National Response Council
NRCC	National Registration Centre for Chemicals
NTSC	National Transportation Systems Center
OECD	Organisation for Economic Co-operation and Development
PACOPAR	Painel Comunitário de Actuação Responsável
PEL	Permissible Exposure Levels
PRA	Probabilistic Risk Analysis
PVC	Polyvinyl chloride
QRA	Quantitative risk assessment
RA	Risk Assessment
RANS	Reynolds Averaged Navier-Stokes models
REACH	Registration, Authorisation and Restriction of Chemicals
REDIPHEM	REview and DISsemination of PHysical Effect Models
RISCAD	Relational Information System for Chemical Accidents Database
RMP	Risk Management Plan

RTP	Rapid Transition Phase
SAFETI	Software for the Assessment of Flammable, Explosive and Toxic Impacts
SAFIR	Safety reporting system
SAWS	Chinese State Administration of Work Safety
SB	Squared Bias
SBL	Stable Bondary Layer
SDSD	difference between the standard deviations of the simulations and measurements
SMEDIS	Scientific Model Evaluation of Dense Gas Dispersion Models
SMPC	Serviço Municipal de Protecção Cível
SMS	Safety Management System
SNPC	Serviço Nacional de Protecção Cível
STEL	Short Term Exposure Limits
TCDD	2,3,7,8-Tetrachlorodibenzo-p
TLV	Threshold Limit Values
TNO	Netherlands Organization for Applied Scientific Research
TüV	Technischen Überwachungsverein Norddeutschland e. V.
UFL	Upper Flammability Limit
UK	United Kingdom
UN	United Nations
UN/ECE	United Nations/Economic Commission for Europe
UNEP	United Nations Environment Program
UNISDR	United Nations International Strategy for Disaster Reduction
UN-OCHA	United Nations Office for the Coordination of Humanitarian Affairs
UNSCEAR	United Nations Scientific Committee on the Effects of Atomic Radiation

USA	United States of America
USCG	United States Coast Guard
USEPA	United States Environmental Protection Agency
USSR	Union of Soviet Socialist Republics
VDI	Association of German Engineers [in german]
VG	Grometric variance
VROM	Dutch National Institute of Public Health and the Environment
WHO	World Health Organization

Notation

A	Constant [-]
A_h	Cross-sectional area of source aperture [m ²]
A_p	Pipe cross-sectional area [m ²]
A_{pl}	Liquid pool surface cross-sectional area [m ²]
B_o	Bowen ratio [-]
$c(z)$	Concentration vertical profile [μg.m ⁻³]
C^*	Dimensionless concentration [-]
C^*_{max}	Representative maximum concentration in the plume centre line [-]
c_1, c_2, c_3	Empirical constants (net radiation calculation) [W.m ⁻² .K ⁻⁶ , W.m ⁻² , -]
C_b	Bow-down correction factor [-]
C_D	Discharge coefficient of the source point [-]
C_D	Drag coefficient [-]
$C_{measured}$	Concentration value measure during experimental tests [% vol.vol ⁻¹]
$C_{modelled}$	Concentration value modelled by EFRHA model [% vol.vol ⁻¹]
C_p	Specific heat capacity at constant pressure [J.kg ⁻¹ .K ⁻¹]
C_{pa}	Specific heat capacity of atmospheric air gas at const. pressure [J.kg ⁻¹ .K ⁻¹]
C_{pL}	Specific heat capacity of Liquid at constant pressure [J.kg ⁻¹ .K ⁻¹]
C_{pV}	Specific heat capacity of gas at constant pressure [J.kg ⁻¹ .K ⁻¹]
C_{vV}	Specific heat capacity of gas at constant volume [J.kg ⁻¹ .K ⁻¹]
d	Displacement [m]
D_c	Cloud diameter [m]
D_c	Cloud width [m]
$dM_{pl}(t)/dt$	Overall mass balance [kg.s ⁻¹]
d_p	Pipe cross-sectional diameter of the pipe [m]

dT_{pl}/dt	Variation of the pool temperature [K.s ⁻¹]
e_{sf}	terrain surface elevation [m]
f	Coriolis parameter [s ⁻¹]
F	Frictional flow reduction factor [-]
$FAC2$	geometric fraction within a factor of 2 [-]
FB	Fractional bias [-]
f_D	Darcy friction factor [-]
f_F	Frictional Fanning factor [-]
Fr	Froude number [-]
g	Gravitational acceleration [m.s ⁻²]
$g(\bar{\rho} - \rho_a)$	Cloud buoyancy [kg.m ⁻³]
G_{ERM}	Equilibrium mass flux [kg.m ⁻² .s ⁻¹]
G_{SUB}	Subcooled mass flux [kg.m ⁻² .s ⁻¹]
H	Height [m]
H	Sensible heat flux [W.m ⁻²]
h	Cloud height [m]
h	Reference height [m]
H_{bd}	Building height [m]
h_n	location of the orifice from the vessel base [m]
h_L	Relative liquid height above the failure opening [m]
h_{pl}	Depth of the pool [m]
H_{vap}	Heat of vaporization at T_0 [J.kg ⁻¹]
$H_{vap}(T_{pl})$	Heat of evaporation at pool temperature [J.kg ⁻¹]
i	Step counter [-]
k	von Karman constant [-]
k_i	Semi-empirical coefficient [-]

$K_m(t)$	Mass transfer coefficient related to concentration [m.s ⁻¹]
L	Monin-Obukhov length [m]
l_p	Length of the pipe/pipeline [m]
M	Molar mass [g.mol ⁻¹]
m_0	Initial total gas mass contained in the pipe [kg]
MG	Geometric mean bias [units ²]
M_i	Measured value [units]
$m_{L,0}$	Initial liquid mass in the vessel [kg]
M_{pl}	Liquid pool mass [kg]
$m_{V,0}$	Initial vapour mass in the vessel [kg]
n	Fractional cloud cover [-]
n_{eq}	Equivalent cloud cover [-]
N_F	Non-equilibrium dimensionless parameter [-]
$NMSE$	Normalised mean square error [-]
N_t	Total number of steps [-]
P	Pressure [Pa]
P	Total pressure at opening [Pa]
P_0	Initial stagnant initial pressure in the vessel [Pa]
P_a	Atmospheric pressure [Pa]
P_v^0	Initial saturation vapour pressure at T_0 [Pa]
$P_v^0(T)$	Saturated vapour pressure as a function of temperature [Pa]
P_v^{sat}	Saturation vapour pressure [Pa]
q'_{rel}	Liquid spill rate [kg.s ⁻¹]
q_0	Initial gas release rate [kg.s ⁻¹]
q_{co}	Source volume flow rate [m ³ .s ⁻¹]
$Q_{i,0}$	Initial volume of instantaneous puff [m ³]

q_s	Hazmat gas mass outflow rate [$\text{m}^3.\text{s}$]
$q_{s,L}$	Spilled liquid mass outflow rate [$\text{kg}.\text{s}^{-1}$]
q_{s0}	Initial mass flow rate of pure vapour [$\text{kg}.\text{s}^{-1}$]
q_{sc}	Hazmat steady-state (continuous) mass flow rate [$\text{kg}.\text{s}^{-1}$]
q_{sF}	Two-phase hazmat mass flow rate [$\text{kg}.\text{s}^{-1}$]
q_{sh}	Hazmat gas mass flow rate through the pipe opening [$\text{kg}.\text{s}^{-1}$]
q_{sL}	Liquid hazmat mass flow rate [$\text{kg}.\text{s}^{-1}$]
q_{sp}	Hazmat mass flow rate through the pipe [$\text{kg}.\text{s}^{-1}$]
q_{srel}	Hazmat liquid spill rate for liquid pool formation [$\text{kg}.\text{s}^{-1}$]
q_{sV}	Hazmat mass vapour rate from PLG release [$\text{kg}.\text{s}^{-1}$]
q_{sVp}	Hazmat mass liquid evaporation rate from liquid pools [$\text{kg}.\text{s}^{-1}$]
r	Radius [m]
r	Correlation coefficient [-]
R	Gas constant [$\text{J}.\text{mol}^{-1}.\text{K}^{-1}$]
R_0	Clear sky incoming solar insolation [$\text{W}.\text{m}^{-2}$]
$r_a(\phi_s)$	Surface albedo as a function of solar elevation angle [-]
r_a'	Noontime surface albedo (for the sun on the meridian) [-]
Re	Reynolds number [-]
R_i	Richardson number [-]
R_n	Net radiation [$\text{W}.\text{m}^{-2}$]
$r_p(t)$	Liquid pool surface radius as a function of time [m]
\bar{R}_{sol}	Incoming solar radiation [$\text{W}.\text{m}^{-2}$]
S_1	Shape parameter [-]
SB	Squared bias [units ²]
Sc	Schmidt number [-]
$SDSD$	Difference between the standard deviations of modelled results and

	observations [units ²]
S_i	Simulated value [units]
t	Record hour after sunrise [s]
T	Temperature [K]
t	Time after the start of the release [s]
t	Time after starting the simulation [s]
T_0	Initial hazmat storage/transport temperature [K]
T_a	Atmospheric temperature [K]
$T_{a,S}$	Ambient sub-soil temperature [K]
T_B	Boiling point temperature [K]
t_B	Time constant in the Wilson method [s]
t_{bd}	Blow-down time [s]
T_c	Critical temperature [K]
t_E	Maximum time validity model [s]
t_i	Time for the step i after the start of the release [s]
T_{melt}	Melting point temperature [K]
T_{pl}	Temperature of the liquid pool [K]
t_{sc}	Duration of hazmat steady-state (continuous) outflow [s]
T_{sim}	Total time of simulation period [s]
t_v	Initial vapour outflow blow-out period [s]
u	Wind velocity [m.s ⁻¹]
u^*	Surface friction velocity [m.s ⁻¹]
u_a	Ambient air horizontal velocities along x [m.s ⁻¹]
u_{entr}	Air entrainment velocity [m.s ⁻¹]
u_h	Wind velocity at reference scale [m.s ⁻¹]
u_{inf}	Dense gas inflow velocity [m.s ⁻¹]

u_L	(Average) Liquid flow velocity inside the pipe [m.s ⁻¹]
u_{ref}	Wind velocity at reference measurements height [m.s ⁻¹]
u_s	Sonic velocity in the gas [m.s ⁻¹]
$ u_{auv} $	Ambient fluid velocities along (x,y) respectively (u_a, v_a) [m.s ⁻¹]
$ u_{uv} $	Depth-averaged velocity (\bar{u}, \bar{v}) [m.s ⁻¹]
\bar{u}, \bar{v}	Horizontal velocity components [m.s ⁻¹]
$ u_{uv} $	Ambient fluid velocities along (x,y) respectively (u_a, v_a) [m.s ⁻¹]
v_a	Ambient air horizontal velocities along y [m.s ⁻¹]
VG	Geometric variance [units ²]
V_p	Total volume of the gas inside the pipe [m ³]
V_V	Vessel volume [m ³]
V_x	Turbulent shear stress forces along x [Pa]
V_y	Turbulent shear stress forces along y [Pa]
w^*	Convective velocity scale [m.s ⁻¹]
x	Quantity under analysis [-]
x,y,z	Cartesian coordinates [m]
Y	Expansion factor [-]
ψ	Outflow coefficient [-]
Y	Expansion factor
z	Height [m]
z	Compressibility factor [-]
z_0	Surface roughness length [m]
z_i	ABL mixing height [m]
z_{ic}	ABL convective mixing height [m]
z_{im}	ABL mechanical mixing height [m]
z_{ref}	Reference height [m]

β_m	Constant [-]
γ	Specific heat capacity ratio [-]
ΔP	Total pressure drop between the vessel and the ambient [Pa]
ΔP	Pressure drop over the pipe [Pa]
ΔP_h	Pressure drop over the downstream opening in the pipe [Pa]
ΔP_p	Pressure drop over the pipe [Pa]
ΔP_L	Pressure drop over the pipe [Pa]
ζ	Constant of proportionality of turbulent shear stress [-]
θ	Potential temperature [K]
θ^*	Potential temperature scale [K]
ρ	Density of air [kg.m ⁻³]
$\rho(z)$	Vertical distribution of density [kg.m ⁻³]
ρ_0	Initial hazmat gas density [kg.m ⁻³]
ρ_a	Atmospheric air density [kg.m ⁻³]
ρ_F	Two-phase mixture density [kg.m ⁻³]
ρ_g	Gas density [kg.m ⁻³]
ρ_L	Liquid density [kg.m ⁻³]
$\rho_{sL,0}$	Initial liquid density [kg.m ⁻³]
$\rho_{v,0}$	Initial vapour density [kg.m ⁻³]
ΣH	Sum of the surrounding environment heat fluxes, from soil, air, solar radiation, long wave radiation and mass [J.m ⁻² .s ⁻¹]
ΣK_f	Sum of the individual excess head loss terms [-]
σ_{SB}	Stephan-Boltzmann constant [W.m ⁻² .K ⁻⁴]
σ_y	Standard deviation of the maximum concentration horizontal distribution [-]
τ	Time scale controlling the temporal interpolation of z_{im} [s]
τ_{cr}	Sonic blow time [-]

τ_s	Subsonic blow time [-]
τ_v	Time constant [s]
ν_{fg}	Change in specific volume from liquid to vapour [$\text{m}^3.\text{kg}^{-1}$]
ϕ	Filling degree [$\text{m}^3.\text{m}^{-3}$]
ϕ_{crit}	Critical solar elevation angle [$^\circ$]
ϕ_L	Liquid filling degree [$\text{m}^3.\text{m}^{-3}$]
ϕ_s	Solar elevation angle [$^\circ$]
Φ_m	vapour mass fraction in the two-phase flow [$\text{kg}.\text{kg}^{-1}$]
Φ_V	Vapour mass fraction in the two-phase flow [$\text{kg}.\text{kg}^{-1}$]
$\Phi_{V,F}$	Flash fraction [$\text{kg}.\text{kg}^{-1}$]
Ψ_m	Integrated forms of the similarity function [-]
ω	Pitzer factor [-]
α	Fraction parameter[-]
$\alpha_2, \alpha_3, \alpha_7$	Empirical constants [-]
$\bar{\rho}$	Depth-averaged hazmat gas density [$\text{kg}.\text{m}^{-3}$]

Overlines

\bar{X}	Average Value
-----------	---------------

Subscripts

X_a	Atmospheric conditions
X_s	Hazmat gas state
X_{sL}	Hazmat liquid state
X_{svp}	Hazmat evaporation
X_0	Initial conditions of hazmat
X_{sF}	Hazmat two-phase state

X_p	Pipe/pipeline
X_v	Vessel
X_V	Hazmat Vapour
$X_{V,F}$	Hazmat vapour fraction of flashing
X_{crit}	Critical condition
X_{fg}	Two-phase mixture
$X_{V,0}$	Initial conditions of Vapour fraction
$X_{L,0}$	Initial conditons of Liquid fraction
X_g	Pure gas state
X_x	Along x
X_y	Along y
X_{uv}	Along (x,y)
X_{auv}	Ambient Fluid Velocities along (x, y) respectively

CHAPTER 1

1. INTRODUCTION

Public awareness on risks posed by the use of *hazardous materials/substances* (hereinafter named *hazmat*) increased markedly over the last decades due to the expansion and scale-up of reported severe accidents/disasters, in particular since the 1960s and 1970s. The attention to this problem is continuously brought worldwide by examples of ‘*major disasters*’, either they have a natural or man-made (technological) origin. Technological disasters, such as *major industrial accidents* (MIA) or terrorist attacks are not rare events and consequences on humans and the environment have been extensively discussed in the literature [e.g. Lees, 1996; Kirchsteiger, 2001; Nivolianitou *et al.*, 2006; Gunn, 2008; European Environmental Agency (EEA), 2010]. Moreover, the extensive industrial development next to (progressively more densely) populated areas, clearly leads to the possibility of accidents causing mass casualties and a dramatic escalation of potential financial, social and environmental repercussions of such events [Lari *et al.*, 2009]. Despite the growing understanding and significant efforts on the mitigation of technological hazards, the assessment and reduction of related risks and impacts continues to challenge scientific, safety and regulatory prone communities [Tyagunov *et al.*, 2005]. Consequently, the attempt to control and predict such hazards and potential consequences has become a recognized strategic goal component of emergency planning and response, risk analysis and safety regulatory instruments [Durham, 2003].

1.1 Industrial accidents involving hazardous materials

Industrial development provides prosperity, high standards of living and is considered a key measure of progress but, as all physical human activities, industrial activities involve risks to humans and the environment. Production, storage and transportation of hazmat are processes of vital economic importance for any advanced and technologically complex society, which are always coupled with an increase of the number of industrial facilities and hazmat quantities handled [Mannan, 2005; Guedes *et al.*, 2009]. Nonetheless, this modification requires a continuous learning process to deal with the constant threat of technological disasters generated by the development of new and more complex technologies. Moreover, this learning process is frequently based on the study of previous MIA, as well as, on the compilation and comprehensive analysis of data.

1.1.1 Concepts

The potential for MIA has emphasized the need for a clearly defined and systematic approach to evaluate and control hazmat process, storage or transportation, in order to protect workers, the public and the environment. As a result, various definitions of relevant concepts have been proposed and extensively used in regulatory and scientific contexts.

Commonly, an *accident* can be defined as ‘an unfortunate incident that happens unexpectedly and unintentionally, typically resulting in damage or injury’, as cited in the *Oxford Dictionary* [Oxford Dictionaries, 2010]. When considered in the context of industrial activity and associated risks, a *MIA* is ‘an occurrence such as major emission, fire, or explosion resulting from uncontrolled developments in the course of the operation of any industrial plant (storage, process or transportation, leading to serious danger to human health and/or the environment, immediate or delayed’. Such incidents/events can take place inside or outside the plant involving one or more dangerous substances.

Everyday life human activity entails a variety and degrees of *hazards* and *risks*. These terms are familiar and intuitive to many of us. However, they are regularly treated as interchangeable synonymous in many fields and activities including economics, business, sports, industry, even not always referred to with exactly the same meaning. Consequently, this has led to a sort of ambiguity in the use and definition of these concepts over the last years [Christensen *et al.*, 2003]. The *Oxford English Dictionary* provides again some insights defining *hazard* as ‘a possible source of danger or risk’ and *risk* as ‘a situation involving exposure to danger’ or ‘the possibility that something unpleasant will happen’ [Oxford Dictionaries, 2010]. Nonetheless, in spite of being relatively new and still in development, modern engineering sciences and regulatory communities have also proposed guidance definitions for these concepts over the last years, as follows.

In a technical interpretation, *hazards* can be defined as ‘the source of danger, that may be an intrinsic phenomenon, human activity, a chemical or physical condition that has the potential for causing damage to people, property, or the environment and may or may not lead to an emergency or disaster’ [Greenberg and Cramer, 1991]. Furthermore, the Center for Chemical Process Safety [CCPS, 1999] and the United Nations International Strategy for Disaster Reduction [UNISDR, 2009] argue that *hazards* can be quantitatively described by the likely frequency of occurrence and different intensities of consequences determined from historical data or scientific analysis. Their origin may be purely natural (*e.g.* earthquakes, storms, floods, forest fires), technological (*e.g.* industrial accidents, terrorist attacks), or a mixture of both (*e.g.*

sinking of an oil tanker in a winter storm at sea, explosion of tank during earthquake) [Slovic, 2000]. In any case these events can lead to threats and damages to people, the environment or material assets. While natural hazards are purely natural origin processes or phenomena; technological hazards refer to failures of man-made systems, occurring accidental or deliberately with minor or no warning preceding the event, that have the potential to cause fatalities and/or casualties and produce significant damage to structures and environment. In the context of industrial and transportation activities, technological hazard events often involve the release of hazmat, fires or explosions with severe impacts. Consequently, the assessment of technological risk has been recognised to be more complex than natural risk and then, a target of numerous research works [e.g. Covello, 1982; Sherif, 1990; Shaluf *et al.*, 2003; Schmidt-Thomé, 2005; EEA, 2010], given the influence of human activity in its occurrence, prevention and impacts mitigation.

On the other hand, the word *risk* has two distinctive connotations: in popular usage the emphasis is generally placed on the concept of possibility for a particular danger, harm or hazard to occur, such as in the 'risk of an accident'; whilst in technical emphasis is on the consequences, in the form of 'potential losses' for some particular cause, place and period [Smith, 1996; Oxford Dictionaries, 2010]. In 'professional and engineering sciences' *risk* is regularly defined as the 'combination of the consequences of an event (hazard) and the associated likelihood (probability) of its occurrence' [World Health Organization (WHO), 2004; Vose, 2008; International Electrotechnical Commission and International Organization for Standardization (IEC/ISO), 2009]. Notwithstanding, *risk* is a complex function of the degree of hazard to a certain system (technological or environmental), the likelihood that a *hazard* results in an undesired event and the vulnerability of the system into which the undesired event may develop its consequences [Kirchsteiger *et al.*, 1998]. Therefore, it is possible to mention that *risks* are actually the consequences if hazards do materialize (occur).

1.1.2 Historical overview of major industrial accidents

The history of industrial activities (including transportation and storage) is replete with reported MIA. Since the industrial revolution numerous and severe MIA have been reported almost every year, causing major fatalities and asset damage, but most of all, highlighting the resulting potential, and sometimes, devastating social, financial and environmental repercussions [Carol *et al.*, 2002; Tavares *et al.*, 2010]. Even with the increasing number of MIA reported since the beginning of the 20th century, a drastic raise is observed since the 1970s.

Figure 1.1 illustrates the total number of technological disasters (comprising accidents in industrial and transportation activities) reported worldwide since 1900 to present (2009).

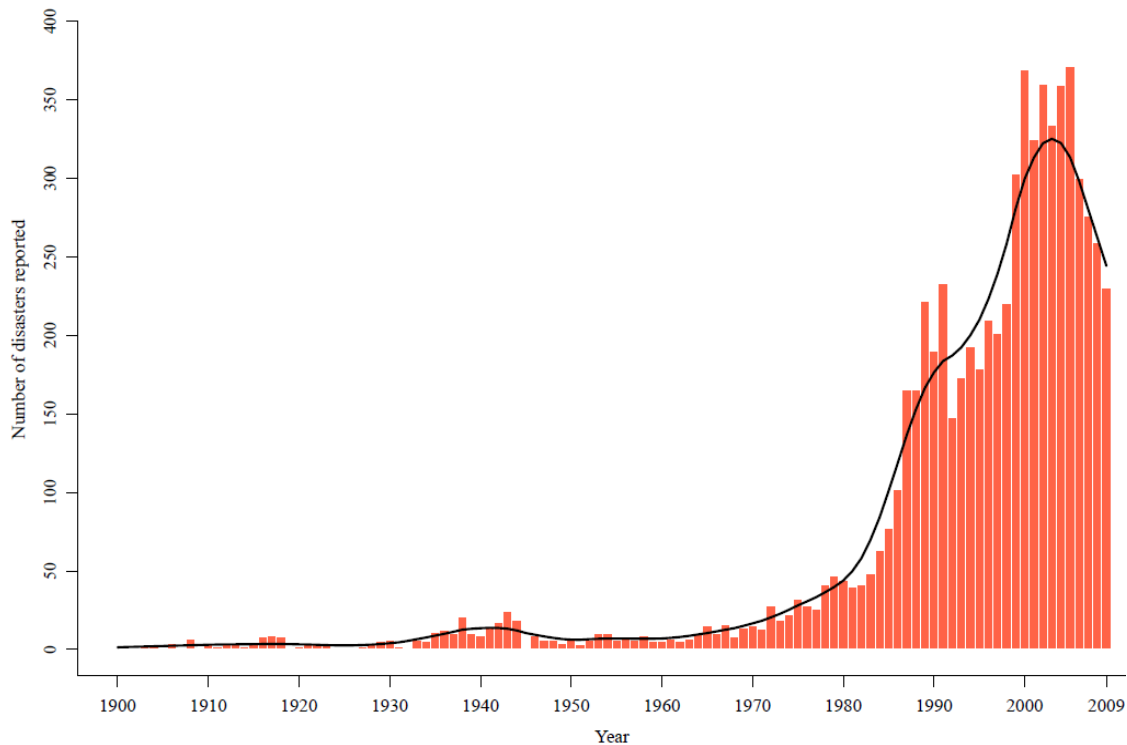


Figure 1.1 - Time evolution of technological disasters reported between 1900 and 2009 [URL1.2].

Time evolution behaviour of major technological disasters reported between 1900 and 2009 can be directly linked with the intense industrial development worldwide. From Figure 1.1 it is perceptible a relatively reduced number of MIA reported between 1900 and 1950s, despite the noticeable higher values during the 1940s (seriously affected by the World War II). However, a drastic raise of reported MIA is observed from the second half of the 20th century onward, largely caused by the rapid industrial development commonly next to (gradually more densely) populated areas. Along history, a large number of reported MIA, including the ones summarized in Table 1.1, became known mostly due to their consequences on people and the environment, illustrating the myriad ways in which human or equipment failures, at industrial and transportation activities, may cause accidents leading to large impacts on human health and environment [EEA, 2003; Lindberg, *et al.*, 2010].

Table 1.1 lists some noteworthy MIA reported worldwide over the last decades highlighting the correspondent type of accident and the estimated number of people death and injured based on available information in the literature and databases.

Table 1.1 – Some noteworthy reported major industrial accidents worldwide. ^(a)

Year	Location	Products involved	Type of accident	Death	Injured
1947	Texas City, USA	Chemicals	Explosions	581	≈5,000
1957	Mayak, USSR	Nuclear	Explosion	200	≈8,000 ^(b)
1957	Windscale, UK	Nuclear	Fire	-	≈200
1974	Flixborough, UK	Cyclohexane	Explosion	28	89
1975	Beek, Netherlands	Ethylene	Vapour cloud explosion	14	109
1976	Seveso, Italy	TCDD Dioxin	Explosion and dispersion	0	37,000
1977	Columbia, USA	Ammonia	Toxic gas dispersion	30	22
1978	Los Alfaques, Spain	Propylene	Fireball (road transport)	216	200
1980	Danaciobasi, Turkey	Chemicals	Unknown	107	0
1984	México city, México	Liquefied Pressurized Gas	Fire and explosion	550	23
1984	Bhopal, India	Methyl Isocyanate	Toxic gas dispersion	22,000 ^(c)	0
1986	Chernobyl, Ukraine	Nuclear	Explosion and fire	60	Unknown
1986	Basel, Switzerland	Chemicals	Fire	0 ^(d)	0
1988	North Sea, UK	Oil, gas	Fire	167	0
1989	Acha Ufa, USSR	Gas	Explosion (pipeline)	575	0
1989	Pasadena, USA	Polyethylene	Explosion	23	120–300
1991	Livorno, Italy	Naphtha	Transport accident	141	0
1996	Alberton, USA	Chemicals	Spill (train transport)	1	300
2000	Baia Mare, Romania	Cyanides	Spill	0 ^(d)	0
2000	Enschede, Netherlands	Fireworks	Explosion	23	947
2001	Toulouse, France	Ammonium nitrate	Explosion	30	2,242
2004	Ghileghien, Belgium	Liquefied Natural Gas	Explosion	24	131
2005	Texas City, USA	Chemicals	Explosion	15	170
2005	Buncefield, UK	Fuel	Explosion and fire	0	43
2009	Viareggio, Italy	LPG	Fire (train transport)	31	+30
2010	Louisiana, USA	Oil	Explosion and spill	11	0
2010	Bonaire, USA	Oil	Explosion and fire	0	0
2010	Ajka, Hungary	Alumina sludge	Spill	10	120–150
2011	Sendai, Japan	Nuclear	Explosion ^(e)	0	7

(a) Information compiled from MARS, EM-DAT and FACTS databases.

(b) More than 8,000 deaths from health problems caused by exposure have been reported until 1992.

(c) Around 22,000 deaths (with direct or indirect exposure consequences) have been reported until 2004.

(d) No fatalities but large environmental damage.

(e) Effects on humans and the environment have not yet been estimated

One of the worst MIA disasters reported in North America occurred in Texas City, in the United States of America (USA) in the morning of 16th April 1947. A chain of catastrophic fires

and explosions that destroyed the entire chemical complex facilities and the surrounding populated area started with a small fire on bags of ammonium nitrate fertilizer in the hold of a cargo ship anchored at the sea Port complex. The fire and explosions detonated approximately 3,250 tonnes of ammonium nitrate and 1,800 tons of sulphur [Stephens, 1993]. The official death toll was 581 people (including the entire Texas City Firefighters Department crew), 5,000 people were injured and 113 classified as missing [URL1.3].

Since the 1970s an increasing number of severe MIA events have been reported with major casualties, financial, social and environmental repercussions. The explosion and subsequent fire at a petrochemical site close to Flixborough, in United Kingdom (U.K.) on 1st June 1974, lead to a widespread public outcry over industrial activities safety, and significant tightening of regulations covering hazardous industrial processes [Mannan, 2005]. According to Her Majesty's Stationery Office (HMSO) [1975], in the explosion, 28 people were killed and 89 injured (36 workers and 53 off-site). Around the 'ground zero' area, 1800 buildings within a 1.6 km radius of the site were damaged. Notwithstanding the level of destruction, shown in Figure 1.2, the number of fatalities was relatively reduced because the accident took place on a Saturday [Health and Safety Executive (HSE), 1975].

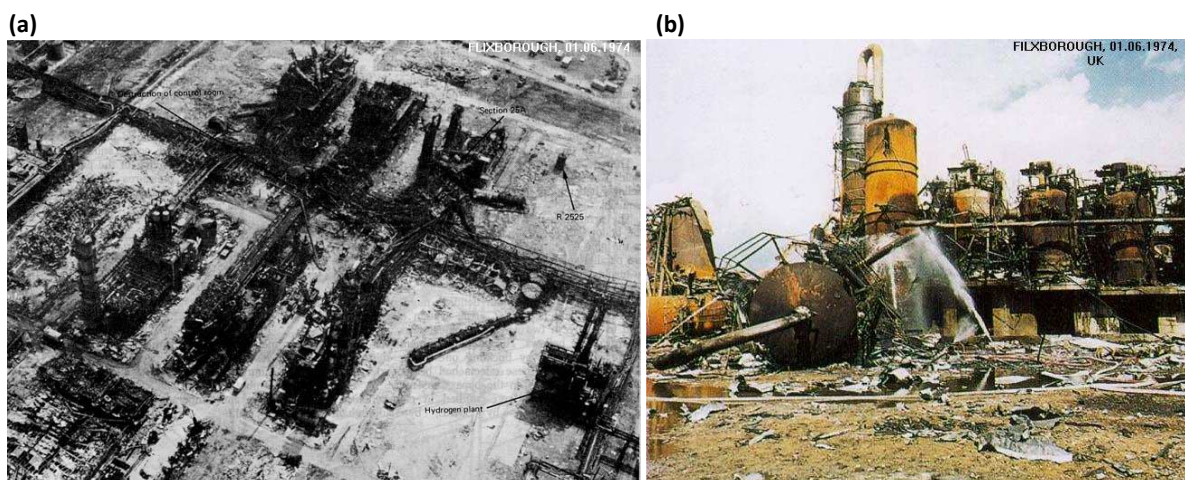


Figure 1.2 - Aerial (a) and local (b) views over Flixborough explosion Ground Zero area [HMSO, 1975].

Post-accident investigations concluded that human failure was the cause of the rupture that originated the release and ignition of about 40 tonnes of cyclohexane [Lees, 1996]. This accident endorsed a significant improvement on maintenance operations procedures and checklists in petrochemical industries. This event is often considered the genesis for the development of new regulatory and safety procedures and regulatory documents at European Union (EU) level [Marshall, 1987; Høiset *et al.*, 2000].

Two years later, the release of about 30 kg of TCDD dioxin (2,3,7,8-Tetrachlorodibenzo-p-dioxin) on 10th June 1976, at the Industrie Chimiche Meda Società Azionaria (ICMESA) chemical plant located in Seveso (Italy), caused extensive impacts in both humans and the environment. Approximately 37,000 individuals were affected by direct and/or indirect exposure to TCDD [Rice, 1982]. Although there were no immediate human casualties, as in previously described accidents, delayed and indirect effects resulted in thousands of animals died, or killed to prevent further impacts along the food chain, buildings were demolished, and residents were forced to leave the area [Wettig *et al.*, 1999]. Delayed exposure effects on humans, like chemical burns and chloracne were observed in many of the affected people. The Italian public authorities lift temporarily the law banning abortion, allowing several pregnant women to terminate pregnancies voluntary [Bertazzi, 1991]. Studies on long-term effects of mortality and cancer incidence on resident populations have been conducted in the following years to evaluate the carcinogenic risks posed by TCDD, such as Bertazzi *et al.* [1998] or Pesatori *et al.* [2009]. In the light of this MIA event, the development and implementation of a new European legislation aiming at the prevention and control of accidents involving hazmat was emphasized and put into practice. As a result, the European Directive 82/501/EEC, also called 'Seveso Directive' (to maintain the memory of the consequences of this event) on the major accident hazards of certain industrial activities was prepared and adopted EU-wide in 1982.

For the worldwide chemical industry, the Bhopal (India) toxic gas release in 1984 can be considered the worst MIA ever recorded [Willey *et al.*, 2005]. On the night of 2nd to 3rd December 1984, a runaway chain of chemical reactions caused the release of about 45 tonnes of MIC (methyl isocyanate) at the Union Carbide Corporation industrial plant close to Bhopal. MIC gas cloud drifted over the densely populated Bhopal neighbourhoods around the industrial installations. The impact on people living close to the chemical plant was immediate and devastating, many died in their beds, others staggered from their homes, blinded and choking, to die in the street (see Figure 1.3) [Shrivastava, 1992].

The final death toll was estimated to be between 15,000 and 22,000 people, comprising immediate and delayed fatalities [Willey, 1998]. Some half a million survivors suffered several health problems caused by the exposure to MIC. The attention of international media, *e.g.* the Time magazine cover shown in Figure 1.4, as well as information and investigation reports, were a key factor for the increase of public awareness about the potential impacts of industrial accidents.



Figure 1.3 - Time magazine front cover reporting Bhopal accident [URL1.4].

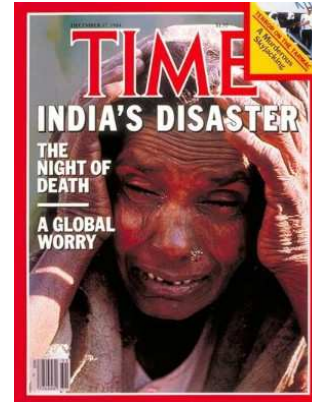


Figure 1.4 - Time magazine front cover reporting Bhopal accident [URL1.5].

Severe MIAs have also been reported in the energy production industry. Among the most studied and known events in this sector, over the last decades, the 1986 explosion at the Chernobyl nuclear power plant in Ukraine (former Union of Soviet Socialist Republics (USSR)), can be considered one of the two¹ worst accidents in history with a level 7 event on the International Nuclear Event Scale [Gunn, 2008]. Although precise causes of the accident still remain uncertain, it is generally believed that a series of incidents leading to an explosion followed by a fire and nuclear meltdown was caused by a combination of reactor design flaws and operator error. The explosion resulted in the collapse of part of the building (see Figure 1.5) and the release of a radiation cloud into the atmosphere, ejecting about 8 tonnes of radioactive material during the following two weeks after the incident. Released material was widely carried away in the form of gases and dust particles (mostly Cesium-137 - ^{137}Cs) by air circulation and mainly deposited over the territory of Ukraine, Russia and Belarus (see Figure 1.6) [Bennet *et al.*, 2006].

However, the extension of the dispersion and deposition of radioactive matter (^{137}Cs) reached outlying countries like Austria, Greece or Italy [EEA, 2003], as illustrated in Figure 1.6, and even the USA as reported by the United Nations Scientific Committee on the Effects of Atomic Radiation (UNSCEAR) [2008]. After the accident, the damaged reactor was sealed in a 'sarcophagus', keeping the other operating until November 2000 [URL1.6].

The main reported casualties were among the fire-fighters including those who attended the initial small fires. By mid-2005s, fewer than 60 deaths could be linked directly to Chernobyl

¹ The second level 7 nuclear accident event occurred in Fukushima (Japan) nuclear power plant involving a series of explosions after being struck on 11th March 2011 by the tsunami wave formed by an earthquake of magnitude between 8 and 9 in Richter seismic scale.

(mostly workers who were exposed to massive radiation during the accident or children who developed thyroid cancer) [UNSCEAR, 2009].



Figure 1.5 - Aerial view over the nuclear reactor after the explosion at Chernobyl plant [URL1.7].

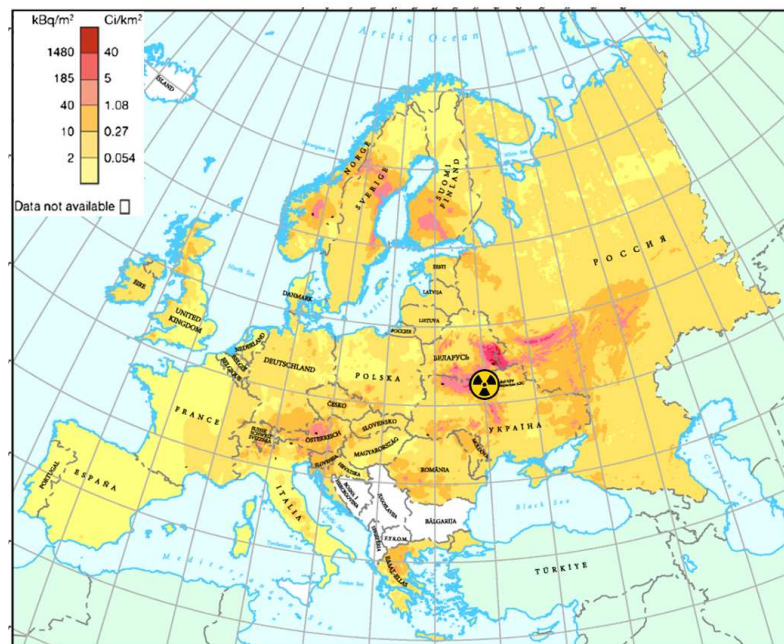


Figure 1.6 - Ground deposition of ¹³⁷Cs radionuclide in Europe after the Chernobyl accident [EEA, 2003].

Estimates of the eventual death toll from Chernobyl vary widely. Aiming to provide valuable information and evaluate the real consequences of this event, an initiative of the International Atomic Energy Agency (IAEA) in collaboration with the WHO, United Nations (UN), Food and Agriculture Organization (FAO), United Nations Environment Program (UNEP), United Nations Office for the Coordination of Humanitarian Affairs (UN-OCHA), UNSCEAR and the World Bank, created the UN Chernobyl Forum as a contribution to the United Nations' ten-year strategy for Chernobyl program, launched in 2002 [URL1.8]. The main purpose of this Forum is the provision of scientific information concerning the 'real' consequences from the accident on population and the environment in the most affected countries.

After the accident, an increase in thyroid cancer was found in children exposed to fallout from the accident [IAEA, 2006]. In 2000, about 2,000 cases of thyroid cancer had been reported in those exposed as children in the former Soviet Socialist Union, and in 2005, the number was estimated at 4,000 [WHO, 2005]; the latest estimate for the year 2056 ranges from 3,400 to 72,000 [Cardis *et al.* 2005]. The effects are not limited by national boundaries and more than 20 years after the accident, people in the affected countries had not yet precise and clear scientific consensus and knowledge on the health, environmental and socio-economic consequences of the accident [Baverstock and William, 2006; IAEA, 2006].

Entering the 21st Century, a major explosion at the Azote de France (AZF) fertilizer plant, located 3 km from Toulouse (France), on 21st September 2001, caused the destruction of the entire industrial complex (see Figure 1.7 and Figure 1.8), killed 30 people (21 on-site and 9 off-site), and injured nearly 2,242, many of them seriously [Cahen, 2006]. As illustrated in Figure 1.7, the accident generated a crater in the industrial facility and also affected two other chemical plants in the vicinity.



Figure 1.7 - View over crater formed during the explosion of AZF plant in Toulouse [URL1.9].



Figure 1.8 - View of the AZF fertilizer plant structure after the explosion [URL1.10].

Various investigations have been performed in the following years trying to establish the chain of events that caused the explosion [e.g. Barthelemy *et al.*, 2001; Dechi *et al.*, 2004], however the precise technical explanation for this disaster remains unanswered. According to the judicial enquiry, the explosion was caused by a human handling error [Barthelemy *et al.*, 2001]. However, AZF suggests another hypothesis through its own commission of enquiry, claiming that the explosion was caused by an electric arc between two transformers located outside the plant [Dechy *et al.*, 2004]. This accident involved considerable damage to the structure in the industrial complex as shown in Figure 1.8, but also, over surrounding residential areas and affected the electricity distribution system in the region.

The explosion was one of the worst industrial disasters in France, and the third major chemical disaster after the accident in Seveso (Italy, 1976).

The recent events on the 11th December 2005 at Buncefield fuel depository in Hertfordshire (U.K.) were possibly the largest explosion in Europe since the World War II, as reported by the Buncefield Major Incident Investigation Board (BMIIB) [BMIIB, 2006]. The incident caused injuries on 43 people and left a scene of devastation (see Figure 1.9). Both industrial complex and surrounding area were evacuated leaving some 2,000 people displaced [BMIIB, 2008a].

Initial findings of the BMII investigation [BMIIB, 2006] pointed to an instrumentation failure with a leak of aviation fuel spilled into a bund for several hours generating vast quantities of vapour, as high-level gauges failed to detect that the tank was full. A total of 20 tanks and

building structures were involved in the incident. Environmental issues related to the disaster do not appear to have long-term implications with regard to water pollution as the heavily contaminated firewater was contained on site. Even with the intense and dense cloud of smoke observed (see Figure 1.9) that lasted for days, it was classified as irritant, rather than being toxic, based measurements at both air and ground levels [BMIIB, 2008a,b].

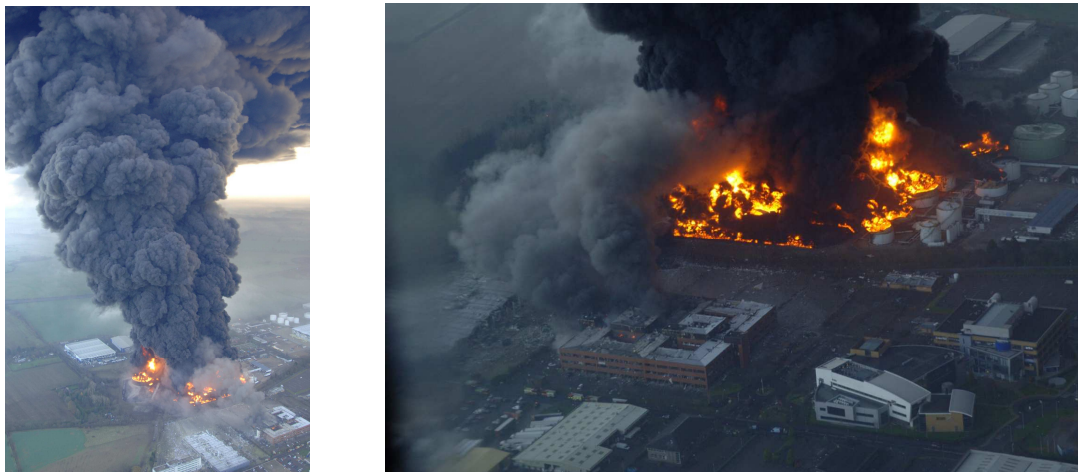


Figure 1.9 – Aerial photographs of Buncefield explosion and resulting fire [URL1.11].

Following the extensive investigation, major changes on land-use planning and control of societal risks around hazards sites measures, as well as, safety and environmental standards for fuel storage sites have been recommended by both BMIIB and the British HSE [BMIIB, 2008c; HSE, 2009].

Notwithstanding the extensively investigated MIA that occurred in industrial sites, the transportation sector has also been target of numerous studies given the severe accidents involving the release of hazmat also reported over the last decades [*e.g.* Vílchez *et al.*, 1995; Oggero *et al.*, 2006; Ellis, 2011; Ronza, 2007]. A recent well-known accident involving transportation of hazmat was the train accident followed by explosions and pool fires that occurred on 29th June 2009 at Viareggio (Italy) railway station. Figure 1.10 shows two aerial photographs taken at Viareggio train station area after the explosion and subsequent fire.

One of the 14 transported tank wagons went off the rails and got damaged causing the release and spread of liquefied pressurized gas (LPG) with subsequent explosion and fire. The LPG gas cloud dispersed radially from the derailed tank mainly across the railway line, due to rather calm weather conditions. A narrow long street parallel to the railway line comprising more than 42 buildings was also affected (see Figure 1.10).



Figure 1.10 - Aerial photographs of Viareggio trains station explosion and resulting fire [URL1.12].

A large number of buildings surrounding the train station were destroyed by explosions or fires. A total of 31 people died and more than 30 people were seriously injured and about 1,100 inhabitants had to evacuate their houses for safety reasons either due to unsafe buildings or to areas exposed to further risks [Manca *et al.*, 2010]. Consequences and fatalities of the accident would have been even worse if the station master had not stopped two passenger trains that were arriving in Viareggio a few minutes later [Dellacasa, 2009]. As far as the transportation of dangerous goods, the Viareggio accident can be considered the worst railway accident that ever happened in Italy [Landucci *et al.*, 2011].

Over the last decades, various theories tried to explain the reason for the continuous occurrence of accidents, regardless the numerous safety measures and large efforts on prevention and control of MIA. Normal accidental theorists, like Perrow [1999], defend that accidents still happen since companies with major accident hazards have increasingly complex technology and tightly coupled processes, which result in situations where accidents just happen because the learning process is handicapped [Lagadec, 1997]. Others, such as Hopkins [2005], claim that this complexity is what makes accidents so predictable. Nevertheless, it is generally recognized that past accidents represent important ‘experimental data’ and are essential sources for updating state-of-the-art requirements in process safety [Uth, 2004]. Valuable lessons and knowledge are continuously gained analyzing past MIA events in finding better ways to manage most frequent causes of failure, safety and emergency response. Thus, accident investigation is an indispensable source for further developments on accident prevention and control measures [Uth, 1999].

1.1.3 Available information of major industrial accidents

Over the last decades, there has been a strong enforcement for industries to report abnormal and MIA events, making more and 'transparent' the information available to public, analysts, regulatory and scientific prone communities. At the same time, industrial activities face more stringent execution by regulatory authorities with respect to *Risk Assessment* (RA) for prevention and reduction of risks and implementation of emergency planning and response strategies.

The increased awareness and impetus prevention and control of MIA resulted in greater transparency and on the development of databases aimed to compile reported MIA events [e.g. Kletz, 1988; Drogaris, 1993; Khan and Abbasi, 1995; Kirchsteiger, 2001; Hadad *et al.*, 2007]. Mainly supported by the interest to investigate past events, but also estimating present and future trends, different databases have been developed by national or international, public or private institutions, focusing on reporting relevant information of current and past industrial accidents and subsequent consequences. In most available databases, information concerning accident type and hazmat involved, main causes and effects, as well as efficiency on emergency response and lessons learned are compiled [Nivoulitanitou *et al.*, 2006]. Table 1.2 summarizes basic and relevant information of some of the best-known and most used MIA reporting databases.

Table 1.2 - Examples of available databases of MIA reports.

Name	Agency	Time covered	# reported accidents	Area covered by data
EM-DAT	CRED	1900 to present	> 19,000	Worldwide
MARS	MAHB	1980 to present	743	EU and OECD countries
FACTS	TNO	Late 1970s to present	24,100	Worldwide
MHIDAS	HSE	1964 to present	11,000	Worldwide
ARIA	MEESDS	1992 to present	37,000	France/Worldwide
ERNS	USEPA	1987 to present	275,000	USA
APELL	UNEP	1970 to present	not available	Worldwide
RISCAD	AIST & JST	1949 – 2006	4796	Japan
RMP	USEPA	1990 to present	> 15,5000	USA
IRIS	NRC	1990 to present	> 605,000	USA
AIS	SAWS	2000 to present	20,000	China

The Centre for Research on the Epidemiology of Disasters (CRED) with the collaboration of WHO created in 1980 the Emergency Events Database (EM-DAT), intended to compile,

validate and analyze information on major natural and technological disasters reported worldwide [URL1.2]. More than 19,000 reported events are compiled since 1900 to present (June, 2011) (see Figure 1.1). The most used and recommended (in European legislation) database EU-wide is the Major Accident Reporting System (MARS) database [URL1.13], created in 1984 to be used within the framework of the SEVESO Directives of the European Commission (EC) and managed by the EU's Major Accident Hazard Bureau (MAHB). Major accidents, near-events (near misses) and other events (incidents), occurred in EU and the Organisation for Economic Co-operation and Development (OECD) countries, are the main types of events reported in MARS database [Rasmussen, 1996]. A total of 743 reported events are currently listed in MARS (until June 2011), referring to 660 major accidents, 8 near misses and 75 other events. Other extensively used European databases are the Dutch Failure and Accidents Technical information System (FACTS) database [URL1.14] from the Netherlands Organization for Applied Scientific Research (TNO), the British HSE Major Hazard Incident Data Service (MHIDAS) database [HSE, 2006] or the French Analyse, Recherche et Information sur les Accidents (ARIA) database [URL1.15] from the French Ministry of Ecology, Energy, Sustainable Development and the Sea (MEESDS).

One of the most used databases in the United States of America (USA) is the Risk Management Plans (RMP) database [URL1.16], developed by the United States of America Environmental Protection Agency (USEPA), comprising more than 15,500 accident events (until June, 2011) in American industrial activities. Other American databases are the United States Incident Reporting Information System (IRIS), [URL1.17] developed by the National Response Centre (NRC) and the Emergency Response Notification System (ERNS) [USEPA, 1989], which results from a cooperative effort among USEPA Headquarters, the Department of Transportation (DOT), National Transportation Systems Center (NTSC), the ten EPA Regions, the United States Coast Guard (USCG), and the National Response Center (NRC). Both IRIS and ERNS databases compile information concerning both major and minor abnormal events at industrial activity involving the release of hazmat.

In the Asian context, both Japan and China also developed industrial accidents reporting databases systems. The Japanese Relational Information System for Chemical Accidents Database (RISCAD) [URL1.18] is maintained by the Japanese National Institute of Advanced Industrial Science and Technology (AIST) and the Japan Science and Technology Agency (JST) and includes data on accidents caused by explosives, high pressure gas, chemical substances and chemical plants [He *et al.*, 2011]. Additionally, the Accident Inquiry System (AIS) database was developed and managed by the Chinese State Administration of Work Safety (SAWS) and

the Ministry of Environmental Protection (MEP). It is one of the official Chinese abnormal events reporting systems for all types of work safety accidents in China [Hou and Zhang, 2009], compiling information regarding around 20,000 reported accidents since July 2000 [He *et al.*, 2011]. Other Chinese industrial accident reporting systems include the Chemical Accident Case database (CAC) of the China Chemical Safety Association (CCSA) affiliated to SAWS and the Daily Accident Information (DAI) of the National Registration Centre for Chemicals (NRCC) affiliated to SAWS [He *et al.*, 2011].

Apart the differences of objectives or coverage (types of events, area and period of time), available databases make possible historical statistical and trend analyses, providing valuable information for the understanding of the various steps that can and/or need to be accounted in environmental and risk/safety assessment studies [Nivolianitou *et al.*, 2006]. As a result, they have also supported, over the last decades, the development of new policy and decision making instruments adopted at national and international levels [Vílchez *et al.*, 1995; Zhang *et al.*, 2008]. Worldwide regulatory, analysts and research prone communities have been investigating the events compiled data in order to identify common trends of accidents precursors (*i.e.* causes of the event), typical casualties, as well as estimated risks and consequences. For instance, CRED continues to update EM-DAT database and examine worldwide major technological disasters trends based on reported data concerning the number of events and people killed and affected, generating information such as presented in Figure 1.1 and Figure 1.11.

Examining Figure 1.11 it is possible to observe a slender increase of the number of reported accidents since the 1930s; with a marked raise between 1970s and 2000s, followed by a strong inversion until 2010. Such variation clearly reflects the intense industrial development occurred during the second half of the 20th century. A noticeable resemblance between the number of reported event and number of people reported killed is visible along the analyzed period. Nevertheless, the estimated total number of reported people affected shows some deviations from overall behaviour, in particular in 1957, or even between 1970 and 1995. The 'isolated peak' of the number of affected people in 1957 results mainly from the accidents occurred at the Mayak Nuclear Power Plant (Russia) and at the Windscale Nuclear Power Plant (U.K.) (listed in Table 1.1) [URL1.2]. Moreover, a marked increase of the total number of people reported affected is observed in 1970s-1980s, mainly due to various MIA, such as the ones happened in Seveso (1976) and Bhopal (1984); and a significant decline observed during the period 1980-1990. This variation reflects the enhancement of safety and control measures in industrial activity. Still, between 1995 and 2009 all three trend lines show a similar tendency

(shape) of augment until the year of 2000, followed by a significant decrease trend. Detailed graphical representations of reported fatalities and affected people by MIA are presented in Figure A.1 (Appendix A).

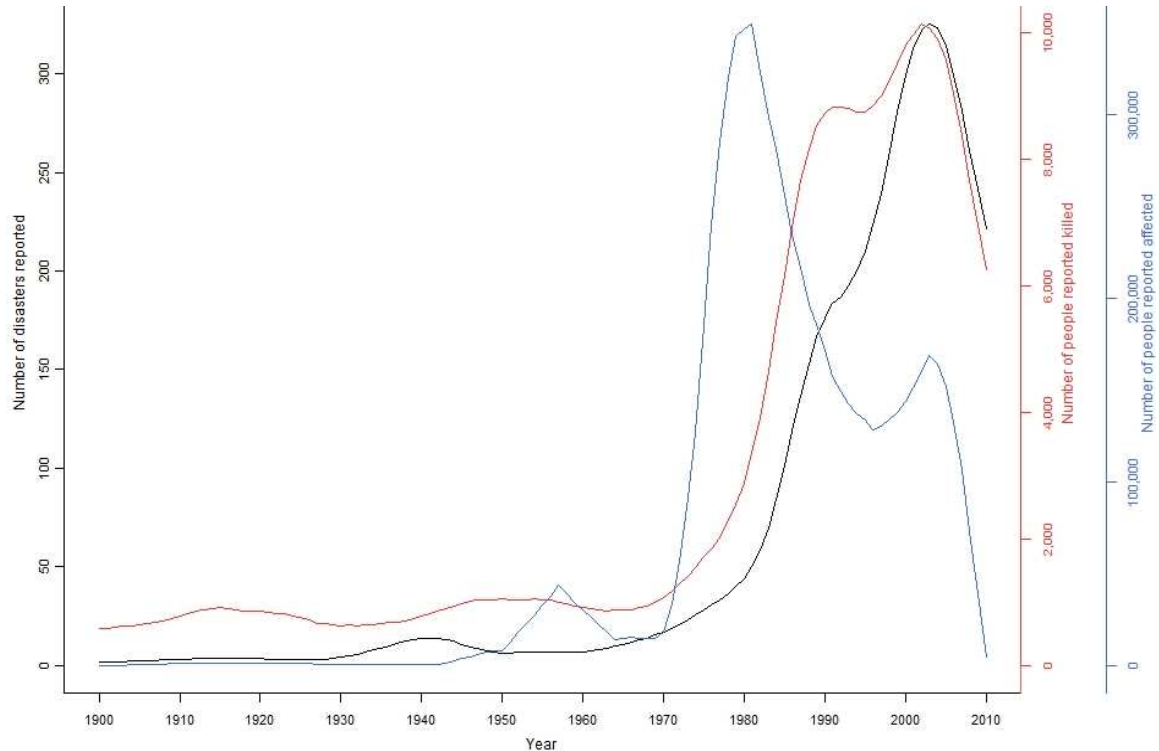


Figure 1.11 – EM-DAT reported technological accidents summary for the period 1900-2010 [URL1.2].

Sonnemans *et al.* [2003] investigated 17 accidents that occurred in the Dutch petrochemical industry sector and demonstrated qualitatively that if accident precursor (failure) information had been recorded, with proper measures to control future occurrences such accidents could have been foreseen and possibly prevented. In another study, Sonnemans and Korvers [2006] observed that even after recognizing accident precursors and disruptions, the operating systems inside companies often fail to prevent accidents. Uth [1996] and Uth and Wiese [2004] evaluated general main features and lessons learnt from the major accident and near miss events in Germany between 1993 and 1996. The results underlined the importance of maintenance, detailed knowledge of chemical properties, human factor issues and the role of safety organization. Elliott *et al.* [2004] analyzed the frequency and severity of accidents reported in the RMP database with respect to socio-economic factors and concluded that larger hazardous chemical companies are located in countries with larger African-American populations and with both higher median incomes and higher levels of income inequality.

Accident trends evaluation studies made by the EEA [2003] showed that between 1971 and 1992 there was, on average, one technological accident every year in Europe with a total

number of 25 or more reported fatalities. Even so, these accidents claimed only a fraction of the lives lost compared to natural hazardous events (approximately 5% of the total in the period 1985–96 in Europe) [EEA, 2003]. More recently, EEA [2010] analyzed and mapped MARS database reported MIA and related impacts (in particular fatalities) during the period 1996-2009. Figure 1.12 shows the reported and analyzed MIAs (light blue) and related fatalities (dark blue) between 1996 and 2009 EU-wide. Given the lack of reported information in 1996 and 1997, MIA fatalities were only analyzed between 1998 and 1997.

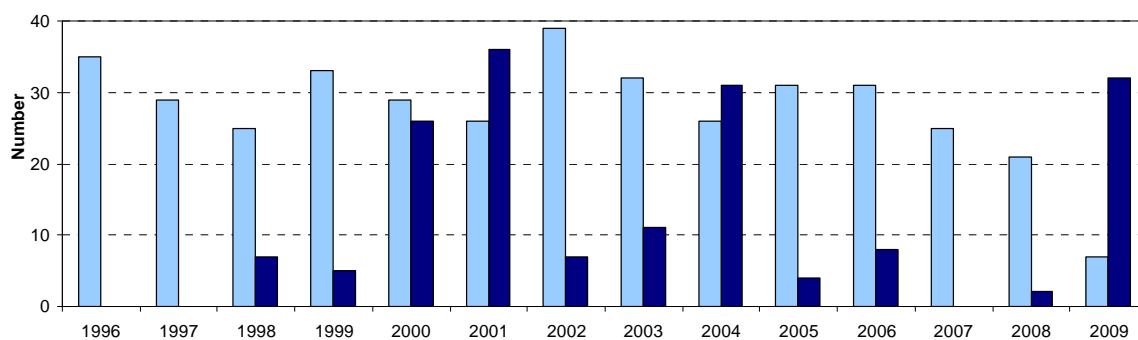


Figure 1.12 – MIA (light blue) between 1996 and 2009 and related fatalities (dark blue) between 1998 and 2009 reported in MARS database [EEA, 2010; URL1.11].

Between 1996 and 2009, a total of 389 events were reported (12 oil spills, 370 major accidents and 7 toxic liquid spills) in the MARS database [URL1.13]. After having increased steadily until 1996 [EEA, 2003] the annual number of industrial accidents has been more or less stable since then (around 28 major accidents per year). Although the number of serious accidents has remained more or less constant, in general they tend to be less severe following the decreasing behaviour of overall technological accidents worldwide previously presented in Figure 1.11. A detailed analysis of reported data based on Figure 1.12 shows that the highest number of events were reported in 2002 (39 events), in contrast with 2009 (7 events). The nature of these incidents varies from major spills, to partial or total destruction of an industrial plant with serious environmental implications and human cost [EEA, 2010]. A continuous decline is observed after 2006 reaching the minimum number reported in 2009. Such behaviour may be the result of the implementation of more recent safety and regulatory requirements in European countries. Nevertheless, the analysis of the total number of MIAs is not straightforward, due to the continuous increasing population of covered establishments, the 2 EU enlargements during this period (2004 and 2007), but also the permanent enforcement and implementation of safety and regulatory requirements EU-wide.

Concerning the total number of reported fatalities caused by MIA (in MARS database) no obvious trend is observed between 1998 and 2009, as well as, there is not a direct correlation

with the total number of MIA. For instance, 2001, 2004 and 2009 show the highest number of reported fatalities, despite the reduced number of reported MIA. Nonetheless, the high number of fatalities in 2001 and 2009 is mostly related to Toulouse (2001) and Viareggio (2009) incidents. In 2002, even with the peak number of reported MIAs (39), the number of fatalities is small. EEA [2010] also verified that, between 2003 and 2009, a total of 27 industrial accidents in Europe with human casualties were reported in MARS database, in addition to 34 accidents that resulted in injuries to people [EEA, 2010]. Most of the victims were workers of chemical plants. In contrast, in the same period there were only 22 incidents with impacts on the environment.

From another perspective, Nivolianitou *et al.* [2006] analyzed the various types of industrial activities involved in MIA reported in MARS during the period between 1985 and 2002. In general the authors concluded that release of hazmat was the most observed type of accident, followed by fires and explosions. Moreover, petrochemical industry was one of the most affected industrial fields, with a percentage of 17% of the total reported events (see Figure 1.13), with the exception of general chemical industrial activities covering around 32%.

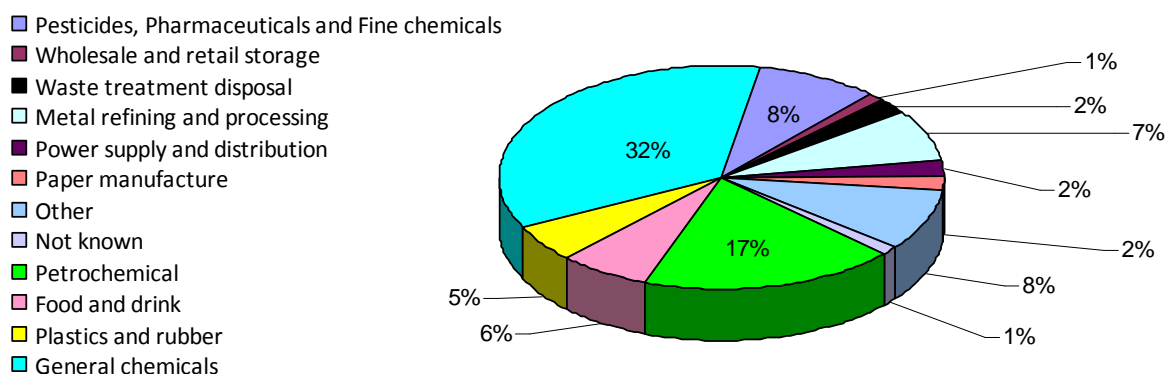


Figure 1.13 - Percentage of MIA reported in MARS database per type of industry in the period 1985-2003 [Nivolianitou *et al.*, 2006].

Nivolianitou *et al.* [2006] also determined that in most cases, Liquefied Pressurized Gas (LPG) and petroleum related substances were the most involved hazmat in reported MIA, followed by Liquefied Natural Gas (LNG), heavy hydrocarbons, hydrogen and ethylene. Moreover, the same authors concluded that the human factor (in 40% of the cases) and the equipment (in 44% of the cases) are the main causes of MIA in the petrochemical industry, similarly to the previous (global) analysis of Rasmussen [1996] (see Figure 1.14). Earlier, Rasmussen [1996] verified that mechanical failures (44%) and operator errors (22%) were the most common immediate causes of the accidents reported in MARS database between 1984 and 1993, as

shown in Figure 1.14. However, in the same study the author stated that the dominant underlying causes identified were poor safety and environmental management.

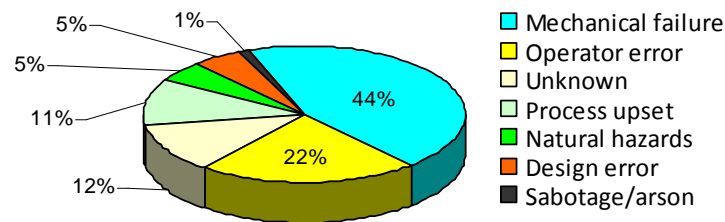


Figure 1.14 - Causes of major accidents in the process industries [Rasmussen, 1996].

The age of process plants is also a relevant factor of risk for the occurrence of major accidents as the probability of 'wear-out' failure increases with age [M&M Protection Consultants 1997]. Other relevant research findings on safety revealed that human factor plays a fundamental role in an organisation's safety performance [Hughes and Kornowa-Weichel, 2004]. Nivolianitou *et al.* [2004] concluded that human factor is considered to contribute by over 80% to accidents occurring due to the high reliability of electronic and mechanical components and the new role of human operators in complex systems. Employees can be considered the last barrier against risks, and their behaviour is critical for avoiding both material and personal losses [Hofmann and Stetzer, 1996]. However, unsafe worker behaviour is frequently the result of latent failures in the organisation and its management system that predispose workers to act unsafely [Sonnemans and Körvers, 2006]. Such 'defects' or unsafe actions include, particularly, the lack of instructions or appropriate training [Attwood *et al.*, 2006], demotivation [Kletz, 1993], lack of work procedures, poor design of tasks, lack of control, low management commitment to safety [Rundmo, 1996], and, in short, inadequate safety measures and management systems [Hofmann, *et al.*, 1995; Kwon, 2006]. More recently, Jacobsson *et al.* [2010] analyzed the main causes of updated MARS reported MIA and concluded that for 67 % of the reported events, the dominant underlying causes were poor safety and environmental management. This means that both mechanical failures and operator errors can likely be due to some kind of management failure, which is thus the underlying cause.

The intense industrial development observed during the last decades also generated a significant increase of transportation flows of hazmat through roads, railways, rivers, seas and pipelines. Unlike fixed plants, hazmat transport is less controllable because it is not set in a 'rigid' location, but in a dynamic scenario influenced by numerous factors. Considering that transportation of hazmat creates numerous opportunities for the occurrence of accidental releases due to traffic accidents, train derailments, shipwreck at sea, equipment failures and

human errors, among other causes, is important also to investigate past accidents in the hazmat transportation sector. A large number of serious transport-related accidents have been reported over the last years, with particular incidence in road (e.g. cistern trucks), railways (train wagons), but also in pipeline systems. Bernatik *et al.* [2008] analyzed historical data concerning hazmat transportation incidents reported in USA by transportation mode during the period of time between 1997 and 2006. Pipelines are generally considered as the safest way to transport hazardous substances [Mitchison, 1999]; yet this mode of transportation has the potential for creating major-accident hazards and reported accidents over the last decades [Kishawy and Gabbar, 2010]. One of the worst accidents occurred in Apawor (Nigeria) in 1998 where a blast from a leaking petrol pipeline killed 701 persons [URL1.10]. Concerning railway transportation modes, in addition to the previously described Viareggio, Italy (2009), another recent reported event with a high number of fatalities is the train accident occurred in Ghislenghien, Belgium, in 2004 [EEA, 2010].

Accidents involving hazmat are also reported in sea ports every year [Ronza, 2007]. According to Darbra and Casal [2004], hazmat gas releases are the most common type of accident in sea ports, followed by fires, explosions and gas clouds, similarly to petrochemical industry trends. In the same study Darbra and Casal [2004] showed that, from a total of 471 accidents inside ports areas, 83% during the last 20 years and 59% in the past decade. An increasing trend regarding the frequency of occurrence in port activity and sea transport of hazmat has been observed over the last decades, as analyzed by Ronza [2007].

With similar importance is the investigation of MIA involving 'domino' effects, *i.e.* accidents where a release of hazmat in a process unit becomes the trigger and will damage one or more other process units, causing a chain of additional accident events [Darbra *et al.*, 2010]. Domino accidents may start from an initial incident, with fires being the most frequent cause in industrial installations, followed by explosions and gas clouds [Darbra *et al.*, 2010]. Several authors have analyzed relevant aspects involved in domino accidents, in particular their frequency, likelihood and consequences [e.g. Bagster and Pitblado, 1991; Khan and Abbasi, 1999a, 2001; Kourniotis *et al.*, 2000; Cozzani and Salzano, 2006; Darbra *et al.*, 2010; Abdolhamidzadeh *et al.*, 2011]. For instance, Kourniotis *et al.* [2000] statistically analyzed a set of chemical accidents showing different characteristic patterns in terms of fatalities caused and domino effects likelihood depending on the type of substances involved. More recently, Darbra *et al.* [2010] and Abdolhamidzadeh *et al.* [2011] analyzed the main features and causes of domino accidents sequences in terms of types of industries and substances of past recent events. The analysis showed that the most frequent causes of domino accidents in

process/storage plants and in the transportation of hazmat are external events and mechanical failure. Storage areas and process establishments are by far the most common settings for domino accidents. Moreover, flammable materials were involved in the majority of accidents involving explosions and fires.

In addition to the statistical investigation of 'typical' historical events, it is vital to examine spatial distribution of such events at regional, national or international level. Among other studies, the EEA [2010] analyzed the spatial distribution of reported technological events, by type occurred during the period between 1998 and 2009. Figure 1.15 shows the spatial distribution and type of accidents reported EU-wide between 1998 and 2009.

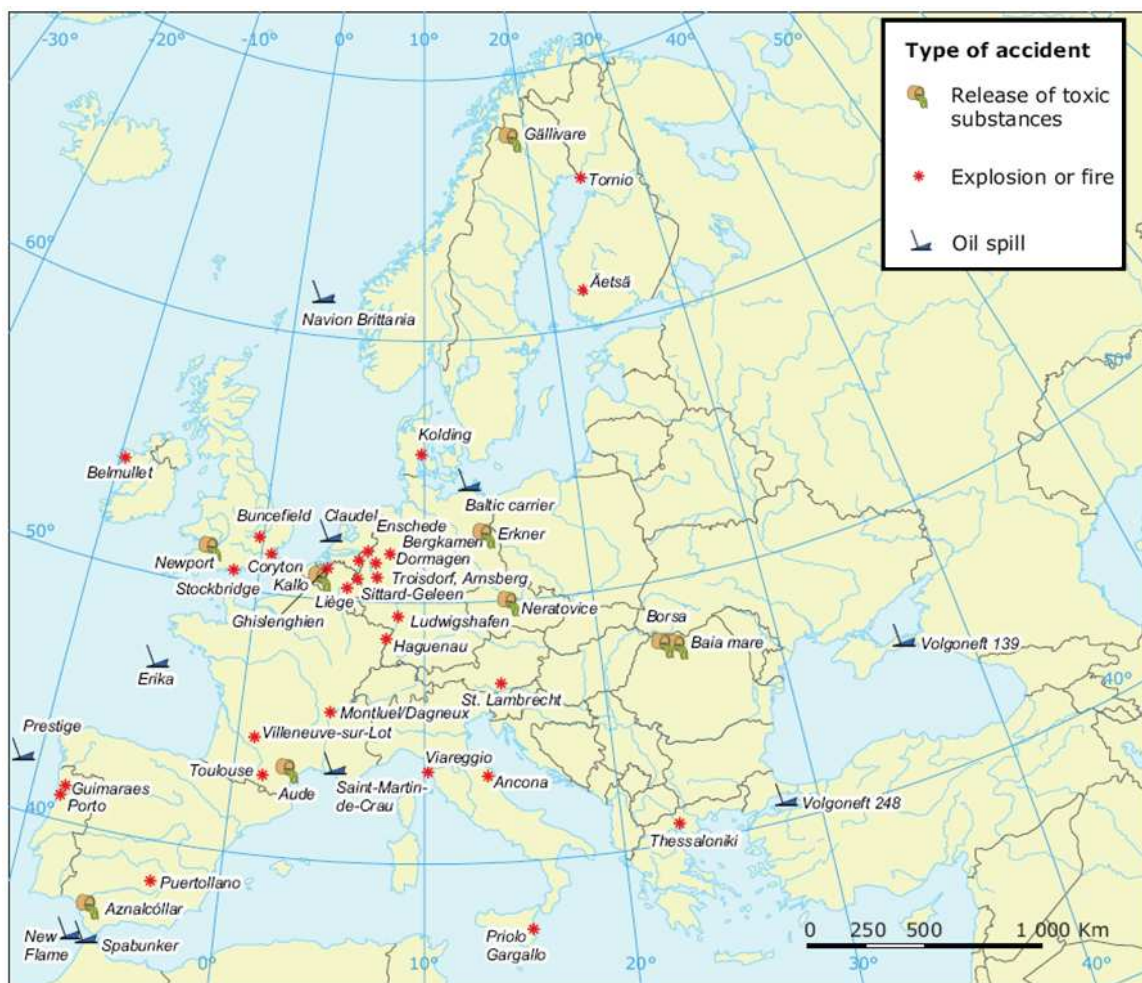


Figure 1.15 -MIA in Europe reported between 1998 and 2009 in MARS database [EEA, 2010].

The distribution of disasters caused by technological accidents is not uniform in the various EU member states. As expected, most of MIAs are concentrated in the countries with the highest number of hazardous industrial activities and it is possible to verify that France and Germany reported by far the highest number of accidents, followed by the U.K. and the

Netherlands [EEA, 2010]. Two major technological accidents were reported in Portugal between 1998 and 2009. On 24th October 1998, a crude oil spill followed by ignition in the beach of Aterro, close to the ocean terminal of the petrochemical refinery at the Port of Leixões (Porto), caused one fatality and several injuries, but also water contamination [URL1.13]. Also, on 13th August 2001, an explosion followed by fire in a firework storage facility located in Guimarães killed 6 persons and injured 1, seriously damaging the industrial infrastructures [EEA, 2010].

MIA events raised public awareness about the potential effects of technology [Willey *et al.*, 2005] and their impacts and consequences on- and off-site human health and environment, highlighting the need to develop regulatory and safety strategies to prevent and control accidents, but also, to reduce their consequences [Cozzani *et al.*, 2006]. This increasing emphasis on industrial activity safety over the last decades also led to the development and implementation of powerful RA procedures [*e.g.* Fang *et al.*, 2004; Reniers *et al.*, 2005] and regulatory instruments, each time more supported by computational tools [Dechy *et al.*, 2009], particularly at European level.

1.2 European regulatory instruments on industrial accidents

Apart from their serious impacts, MIA can also contribute to beneficial transformations on safety and regulatory instruments [Dechy *et al.*, 2009]. Recognising that accidents do happen, regulatory authorities and industrial operators long have assumed that regulations play an important role in controlling risks. Thus, aiming to control and prevent MIA hazards and related consequences, regulatory and guidance documents/instruments have been prepared and adopted over the last decades worldwide. The history of safety and prevention regulation of MIA involving hazmat can be traced back to the beginnings of industrial revolution. One of the first regulatory documents was a French decree published in 1810, focusing activities with major risks, after the occurrence of a major dust explosion in 1795 at Grenelle (France), where around 1,000 people were killed [Vierendeels *et al.*, 2011]. Since then, other European countries prepared and adopted their own MIA regulations and control instruments at national and international levels, most of them regretfully stirred by severe MIA. Nonetheless, main issues on prevention of consequences to human health and environment were integrated in disaggregated and widespread coverage documents, until the beginnings of the 1980s, when a series of Directives (the so-called Seveso Directives) were adopted EU-wide. Since then, this series of Directives became the main European regulatory instruments on prevention of major

accidents involving hazmat and limitation of their consequences for people and the environment.

1.2.1 The 'Seveso Directives Regime'

The severe MIA occurred in Flixborough and Seveso, among others, led to long discussions EU-wide (particularly at EC and European Parliament) and awareness for the need of (inter)national action because of the 'dread, nature and uncontrollability of the hazards' at stake [Arcuri, 2005]. The revision was also motivated because most of the 'best policies', accounting to protection of people and the environment, were in general disaggregated in various Directives and Regulations in different areas of action at both national and EU level. Consequently, since 1982 a set of new regulatory instruments regarding prevention and control of accidents involving hazmat have been adopted and continuously upgraded, in particular the often named '*Seveso Directives Regime*', by virtue of the publication of a series of Directives and related Amendments following the Seveso MIA. Additional international regulatory instruments (Conventions and Regulations) have been adopted to assure a broad protection to human health and the environment from MIA and hazmat handle. Figure 1.16 schematizes the chronological evolution of most important EU regulatory instruments adopted over the last decades in this field and relevant MIA that emphasized the need to revise and adopt or upgrade the contemporary legislation.

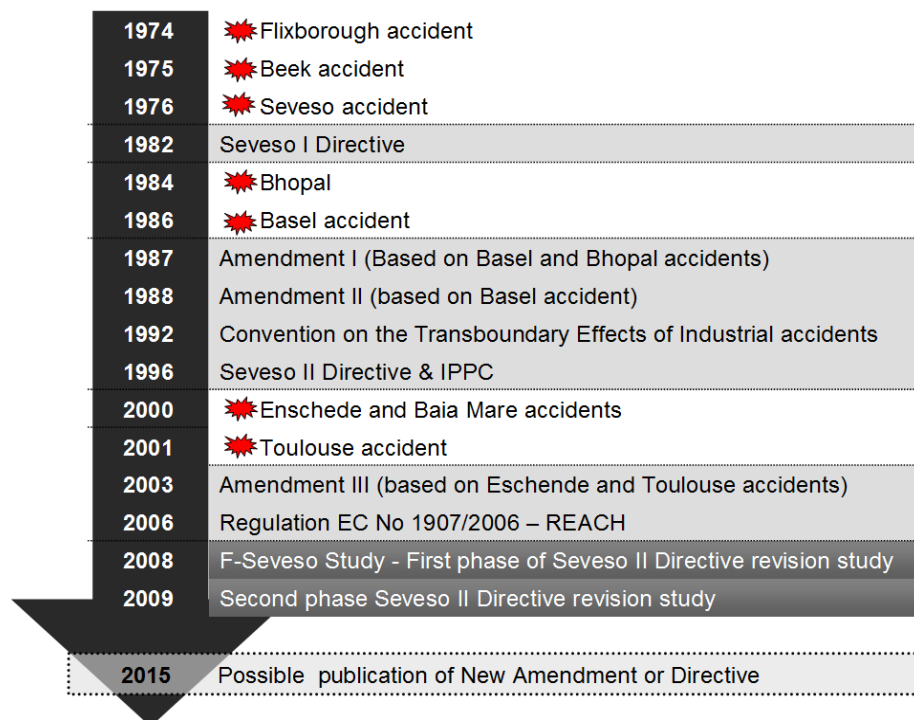


Figure 1.16 – Scheme of chronological evolution of EU regulation and relevant MIA EU-wide.

The first European Directive directly treating MIA involving hazmat was the Directive 82/501/EEC, often called '*Seveso I Directive*', published in 1982. The preparation of this document was a response of the increased awareness of consequences from severe MIA EU-wide (see Figure 1.16 and Table 1.1). The mere fact that the Directive was named after one of them reflects the magnitude of MIA as an influential parameter for changing legislation and regulatory instruments.

The Seveso I Directive was mainly focused on the prevention and control of MIA which might result from certain industrial activities and the limitation of their consequences for man and the environment. The aim was the reduction of the source and incidence of technological risks by analyzing the causes, inspecting the establishments and creating an accident prevention system, assuring internal and external safety to industrial installations. The document also integrated a list of covered particular operators and storage facilities EU-wide supplemented by a list of 180 dangerous substances (Annexes I and II of Directive 82/501/EEC).

A key aspect of this Directive was the mandatory provision, by industrial operators, of information on safety measures and on the correct behaviour to adopt, in case of the occurrence of a MIA. Additionally, transfer of safety and reporting responsibilities to operators, instead of the traditional 'role of authorities' was a relevant initiative. For instance, operators must take all the measures necessary to prevent MIA, to limit their consequences for persons and the environment and report, in a transparent way, relevant information on industrial activity and eventual 'abnormal events'. Even with the large coverage range, Wettig and Porter [1999] argued that this Directive's main scope was more focused on the protection of persons than on the protection of the environment.

In the light of the MIA occurred in Bhopal (1984) and Basel (1986), the original Directive was amended twice by the Directive 87/216/EEC in 1987, and by the Directive 88/610/EEC in 1988. Both amendments extended the range of covered installations (including storage of hazmat) and substances, to broadening the scope of the Directive. Also the improvement of public information requirements and reporting systems and safety instruments aiming to increase transparency of safety measures were focused in the amendments.

Driven by major revisions performed following the resolutions of the fourth (1987) and fifth (1993) European Action Programmes on the Environment, further refinement of the original Directive was deemed necessary to expand the area of application and to enhance setting up

improved safety management systems within industrial activities [Wettig *et al.*, 1999]. The revision of the original Directive showed that major modifications should be made and an entirely new Directive adopted instead of preparing a third hypothetical amendment [Wettig and Porter, 1999]. The explanatory memorandum of the EC COM(94)4 also mentioned that an analysis of the 130 major accidents reported between 1982 and 1994 showed that about 95 % could have been prevented by the application of existing knowledge and proper management and operational procedures [Walker, 1995]. Furthermore, changes in the EU system of classification of dangerous substances to which the Directive refers, among other issues and limitation/gaps, emphasized the need for the adoption of an entirely new Directive in 1996 – Directive 96/82/EC also called '*Seveso II Directive*'. This Directive was adopted by the Council of the European Union on 9 December 1996 and the Member States had until February 1999 to turn the obligations of the Directive mandatory for industry and public authorities responsible for its implementation and enforcement.

The main scope of Seveso II Directive has been broadened and simplified at the same time, covering both, industrial 'activities' and storage of hazmat. Instead of the previous 'static list of operators, depending on the level of potential hazards (quantities of hazardous substances) a '*two-tier establishments regime*' (i.e. a two levels of risk coverage regime of industrial establishments – upper- and lower-tier establishments) is defined. It also covers establishments, defined as 'the whole area under the control of an operator where hazmat are present in one or more installations, including common or related infrastructures or activities', without the need to define the term industrial activity. At the same time, the list of hazardous substances was also reduced to around 50 substances, referring additional related Regulations. New duties for both industry and administrative bodies/authorities comprise the preparation of internal and external emergency plans and the evaluation of possible accident effects including potential domino effects among other requirements. In addition, the implementation of a Safety Management System (SMS) is also mandatory, to assure the use of suitable measures to control the foreseeable hazards, and these are properly managed and continuously upgraded so as to be effective at all times. The most practical outcome of SMS outputs is the explanation of accidental scenarios (covering both most plausible and worst-case) and prevention/control measures taken by industry and authorities.

A new series of MIA (Baia Mare, Enschede and Toulouse) allied with studies on carcinogens and substances dangerous for the environment and with changes in the EU system of classification of hazmat to which the Directive refers highlighted the need to review the Seveso II Directive. Hence, this Directive was amended in 2003 by the Directive 2003/105/EC.

Risks arising from storage and processing activities in mining, from pyrotechnic and explosive substances and from the storage of fertilizers are now included. Other minor changes taking into account the changes of the hazmat classification and the introduction of new technologies and industrial activities were also performed.

Due to modifications of the EU system of classification of dangerous substances to which the Directive refers (see subsection 1.2.3), a 'two phases' review study of currently implemented Seveso II Directive started in 2008 by EC [URL1.19]. The main objective of this study is to assess its effectiveness and identify possible improvements [COM(2010)781-SEC(2010)1590]. The study was also extended to a wider revision of the Directive because its basic structure and main requirements have remained essentially unchanged since its adoption. The first phase of the review ('Study of the Effectiveness of the Seveso II Directive'), conducted in 2008 and known as the 'F-Seveso' study showed that no real need for significant legislative change is required, despite some identified inconsistent implementations of the Directive at national and regional EU-level [COM(2010)781-SEC(2010)1590]. The second phase of the study started in 2009 and was launched to examine the effectiveness of the main requirements imposed on public authorities. Among others, the main conclusions emerging from the second study are: no fundamental changes to the Directive are necessary; the existing approach should be maintained; but, there is a need to clarify/update some provisions. Additionally, improvements can be made to the implementation and enforceability of the Directive, but any changes should avoid adding administrative burdens. Overall, the revision study of the Directive showed the need of minor changes and on 21 December 2010 the EC adopted a proposal for a new (Amendment) Directive that would repeal and replace the current Directive, by the 1st June 2015 [URL1.19].

1.2.2 Seveso establishments EU-wide

Within the context of Seveso II Directive around 10,000 establishments (upper- and lower tier establishments) are currently covered EU-wide, heterogeneously distributed by member states (see Figure 1.17 and Table A.1 in Appendix A). These establishments include a diverse number of industrial sectors EU-wide that store, process or handle hazmat, mainly in the chemicals, petrochemicals, storage, and metal refining sectors [COM(2010)781-SEC(2010)1591] as listed in Table A.2 (Appendix A). Overall, the number of lower tier is in general higher than upper-tier establishments, excepting for Austria, Czech Republic, Cyprus, Germany, Malta, Netherlands, Slovakia and Sweden as graphically presented in Figure 1.17. As expected, the most heavily industrialized countries in Europe (Germany, UK, Italy, France and Spain) have

more than 500 sites, corresponding to about 63 % of the total number. Despite the number of lower-tier establishments, special attention is usually taken to upper-tier establishments given their enhanced hazards and risk to neighbouring and progressively denser urban/populated areas.

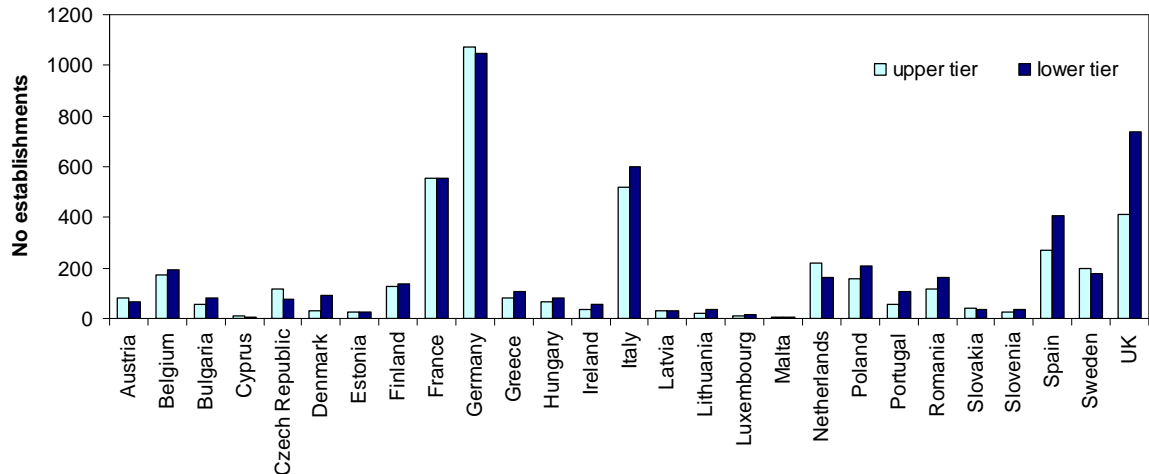


Figure 1.17 - Seveso establishments by EU member state and tier class in 2009 [COM(2010)781-SEC(2010)1591].

For instance, EEA [2010] analysed the distribution of upper-tier establishments per country in the last years, which is presented in Figure 1.18.

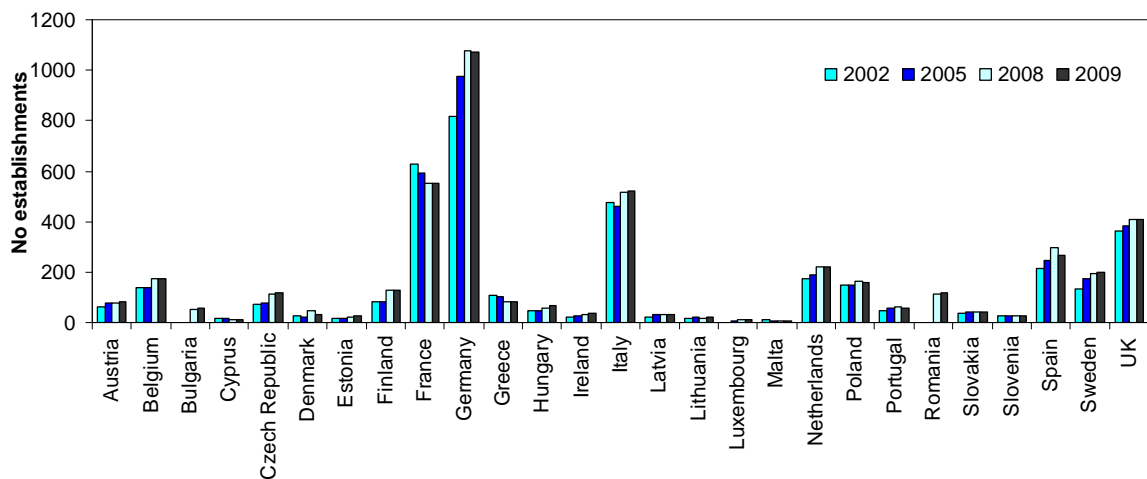


Figure 1.18 - Upper-tier establishments per EU member state: 2002, 2005 and 2009 [2009 [COM(2010)781-SEC(2010)1591].

Figure 1.18 reveals the 'irregular' trends of the number of Seveso establishments. While in some countries the total number of upper-tier sites increases mainly between 2002 and 2008 (Belgium or Germany), others decrease regularly (Cyprus, France and Greece). As regards to

Portuguese Seveso establishments (mostly chemical facilities), despite the clear increase between 2002 and 2008, a slight decrease between 2008 and 2009 is observed.

Given the number of upper-tier and 'constant threat/risk' of occurrence of MIA allied with the visible expansion of urban/populated areas gradually closer to industrial establishments, it is important to develop and implement regulatory and safety instruments, as well as, risks and consequences evaluation methodologies supported by computational modelling instruments.

1.2.3 Other relevant European regulatory instruments

In addition to Seveso Directives, broader European Regulations for the protection of human health and the environment have also been implemented EU-wide, such as the Commission's Directive 96/61/EC on Integrated Pollution Prevention and Control (IPPC) Directive or the Regulation (EC) No 1907/2006 also called REACH (Registration, Authorisation and Restriction of Chemicals) Directive (2006) and the Regulation (EC) No 1272/2008 (2008). In spite of their specific objectives, these documents 'help' achieving the objectives of Seveso Directives by promoting integrated approaches that contribute to a greening of industrial establishments so that the impact of any accident would be minimized.

The IPPC Directive was adopted in 1996 and can be considered one of the most important initiatives aiming the 'protection of the environment as a whole', based on a common rules permitting system to control the environmental impacts (regular emissions into air, water, and land, use of raw materials, energy efficiency, and generation of waste) of certain industrial and agricultural activities [Emmott and Haigh, 1996]. Permits must contain emission limit values based on 'Best Available Techniques' (BATs), referring to technologies and ways in which an installation is designed, built, maintained and operated that are most advanced and effective in preventing or reducing emissions, taking into account economical and technical viability and their costs and advantages. It covers mostly large industrial installations, since for the majority of sectors there are already established production capacity thresholds, excluding the smallest installations [Emmott, 1999]. This Directive has a number of interactions with institutions and other Directives covering different fields, including the Seveso II Directive.

Recently (2007) the EC adopted the Proposal COM(2007)844-2007/0286(COD) for a new Directive on industrial emissions. The proposal recasts existing Directives related to industrial emissions into a single clear and coherent legislative instrument, in particular the IPPC Directive. As a result, the IPPC Directive has been codified in the Directive 2008/1/EC concerning integrated pollution prevention and control. The codified act included all the

previous amendments to the IPPC Directive and introduced some linguistic changes and adaptations. Currently, around 52,000 industrial installations are covered by IPPC Directive EU-wide (significantly higher than the currently covered 10,000 'Seveso establishments').

In regards to harmonized systems of classification, control, labelling and cataloguing guides of hazmat to which Seveso II Directive refers, the most important documents are the Regulation (EC) No 1907/2006 often called REACH and the Regulation (EC) No 1272/2008 also called Regulation for 'Classification, Labelling and Packaging' (CLP).

REACH is the EC Regulation on chemicals and their safe use and was adopted in 2006 entering into force one year later. It deals with the registration, evaluation, authorisation and restriction of chemical substances. The main goal of this Regulation is to improve the protection of human health and the environment through a better and earlier identification of the intrinsic properties of chemical substances. At the same time, it intends improving innovation and competitiveness of EU chemicals industry. REACH also calls for the progressive substitution of the most dangerous chemicals when suitable alternatives have been identified. The Regulation places greater responsibility on industry to manage the risks from chemicals and to provide safety information on the substances. Operators are required to gather information on the properties of their chemical substances, which will allow their safe handling, and to register the information in a central database run by the European Chemicals Agency (ECHA). This Agency acts as the central point in the REACH system: it manages the databases necessary to operate the system, co-ordinates the in-depth evaluation of suspicious chemicals and is building up a public database in which consumers and professionals can find hazard information.

The CLP Regulation incorporates the chemical substances and mixtures classification criteria and labelling and packaging rules agreed at UN level by the so-called Globally Harmonised System of Classification and Labelling of Chemicals (GHS). This Regulation intends protecting workers, consumers and the environment by means of labelling what reflects possible hazardous effects of a particular chemical. It is expected to facilitate global trade and the harmonised communication of hazard information of chemicals, but also, to promote regulatory efficiency. It complements REACH, replacing previous Directive 67/548/EEC and Directive 1999/45/EC. New classification criteria, hazard symbols (pictograms) and labelling phrases are introduced considering the current EU legislation.

Recognized the importance and urgency of preventing serious adverse effects of MIA on human health and the environment also at a broader transboundary (international level), and

of promoting all measures to stimulate the rational, economic and efficient use of preventive, preparedness and response measures, the Convention on the Transboundary Effects of Industrial Accidents was prepared in 1992. It was elaborated under the auspices of the United Nations/Economic Commission for Europe (UN/ECE) and signed in Helsinki in 1992, entering into force in 2000 in most countries. The main objective of the Convention is to enhance individual and collective national responsibility and capacity in the prevention and control of industrial accidents capable of causing transboundary effects, with a view to protecting human life and environmental safety [UN/ECE, 1992]. It also provides measures to prevent industrial accidents, preparedness for and response to accidents that can lead to transboundary effects, including the impact of accidents caused by natural disasters; promoting an international cooperation on mutual assistance, research and development, exchange of information and technology to prevent industrial accidents.

Considering the continuous occurrence of MIA, adopted control and prevention regulatory instruments and the number of 'hazardous' establishments (gradually closer to urban/populated areas), it is essential the development and implementation of risk and consequences evaluation methodologies supported by computational modelling tools.

1.3 Research objectives and structure of the thesis

This introductory chapter has shown that, even not an everyday phenomenon, technological accidents involving the release of hazmat gases are continuously reported worldwide with significant impacts on human health and environment. This has led to an increased public, regulatory/safety and scientific awareness of the consequences from exposure to hazmat released into the atmosphere and a renewed interest in assessing risks from technological accidents occurring in industrial and built-up urban environments. As a result, with the aim of supporting regulatory instruments and risk analysis, particularly consequence analysis methodologies, several numerical models have been developed and implemented over the last decades for the prediction of hazard areas affected by accidental releases of toxic gases.

Moreover, modelling accidental release is nowadays required in the frame of quantitative risk analysis and European regulatory instruments (*e.g.* EU Seveso Directives), for a variety of reasons: analyzing different accident scenarios, preparing emergency response plans and optimal countermeasures, but also real-time consequence analysis and emergency response. Depending on the demand and main purposes of application, the choice of appropriate modelling tools is up to the authorities, industrialists and analysts. Even with the number of

available consequence analysis modelling tools/software packages, most comprise either simple modelling approaches that can not properly represent the actually occurring real conditions in industrial and built-up areas, or complex modelling system that turn the tool powerless to provide fast response information, especially in case of emergency response to industrial accidents. Thus, a major challenge in applied environmental sciences is the development of fast run local-scale modelling tools able to be used in consequence analysis for tracking and predicting short-term pollution episodes and effects from exposure to hazmat gas released in industrial and neighbouring built-up environments. Endorsed by the continuous improvements on computational hardware capacity, the development of new numerical tools incorporating state-of-the art modelling techniques is of great importance for assessing technological risks and for consequence analysis in industrial and urban areas.

In this sense, the present thesis intends to contribute to consequence analysis modelling of hazmat risks on humans in industrial and built-up areas. The main goals are:

- (i) The development of the Effects of Released Hazardous gAses (EFRHA) model, an integrated consequence analysis computational modelling tool designed to simulate short-term pollution episodes in case of hazmat gas accidental release into the atmosphere;
- (ii) The evaluation of the EFRHA model suitability to predict concentration fields of hazmat gases (heavy and passive) based on the its application to specific and typifying test case scenarios and modelling conditions; and
- (iii) The application of the developed model to a demonstrative case study in the scope of consequence analysis.

The EFRHA model is designed to be used in consequence analysis studies, enabling the estimation of potential consequences to human health in case of accidental release of hazmat gases in industrial and built-up environments, determined in the form of concentration fields as a function of time.

The thesis is organized in six main chapters addressing the theoretical and scientific background, development and validation, and finally, application of the developed model and main findings.

Chapter 2 contains the scientific background of quantitative risk analysis, focusing on consequence analysis of industrial hazmat gas releases and applied modelling techniques. Main features of hazmat gas accidental release and dispersion modelling are presented and interpreted in the light of current understanding of hazmat dense and passive gas release and

dispersion phenomena. An overview of consequence analysis physical and numerical modelling is provided, highlighting the well-known work carried out over the last years to numerically describe hazmat gases accidental release and atmospheric dispersion.

Chapter 3 describes the core structure and mathematical formulation of the developed model. The different modules that compose this numerical tool and implemented modelling approaches are explained. Hazmat outflow rate (source term) and dispersion simulation are key modules for the output concentration field required for the estimation of consequences from the exposure to hazmat gas. The model main input and output data are also discussed.

In chapter 4, the EFRHA model is validated and results interpreted. This evaluation process is composed by a set of four independent stages. The first two stages consisted on the preliminary individual assessment of EFRHA Meteorology and Source Term Modules consistency. The third stage comprised the validation of EFRHA reliability to predict hazmat gas dispersion in obstructed areas. Finally, in the last stage EFRHA aptness to simulate heavy hazmat gas accidental release and dispersion scenarios is assessed in its entire scope.

Chapter 5 presents a demonstrative application of the EFRHA model to a case study illustrating its reasonability to estimate potential consequences to humans from hazmat gas accident scenarios in industrial and built-up areas. The definition of hypothetical accident scenarios, as realistic as possible, based on industrial activity and neighbouring built-up structure allows discussing the applicability and model's main outputs quality, as well as, the influence of input data for real case accident scenarios.

Finally, main conclusions and outcomes of the present work are addressed in Chapter 6.

CHAPTER 2

2. QUANTITATIVE RISK AND CONSEQUENCE ANALYSIS: SCIENTIFIC BACKGROUND

This chapter presents the scientific background of the thesis main subject: *Quantitative Risk Analysis* (QRA) and *Consequence Analysis* (CA) modelling of MIA involving hazmat gas release into the atmosphere. Up-to-date QRA and CA theoretical and modelling approaches are described. Physical and numerical modelling techniques for the description of hazmat gas accidental release and atmospheric dispersion main features are addressed, without forgetting examples of relevant work conducted over the last years. Finally, main advantages and limitations of available CA numerical modelling techniques and tools are discussed emphasizing the selections and approaches considered in the present work.

2.1 Quantitative risk analysis of industrial accidents

Fear of technological hazards has been present worldwide since the industrial revolution and 'responses' seem to oscillate along the spectrum of prohibition, prevention, precaution, foresight and 'blind euphoria' followed by a belief in scientific and technological progress from the second half of the 20th century onward. This change, deeply influenced by the sequence of serious MIAs, introduced major changes on the perception of risks; and therefore, new methods and tools (technical and regulatory instruments) have been developed to assess risks of MIA [Tixier *et al.*, 2002].

As a result, QRA methodologies 'emerged' worldwide since the mid-1970s with ever-increasing importance becoming the 'scientific pillar' of regulatory, control and prevention instruments, as an important and practical tool of *Risk Assessment* (RA) studies to map and quantify specific risks identified in hazardous industrial and transportation activities [Kolluru, *et al.*, 1996; Vose, 2008]. However, given the ambiguity associated to hazard and risk concepts, both RA and QRA definitions and methodologies/techniques are also commonly influenced by some misunderstanding and controversy [Kirchsteiger, 2002].

In 'professional and engineering sciences' context, QRA can be defined as the methodology or process intended for identifying and assessing the impact, frequency of occurrence and magnitude of consequences and effects of the human activities on systems with hazardous characteristics, *i.e.* the various types of risks associated to a given industrial installation [Lees,

1996; ICE/ISO, 2009]. Its methodologies are based on engineering evaluation and mathematical techniques, combining estimates of incident consequences and frequencies (probability of likelihood) to make decisions, either through a relative ranking of risk reduction strategies or through comparison with risk targets [CCPS, 2000; Ale, 2009]. When applied to 'hazardous industries' (e.g. Seveso establishments), QRA is intended to evaluate and estimate the risks of a system or its elements and provide authorities with relevant information [Pietersen and van het Veld, 1992].

Nowadays, the diversity in QRA methodologies and techniques is such that there are many appropriate techniques for any circumstance and the choice has become more a matter of taste [Reniers *et al.*, 2005; Marhaviilas *et al.*, 2011] Notwithstanding the wide variety of methodologies developed over the last decades, 'full QRA methods' comprise five main steps [Vose, 2008], namely: 1 - scope and objectives definition; 2 - hazards identification and accident scenarios definition; 3 - frequency and probability estimation; 4 - effects and consequences estimation; and finally, 5 - risks estimation. Figure 2.1 schematizes the five main steps of 'full QRA methods'.

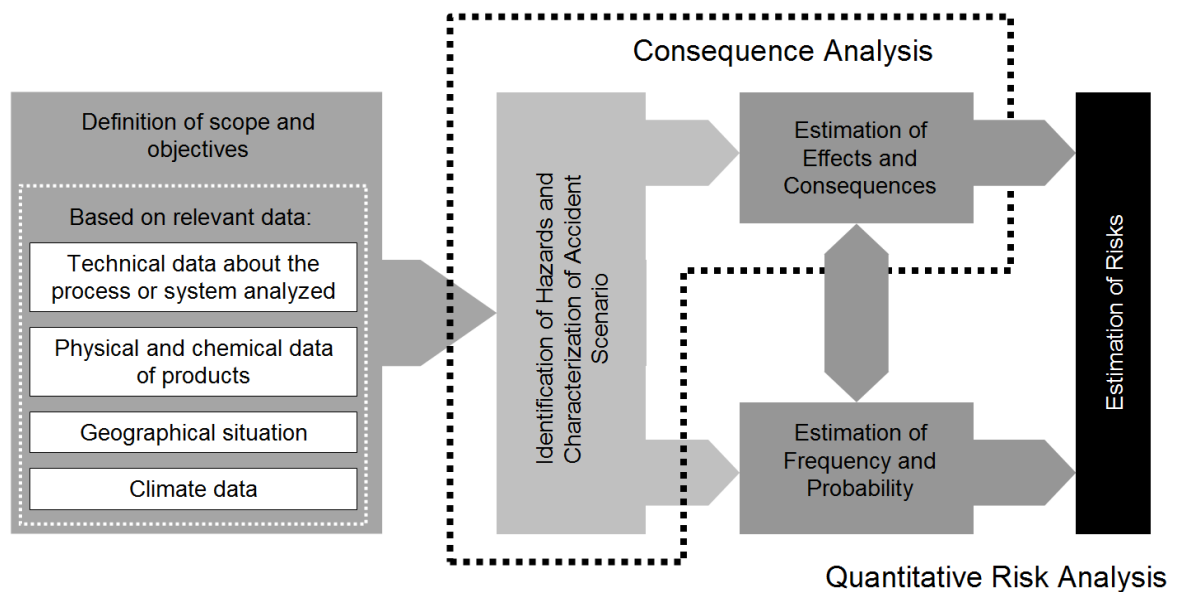


Figure 2.1 - Scheme of quantitative risk analysis methodology [based on Mannan, 2005].

The first step consists of defining the main scope and objectives of the QRA study. Relevant information is collected for an accurate/appropriated characterization of the studied system (e.g. hazmat properties, geographical, meteorological and site-specific data). A balance is established between the intended scope and objectives with available data and expected results (quantified risks). Next (step 2) hazards and related accident scenarios are identified based on compiled information. Most frequent or plausible and worst-case scenarios can be

defined, according to the characteristics of the studied system and main purposes of the QRA. Both steps 1 and 2 are essential for establishing the basis of the QRA study [Tixier *et al.*, 2002].

A pure probabilistic approach is considered for the estimation of the frequency and probability (likelihood) of occurrence of the identified hazards in step 3, through the application of vulnerability and probability models or simply statistical data [Ale, 2009]. Despite its relevance to assure a precise and complete QRA study, this step is applied if the minimum required information for the estimation of probability and frequency is available. In step 4, the magnitude of consequences and effects from the target hazards of accident scenarios are quantified through the application of deterministic approach mathematical techniques [Mannan, 2005], in accordance with previous steps information. Finally, risks (usually refereeing to individual, social or environmental risks) are estimated in step 5, as a function of frequency/probability (step 3) and the magnitude of consequences (step 4).

QRA main outcomes can be directly analyzed or used in the context of RA studies, to evaluate the current situation and introduce (if necessary) relevant modifications or corrective actions/measures on the most severe risks identified [see Vose, 2008; Ale, 2009].

Albeit the variety of suggested QRA methodologies and related approaches or techniques, Kirchsteiger [1999] argued that a valid estimation of risk does not necessarily entails all five main steps. Hence, depending on the degree of accuracy and available input data, QRA studies can consist on combinations of steps, namely: (i) steps 1 and 2; (ii) steps 1 to 4; (iii) steps 1, 2 and 4; or (iv) steps 1 to 5 ('full QRA study'). Whatever approaches and techniques are used, three main elements are always present: (a) the expected output data; (b) the available input data; and (c) the selected method. Indeed, analysts usually predefine the expected outputs according to the identified hazards; next they collect information related to the target system and main purpose of the QRA study, and finally choose the most appropriated approaches and techniques. Furthermore, as highlighted in Figure 2.1, CA methodologies overlap QRA steps 2 (identification of hazards and accident scenarios) and 4 (estimation of consequences).

In general, it is possible to identify two 'distinct' approaches as the main basis of QRA methodologies: probabilistic and deterministic [Mannan, 2005; Ale, 2009]. These can be implemented individually or combined in QRA studies, depending on the main purpose, available information and the degree of complexity [Vose, 2008]. Table 2.1 summarizes some of the most known and extensively used QRA techniques, as a function of the considered

approach methodology, based on Tixier *et al.*, [2002], Casal [2008] and Marhavidas *et al.* [2011] reviews.

Table 2.1 - Examples of QRA techniques as a function of the approach methodology [based on Tixier *et al.*, 2002; Casal, 2008].

Approach	Qualitative techniques	Quantitative techniques
PRA	<ul style="list-style-type: none"> - Accident Sequences Precursor (ASP) [Holmberg, 1996]; - Delphi Technique [Rogers, 2000]; - Earthquake safety of structures and installations in chemical industries [Jezler, 1998] 	<ul style="list-style-type: none"> - Defi method [Rogers, 2000]; - Event Tree Analysis (ETA) [Gadd <i>et al.</i>, 1998; Nicolet-Monnier, 1996]; - Fault Tree Analysis (FTA) [Casal, 2008]
DTA	<ul style="list-style-type: none"> - What if? Analysis [Rogers, 2000]; - Task Analysis (TA) [Rogers, 2000]; - Hazard and Operability (HAZOP) [Kennedy and Kirwan, 1998]. 	<ul style="list-style-type: none"> - Methodology of domino effects analysis [Dolladille, 1999]; - Methods of potential risk determination and evaluation [Jager and Kuhnreich, 1998]; - SAATY methodology [Troutt and Elsaid, 1996]
PRA & DTA	<ul style="list-style-type: none"> - Maximum Credible Accident Analysis (MCAA) [Khan and Abbasi, 1998]; - Reliability Block Diagram (RBD) [Rogers, 2000]; - Safety Culture Hazard and Operability (SCHAZOP) [Kennedy and Kirwan, 1998]. 	<ul style="list-style-type: none"> - Quantitative Risk Assessment QRA [Ale, 2009]; - Facility Risk Review [Schlechter, 1996]; - Probabilistic Safety Analysis PSA [Papazoglou <i>et al.</i>, 1992]; - Rapid Ranking RR [Larson and Kusiak, 1996].

The *Probabilistic Risk Analysis* approach (PRA) is a systematic and logical method aimed at identifying and assessing risks to people and the environment based on the analysis of probability or frequency of hazardous events or on the occurrence of potential accidents [Kirchsteiger, 1999], This approach is commonly applied for safety-related hazards in complex technological systems, often supported by the use of past accidents databases and probabilistic uncertainty methods [*e.g.* Stamatelatos *et al.*, 2002; Muhlbauer, 2004; Baklanov and Mahura, 2004].

On the other hand, the *Deterministic Risk Analysis* approach, also called *Deterministic Test Case* approach (DTA) was developed to estimate immediate and conditional short-term potential for consequences and damages of the identified accident scenario hazards through the definition of plausible (maximum credible) and/or worst-case scenarios [Sorensen *et al.*, 2010; Díaz-Ovalle *et al.*, 2010]. DTA can be considered the most straightforward approach taking into account hazmat properties, equipment and quantification of the consequences on people, the environment or equipment structures. Moreover, worst- and most credible/plausible case scenarios can be analysed without the need to estimate the probability of occurrence [Ale, 2009; Tavares, *et al.*, 2010].

Although PRA and DTA main principles and techniques are distinct, QRA methodologies can comprise combinations of techniques from both approaches [see Vose, 2008; Marhavillas *et al.*, 2011]). This integration enables conducting a more accurate and realistic estimation of resulting risks. On the risk estimation frontier, Kirchsteiger [1999] discussed the strengths and weaknesses of various PRA and DTA approaches and techniques using past-events examples from nuclear and chemical activities. The author argues that PRA approaches are more complex and cost-effective encompassing data usually not readily available to satisfy the needs for its application, still, results that can be easier to communicate to decision and policy makers are obtained. Nonetheless, it is also stressed the relevance of DTA approaches for fewer complex and more rapid analysis (*e.g.* prediction of consequences and fast information transfer to emergency first responders). Legget [2004], supported by the *Wald's maximin paradigm*² [Wald, 1945], considers that a better assessment for chemical facilities safety should be based on a DTA approach. This approach enables the use of the wisdom of hindsight (experiences of past accidents) and up-to-date knowledge (to evaluate its impact) in forecasting accident situations. DTA approach can also be considered a relevant reference point and link between the past, present, and future accident scenarios investigated with QRA methodologies [Khan and Abbasi, 1995]. Moreover, based on the analysis of 62 suggested QRA techniques, Tixier *et al.* [2002] concluded that the majority is deterministic because historically, operators and public organisations have initially tried to quantify damages and consequences of potential accidents before to understand why and how they could occur, *i.e.* the frequency and probability of occurrence. Regardless of related advantages and shortcomings, neither one of them (separately) is sufficient for a 'full QRA study'.

Independently of the applied approach, qualitative and quantitative techniques (see Table 2.1), with varying complexity, have also been developed and integrated in QRA methodologies, to estimate the magnitude of risks of examined accident scenarios [Marhavillas *et al.*, 2011].

Qualitative techniques are mainly based on the definition and use of subjective criteria to establish a scale of evaluation parameter categories; focusing on compilation and analysis of relevant data, identification of hazards and risks, selection of accident scenarios and classification of potential consequences [Andrews and Moss 1993]. Typically, they include the simplest and subjective procedures based on past field and technical experience [Mannan,

²*Wald's maximum model of uncertainty* was proposed by Wald [1945]. It is a non-probabilistic decision-making approach ranked on the basis of worst-case outcomes. It is frequently used for the definition of worst-case scenarios in Risk Assessment studies.

2005]. These techniques are widely appreciated by stakeholders and regulation prone communities, because they are generally easy to perform, following previous applications or examples, especially where possible deficiencies are highlighted. However, the lack of reproducibility, less accuracy, dependency on previous experience and used terminology can be a barrier to communication (*e.g.* probable, unlikely or extremely unlikely) and turns this techniques more vulnerable to criticism than quantitative methods.

On the other hand, quantitative techniques are used to quantify risks as a function of frequencies and consequences. These techniques comprise different models including vulnerability models, consequence models, and effects models [Casal, 2008]. Regularly a full QRA study requires the use of the various quantitative technique models along the various steps. Despite the notable accuracy and reliability to quantify risks and related frequencies of occurrence and consequences, the characteristics of the various types and natures of models makes these techniques substantially more complex than 'simple' qualitative techniques, due to the level of expertise/experience and amount of information required. It is possible to mention that both QRA and CA methodologies can comprise qualitative and quantitative techniques, independently of the applied approach (DTA, PRA or a combination of both) [Marhavidas *et al.*, 2011]. Despite the accuracy and precision of a full QRA, the usual lack of information, enforces the use of less complex, but still, suitable methodologies to assess consequences and impacts of identified accident scenarios, like the well-established CA methodologies.

2.2 Consequence analysis of industrial accidents

In general, CA methodologies include sets of techniques enabling the estimation of likely physical consequences and their quantification, in the form of damage to human health, property, natural resources or toxic effects, from the defined accident scenario [Casal, 2008]. Since the mid-1980s, a wide variety of both quantitative and qualitative techniques have been developed and applied in CA methodologies, following either individual 'pure' or combined DTA and PRA approaches [Mannan, 2005]. In any case, CA methodologies need at least a DTA approach technique for the estimation of effects and consequences from examined accident scenarios. Thus, to estimate consequences, CA generally comprises the set of four stages schematized in Figure 2.2, namely: (i) Accident scenario definition, (ii) Source term characterization, (iii) Atmospheric dispersion modelling, and finally, (iv) Physical effects and consequences estimation.

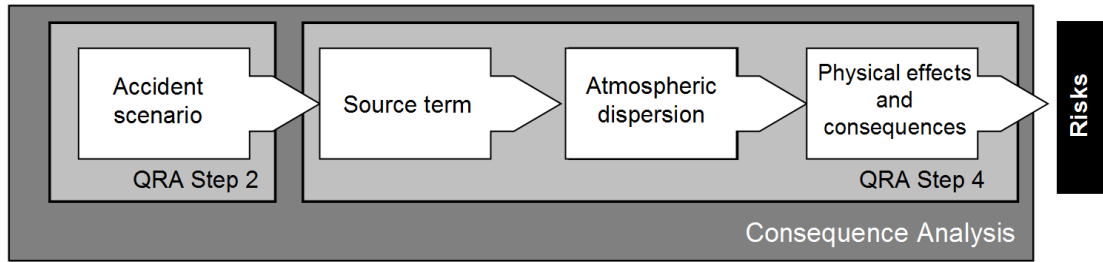


Figure 2.2 – Scheme of consequence analysis methodology [based on CCPS, 1999].

As in QRA, CA studies start with the identification of hazards from initially defined accident scenarios. In view of analyzing accidents involving the release of hazmat gases, potential scenarios include various types of failures, like catastrophic crash of pressurized vessels, small punctures in vessel wall or full bore ruptured pipelines, among other type of malfunctions. To address the characterization of accident scenarios, analysts often consider two main types of potential scenarios [Casal, 2008], namely:

- *Type 1* - hazardous situations that may lead to frequent releases of limited hazmat amounts (e.g. controlled depressurization releases) often-called maximum credible scenarios;
- *Type 2* - sudden catastrophic releases, also known as worst-case accident scenarios.

Whereas *Type 1* accident scenarios often comprise regular or long duration slam safety relief losses frequently considered in PRA approaches; *Type 2* enables assessing the maximum potential hazards of accidents in industrial facilities or equipments, *i.e.* the worst possible accident scenarios (e.g. total crash of a vessel), examined in both PRA and DTA approaches.

Next, accidental release (hereinafter called source term) is quantitatively described in stage 2 by estimating the hazmat gas outflow parameters (e.g. outflow rate, pressure or temperature). Long has been recognised that source term characterization is not a straightforward process, deeply depending on several conditions, such as, type of accident, chemical properties and containment (storage or transportation). As a result, various techniques/models have been developed over the last decades, enabling the description of hazmat gas behaviour during the release process. The most common accident scenarios involve the release and spread of gases or liquids handled in industrial facilities.

Stage 3 comprises CA models specifically developed to describe how the hazmat gas is transported downwind and dispersed in the atmosphere. Generally, this stage is considered the central component of CA studies [CCPS, 1999; Mannan, 2005]. Different models can be applied to accurately predict hazmat gas dispersion depending on the source term accident-

specific behaviour, the hazmat chemical properties and resulting behaviour during the dispersion.

Finally, consequences are estimated in stage 4, in the form of quantified effects and damages, as a function of the affected area and distance, as well as, estimated concentration levels. The dispersion-specific average concentration results are converted into effects on people (injury or death) and environment through their direct comparison with reference exposure limit thresholds depending on the object and purpose of the study. Fires and explosion can also be taken into account in case of flammable hazmat gases [Mannan, 2005]. Moreover, damages may occur as an immediate and direct consequence of the accident, or during the dispersion of the resulting hazmat gas cloud (*e.g.* ignition and explosion of flammable hazmat gas cloud). Notwithstanding the relevance of fire and explosion phenomena, the present thesis will only focus on the consequences from the exposure to the dispersed hazmat gas cloud (*i.e.* any kind of ignition source and related consequences will not be treated in the present work).

Overall, the provision of recognizable measures of consequences, used for the estimation of risks in QRA step 5, depends mainly in the accuracy of the description of: (i) hazmat gas release (*i.e.* source term component), and (ii) hazmat gas cloud atmospheric dispersion. CA modelling results are often presented in the form of risk contour maps and/or number of people potentially affected. In an attempt to simplify analysis's efforts, major developments on CA modelling have been taken and a wide variety and number of computational modelling tools are being implemented in both QRA and CA methodologies.

2.3 Consequence analysis modelling

The need to understand and numerically describe the various stages of accident scenarios involving the release and dispersion of hazmat gases, gave numerical tools a unique value in QRA methodologies and large efforts have been taken in the development and implementation of new and more accurate modelling techniques, assuring a proper quantification of consequences [Casal, 2008]. In fact, it has long been recognized that numerical models can provide valuable information to control and emergency responders to plan, guide and respond adequately in case of accident, also at the very local scale where the risks and threats are potentially high. Nonetheless, the continuous increase in computing power also endorses the development and use of more advanced models, especially, in the context of local- and neighbourhood-scale hazmat gas releases. Moreover, despite of extensive and well studied passive gas dispersion phenomena, the typical denser-than-air gas, *i.e.* with a higher

density than ambient air (hereinafter called '*dense gas*') behaviour, observed in the majority of hazmat gases handled in industrial facilities disables the use of 'traditional' air quality models [Casal, 2008] enforcing the development of adequate computational tools.

In view of the various stages of CA methodologies, it is possible to consider three main types of numerical modelling elements [CCPS, 1999]: (i) source term, (ii) atmospheric dispersion, and (iii) consequences and effects models. The set of elements is, in general, complemented by external models, such as meteorological models, often not considered as 'truly' CA modelling elements, but crucial to assure the accuracy of CA studies. In the literature there are general guidelines for the application of the various CA numerical modelling elements [*e.g.* CCPS, 1999; Fingas, 2002; Mannan, 2005; VROM, 2005a,b,c; Casal, 2008].

2.3.1 Source term modelling

Under normal operating conditions, release behaviour of most hazmat gas occurs in a 'controlled fashion' [Mills and Paine, 1990]. With the exception of fugitive emissions (*e.g.* wind blown dust from a pile), the source term rates are usually described as 'regular steady-state emissions' correlated with process parameters and then somewhat easy to estimate. Conversely, accidental release of hazmat clouds tend to exhibit rapid time variations of the emission rate or phase change and interaction with the immediate surroundings, requiring more complex and not as straightforward approaches as for 'regular emissions' [Hanna and Drivas, 1996]. Hazmat gas release into the atmosphere can be linked with a large diversity of circumstances ranging from slow discharge through a small pinhole failure to rapid discharges resulting from a major rupture of the containment [Jones, 1992].

The release phenomenon depends mainly on the hazmat physical properties; the containment (process or storage) conditions; the way the accident takes place; and possible subsequent mechanical and physical interaction with the immediate surrounding environment, among other factors [Hanna and Strimaitis, 1989; Hanna and Drivas 1996; Dutch National Institute of Public Health and the Environment (VROM), 2005a; Hanna *et al.*, 2008; Brambilla and Manca, 2011]. Notwithstanding the difficulty and uncertainties linked with an accurate characterization of the release [see Hanna and Britter, 2008], typifying and illustrative accident scenarios have been defined and extensively used in CA [Mannan, 2005]. Figure 2.3 illustrates some of the most well-established and characterized typifying accident scenarios considered in CA studies, divided into standard classes also listed in Table 2.2.

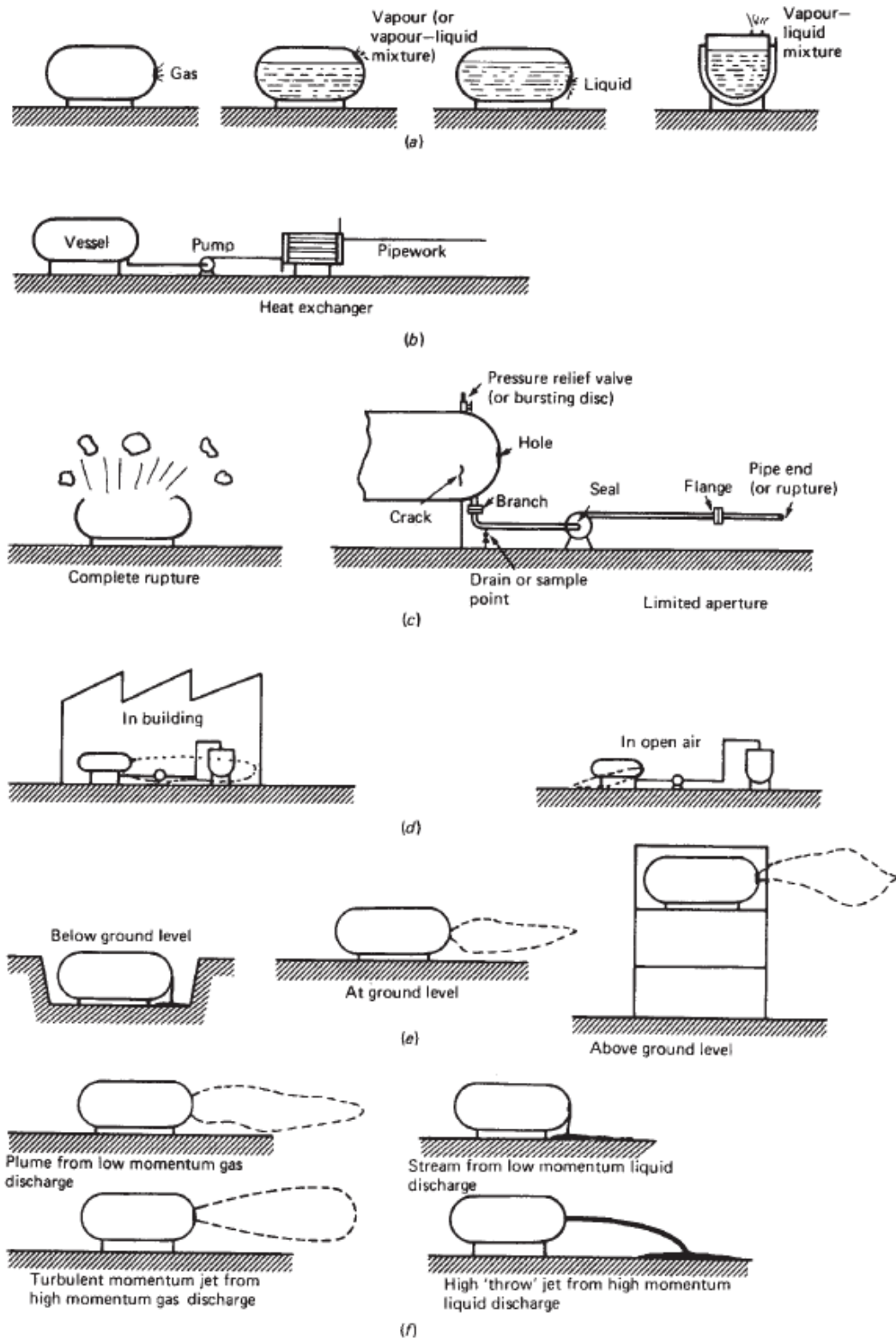


Figure 2.3 - Illustration of some conceivable release mechanisms according to (a) initial condition, (b) container, (c) aperture, (d) enclosure, (e) height, and (f) fluid momentum [Mannan, 2005].

In general, hazmat gas source term scenarios include sudden release, transient spillage, fires or explosions [Hanna and Drivas, 1996]. Among others, the initial conditions, container,

location and height of the aperture, duration and type of outflow or fluid momentum, are used as the most often selection criteria for the characterization of accident outflow conditions in CA studies [CCPS, 1999]. Some of the common used classification criteria and respective classes (illustrated in Figure 2.3) are summarized in Table 2.2.

Table 2.2 – Classification of accidental release situations [based on Mannan, 2005; VROM, 2005a].

Initial conditions	Container	Aperture	Enclosure	Height	Duration/type of outflow	Fluid momentum
Compressed gas	Vessel	Total rupture	Indoor	Below ground level	Instantaneous	Low
Liquid	Other equipment	Limited aperture	Outdoor	At ground level	Finite-duration (constant rate or transient)	High
PLG	Pipework (pipes or pipelines)			Above ground level	Continuous (constant rate)	

The released hazmat gas can be initially contained as a compressed gas, a liquid (cryogenic, sub-cooled, superheated or at normal temperature) or a Pressurized Liquefied Gas (PLG), and therefore released in the same form, excepting PLG, that may be released in the form of gas, liquid or two-phase vapour-gas mixture, depending on the location and type of the aperture (Figure 2.3a). If the release occurs from a container holding PLG, the hazmat will normally be liquid if the aperture is below the liquid level and vapour or two-phase mixture if it is above the liquid level. The container on which the release is defined can be a vessel or other equipments, such as pumps or pipeworks (pipes or pipeline systems) (Figure 2.3b).

The aperture where the release takes place may range from a limited aperture, such as a small hole in a vessel wall, to a large fraction of the envelope of the container in case of a complete rupture of a vessel (Figure 2.3c). The orifice can be a sharp-edge orifice, a conventional pipe branch, a rounded nozzle branch or a crack. The flow through a rounded nozzle is greater than through a conventional pipe branch; however it is the last one that is often considered [Mannan, 2005]. Other kinds of holes include drain and sample points; pressure relief devices (pressure relief valves, bursting discs, and liquid relief valves); seals; flanges or pipe ends.

It is also necessary to consider where the release takes place, distinguishing indoor or outdoor releases (Figure 2.3d). Additionally, the height at which the release occurs (below, at or above the ground) may also affect the release and dispersion behaviour (Figure 2.3e).

In case of liquid spills, possible subsequent evaporation phenomenon must be also examined if liquid pools are formed, because a hazmat gas cloud source could be generated. In general it can be assumed that if a liquid is discharged from a container below the ground level, it may remain completely contained without significant evaporation. However, when occurs at or above the ground level, significant evaporation may happen, generating hazmat gas that may be dispersed over a substantial distance, similarly to 'direct' hazmat gas releases. Moreover, the shape of the liquid pool depends on the presence of retention bunds or other kinds of barriers [Hanna and Drivas, 1996].

The dimensions of the aperture and initial conditions can also affect the momentum of the released hazmat (Figure 2.3f). If hazmat is released in the form of gas, low and high momentum jets can be observed if the gas forms a plume and a turbulent momentum jet, respectively. For liquids, the momentum will only affect the distance of which the liquid will be discharged and form a liquid pool [Lees, 1996]. A more complex approach is required for PLG releases, since both gas and liquid discharges may occur separately or simultaneous. In case of liquid spill, subsequent evaporation or flashing phenomena from the formed liquid pool must be also taken into account [Hanna and Strimaitis, 1989; Witlox *et al.*, 2002].

When analyzed the discharge conditions, the duration and type of outflow rate depend greatly on the type of failure and initial conditions of the hazmat. Three main types of classes can be considered for the duration of the release, namely instantaneous (*e.g.* total collapse of a vessel), finite-duration (*e.g.* relief valve opened for a few minutes) and continuous (*e.g.* long period undetected and uncontrolled release in a piping system) [VROM, 2005a]. As concerns to finite-duration it is possible to consider both transient and continuous release types.

Regardless the influence of the aperture shape, hazmat initial conditions and chemical properties will also affect the behaviour of the gas during the release and atmospheric dispersion regimes. Moreover, it is commonly the case that accidentally released hazmat gases, be they flammable or toxic or both, are often dense gases, as a result of either the properties of the hazmat, the methods of storage or release, or a combination of both [Britter, 1982]. Despite the typical passive or positively buoyant gases (gases with density lower or similar to the air) frequently considered in traditional atmospheric pollution problems [see Zannetti, 1990; Stull, 1997; Seinfeld and Pandis, 2006], a large fraction of existing hazmat has the dense gas behaviour by virtue of having [Britter and Griffiths, 1982; Britter and McQuaid, 1988; Lees, 2006; Green and Perry, 2008]:

- High molecular weight when compared with that of ambient air (*e.g.* chlorine);

- Significantly lower temperature even with low molecular weight (*e.g.* liquefied natural gas (LNG));
- High storage pressure even with low molecular weight, whose vapour at the boiling temperature is less heavy than the environment, but which, due to the release type, produce a cloud including material droplets (*e.g.* failure of ammonia stored at high pressure with formation of aerosol);
- Chemical transformation/reaction of the released material with water vapour in the ambient atmosphere (*e.g.* nitrogen tetroxide, hydrogen fluoride - HF).

Albeit the 'huge' number of hazmat handled in hazardous industry that may form dense gas clouds, interest usually focuses on those that are combustible or toxic, with boiling points below ambient temperature [Britter, 1989]. These are commonly stored or transported as liquids, maintained in that phase at or near to their saturation temperature at atmospheric pressure by refrigeration and insulation, or at ambient temperature by pressurization (*e.g.* PLG or liquefied petroleum gas (LPG)). Among the more prominent and known hazmat that may form dense gas clouds are chlorine, HF, ammonia, propane or LNG.

For instance, chlorine behaves like a dense gas both in liquefied and gas releases. Its normal boiling temperature is $-34\text{ }^{\circ}\text{C}$ and its molecular weight is $71\text{ g}\cdot\text{mol}^{-1}$, which is higher than ambient air ($\approx 28.96\text{ g}\cdot\text{mol}^{-1}$) [Yaws, 1999]. In case of liquefied chlorine releases its density is even higher [Green and Perry, 2008]. HF has a molecular weight of $20\text{ g}\cdot\text{mol}^{-1}$ and a normal boiling point of $20\text{ }^{\circ}\text{C}$, but often behaves like a dense gas [Puttock *et al.*, 1991]. This is because under certain circumstances it undergoes an oligomerization reaction, which has a formula $(\text{HF})_n$; and formed saturated vapour of HF has a molecular weight of $78.2\text{ g}\cdot\text{mol}^{-1}$ at its normal boiling point [Poling *et al.*, 2001]. Ammonia has a molecular weight of $17\text{ g}\cdot\text{mol}^{-1}$ and a normal boiling temperature of $-33\text{ }^{\circ}\text{C}$, but liquid ammonia releases generate dense gas clouds [Yaws, 1999]. If there is no liquid spray, the cloud density will decrease when it mixes with air and it is likely to become a neutral gas; nonetheless, if there is a fraction of liquid spray, the cloud will be dense [Lees, 1996]. Propane has a molecular weight of $44\text{ g}\cdot\text{mol}^{-1}$ and a normal boiling temperature of $-42\text{ }^{\circ}\text{C}$ [Yaws, 1999], so releases of either propane gas or liquefied propane, are always heavy. LNG also originates dense gas releases, not because its molecular weight ($\approx 16\text{ g}\cdot\text{mol}^{-1}$) but due to temperature effects (normal boiling temperature is $-161\text{ }^{\circ}\text{C}$) [Green and Perry, 2008]. Other examples of hazmat used in industry are identified in the literature [*e.g.* Yaws, 1999; Poling *et al.*, 2001; Casal, 2008; Green and Perry, 2008].

To determine the emission rate or volume of hazmat gas, different input data must be defined, depending on the accident release and ambient conditions. Typically, physical and chemical properties of the released material, geometry of the source, characteristics of the ground surface and mitigation measures should be supplied. Main outputs from source term models greatly depend on the type of accident scenario; however, for CA studies of industrial facilities, general and typifying guidelines are often applied to minimize uncertainties of input data gaps [CCPS, 1999; Hanna and Drivas, 1996; Mannan, 2005; VROM, 2005a; Casal, 2008].

Overall, the second stage of CA studies, must be capable to assure a proper numerical description of the outflow conditions (emission rate, temperature, pressure, etc.), but also to determine hazmat gas 'type' (heavy or passive gas) providing accurate and realistic information to reliably perform subsequent atmospheric dispersion modelling.

2.3.2 Atmospheric dispersion modelling

The third stage of CA modelling consists on predicting the transport and atmospheric dispersion and dilution of the formed hazmat gas cloud (passive or dense). It can be considered the 'core' element of any CA methodology [Fingas, 2002], given the need to simulate the concentration fields for further estimation of consequences and damages. During the early instants after the release, hazmat gas behaviour may be dominated by factors arising from the initial containment conditions, influencing the buoyancy (positive, neutral or negative) behaviour. Thus, in addition to the well know dispersion of passive (and neutral) gases regime, hazmat dense (or negatively buoyant) gas behaviour must be also taken into account in CA dispersion modelling techniques [Hanna and Drivas, 1996; Mannan, 2005; Borrego *et al.*, 2009], to properly describe the cloud movement after the release. This requirement is strongly supported by reported MIA involving hazmat gas releases with dense gas mixture clouds observed during the initial instants of the dispersion (*e.g.* Flixborough or Mexico City), in addition to the main findings of a large number of experimental tests [*see* Britter, 1989; Nielsen, 1998; Mannan, 2005, Casal, 2008].

2.3.2.1 Dense gas atmospheric dispersion

Since the 1970s large efforts have been made to understand dense gas dispersion, in particular from sudden (accidental) releases of large quantities of hazmat into the atmosphere [*see* Feldbauer *et al.*, 1972; Te Riele, 1977; Britter and Griffith, 1982]. The interest in studying dense gas dispersion was intensified in the early 1980s onwards [*see* Ermak *et al.*, 1981; Goldwire *et al.*, 1983; Puttock *et al.*, 1984; Britter, 1988, 1998; Nielsen, 1998] leading to the implementation

of relevant large scale experimental trials and the development of a wide variety of numerical models, some of them commonly used in CA, for the chemical and process industries [Nielsen and Ott, 1996; Fingas, 2002; Luketa-Hanlin, 2006; Pontiggia, *et al.*, 2010]. Over the last years a renewed interest on modelling hazmat gas accidental release and dispersion strongly influenced by the need to provide more realistic and accurate tools to support CA studies, but also, due to the developments of computational and hardware capabilities.

The influence of density difference on gas mixing arises primarily from the associated buoyancy force *i.e.* the Archimedean force on a body submerged in a fluid of different density. Although density difference also affects the inertia forces acting on a fluid in motion, the variations to the fluid accelerations are generally assumed to be small when compared with the acceleration arising from buoyancy forces. This assumption is the so-called 'Boussinesq approximation' [Britter and McQuaid, 1988]. The buoyancy forces follow a sign of convention, where negative buoyancy implies a buoyancy force in the opposite direction to the positive direction of the z-coordinate. Hence a dense gas dispersion layer at ground level in the atmosphere may be defined as a negatively buoyant flow (buoyancy force directed to the ground surface). The converse situation is a neutrally or positively buoyant flow. Moreover, it is normal to refer to neutrally buoyant case as a passive gas, although strictly the term implies that the conditions of emission play no dynamic part in the way in which the emission subsequently diffuses into the ambient flow, a condition that will not be satisfied if the emission has significant momentum [Green and Perry, 2008].

Unlike 'traditional' passive gas dispersion, which is entirely governed by the atmospheric turbulence characteristics, the spreading of dense gas is relatively insensitive to variations in meteorological conditions compared to gravity forces and density factors [Jensen, 1981]. Dense gas cloud moving along the ground represents a stably stratified configuration, and it will survive for a considerable time even in the presence of wind. Britter and McQuaid [1988] argued that major physical processes specific for negatively buoyant clouds, include:

- Gravitational velocity field (also called gravitational slumping) is produced by the horizontal density gradients, which is an additional transport mechanism to that provided by the atmospheric flows. This self-generated phenomenon results in clouds with increased spreading in horizontal, and reduced in vertical dimensions. Furthermore, profiles of concentration in the lateral direction are frequently quite uniform with little meandering due to random environmental flow.

- Velocity shear at the cloud interface may lead to a gross intermingling of the cloud with the surrounding air and eventually in the turbulence generation. This mechanism of dilution is of major importance if self-generated velocities are large, compared with the mean wind velocity.
- Vertical density stratification is a direct result of vertical variation of density. Dense gas clouds have negative vertical gradients that may result in turbulence and therefore, turbulence mixing can be strongly reduced or entirely inhibited. This effect can extend to the atmospheric turbulence in the wind flow over the cloud, as well as to the cloud itself.
- Inertia of released gas directly depends upon the material density, *i.e.* depends on the density difference between released material and ambient air. When density difference vanishes, dense gas dispersion approaches to passive gas clouds behaviour.

It is obvious that density difference between the released gas and the ambient air is not the only condition in delineating cloud behaviour; others like volume or volume flux (depending on the type of release), other source term characteristics (*e.g.* source diameter) or atmospheric conditions must be also taken into account for dense gas cloud dispersion analysis. Considering the various conditions, several criteria/parameters have been suggested to numerically determine whether a released hazmat gas will exhibit dense gas behaviour or can, for practical purposes, be treated as a passive gas. One of the most used parameter is the similarity dimensionless Richardson number (R_i) [Britter, 1989; Green and Perry, 2008]. The R_i is the ratio of the buoyancy to the inertia forces, *i.e.*, it represents the ratio of the potential energy due to the density excess inside the cloud with the kinetic energy due to the ambient turbulence. It should be noted that the prevailing estimation of R_i does not conflict with the Boussinesq approximation stated earlier, since the approximation only implies that the influence of density difference on the fluid inertia is small, which doesn't mean that inertia is itself small [Britter and McQuaid, 1988]. Various expressions/conditions have been suggested based on similarity parameters, such as the R_i and experimental tests [*e.g.* Havens and Spicer, 1985; Hanna and Drivas, 1987; Britter and McQuaid, 1988]. For instance, Britter and McQuaid [1988] suggested that a hazmat gas released instantaneously (Eq. 2-1) or continuously (Eq. 2-2) into the atmosphere has dense gas cloud behaviour if the following conditions are satisfied:

$$\left[\frac{(g(\rho_g - \rho_a)/\rho_a) \times Q_{i,0}^{1/3}}{u_h^2} \right]^{1/2} > 0.2 \quad \text{Eq. 2-1}$$

$$\left[\frac{g(\rho_g - \rho_a) \times q_{c,0}}{\rho_a \times u_h^3 \times D_c} \right]^{1/3} > 0.15 \quad \text{Eq. 2-2}$$

In which, D_c is the source or cloud diameter, g is the gravitational constant, u_h is the wind velocity at the reference height h (10 m) $Q_{i,0}$ is the initial volume of instantaneous puff, $q_{c,0}$ is the source volume flow rate for the continuous plume, and finally, ρ_g and ρ_a are the cloud and atmospheric air densities, respectively. For grounded releases D_c is equal to the initial cloud width, while for elevated releases it is the initial diameter or the rupture close to the source or the height of the release further downwind when the cloud touches the ground are used. Nonetheless, the reference limits can not be absolute numbers, which separates the dense gas dispersion from the passive gas dispersion, being used only as guidance [Britter, 1989].

In the early stages of dispersion, the behaviour may be dominated by factors arising from the type of storage and/or release. Continuous releases from pressurized containers may be expected to produce momentum - dominated jets. In case of pressure vessels catastrophic failure (instantaneous release) there will be a rapid 'vapour-flash' in which a thermodynamically determined fraction of the now superheated (with respect to ambient conditions) liquid converts to vapour. It has been observed that for some hazmat the violence of this process ejects a substantial fraction of the residual liquid as fine droplets, producing a cloud consisting of a mixture of air, vapour, droplets of the material and of condensed water. There is, in this case, a substantial initial dilution with air [Britter and McQuaid, 1988].

Observations following accidents or experiments showed that, depending on the release and dispersion mechanisms, hazmat dense gas cloud evolution can be divided into five main phases [Van Ulden, 1986; Britter and McQuaid, 1998]: 1 - emission into the atmosphere, 2 - expansion, 3 - slumping phase, 4 - transition phase, and finally, 5 - passive dispersion phase. Figure 2.4 shows the set of evolution phases identified in dense gas clouds dispersion.

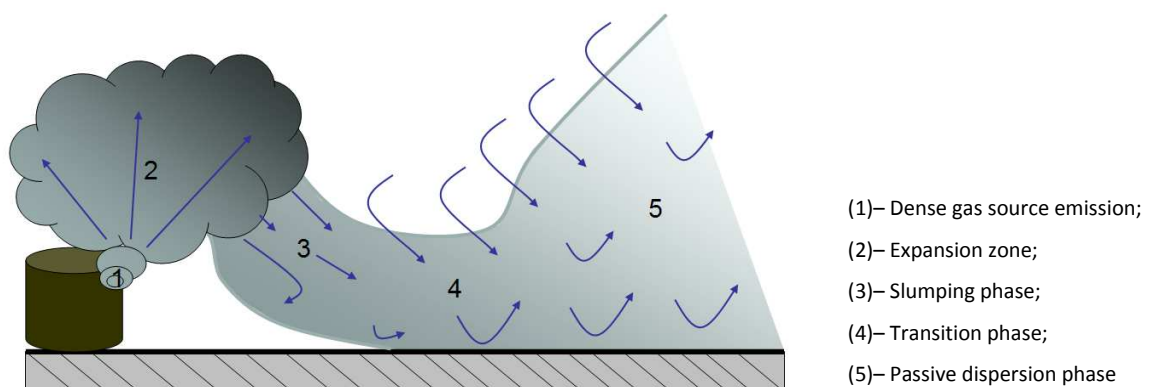


Figure 2.4 - Phases in the dispersion of a dense gas cloud [based on Britter and McQuaid, 1988].

Dense gas source emission phase (1) comprises the failure and accidental release of (liquefied) gas. In case of liquid spills, the evaporation phenomenon must be also considered. This phase is very important for the temporal behaviour of the dispersion [VROM, 2005a]. In an instantaneous release, the 'entire' volume of gas is discharged in a very short time. Alternatively, in finite duration releases, emission occurs during longer periods with time-varying (transient) or steady-state (continuous) outflow rates.

Next, the expansion zone (2) is strongly influenced by the dissipation of stored energy during the process. In some cases, for instance when cold LNG spilled comes in contact with water, an initial rapid vapour expansion, the so-called 'Rapid Transition Phase' (RTP), may occur in certain circumstances [Mannan, 2005]. This expansion is not combustion related, but rather is classified as a physical or mechanical expansion where there is a high-pressure energy release [Luketa-Hanlin, 2006] and a visible vapour volume expansion is observed. In this phase the cloud starts to descend to the ground reaching the slumping phase. Some authors [*e.g.* Van Ulden, 1987; Fingas, 2002; Casal, 2008] consider these first two phases as a single one, covering both emission and expansion mechanisms. In any case, stopped the expansion phase, the cloud starts to 'slump' under the action of gravity and formation of a ground-based cloud.

The slumping phase (3), schematically illustrated in Figure 2.5 for an idealized instantaneous release, occurs when the effects of turbulence and momentum of the ambient air, and surface friction are neglected. Although being observed in all release regimes, the variation of gas cloud shape is more pronounced in case of instantaneous release [Lees, 1996].

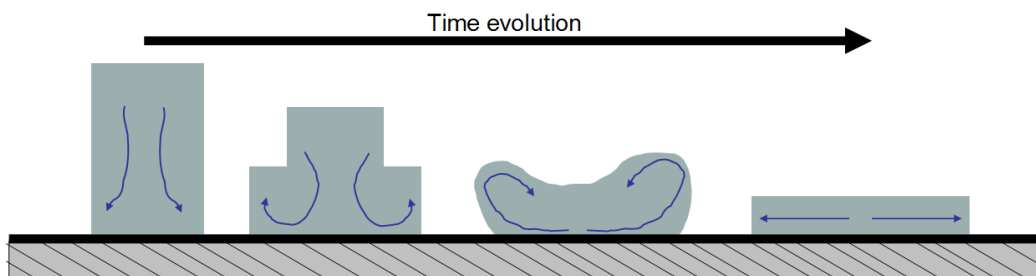


Figure 2.5 – Slumping phase of dense gas cloud dispersion [based on Casal, 2008].

During this phase, entrainment dynamics and mixing of the cloud are exclusively driven by the negative buoyancy of the cloud. A slumping and radially spreading cloud is observed with a more or less pronounced raised edge, sharp radial boundaries and a diffuse top. Substantial mixing takes place at the cloud lateral edges (also called gravity-front), resulting from the self-generated vortices in the extreme lateral areas generated by gravity spreading.

Mixing by atmospheric turbulence at the top of the cloud is eventually suppressed by the density gradient, and turbulence within the cloud is reduced due to the stable stratification, *i.e.* a negative vertical density gradient, of the dense gas layer. Still, the influence of gravity, wind, heat transfer from the environment, may also affect the cloud shape and radial spread [Britter, 1989]. In addition to the ambient air, heating from the ground can also affect the spreading phenomenon in case of cold clouds. As the cloud continues to be diluted, the hazmat concentration continues to fall (though it is important to note that dilution with air will lead also to a cooling effect that may 'compete' with parallel heating processes if droplets are present, since the heat for evaporation must come from the cloud).

After gravity spreading has finished, vertical variation of density in the cloud shows a stable stratification which strongly reduces the dispersion and mixing in the vertical direction. At this level of dilution the density difference becomes negligible, and the transition phase starts (4). Even gravity spreading continues dominating over horizontal atmospheric diffusion; the cloud no longer slumps, because turbulence leads to vertical mixing at a similar or greater rate than the gravity induced slumping motion. Advection by the mean wind happens and surface friction may also affect the gravity spreading. Throughout this period the cloud is being diluted further by air entrainment resulting from the action of turbulence in the ambient flow, and turbulence generated by velocity gradients at the interface between the cloud and the surrounding air. As a result, the sharp-edge cloud transforms into a diffuse cloud.

After the transition phase (4), subsequent cloud behaviour can be described, following neutral or positively buoyant gas dispersion behaviour – passive dispersion phase (5). In this phase the cloud density effects can be neglected. Dispersion by atmospheric turbulence and advection by the mean wind are similar to those for passive gas dispersion. Moreover, as a consequence of the increased lateral spread, dense gas clouds exhibit a lower advection velocity and less meander, or responsiveness to large scale atmospheric motions, than is observed with passive releases [Britter and McQuaid, 1988]. Some of dense gas dispersion phenomenon core features are well replicated in measured observations from large-scale and laboratory experiments on water or land [*e.g.* Koopman *et al.*, 1982a; McQuaid and Roebuck, 1985; Schatzmann *et al.*, 1993; Duijm, 1994; Nielsen and Ott, 1996; Koopman and Ermak, 2007].

Over the last decades, large efforts have been taken for the development and implementation of new and more accurate physical and numerical modelling techniques to understand and describe hazmat dense gas release and dispersion behaviour. Albeit the common purposes, physical and numerical modelling approaches comprise clear differences, concerning the main

intention of application, CA stage(s) covered, complexity and efforts, or even assured quality, among other factors, as discussed by Nielsen [1998].

2.3.2.2 Physical modelling of dense gas atmospheric dispersion

Physical modelling consists on experimental simulation of dispersing gas releases [Duijm *et al.*, 1994] commonly set to provide relevant information to support the development and application of theoretical approaches and/or numerical models. Hazmat gas release and atmospheric dispersion experimental modelling can be conducted on large scale field trials or on reduced scale tests at laboratory facilities (atmospheric boundary layer (ABL) wind tunnels or water channel tunnels) [Lees, 1996]. Large scale experimental tests are mainly intended to observe and collect information on emission and dispersion, without the possibility to isolate specific variables or CA stages. On the other hand, laboratory experiments typically include two main types of tests [Meroney, 1982; Nielsen 1996]: the ones aiming to study in detail a specific process occurring (or variables) on a specific CA stage by isolating or controlling relevant variables; and those involving detailed simulation of the various stages of hazmat accidental release and dispersion.

In general, laboratory wind-tunnel experiments permit a certain degree of control on examined variables (*e.g.* safety, meteorology, site or measurement variables) not often feasible or economic at large-scale trials [Snyder, 1981; Tavares, 2007]. In fact, the main limitations of direct field experiments comprise the simultaneous operation of all governing parameters, as well as, the difficulty in determine which parameters are governing and which are secondary or dispensable parameters [Meroney *et al.*, 1996]. This is the main reason why the majority of the most recent experimental work is being conducted in laboratory wind-tunnel facilities. Nonetheless, in any case, the value of experimental information is a combination of the general usefulness of data and measurement quality [Tavares, 2007].

Most relevant experimental work focusing the release and atmospheric dispersion of hazmat gases (at both large and small scale) is widely reported and investigated since the 1960s [*e.g.* Lapin and Foster, 1957; Seargeant and Robinett, 1968; Van Ulden, 1974; McQuaid, 1979; Puttock *et al.*, 1984; Goldwire *et al.*, 1985; Havens, 1988; Schatzmann *et al.*, 1993; Nielsen *et al.*, 1997; Robins *et al.*, 2001; Hald *et al.*, 2005; Ricciardi *et al.*, 2008].

Most of the 1960s-70s experiments were conducted, aiming to estimate evaporation rate and the maximum distances of danger for flammable (measured as the maximum distance until concentration levels could generate fire or explosion – lower and upper flammability limits,

LFL and UFL, respectively) hazmat gases (e.g. LNG) [Puttock *et al.*, 1982]. Only further experiments (since 1980s) started to consider the dispersion of toxic gases (e.g. ammonia, chlorine) or safer simulants (e.g. carbon dioxide or liquid nitrogen), focused on describing and understanding hazmat gases behaviour during and after the release [Luketa-Hanlin, 2006]. Extensive descriptions and discussion of field experiments are available in the literature and continue to be published, endorsed by the need of experimental data for numerical modelling validation [e.g. Puttock *et al.*, 1982; Meroney, 1987; Nielsen *et al.*, 1997; Mannan, 2005; Luketa-Hanlin, 2006; Casal, 2008]. Table 2.3 summarizes some of the most known reported large and small scale experimental tests carried out since the 1970s focusing dense gas release and dispersion.

Table 2.3 – Summary of well known experimental tests.

Experiment	Location, date and Coordinator	Phenomena involved	References	
Full-scale Field tests	Esso/API	Matagorda Bay, Texas (1971) Esso Company and the American Petroleum Institute	Releases of liquid LNG, fast evaporation, maximum distance to LFL.	Feldbauer <i>et al.</i> , 1972; May <i>et al.</i> , 1973
	Dutch Freon 12	The Netherlands (1973–74) Directorate General of Labour of the Dutch Ministry of Social Affairs.	Dispersion of Freon, simulation of chlorine vapours dispersion generated from a liquid release.	Van Ulden, 1974; Te Riele, 1977
	Porton Down	Porton Down, U.K. (1976–78) Health, Safety Executive, Chemical Defence Establishment of U.K.	Release and dispersion of dichlorodifluoromethane, slumping phase	McQuaid, 1979; Picknett, 1981
	Burro and Coyote field tests	China Lake CA. (1980 and 1981) US Lawrence Livermore Laboratory	Releases of liquid LNG, spill on water pond, fast evaporation and dispersion.	Koopman <i>et al.</i> , 1981; Goldwire <i>et al.</i> , 1983
	Maplin Sands field tests	Maplin Sands, USA (1980) Shell	Dispersion of continuously released propane and LNG, spill onto water.	Puttock <i>et al.</i> , 1984; Colenbrander and Puttock, 1984
	Thorney Island	Thorney Islands, U.K. (1982–84) Health and Safety Executive	Dispersion, release conditions of Propane and LNG, terrain effects, slumping phase behaviour	HSE, 1984; McQuaid, and Roebuck 1985
	Desert Tortoise	Nevada, U.S.A. (1983) US Lawrence Livermore Laboratory	Release, flashing of ammonia jets, dense to passive clouds, non-obstructed flat terrain.	Goldwire <i>et al.</i> , 1985
Wind tunnel tests	FLADIS	Landskrona (1991–1993) Riso, HydroCare, FOA, CBDE	Ammonia release, flashing jet, dense to passive cloud, non-obstructed	Nielsen <i>et al.</i> , 1994; Nielsen, 1996
	EC MTH project and FLADIS	Hamburg, Germany Hamburg University Laboratory (1991)	Continuous and instantaneous releases of Sulphur hexafluoride (SF ₆), flat and obstructed with slopes	Schatzmann <i>et al.</i> , 1991, 1993
	MT-TNO project BA	Apeldoorn, The Netherlands (1988–1990) TNO	Continuous plume, Instantaneous releases (Thorney Isl. No 17), fence	Van Oort and Bultjes, 1991
	EC MTH project BA	Stevenage U.K. (1988–1991) Warren Springs Laboratory	Instantaneous isothermal release of Thorney Island type in 1:100 model scale, Presence of fence	Hall, 1991
	STEP project FLADIS	Apeldoorn, Netherlands (1992) TNO	Continuous plume of SF ₆ gas	Duijm, 1994

One of the first large-scale field experiments focusing the release and dispersion of hazmat gases is the Esso Research and Engineering Company (Esso)/ American Petroleum Institute

(API) field test trials, conducted by the Esso and the API at Matagorda Bay in Texas (USA), in 1971 [Feldbauer *et al.*, 1972]. The series of tests involved instantaneous spills of LNG onto water and extensive measurement of the concentrations during the dispersion of the evaporated hazmat gases [May *et al.*, 1973]. This study focused on LNG fast evaporation behaviour and the estimation of the maximum distances to threshold lower limit flammability level (LFL) concentration. Measurement results were analysed in terms of Gaussian plume profiles showing that the hazmat cloud width to height ratios were in general greater than those appropriated to passive gas releases in any atmospheric conditions. Overall, these tests more or less confirmed the influence of gravitational spreading and the need to account this effect in hazmat dense gas dispersion modelling [Luketa-Hanlin, 2006].

Later, the well-known Lawrence National Livermore Laboratory (LNLL) Burro and Coyote series of full-scale field tests were carried out, as a part of the US Department of Energy's research on the issues of safety of liquefied energy gases [Koopman, 1981] at China Lake, California (USA), between 1980 and 1981. Both series of tests were well instrumented and obtained a fairly comprehensive set of measurements of meteorological parameters and concentration levels [Ermak *et al.*, 1981; Koopman, 1981, 1982a,b].

The Burro tests involved a total of 8 LNG spills onto water in 1980 aiming to determine the dispersion characteristics of large LNG gas clouds [see Koopman *et al.*, 1981]. In all tests, LFL distance first increased and then decreased with time, showing the direct influence of gas source strength on the observed distance to LFL. Moreover, gas cloud orientation and wind-field flow direction were consistent in that the maximum gas concentrations generally lay along the wind-field centreline. To illustrate the dimension of the experiment and observed dense gas dispersion behaviour, Figure 2.6 shows the plume in Burro 8 test after 30 s and the plume in Burro 6 after the quasi-steady state (passive phase) has been reached.

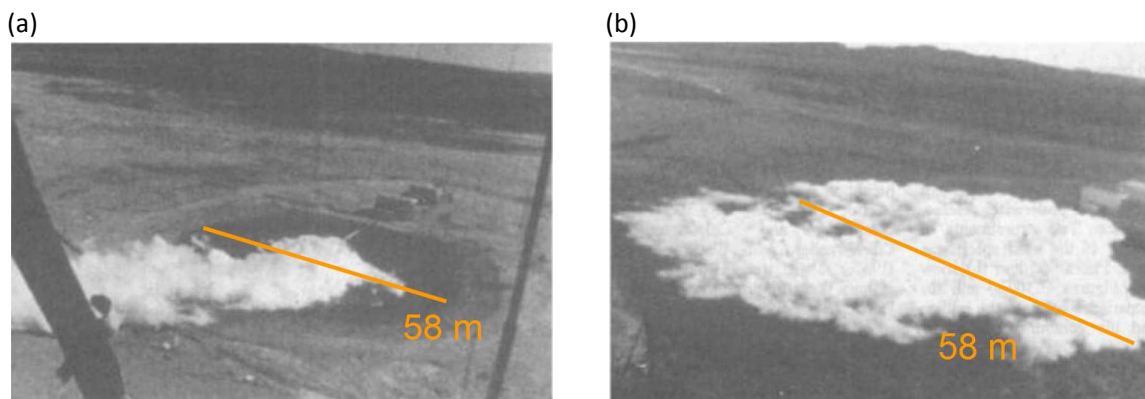


Figure 2.6 – Photographs taken during Burro series: (a) LNG gas plume in Burro test 8 after 30 s; (b) LNG gas plume in Burro test 6 at quasi-steady state [Ermak, *et al.*, 1982].

An exception was reported in one of the tests, in which gas flow was dominated by gravity, producing a highly bifurcated cloud that tended to follow low regions of the terrain [Ermak *et al.*, 1981]. Although data and theory available prior to Burro series indicated that RTP explosions were not likely to occur, numerous explosions were observed, in two tests. Further analyses have been reported by Ermak *et al.* [1982] and Koopman *et al.* [1982a,b, 1989] which also included the comparisons between measured data and numerical models results.

The Coyote tests were performed during the summer and fall of 1981 [Goldwire *et al.*, 1983; LNLL, 1983] as a continuation of Burro tests, with some technical changes (number of tests - 18 tests) and measurement sensors array set up). In addition to the main goals of previous tests, these also aimed investigating the damage of potential fires and RTP explosions resulting from the ignition of LNG spills evaporated hazmat gas clouds [see Goldwire *et al.*, 1983].

In the European context, the series of tests conducted by a consortium led by the British HSE, between 1982 and 1984, at Thorney Island (U.K.), involving the release of a mixture of Freon-12 with nitrogen in a flat terrain over close-cropped grass [McQuaid, and Roebuck 1985] can be considered one of the first relevant studies. The core purpose of these tests was to obtain data which could be used to increase understanding of the mechanisms of hazmat gas dispersion (in the presence or not of simple obstacles) and to validate numerical models.

The main focus was given to report the requirements for meteorological and similarity parameters used in numerical models (*e.g.* atmospheric stability, Monin-Obukhov length (L) or R_i) [Brambilla and Brown, 2010], without reference to the needs of any particular model description [McQuaid and Roebuck, 1985]. The tests were divided into three main phases, with different types of release and terrain set up [see Johnson, 1985; Puttock, 1987b]. Imagery was an important source of data for further evaluation of hazmat dense gas cloud behaviour to determine the cloud area in the first hundred seconds after the release, when the cloud had not reached any sensors [Nussey *et al.*, 1985]. Instantaneous releases were performed using a cylindrical collapsible tent. Figure 2.7 illustrates some snapshots (photographs) taken of the collapsing cloud observed in Thorney Island test 8.

A radially spread of the cloud fronts was observed and the highest peak concentrations were measured at the spreading ring. The presence of obstructions changed greatly the shape and peak concentrations along the cloud radial spread after entering in contact, depending on the geometrical shape and permeability of the barrier [McQuaid, 1987].



Figure 2.7 - Photographs of collapsing cloud observed in Thorney Island Test 8 [Prince *et al.*, 1987].

Continuous release conditions were also tested (phase III) [McQuaid, 1987], maintaining the same goals of previous phases. Main results showed that for high wind velocity, hazmat cloud lateral spread was less and the downwind extent greater. Additionally, the plume was characteristically very shallow, *i.e.* lower height and more extended laterally up to a certain distance from the source.

More recently, a series of full-scale field experiments with liquefied ammonia continuous releases were carried out during the FLADIS Field Experiments conducted in the frame of an European Council of European Commission CEC ENVIRONMENT PROGRAM project [Nielsen *et al.*, 1997]. The objective was to study the dispersion in all its stages, from the source into the regime of passive dispersion.

Despite the 'value' and number of full-scale field experiments, a wide variety of laboratory wind-tunnel experimental studies have also been carried out over the last decades, often in an attempt to reproduce and control relevant parameters or conditions of release and dispersion previously tested at full-scale field experiments. Whatsoever, only in the last years some of these became more known by virtue of the main purposes or results obtained. Among others, wind-tunnel experimental tests have been performed in the scope of European research

projects, such as the EC Major Technological Hazards (MTH) project and FLADIS experiments [Schatzmann *et al.*, 1991,1993] and the STEP project [Duijm, 1994] that replicated the several tests of previous full scale FLADIS experiments, the TNO Division of Technology for Society (MT-TNO) project [Van Oort and Bultjes, 1991], in which the Thorney Island test 7 experiment was simulated, or even the EC MTH project BA [Hall, 1991] that replicated the Thorney Island instantaneous release tests. These projects analyzed different types of release and dispersion in obstructed and unobstructed areas, but in most cases, experimental set up reproduces prior full-scale field trials. Additionally, aiming to reproduce full-scale experimental data in wind-tunnel, Schatzmann *et al.* [1991, 1993] performed the wind-tunnel experiments of the FLADIS project. Different release conditions and hazmat gases were tested in surfaces comprising a wide variety of obstructions set ups. In general, wind-tunnel experiments showed the typical behaviour of dense gas dispersion, highlighting the need for proper description of this behaviour in real and full-scale conditions.

The dispersion of pollutants is relatively well understood in open, unobstructed, nearly flat and homogeneous terrain, but this same unified level of understanding of dispersion in an intrinsically more complex urban environment appears to be lacking. In build-up regimes, new effects come into play as the turbulent flow interacts with isolated or groups of obstacles, taking a large range of shapes, sizes and possible configurations. A number of experimental studies of dispersion in sets of regular obstacles arrays have appeared in the past decade in the literature [*e.g.* Baechlin *et al.*, 1991; Davidson *et al.*, 1995; Macdonald *et al.*, 1997; Allwine, 2004; Ye and Bilitoft, 2004; Bezpalcova and Harms, 2005].

The study of dispersion through idealized arrays of obstacles has shown to be an important method of obtaining a better understanding of the dispersion through a real urban environment [Leitl *et al.*, 2003; Schatzmann and Leitl, 2011]. Although experimental studies considering idealized obstacles arrays can be considered valid simplifications of the real and complex urban environment [Britter and Schatzmann, 2007a], such type of geometries presumably displays some of the characteristics of the more complex, real-world configurations providing some simple physical models. Hence, it is through a comprehensive and controlled study of a wide range of idealized configurations that the underlying physical mechanisms of flow and dispersion in urban terrain can be effectively developed [Gailis and Hill, 2006].

2.3.2.3 Numerical modelling of dense gas atmospheric dispersion

Long has been recognized that numerical modelling is a valuable tool for a reliable application of CA methodologies; the inadequacy of 'conventional' passive gas dispersion models allied with the increased use of hazmat dense gases in industrial activity, enforced the development of models suitable to numerically describe both passive and dense gas dispersion behaviours. Hence, taking into account the number of industrial hazmat that can present dense gas behaviour when accidentally released and the main achievements from experimental studies, it was recognized the need to implement dense gas atmospheric dispersion models in CA modelling coupled with or even replacing traditional passive gas dispersion models. Illustrating the extensive work carried out over the last decades on this topic, a wide number of reviews and/or guidelines of hazmat gas dispersion modelling are given in the literature [e.g. Havens, 1982; Wheatley and Webber, 1985; Britter, 1989; Hanna *et al.*, 1991; MEG, 1994b; Hanna and Drivas, 1996; Fingas, 2002; Mannan, 2005; VROM, 2005a; Hanna *et al.*, 2008], in which different types of models are classified, compared and modelling approaches discussed.

Classification of dispersion models is far away of being consensual depending on author's criteria and selection parameters [Hanna and Drivas, 1996; Markiewicz, 2006]. Yet, authors tend to classify dispersion models using different criteria, including mathematical principles, emission source type and model complexity [Britter, 1989; MEG, 1994a; Hanna and Drivas, 1996]. Therefore, based on the complexity of the mathematical approach, CA dispersion models can be divided into three main classes of models [Britter, 1989; MEG, 1994b; Hanna and Drivas, 1996; Mannan, 2005; Markiewicz, 2006], as summarized in Table 2.4.

Table 2.4 – Classes of CA atmospheric dispersion models.

Class	Model Class	Model Type
I	- Empirical or phenomenological models	<i>Nomograms or simple correlations</i>
II	- Intermediate or integral models	<i>a) Box models</i> <i>b) Uniform or Gaussian plume models</i> <i>c) Generalized plume models</i> <i>d) Integral jet models</i> <i>e) Shallow layer models</i>
III	- Computational fluid dynamic (CFD) models	<i>a) Reynolds Averaged Navier-Stokes models (RANS)</i> <i>b) Direct Numerical Simulation models (DNS)</i> <i>c) Large Eddy Simulation models (LES)</i>

The models increase in complexity and vary according to the focus of application. With the exception of Class I models, generally, most dense gas models include an automatic internal transition to neutral Gaussian dispersion behaviour when the density effects become negligible [CCPS, 1999]. This transition is clear in Class II models, enabling modelling both heavy and passive gas dispersion behaviours along the dispersion process. Following, a brief description of the main characteristics and features of each class is provided, with a particular attention to class II models, which are the basis for the development of the model presented in this thesis.

Class I models can be considered the most simple, allowing determining the relation between the centreline concentration decay and the downwind distance of instantaneous and continuous dense gas releases in flat and grassy terrain. Mathematically, these models are based on the analysis of empirical relations of dimensionless quantities in the form of nomograms or simple correlations obtained from both field tests and wind tunnel tests [Blackmore, *et al.* 1982]. A well-known example of this class is the Britter and McQuaid model.

Class II models comprise a wide variety of intermediate and integral models, divided into five main types of models [MEG, 1994a]: (I) the so-called 'box models', (II) the uniform or Gaussian plume models, (III) the generalized plume models, (IV) the integral plume models, and (V) the shallow layer models. These models typically consider dense gas clouds by analyzing them in terms of a number of regimes. After the initial momentum- and buoyancy-dominated phases, the cloud is usually assumed to be passive.

'Box models' (Type I) have been developed to describe grounded dense gas puffs [McQuaid, 1984]. In general it is assumed that the instantaneously released cloud has a shape somewhat similar to an upright cylindrical box cloud with radius (R) and height (H) [Cox and Carpenter, 1980] as represented in Figure 2.8.

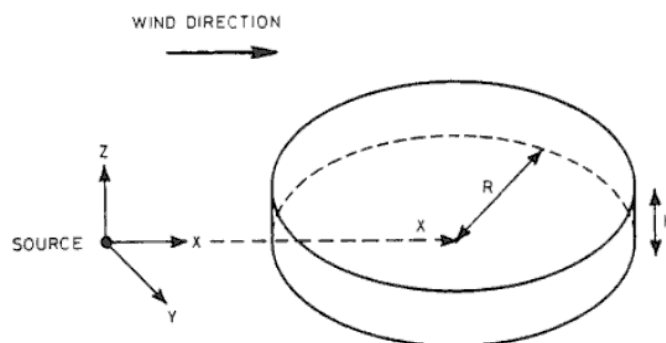


Figure 2.8 - Idealised cloud shape assumed in box models for instantaneous releases [based on Cox and Carpenter, 1980].

Traditional box models assume that all parameters (concentration, density, temperature, enthalpy difference, etc.) are uniformly distributed within the volume [Nielsen, 1994]. Basic ordinary differential equations representing the cloud horizontal spreading, mass and energy conservation, depending only on time, are applied to describe lateral and top entrainment of air (mass exchange) and plume heating. Horizontal spreading of cloud radius is assessed by estimating the self-generated gravitational front velocity [Britter and McQuaid, 1988]. Some variations have been implemented to account the dispersion in slopes [e.g. Webber, 1993, Kunsch and Webber, 2000] or the possibility to the cloud to become elliptical [Britter *et al.* 1991; Nikmo and Kukkonen, 1991], among others. Box model approach has also been extended in to simulate continuous or time-varying releases, in which the total release is divided into a number of cloud puffs, each of which is considered as a separate release and regular shape [e.g. Nikmo and Kukkonen, 1991].

Examples of box models include the DENZ-EDF model [Kaiser and Walker, 1978], the HEGABOX model [Witlox, 1994a], and other models described in the literature [e.g. Eidsvik, 1980; Fay and Zemba, 1985; Cleaver *et al.*, 1994; Kunsch and Fannelop, 1995].

Uniform or Gaussian plume models (Type II) are mainly used to predict the dispersion of continuous steady state grounded hazmat dense gas sources. All basic phenomena associated to dense gas release, such as horizontal spreading, mass exchange between the plume and surrounding environment or plume heating are described by ordinary differential equations similar to the ones used in box models. In uniform plume models, the cloud is assumed to have uniform height and width, concentration and temperature being described by a sort of rectangular box model sort of box model with the downwind development as sketched in Figure 2.9 [Morgan *et al.*, 1983]

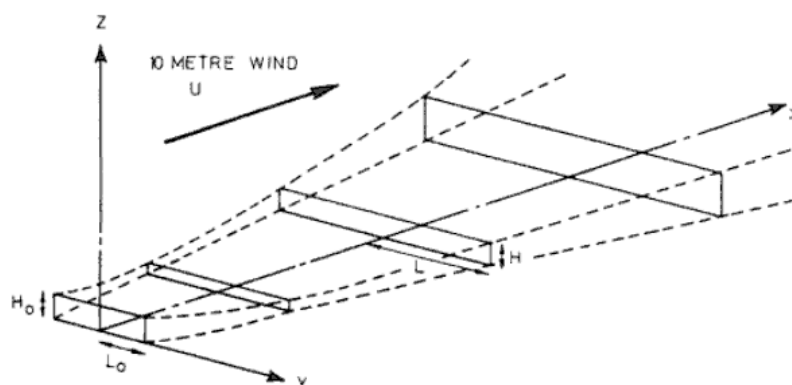


Figure 2.9 - Idealised cloud shapes assumed in uniform models for continuous steady state grounded releases [based on Cox and Carpenter, 1980].

On the other hand, the 'traditional' Gaussian profile is adapted in Gaussian plume models to consider some degree of variation of concentration in the cross section [Markiewicz, 2006]. In both uniform and Gaussian models, the increasing plume width is estimated by the front velocity at the two lateral edges and entrainment of air is described by the entrainment top velocity (top) and the front entrainment velocity (front). Transition between dispersion regimes is already implemented, assuming the traditional Gaussian approach and after reaching the passive plume dispersion behaviour in the far field.

The models described in works of Delvosalle *et al.* [1993], Fay and Zemba [1986] are examples of uniform plume models and the Indian Institute of Technology (IIT) dense gas model [Mohan *et al.*, 1995] is a well-known example of a Gaussian plume model.

Generalized plume models (Type III) can be considered an extension of Type II models in the sense that they consider a greater structure to the spatial variations of dense gas concentration than merely assuming a Gaussian or rectangular profile. Figure shows a schematized representation of Type III model dense gas cloud shape along the dispersion.

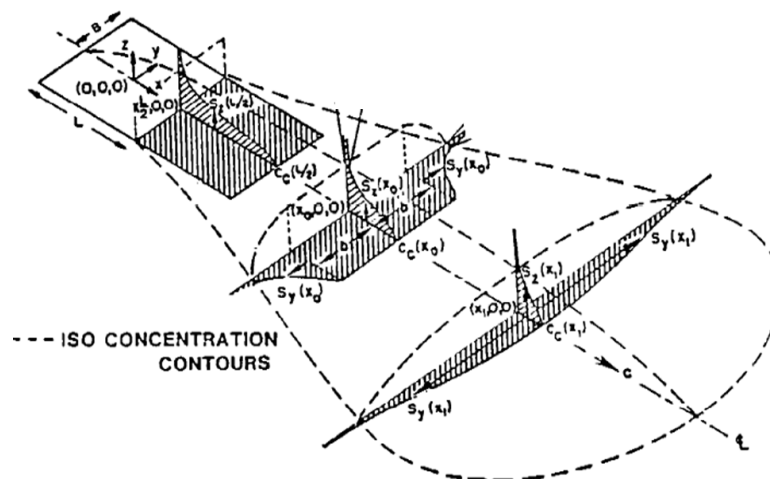


Figure 2.10 – Schematic representation of a Generalized plume model [based on Havens, 1988].

Basic equations describing the gas mass conservation, air entrainment, horizontal crosswind gravity spreading and crosswind diffusion are used to estimate the plume dispersion, in which, concentration is expressed in terms of the centreline ground level concentration, the vertical and horizontal dispersion parameters and plume width. The plume is represented as being composed by horizontally homogeneous cross sections with Gaussian profile edges in the horizontal direction and the exponential profile in the vertical direction as schematized in Figure 2.10. The average transport velocity in the plume is determined adopting a power law profile for the wind velocity and quasi-three-dimensional solutions are obtained by using

similarity profiles. The transition from heavy to passive gas dispersion is taken into account through a smooth or continuous evolution to passive regime based on density difference, eliminating the need of coupling different algorithms [Colenbrander *et al.*, 1980]. Once reached passive gas dispersion regime, the plume dispersion behaviour is performed according to a 'traditional' passive gas dispersion Gaussian model approach.

Examples of Type III models include the HEGADAS model [Witlox, 1994a,b], the DEGADIS model [Havens and Spicer, 1985], the GASTAR model [Britter, 1990] and the SLAB [Ermak, 1990] or even the ALOHA models [Reynolds, 1992].

Integral jet models (Type IV) are typically applied to describe dense gases continuous, elevated or upward momentum (vertical jets) sources, in which the released plume follows a 'ballistic' path before reaching the ground [Nielsen, 1998]. They are based on the integration of conservation equations of mass, species, downwind and crosswind momentum and energy averaged over a jet cross section. The equations directly predict jet variables, such as the concentration, jet velocity, radius or enthalpy, as a function of both downwind distance and time. In these models, the shape of the jet is not needed as a main variable. The jet path is mostly influenced by gravity, drag force of the ambient flow and momentum of the entrained air. Entrainment rate is different from that in the grounded release models, because it mainly depends on a velocity shear, the elevated jet, and the surrounding air. Examples of Type IV models include the HMP model [Hoot *et al.*, 1973], the Ooms model [Ooms, 1972], the AEROPLUME and HFPLUME models [Witlox and McFarlane, 1994], the model described by Muralidhar *et al.* [1995] and more recently the Khan and Abbasi model [1999b].

Shallow layer models (Type V) can be considered the most complex of Class II models, due to their ability to consider topography and build-up effects, as well as, the theoretical principles and modelling approaches [Venetsanos *et al.*, 2003; Markiewicz, 2006]. This type of models use depth-averaged equations obtained by the integration of conservation equations over the fluid depth to describe the flow behaviour based on shallow water equations [Hankin and Britter 1994; Venetsanos *et al.*, 2003]. Formally, shallow layer models describe the cloud by four main variables (cloud depth, two components of velocity (u,v), and cloud concentration) as a function of time and (two-dimensional) ground position [Hankin, 1997]. The cloud depth is defined in terms of vertical concentration distribution and variables are often referred to as depth averaged [Hankin and Britter, 1994]. It is assumed that pressure distribution is hydrostatic within the main body of the cloud; and dispersion mainly occurs due to special processes at the leading edge. Among others, examples of Type V models include the

SHALLOW model [Webber, 1993], the SLAM model [Ott and Nielsen, 1996], the TWODEE model [Hankin, 1997], the DISPLAY-2 model [Venetsanos *et al.*, 2003] or more recently the TWODEE-2 model [Folch, *et al.*, 2009] and the QUIC modelling system [Brambilla *et al.*, 2009].

With the continuous increase of hardware capabilities and the optimisation of numerical methods, Class III computational fluid dynamics (CFD) models have become an attractive tool to predict flow and concentration fields in complex topography and build-up areas [Costa, 2008]. These models allow determining the dispersion phenomena associated to instantaneous, continuous and transient hazmat gas releases. Furthermore, in contrast to previous classes, CFD models have the capability to description of the flow around obstacles in a 'more realistic way' [Duijm *et al.*, 1996; Cormier *et al.*, 2009; Schatzmann *et al.*, 2010] Fully 3-dimensional (3D) conservation equations provide precise information of spatial and temporal distribution of hazmat gas in complex topography and/or build-up environments, even close to the source. Class III models can be divided into three distinct types: (I) Reynolds Averaged Navier-Stokes equation (RANS), (II) Direct Numerical Simulation (DNS), and (III) Large Eddy Simulation (LES) modelling [Borrego *et al.*, 2004; Pontiggia *et al.*, 2009].

RANS model (Type I) is a CFD modelling technique that uses turbulence models to simulate the turbulent flow. This approach may be used with a finite element method to estimate the cloud in a 3D configuration. The most popular closure model for RANS models is the $k-\varepsilon$ two-equation model, since it has been proven to assure reasonable results and good stability [e.g. Luketa-Hanlin *et al.*, 2007; Costa, 2008]. Nowadays, RANS models are often used in industrial and engineering applications. Despite its known limitations, for instance the tendency to over-predict pollutants concentration in the far field under some atmospheric conditions, $k-\varepsilon$ model typically results into reasonable agreement with experimental information concerning mean flow and pollutant concentration [see Würtz *et al.*, 1996; Gilham *et al.*, 2000; Baik and Kim, 2002; Schatzmann and Leitl, 2002]. Currently, the DNS is very computationally demanding limiting its application to very simple cases [Pontiggia *et al.*, 2009]. An intermediate solution is represented by LES models. In this type of class III models, the time-dependent flow equations are solved for the mean flow and the largest eddies through the use of models for simulating the effects of isotropic dissipating eddies [Qin *et al.*, 2009].

Some of well-known CFD models commonly applied to dense gas dispersion include: the FEM3 model [Gresho *et al.*, 1983], FLUENT [URL2.2; Gavelli *et al.*, 2006], CFX [URL2.2; Sklavounos and Rigas, 2004], FLACS [URL2.3; Hanna *et al.*, 2004] or the VADIS model [Martins, 1998; Borrego *et al.*, 2004]. Whereas CFX and FLUENT models are general-purpose

CFD codes not specifically designed to model hazmat gas dispersion; both FEM3 and FLACS models have been specifically developed to model hazmat gas dispersion.

As shown in this section, there is a plethora of dispersion models of varying complexity that can be applied and implemented in CA studies. Currently, Class II models, particularly Types II - IV, are almost exclusively integrated in CA methodologies and Class III just starting to be applied [Hanna *et al.*, 2008]. For instance, ALOHA, DEGADIS, GASTAR or even SLAB models (Class II models) are being widely used in CA studies over the last two decades, given their convenience of fast computational run time and easiness use. Yet, their selection/application is not consensual and always allied with limitations or assumptions. Over the last years, numerous studies compared the performance of some Classes II and III models in CA studies [e.g. Nussey *et al.*, 1992; Würtz *et al.*, 1996; Hankin, 1997; Hankin, 2003; Hanna *et al.*, 2009; Schatzmann *et al.*, 2010] demonstrating the reasonability of Class II models to provide satisfactory results for dispersion in flat terrain cases where the main concern is ground level concentration fields along the downwind directions; whilst Type V of Classes II and Class III models are capable to produce reliable results, including complex and/or built-up areas.

Apart from the extensive use of Class II models (Types II - IV) in CA studies, their application neglecting the effects of complex terrain or presence of obstacles is becoming increasingly unacceptable due to the need to replicate as realist as possible hazmat gas cloud behaviours in industrial and built-up areas [Nussey *et al.*, 1992; Mannan, 2005]. Additionally, Class III RANS models are starting to be applied in CA studies given their multi-task capacity [Würtz *et al.*, 1996; Gilham *et al.*, 2000; Schatzmann and Leidl, 2002; Kim and Baik, 2003; Schatzmann *et al.*, 2010]. Nonetheless, the required computational efforts and level of expertise motivates the remaining use of Class II models, mainly by virtues of the associated low cost and expertise skills required, especially supporting limited time decision and emergency response. For that reason, is important to develop alternative models that maintain the simplicity of Class II models but enabling considering atmospheric dispersion in industrial and built-up areas, as realistic as possible.

A possible alternative is the 'commonly forgotten' Shallow layer (Class II Type V) models [Venetsanos *et al.*, 2003]. As explained before, these models are suitable to realistic assess the effect of complex topography on dense gas dispersion [Folch *et al.*, 2009]. This type of models also presents some disadvantages, especially more computational run time than Class II Types I - IV, but still significantly lower than Class III models. Moreover, based on the literature [e.g. Meroney, 1987; Britter, 1989; Ott and Nielsen, 1996; Hankin, 1997; Venetsanos *et al.*, 2003;

Brambilla *et al.*, 2009] Shallow layer models have some advantages over other Class II models. Recent developments emphasized the potential application in CA studies, given their capability to describe the release and account (in a relatively simple way) the influence of major obstructions on hazmat gas atmospheric dispersion in complex terrain and/or built-up areas [see Hankin, 2003; Brambilla *et al.*, 2009; Folch *et al.*, 2009]. Therefore, the development and implementation of new shallow layer models can represent an alternative to currently applied Classes II and III models, in an attempt to replicate hazmat gas dispersion in industrial and built-up areas with relatively low computational efforts.

2.3.3 Meteorological modelling

In addition to hazmat gas source term characterization, atmospheric dispersion modelling critically depends on the accuracy of atmospheric physical processes numerical description and especially the meteorology characterization. Aiming to understand the role of meteorology on pollutants dispersion, a wide number of studies have been conducted and models developed over the last decades [*e.g.* Monin and Obukhov, 1954; Turner, 1964; Hanna and Chang, 1992; Karppinen, 2001; Allwine *et al.*, 2002; Cimorelli *et al.*, 2004; Palau *et al.*, 2005; Monache *et al.*, 2009]. Overall, it is consensual that dispersion is particularly affected/controlled by meteorological conditions, particularly the wind (velocity and direction), atmospheric turbulence and the occurrence of inversion layers, ambient temperature and mixing height [Karppinen, 2001]. Consequently, a proper description of these meteorological and atmospheric boundary layer (ABL) stability conditions is of substantial importance for the performance quality of the atmospheric dispersion modelling element [Hewitt and Jackson, 2003; VROM, 2005a].

Bearing in mind that turbulence and mixing height parameters are not measured in routine monitoring stations (as wind velocity and direction or temperature profiles), they have to be inferred from the available measurements through the application of theoretical and mathematical methodologies (parameterisation schemes). These methodologies can be implemented in integrated or separated meteorological pre-processing models. Thus, even not considered a 'truly' CA modelling element, meteorological modelling must be also integrated and applied to assure a proper characterization of meteorological and ABL conditions for further atmospheric dispersion modelling. Taking into account the main purposes of application of CA modelling tools, meteorological models commonly used consist of diagnostic tools, which use mainly past, present or hypothetical meteorological data.

In spite of the wide variety of meteorological models currently available, the majority integrates the 'Monin-Obukhov Similarity Theory' (MOST) principles for the treatment of meteorological information and estimation of ABL scaling parameters. It is also common the use of the surface momentum and energy fluxes method originally suggested by van Ulden and Holtslag [1985], with a separated treatment for convective and stable conditions [see Monin and Yaglom, 1971; Karppinen, 2001; Cimorelli *et al.*, 2004]. In general, ABL scaling parameters (*e.g.* Monin-Obukhov length, surface friction velocity or surface heat flux) are estimated from routine or representative surface and upper air meteorological measurements. As regards to mixing heights, various mathematical schemes and approaches have been suggested and applied to determine ABL mixing heights during day and night periods [see Seibert *et al.*, 1998; COST 715, 2002; Baklanov *et al.*, 2006].

Despite the limitations discussed by Högström [1996], Seibert *et al.* [1998], Venkatram [2004], Zilitinkevich *et al.* [2007] or Monache *et al.* [2009], or even the new modelling similarity approaches proposed recently [see Laubach and McNaughton, 2009], McNaughton [2009] stated that MOST approach can work reasonably well, if not perfectly, with experimental field meteorological data. More realistic meteorological models, such as the 3D full-physical models (*e.g.* the Mesoscale Meteorological (MM5) [URL2.4] or Weather Research Forecast (WRF) [URL2.5] models) can be applied, however, the degree of complexity, expertise and run time still limits their application by analysts or emergency response.

2.3.4 Effects modelling

The assessment of consequences and damages from examined accident scenarios depends on the object of the CA study, providing reliable information of effects in human health, structures or the environment. For the purpose of assessing effects on human health, consequences can be expressed in the form of deaths or injuries [CCPS, 2000]. In case of physical structures, effects are expressed as damages or monetary losses. Environmental effects may be more complex, and can include impacts on animal life or plants, soil or water contamination, and other impacts. However, within the scope of CA studies in industrial activities, environmental effects are usually not taken into account [CCPS, 1999; VROM, 2005c], being examined in the frame of other studies, such as environment impact evaluation.

Over the last decades, several ways to quantify the effects from specific incidents have been developed and applied in CA studies [Mannan, 2005]. The most frequently used method of assessing the consequence of accidents is the 'Direct effects model' [CCPS, 1999], which estimates the effects on people and structures based on predetermined criteria (*e.g.* death or

crashes in a building). Contrarily to previous modelling approaches (source term or dispersion modelling), consequences cannot take the form of discrete functions [CCPS, 2000], given the variety and number of variables that must be considered (*e.g.* age, health conditions, period of exposure, resistance, etc.). Yet, depending on the type of accident, different modelling approaches have been developed and implemented in CA studies, for instance, the statistical methods of dose-response and probit functions, the toxic gas effects models, the thermal effects models or the explosion effects models [Mannan, 2005; VROM, 2005b,c]. Overall, the name of each reflects the type of incident and related consequences examined, with the exception of the statistical methods that can be applied for various incidents. Whereas thermal and explosion effects models predict the consequences on humans and structures from fires and explosions respectively; toxic gas effects models are applied when examined accidental release and atmospheric dispersion of hazmat gases. Despite the broad range of application, the statistical methods are mostly applied when PRA approaches are used in the CA study [VROM, 2005c]. Regardless the relevance of the various consequences models, in view of the main purpose of the present thesis, only toxic gas effects modelling approach is presented.

In general, toxic gas effects models are employed to assess the consequences to human health as a result of exposure to a known hazmat gas concentration for a known period of time [CCPS, 1999]. Direct comparison of estimated hazmat concentrations at specific locations against reference safety toxicological criteria (safety threshold limits) intends estimating the magnitude of potential effects on human health from the exposure. Within the frame of CA studies, effects models directly use concentration fields produced by the dispersion models.

Taking into account the nature of potential consequences from accidents involve the release of hazmat gases, only effects on human health and related safety threshold limits are considered [CCPS, 1999]. These safety threshold criteria are based on the combination of results from animal experiments, observations of long- and short-term human exposures, and expert judgement [CCPS, 2000]. Some of the widely used safety threshold limits, extensively described in the literature, include *Emergency Response Planning Guidelines for Air Contaminants* (ERPGs), *Threshold Limit Values* (TLVs), *Short-Term Exposure Limits* (STELs), *Permissible Exposure Limits* (PELs) or even the *Acute Exposure Guideline Limits* (AEGs) [Hanna and Drivas, 1987; Fingas, 2002; VROM, 2005b,c; Casal, 2008] among others considered in emergency response planning, occupational health and safety in industrial environments [AIHA, 2004; Casal, 2008]. Often, these criteria comprise different degrees/levels of consequences as a function of the exposure period (*e.g.* STEL 15 minutes or AEG-1 for 1 hour of exposure). In addition to toxicological consequences, flammability limits (LFL and upper flammability limit

(UFL)) can also be considered when potential occurrence of ignition is considered [Fingas, 2002; Casal, 2008]. Nonetheless, in the present thesis will only be focused the toxicological thresholds considered for the estimation of short-term pollution episodes.

Potential consequences can be estimated in various forms, depending on the degree of available information or purpose of application. The simplest comprise the estimation of areas potentially affected by concentrations above threshold limits. Direct comparison of predicted concentration-time fields' against reference limits is performed and outcomes are produced in the form of risk contours maps. More complex approaches enable the estimation of potential effects on humans by crossing information from detailed characterization of the accident concentration field and the population spatial distribution [Tavares *et al.*, 2010]. In this case, the quantification of effects is presented in the form of risk contour maps, hazardous cloud footprints as a function of time and effective number of people affected by concentrations above the examined threshold limits [CCPS, 2000; Ale, 2009; Pontiggia *et al.*, 2009]. Nonetheless, if detailed information on local population of vulnerable spots is available, the number of people potentially in risk to suffer health problems can be also estimated.

2.4 Synthesis

Since the mid-1970s, QRA methodologies 'emerged' worldwide with ever increasing importance as the 'scientific pillar' of regulatory, control and prevention instruments to quantify the impact, frequency/probability of occurrence, consequences and risks of technological hazards identified in hazardous industrial and transportation activities. 'Full QRA' studies comprise five main steps for the estimation of risks from identified and examined accident scenarios based on probabilistic and/or deterministic approaches and qualitative and/or quantitative techniques. Considering the estimation and assessment of consequences the central focus of QRA studies, new and more complex CA methodologies (overlapping QRA steps 2 and 4) have been developed and applied over the last years, strongly supported by numerical modelling tools.

The need to understand and numerically describe the various stages of accident scenarios involving the release and dispersion of hazmat gases, gave to numerical tools a unique value, and it possible to identify three main types of CA numerical modelling elements: source term, atmospheric dispersion and effects models.

Considering the wide variety of release conditions, a large number of source term models have been developed to account for the various types of failure and initial containment

conditions of the hazmat gas accidentally released, commonly defined by typifying accident scenarios. A plethora of different dispersion models of varying complexity (divided in three main classes) has been developed and integrated in CA methodologies over the last decades, to estimate concentration fields as a function of time. Currently, Class II models (integral and intermediate), particularly Types II - IV, are almost exclusively integrated in CA, and Class III (CFD models) are just starting to be applied. Contrarily to 'traditional' air quality modelling tools, CA dispersion models essentially comprise models able to predict the dispersion of dense gas in industrial and built-up areas. Additionally, meteorological modelling tools, in general based on the MOST principles, provide information to numerically describe the meteorological and ABL conditions during the release and dispersion phenomena. Finally, the magnitude and extension of predicted consequences/effects from the accident scenario hazards are estimated in the effects models, based on direct comparisons of estimated concentrations fields and reference toxicological criteria (exposure threshold limits).

Despite the extensive use of both simple (Class II Types II - IV) and more complex (Class III) models in CA studies, a remaining and major challenge to overcome their constraints and limitations, entails the development of intermediate (Class II) local-scale dispersion models, able to predict short-term pollution episodes from accidents involving the release of hazmat gases in industrial and/or built-up urban areas, in a more realistic but still simple way.

A possible alternative are the 'commonly forgotten' shallow layer (Class II Type V) models. These models are suitable to describe in a realistic, but still relatively simple way, the influence of complex topography and obstacles on hazmat gas dispersion. Even requiring more computational run times than other Class II models, this is significantly lower than Class III models, enabling their use in CA studies for industrial and built-up areas, as well as, to support decision and emergency planning and response in reasonable run time.

CHAPTER 3

3. DEVELOPMENT OF THE EFFECTS OF RELEASED HAZARDOUS GASES MODEL

This chapter presents the development of the *EFfects of Released Hazardous gAses* model (EFRHA), specifically designed to predict short-term pollution episodes from accidental releases of hazmat gases into the atmosphere in industrial and built-up areas. Its general structure, modules and main input/output data are described. Main features of implemented modelling algorithm techniques and approaches to numerically describe the various stages of the release and atmospheric dispersion of hazmat gases, as well as, the influence of environmental conditions are also addressed.

3.1 General structure of the EFRHA model

With the purpose of overcoming some of recognized constrains of Class II models/software packages currently applied in CA studies, the PC-based EFRHA model (written in the FORTRAN® 95 programming language) was developed for the estimation of short-term pollution episodes and consequences from accident scenarios involving the release and dispersion of hazmat gases in industrial and urban areas. Intended to be used by expert modellers, analysts and industrialists, but also, by less specialized regulatory and emergency or safety operators, the design of EFRHA model kept a compromise between the simplicity of Class II dispersion models and an increased modelling capability to account the influence of obstructions (complex terrain and/or obstacles) on hazmat gas atmospheric dispersion. Also, aiming to facilitate its use, up-to-date numerical methods usually applied separated in the various CA modelling elements and relevant databases were implemented, reducing the requirements of input and 'interim' data. As a result, a minimum number of strict mandatory user defined information was established, simplifying the complexity and effort on preparing/collecting input data, but also, enabling the application of the developed model, especially when limited input information is available, particularly if not easily accessible by the potential user.

Considering the overall structure (see Figure 2.2) and requirements of CA studies and the process stages and modelling elements, the EFRHA model is designed to run as a five sequential steps modules: (1) Meteorological Module (EMM); (2) Terrain Module (ETM); (3)

Source Term Module (ESTM); (4) Dispersion Module (EDM); and finally (5) Effects Module (EEM), as schematized in Figure 3.1a. The organization of the modules follows the needs of information processing flow, to properly describe the source term and hazmat gas dispersion phenomena based on the defined accident scenario conditions, without forgetting the influence of surrounding environment, according to the structure presented in Figure 3.1b. Figure B.1 (Appendix B) shows a more detailed scheme of organization of the implemented modules and data used/produced in each.

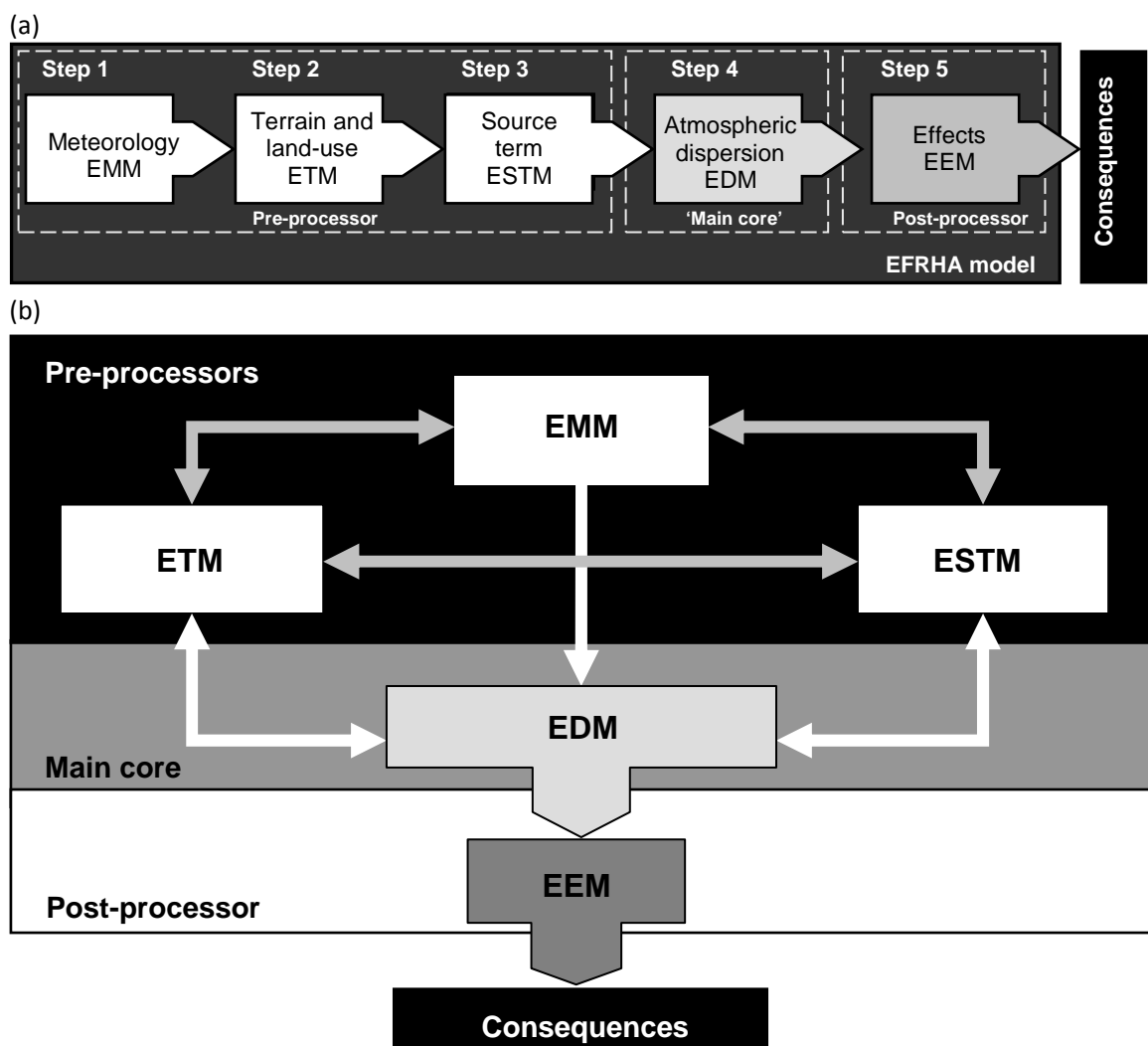


Figure 3.1 - EFRHA model: (a) organization of the steps modules, and (b) basic structure with data flow along the simulation process.

Even considering EDM the main core of the EFRHA model, additional related models have been implemented in the developed model in the form of pre- (EMM, ETM and ESTM) and post- (EEM) processors. The calculation starts with the treatment of meteorological input data and the estimation of ABL scaling parameters in the EMM. Topographical and obstacles input

information is processed and wind fields generated in ETM. Next, ESTM estimates the hazmat gas mass flow rate applying well-established source models according to the defined accident scenario characteristics. Atmospheric dispersion of the released hazmat gas in industrial and built-up areas is numerically described in EDM using an up-to-date Class II Type V modelling approach. Finally, potential consequences and effects on human health are determined in EEM based on direct comparisons of predicted concentrations temporal and spatial distribution against standard safety threshold limit values.

Modelling schemes used in the simulation directly depend on various criteria, such as, the main purpose of the CA application, selected input modelling options, available information or type of the accident scenario evaluated. Detailed datasets of meteorological, terrain (surface, land-use and obstacles) and source information/parameters must be generated and/or provided along the modelling process to properly estimate the consequences of exposure to short-term pollution episodes from hazmat gas accidental release into the atmosphere in industrial and/or built-up areas. Nonetheless, the developed model is structured to simplify the definition of input information and data flow along the various modules, maintaining continuous verification of generated and transferred data, as well as, access to internal databases.

Unlike most CA models or software packages currently applied in CA studies, the developed model is prepared to bypass 'pre-processing' modules, if correspondent outputs (EFRHA's interim information) have already been estimated. For instance, if the same meteorological data is considered for various accident scenarios, EMM only needs to be run in the first simulation and therefore bypassed in the following, if it is assured the completeness of generated interim information and is accessible by the user. This option is of particular interest, especially in case of multiple runs under the same environment conditions, reducing the process time.

In order to avoid errors or erroneous results (especially in interim modelled information), a continuous evaluation and consistency check procedure/test is implemented in the algorithm to assure that processed information (either input and output) is valid, *i.e.*, within ranges of recommended valid data limits. Two main consistency check procedures are implemented in all the modules and model main algorithm to verify if processed data is valid to continue the simulation without producing erroneous outputs. The process is based on direct comparisons of input/output data against acceptance limits, according to modelling requirements and

recommendations available in the literature [e.g. Britter, 1990; USEPA, 2004a,b; TNO, 2005; VROM, 2005a; Borrego *et al.*, 2009].

Following, mathematical methods and modelling approaches implemented in the various modules of the EFRHA model are presented, justifying the selection and adopted approaches and assumption.

3.2 EMM – EFRHA Meteorological Module

The EMM is designed to process meteorological data and numerically describe the ABL conditions, in the form of ABL scaling and mixing height parameters, during the period of simulation, according to the structure presented in Figure 3.2.

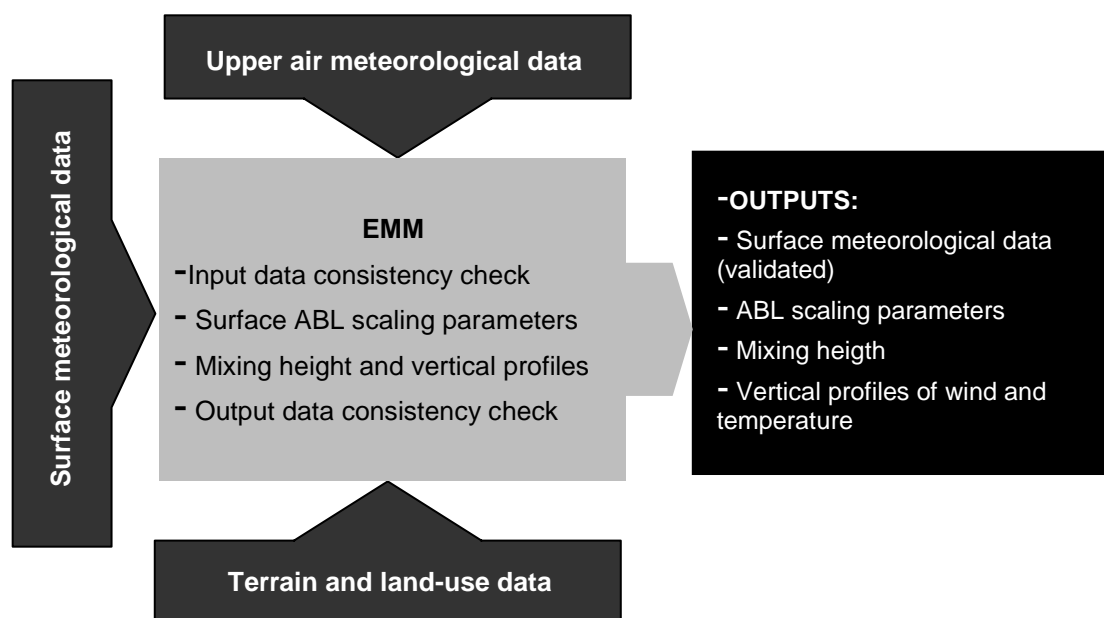


Figure 3.2 – Schematic representation of EMM structure and data flow.

Unlike most CA models/software packages, the user does not have to provide all input meteorological parameters, especially the ones rarely measured in routine meteorological monitoring stations and which the estimation may require a certain degree of expertise (e.g. ABL scaling parameters).

The minimum input data requirements of EMM include measurements from an onsite or representative surface monitoring station and terrain surface and land-use characteristics. If the period of simulation includes daytime and/or after daytime hours, it is necessary to provide, at least, the early morning upper air radiosonde data. The complete list of input meteorological data considered by EMM is listed in Table B.1 (Appendix B). Apart from the

recommended use of the strict mandatory list of input parameters, the module is also prepared to 'read' both input and output meteorological parameters previously estimated by EFRHA or other meteorological model (e.g. mesoscale weather forecast models).

In any case, direct comparisons of input and output data with acceptance limits established in accordance with the literature and meteorological models currently available [e.g. Reynolds, 1992; Cambridge Environmental Research Consultants (CERC), 2002; USEPA, 2004b; TNO, 2007] are performed, following the philosophy of continuous consistency data check. Moreover, although 'traditional' CA studies apply representative average and 'constant' meteorological conditions for the entire period of simulation, EMM is designed to process meteorological information for short and long periods of recorded data of varied temporal resolution. This capability is of significant importance for ESTM and EDM calculation processes.

The EMM modelling approach is based on the quantitative MOST approach through the integration of the commonly applied surface momentum and energy fluxes relationships method, with a separated treatment for convective and stable conditions [Ulden and Holtslag, 1985; Cimorelli *et al.*, 2005]. It is assumed that mean wind and temperature profiles and turbulent velocities in the ABL can be completely determined by scaling lengths (surface roughness length (z_0), displacement length (d) and L), and scaling velocities – surface friction velocity (u^*) and the convective velocity scale (w^*) [see Deardorff, 1970 Seinfeld *et al.*, 2006]. It is also considered that fluxes are constant with height and the mean wind follows a logarithmic profile, with an adjustment for diabatic flows [Hanna and Britter, 2002].

During the period of simulation, meteorological and turbulence conditions are numerically described by estimated ABL scaling parameters, according to the two stages calculation process schematized in Figure 3.3.

The first stage comprises the determination of the period of the day (day or night time period), prevailing stability conditions (convective or stable) and the estimation of the following ABL scaling parameters: L , u^* , sensible heat flux (H) and potential temperature scale (θ^*).

At a first analysis, the period of the day is determined based on the estimation and comparative analysis of solar elevation angle (ϕ_s) and critical solar angle (ϕ_{crit}) at the moment of meteorological data. The estimation of ϕ_s is based on the general method described in VROM [2005a], whereas ϕ_{crit} is estimated as presented by Cimorelli *et al.* [2004]. If $\phi_s > \phi_{crit}$, it is

considered to be at daytime; otherwise it is assumed night time. This initial process is of significant importance for further estimation of ABL mixing heights in stage 2.

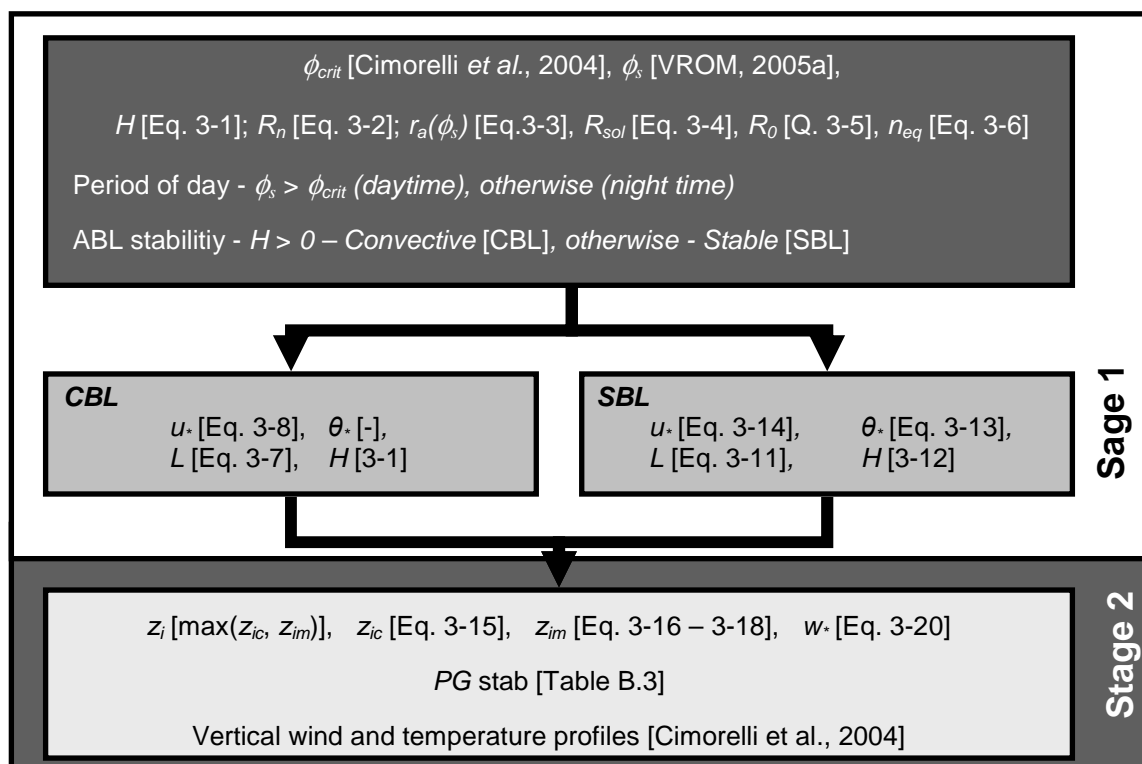


Figure 3.3 - General calculation equations flowchart of EMM.

Taking into account that different approaches are applied for stable and convective conditions, prevailing stability conditions are also determined by the estimation of H (Eq. 3-1), assuming that $H < 0$ - stable; $H > 0$ - convective and $H = 0$ - neutral [Seinfeld *et al.*, 2006]. The expression to estimate H was derived by Holtslag and van Ulden [1983] from the energy balance at the earth's surface for rural sites, using the Oke's [1978] approach at the earth's surface for rural sites, as follows:

$$H = \frac{0.9R_n}{\left(1 + \frac{1}{B_o}\right)} \quad \text{Eq. 3-1}$$

In which R_n is the net radiation and B_o is the Bowen ratio. The B_o is an indicator of surface moisture, and expresses the ratio between the H to the latent heat flux. Standard default values of B_o are widely compiled in the literature [e.g. Paine, 1987; Seinfeld *et al.*, 2006], ranging from less than 0.001 m over a calm water surface to 1 m or more over a forest or urban area, depending on land use type, season, moisture conditions and period of day, among other criteria. In EFRHA, the B_o is processed in ETM as further described (see Section 3.3).

If measurements of R_n are not available, it is estimated from the insolation and the thermal radiation balance at the ground following the method of Holtslag and van Ulden [1983] as:

$$R_n = \frac{[1 - r_a(\phi_s)]R_{sol} + c_1 T_a^6 - \sigma_{SB} T_a^4 + c_2 n}{1 + c_3} \quad \text{Eq. 3-2}$$

In which $c_1=5.31 \times 10^{-13} \text{ W.m}^{-2}.\text{K}^{-6}$, $c_2=60 \text{ W.m}^{-2}$ and $c_3=0.12$ are constants, $r_a(\phi_s)$ is the albedo as a function of ϕ_s , R_{sol} is the incoming solar radiation, $\sigma_{SB}=5.67 \times 10^{-8} \text{ W.m}^{-2}.\text{K}^{-4}$ is the Stefan-Boltzmann constant, T_a is the reference ambient temperature and n the fractional cloud cover.

$$r_a(\phi_s) = r_a' + (1 - r_a') \exp[-0.1\phi_s - 0.5 \times (1 - r_a')^2] \quad \text{Eq. 3-3}$$

where r_a' is the $r_a(\phi_s=90^\circ)$ for the sun on the meridian, which is specific for the surface characteristics of the site. In the open literature standard default values for $r_a(\phi_s)$ is available and recommended [USEPA, 2004b].

If R_{sol} is not available in input data, it is computed from ϕ_s , n and the incoming solar radiation for clear skies (R_0) following the Kasten and Czeplak [1980] expressions, given by:

$$R_{sol} = R_0 (1 - 0.75n^{3.4}) \quad \text{Eq. 3-4}$$

$$R_0 = 990(\sin \phi_s) - 30 \quad \text{Eq. 3-5}$$

If measurements of n and R_{sol} are not available, a default value of $n=0.5$ is assumed in Eq. 3-2 and Eq. 3-4; however, if observations of R_{sol} are available, an equivalent fractional cloud cover (n_{eq}) is calculated from Eq. 3-6, such that

$$n_{eq} = \left(1 - \frac{R_{sol}/R_0}{0.75}\right)^{3.4} \quad \text{Eq. 3-6}$$

Finally, if $H < 0$ it is assumed that the atmosphere is stable, otherwise convective stability conditions are considered. In case of different results obtained by the previously describe methods, prevails the result of the estimation of H .

Known the relation between ABL stability and H , the implemented approaches and expressions used to estimate L and u^* and θ^* are 'selected' depending on the determined stability condition [Venkatram, 2004]. In case of atmospheric convective or unstable conditions (CBL), the L and u^* are estimated using Eq. 3-7 and 3-8 to 3-10; otherwise, under stable conditions (SBL) the L , u^* and θ^* are estimated using the set of Eq. 3-11 to 3-14; as schematized in Figure 3.3.

According to the MOST approach, the effects of ABL stability on the wind profile can be completely determined by L [Hanna and Britter, 2002], which provides a measure of stability and can be interpreted as the height above the ground where turbulence generated by wind shear equals the turbulence dissipated by the heat flux [Wyngaard, 1988], estimated as:

$$L = \frac{-\rho_a C_{pa} T_a u_*^3}{k g H} \quad \text{Eq. 3-7}$$

In which $g=9.8 \text{ m.s}^{-2}$ is the gravitational acceleration, $k=0.41$ is the von Karman constant, C_{pa} is the specific heat capacity of air at constant pressure, and T_a is the reference ambient temperature representative of the surface ABL. Eq. 3-6 shows that L depends directly from the estimation of both H and u_* . Therefore, the estimation of L and u_* is performed simultaneously through an iterative process. The methods implemented for the estimation of these ABL scaling parameters differ according to ABL stability conditions, as further presented.

During CBL conditions, u_* and L are computed through a surface similarity iterative method (Eq. 3-7 to Eq. 3-10) until the convergence less than 1% is reached. In this case it is used the value of H initially estimated from Eq. 3-1. The iterative method is initialized assuming neutral conditions (*i.e.*, $L = \infty$), $\Psi_m = 0$, and $u = u_{ref}$. In each step, u_* is computed by the expression of Panofsky and Dutton [1984] as follows:

$$u_* = \frac{k u_{ref}}{\ln(z_{ref}/z_0) - \Psi_m \{z_{ref}/L\} + \Psi_m \{z_0/L\}} \quad \text{Eq. 3-8}$$

In which u_{ref} is the wind velocity at reference measurements height z_{ref} , and z_0 is the roughness length. The integrated forms of the similarity functions Ψ_m 's are evaluated by Panofsky and Dutton [1984] as:

$$\begin{cases} \Psi_m \left\{ \frac{z_0}{L} \right\} = 2 \ln \left(\frac{1 + \mu_0}{2} \right) + \ln \left(\frac{1 + \mu_0^2}{2} \right) - 2 \tan^{-1} \mu_0 + \frac{\pi}{2} \\ \Psi_m \left\{ \frac{z_{ref}}{L} \right\} = 2 \ln \left(\frac{1 + \mu_1}{2} \right) + \ln \left(\frac{1 + \mu_1^2}{2} \right) - 2 \tan^{-1} \mu_1 + \frac{\pi}{2} \end{cases} \quad \text{Eq. 3-9}$$

with μ_0 and μ_1 calculated from:

$$\begin{cases} \mu_0 = (1 - 16 \cdot z_0 / L)^{1/4} \\ \mu_1 = (1 - 16 \cdot z_{ref} / L)^{1/4} \end{cases} \quad \text{Eq. 3-10}$$

Alternatively, under SBL conditions u^* and L are estimated recurring to a simpler empirical approach suggested by Venkatram [1980], because Oke's [1978] approach used for the estimation of H (Eq. 3.1) is unreliable in the SBL conditions.

The L can be expressed as:

$$L = \frac{T_a}{kg\theta^*} u_*^2 \quad \text{Eq. 3-11}$$

Venkatram [1980] observed that an empirical relationship (Eq. 3-12) can be established between θ^* and H given by:

$$\theta_* = -\frac{H}{(\rho_a C_{pa} u_*)} \quad \text{Eq. 3-12}$$

In stable conditions, the θ^* can then be calculated from the empirical form considering the cloud cover [van Ulden and Holtslag, 1985] as:

$$\theta_* = 0.09(1 - 0.5n^2) \quad \text{Eq. 3-13}$$

As regards to u^* , it is considered the Panofsky and Dutton [1984] expression for the wind velocity profile:

$$u = \frac{u_*}{k} \left[\ln\left(\frac{z}{z_0}\right) + \frac{\beta_m z_{ref}}{L} \right] \quad \text{Eq. 3-14}$$

where $\beta_m = 5$. Substituting Eq. 3-11 into Eq. 3-14 and modifying the expression is obtained a quadratic solution that simplifies the estimation of u^* [Venkatram, 2004]. The solution for L , u^* and θ^* is then found through an iterative process by the continuous application of the Eq. 3-11 to Eq. 3-14 [Hanna and Chang, 1993]. Reached the acceptable degree of convergence lower than 1%, H is estimated from Eq. 3-11 and final value of L is estimated from Eq. 3-10. Detailed description of the implemented methodology for stable conditions is presented in Cimorelli *et al.* [2005].

Next, surface energy flux balance and mixed-layer parameters are estimated in the second stage, in the form of ABL mixing height (z_i), convective (z_{ic}) and mechanical mixing heights (z_{im}), the w^* and vertical profiles of meteorological parameters. The estimation of z_i depends on both z_{ic} and z_{im} , as a function of the prevailing ABL stability conditions. During CBL conditions, z_i is considered to be the larger of z_{ic} and z_{im} ; whilst under SBL conditions, mechanical processes are dominant and z_i is directly estimated by the estimated z_{im}

[Venkatram, 2004]. In an attempt to facilitating the application of EFRHA model even in case of limited input meteorological information, two distinct modelling techniques are implemented in EMM for the estimation of ABL mixing height parameters (z_i , z_{ic} , z_{im} and w^*) depending on the availability of early morning upper air data for the period of time considered.

If early morning upper air data is available, CBL conditions are considered and no measurements of the mixing height are input, z_{ic} is calculated with the simple one-dimensional energy balance model developed by Carson [1973] and modified by Weil and Brower [1983] given by:

$$z_{ic} \theta\{z_{ic}\} - \int_0^{z_{ic}} \theta\{z\} dz = (1 + 2A) \int_0^t \frac{H\{t'\}}{\rho_a C_{pa}} dt' \quad \text{Eq. 3-15}$$

In which θ is the potential temperature, $A = 0.2$ and t is the record hour after sunrise, requiring the continuous contribution of H along the daytime period. In case of additional upper air vertical profiles are available during daytime EMM is prepared to continuously use this information to correct the estimated parameters time evolution.

On the other hand, if early morning upper air data is not available, the default standard values listed in Table B.3 (Appendix B) suggested by the European ARIA-EIA project [URL3.1] are considered for the estimation of z_{ic} and therefore z_i during daytime periods. The selection of the z_{ic} value is based on the well-established Pasquill-Gifford (PG) stability classes determined from the ranges of L values relations suggested in the literature [see Seinfeld *et al.*, 2006], as presented in Table B.3 (Appendix B). Despite the clear uncertainties associated to this assumption, the implementation of this methodology intends overcoming the 'common' limitation and allowing the estimation of consequences from the accident scenario analyzed even in case of limited input information.

As regards to z_{im} , EMM integrates different approaches depending on ABL stability conditions. Under SBL conditions, z_{im} is estimated by the lower of the expressions suggested by Zilitinkevich [1972] (Eq. 3-16) and Venkatram [1980] (Eq. 3-17) as mentioned in Seibert *et al.* [1998] and COST 715 [2002] given by:

$$z_{im} = 0.4 \left(\frac{u_* L}{f} \right)^{1/2} \quad \text{Eq. 3-16}$$

$$z_{im} = 2300 \times u_*^{3/2} \quad \text{Eq. 3-17}$$

where f is the Coriolis parameter.

During CBL conditions, z_{im} is estimated using the expression suggested by Venkatram [1980] (Eq. 3-17) [Cimorelli *et al.*, 2005]. To avoid estimating sudden and unrealistic drops in the shear-induced turbulent layer, the time evolution of z_{im} is computed following Venkatram [1982] approach in which the current 'corrected' value of $(z_{im}(i))$ is 'smoothed' based on previous record $(z_{im}(i-1))$ given by:

$$z_{im}(i) = z_{im}(i-1) \times e^{(-\Delta t/\tau)} + z_{im}(i) [1 - e^{(-\Delta t/\tau)}] \quad \text{Eq. 3-18}$$

In which the time scale τ is estimated by:

$$\tau = z_{im}(i-1) / (2u_*(i)) \quad \text{Eq. 3-19}$$

In the estimation of τ , while $z_{im}(i-1)$ corresponds to previous record, $u_*(i)$ is the estimated value for the current record [Cimorelli *et al.*, 2004].

Finally, w_* , used to characterize the convective portion of the turbulence during CBL conditions [Wyngaard, 1988], is calculated as follows:

$$w_* = \left(\frac{gH z_{ic}}{\rho_a C_{pa} T_a} \right)^{1/3} \quad \text{Eq. 3-20}$$

Vertical profiles of temperature and wind velocity are determined using the similarity parameterizations and power law profile approaches described by Karppinen [2001] and Cimorelli *et al.* [2005].

Overall, implemented ABL scaling parameters modelling approaches enable an accurate, but at the same time simple and fast-run technique to provide reliable information for subsequent modules. In order to assure that reliable interim meteorological and ABL scaling parameters are provided to subsequent modules, a consistency check is performed covering all estimated meteorological and ABL scaling and mixing height parameter.

In case of bypass, or direct provision of output parameters values (*e.g.* from previous runs), EMM checks the consistency of the complete set of 'input parameters'. An alternative procedure to the EMM bypass option is to derive the necessary meteorological data from weather forecast models (*e.g.* MM5 [Dudhia *et al.*, 2001] or WRF [Michalakes *et al.*, 2004] forecast models) or previous EFRHA model meteorological simulations available for the same location and period of time and directly provide the complete list of input data considered in EFRHA meteorological input file.

3.3 ETM – EFRHA Terrain Module

The ETM aims processing topographical, land-use and obstacles data, as well as, the spatial distribution of receptors and sources within the simulation domain area 'boundaries'. Apart from input and output data consistency check procedures, the ETM is structured in two main stages of data process: (i) surface and land-use characteristics, and (ii) estimation of average wind fields. Figure 3.4 shows the basic structure of the ETM and data flow.

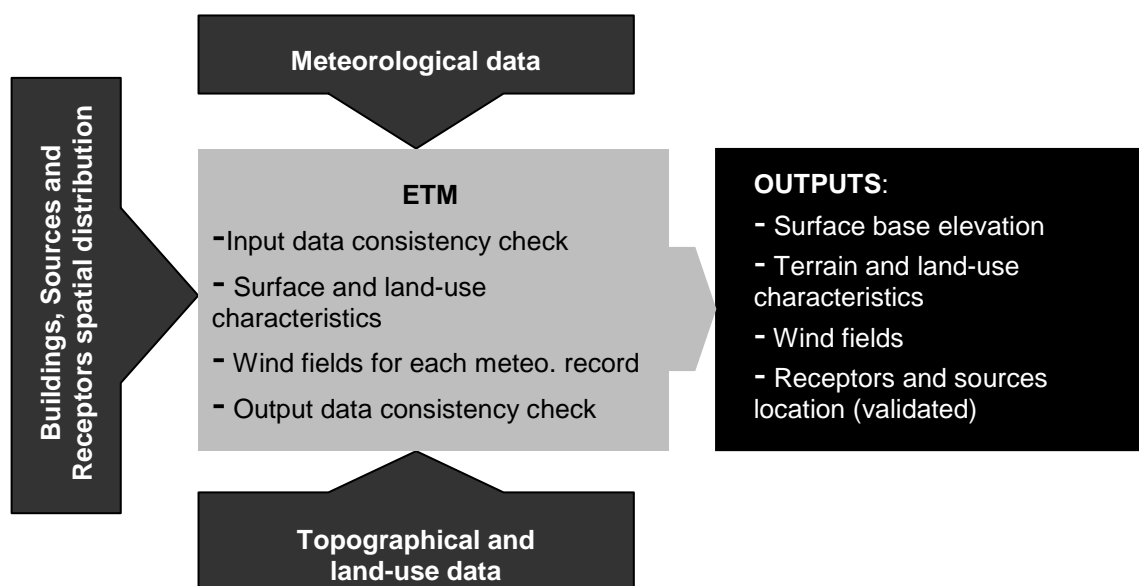


Figure 3.4 – ETM basic structure with the different stages of process.

ETM main inputs comprise information concerning the spatial distribution of receptors, sources and buildings, surface and land-use information and meteorological information.

Attempting to integrate up-to-date Geographical Information System (GIS) tools formats or other types of information, this module relies on a regular Cartesian coordinate system where true north is always upward in the positive y and east is always to the right in the positive x directions, independently to wind direction as illustrated in Figure 3.5.

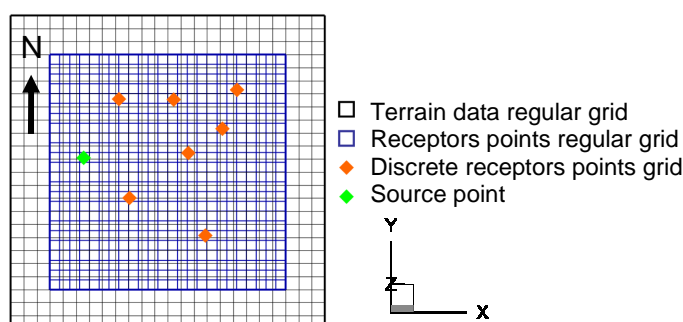


Figure 3.5 – Schematic representation of terrain, receptors and source gridded data used in EFRHA.

Regular and discrete gridded terrain data can be used to characterize both terrain (terrain topography and land-use) and receptors spatial distribution. Sources are defined by the spatial location of the source centre point initially defined by the user and dimensions are further defined according to the type of accident and outflow conditions (see Section 3.4). Additionally, if relevant obstructions (*e.g.* buildings) are considered, their spatial distribution and geometries are also input, directly by the user or through preliminary data process procedures using GIS software with the terrain topography information. Spatial distribution and dimensions of receptors grids, sources and obstacles (if present) are checked against terrain domain gridded data and 'boundaries', to guarantee the reliability and completeness of processed data for the correct data treatment and further transfer to EDM.

The first stage of ETM comprises the treatment of input land-use and terrain surface base elevation data. Land-use is characterized by the z_0 , B_0 and $r_a(\phi_s)$ values. Estimated, measured or even default values available in the literature based on the type of land-use and period of the year [*e.g.* USEPA, 2004b; Seinfeld *et al.*, 2006; Turner and Schulze, 2007] can be used to characterize the study area surface, defined by one of two alternative approaches.

If detailed information for the gridded terrain domain area is available (*i.e.* spatial distribution of the analyzed parameters), values for terrain base elevation, z_0 , B_0 and $r_a(\phi_s)$ in each receptor point are determined by interpolation from the closest terrain grid point's data. Alternatively, if limited information of spatial distribution is available, or is relatively uniform, predominant terrain features can be supplied for various wind direction sectors (up to 16 sectors) about the major variations in terrain and land-use characteristics. Values for z_0 , B_0 and $r_a(\phi_s)$ in each receptor point are determined based on the wind direction recorded during the period of simulation and correspondent sector.

As regards to the effective surface elevation at receptors locations, the interpolation of terrain surface elevation height values in each receptor from the closest terrain grid point's data is performed (from a reference base level elevation).

Next, average wind fields are estimated for the simulation domain to account, in a more realistic way, the influence of terrain and obstructions on hazmat gas dispersion behaviour. Two distinct situations are considered in ETM:

- (i) Flat terrain without any obstruction,
- (ii) Complex or obstructed terrain.

While in the first a uniform wind flow is considered, using only the mean wind direction measured in each meteorological record; in case of obstructed, a spatially variable wind field for each meteorological record must be estimated. In order to account the presence of obstructions, but at the same time maintaining the somewhat straightforwardness of EDM modelling approach, quasi-steady-state average gridded wind fields are estimated based on the Diagnostic Wind Model [Douglas and Kessler, 1990] principles for each meteorological record. Mean wind fields are adjusted based on the obstructions spatial distribution and a divergence minimization is performed to ensure mass conservation [Folche *et al.*, 2009]. This option is also prepared to process multiple wind fields records based on the meteorological records initially defined by the user. In addition to the capability to account, in a relatively simple way the presence of obstructions, it also enables considering variation of wind direction during the period of simulation, independently if obstructions are considered or not.

3.4 ESTM – EFRHA Source Term Module

Aiming to numerically describe the hazmat gas release phenomenon, the ESTM comprises a set of up-to-date source models recommended for the wide variety of accident situations commonly analyzed in CA studies. Taking into account the number and types of source models, ESTM is divided in four sub-modules based on the initial hazmat physical state and scenario conditions: (i) ESTM1 – compressed gas, (ii) ESTM2 – non-boiling liquid, (iii) pressurized liquefied gas, and (iv) evaporation of liquid pool, as schematized in Figure 3.6.

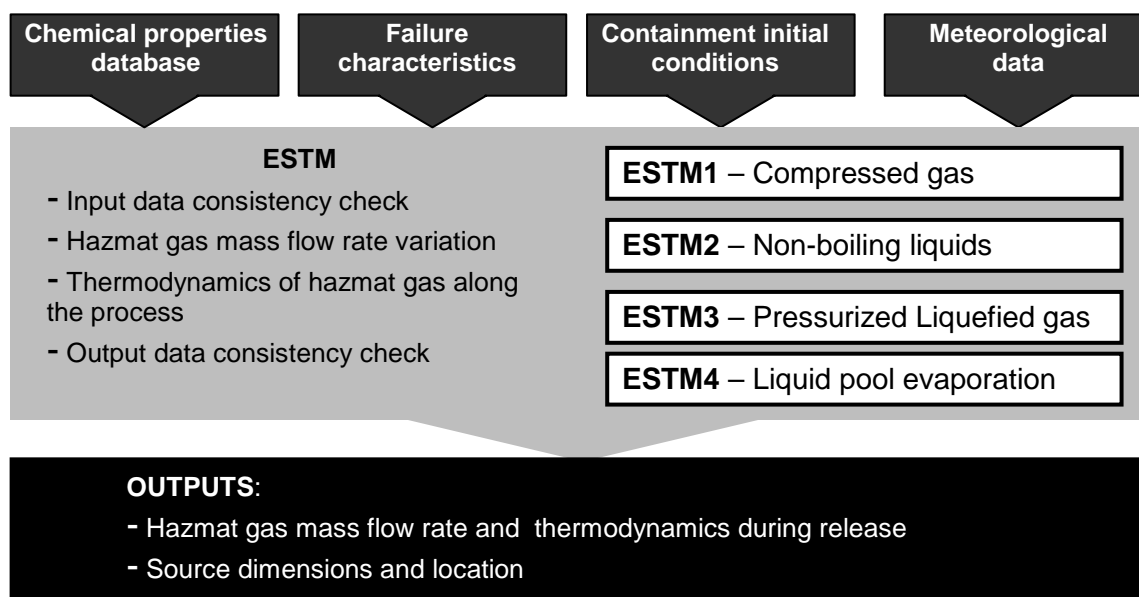


Figure 3.6 – ESTM basic structure with data flow.

Three distinct initial physical states can be considered: pure gas (from compressed gas or vapour fraction of PLG), pure liquid (from non-boiling liquids or liquid fraction of PLG) and two-phase mixtures (mixtures of vapour and liquid from PLG) [Green and Perry, 2008]. Depending on the initial physical state, varying degrees of calculation ‘complexity’ are implemented, as further described.

In any case, to assure a proper characterization of hazmat initial containment conditions for the selected scenario, an initial consistency check of user defined input information and internally estimated chemical properties is conducted prior the ‘selection of the sub-module’. Input information concerning initial containment conditions, failure type/mode (*i.e.* the way the release takes place) and chemical properties parameters is directly compared against ranges of recommended acceptance limits [see Britter 1990; TNO, 2007; Reynolds, 1992]. Additionally, in view of guaranteeing the selection of the most appropriated modelling approach, the ‘real physical state’ of the hazmat prior the release is verified by means of the criteria listed in Table 3.1.

Table 3.1 – Thermodynamic states [VROM, 2005a].

Physical state	Thermodynamic conditions
Compressed gas	$T_0 > T_c$ or $P_0 < P_v^0(T)$
PLG	$P_0 = P_v^0(T)$
(non-boiling) liquid	$T_{melt} < T_0 < T_B$

Initial hazmat storage/transport temperature (T_0) and pressure (P_0) are directly compared with correspondent critical temperature (T_c), boiling point temperature (T_B), melting point temperature (T_{melt}) and the estimated saturated vapour pressure ($P_v^0(T)$) to confirm/define the ‘real’ hazmat physical state prior to the release and then select the most appropriated source model. In view of considering the most common release scenarios examined in CA studies, the set of outflow conditions listed in Table 3.2 distributed by the four main sub-modules can be processed by ESTM, as a function of the initial hazmat physical state.

According to Table 3.2, ESTM is designed to estimate the mass flow rate of: pure gas (from compressed gas or vapour fraction of PLG); pure liquid (non boiling liquid or liquid fraction of PLG); and two-phase mixtures (vapour and liquid mixtures PLG) release scenarios. Whereas for ‘pure gas’ releases, the calculation process is more or less straightforward, considering directly the estimated mass flow rate; ‘pure liquid’ outflows require the estimation of the liquid spill outflow and further evaporation rate (if applicable). A more

complex approach is required for two-phase outflows from PLG depend in the liquid and/or vapour fraction.

Table 3.2 - ESTM sub-modules and integrated release scenarios.

Sub-module	Initial physical state	Outflow condition
ESTM1	Compressed gas (q_s)	<ul style="list-style-type: none"> - Totally collapsed vessel - Vessel through small leak from <ul style="list-style-type: none"> a) hole in vessel wall b) hole in vessel piping - Full bore ruptured pipeline - Pipeline through small leak - Full bore ruptured piping system - Piping system through small leak
ESTM2	Non-boiling Liquids (non-boiling or refrigerated) (q_{sl})	<ul style="list-style-type: none"> - Totally ruptured vessel - Vessel through small leak <ul style="list-style-type: none"> a) hole in vessel wall b) hole in vessel piping - Full bore ruptured pipeline
ESTM3	PLG (saturated and refrigerated) (q_{sF}, q_{sV}, q_{sL})	<ul style="list-style-type: none"> - Totally ruptured vessel - Vessel through small leak <ul style="list-style-type: none"> a) hole in vessel wall b) hole in vessel piping - Full bore ruptured pipeline - Pipeline through small leak
ESTM4	Liquids (q_{svp})	<ul style="list-style-type: none"> - Evaporation from spill of non-boiling and boiling liquids

In order to cover both, short and long term release situations, as well as, controlled and uncontrolled outflows, the ESTM algorithm is prepared to process instantaneous, continuous (steady-state) and transient (time-varying) releases. In case of continuous releases, the user provides the finite-duration steady state emission rate (q_{sc}), corresponding duration (t_{sc}) and the cross-sectional area of the source aperture (A_h), independently of the containment equipment. In this case, if a pure gas release is defined, the ESTM checks the consistency of user defined input data and processes the information to be properly used in EDM; however, if is assumed a liquid of two-phase outflow, the ESTM checks the consistency of input information and estimates the resulting evaporation rate (in ESTM4). As regards to instantaneous release scenarios, the calculation process is similar to previously described for continuous, however is assumed the instantaneous release of the all hazmat volume.

Alternatively, transient release scenarios can be considered the most complex release situations, requiring the integration of source models developed to numerically describe the variation of the outflow rate under specific conditions and initial conditions. Independently of the selected sub-module, the source term calculation process only continues while the set of control conditions listed in Eq. 3-21 is satisfied.

$$t_i \leq T_{sim} \quad P \geq P_a \quad T > T_{melt} \quad i \leq N_t \quad \text{Eq. 3-21}$$

In which t_i is the time for the step i after the start of the release, T_{sim} is the period of simulation defined by the user, P is the pressure of the hazmat gas, P_a is the atmospheric pressure, T is the temperature of the hazmat gas, T_{melt} is the typical melting temperature of the hazmat and finally N_t is the total number of steps defined by the user. Such conditions assure the consistency and accurate numerical description of hazmat gas outflow and remaining stored/transported fraction along the simulation time steps. Additional criteria may be considered to control the calculation process, depending on the selected modelling approach and input data, extensively described in the literature [e.g. Hanna and Drivas, 1996; CCPS, 1999; Fingas, 2002; Mannan, 2005; VROM, 2005a].

In general, implemented models provide the variation of outflow conditions along the simulation period while internal conditions and remaining stored/transported hazmat amount are 'sufficient enough' to continue the process. Following, source term modelling approaches implemented in the various ESTM sub-modules to estimate outflow conditions are further described.

3.4.1 ESTM1 – Compressed gas

In spite of the wide variety of accident scenarios implemented in ESTM1, emission from initially compressed gas containers always results in the release of pure gases into the atmosphere. In addition to the effortless approaches implemented for instantaneous and continuous releases (previously described), transient outflow scenarios can be characterized for the various types of containment equipments commonly present in industrial environments, through the application of different and varying mathematical and theoretical methods.

Based on Table 3.2 it is possible to mention that, ESTM1 comprises the most 'broadening' set of potential accident scenarios (if compared with non-boiling liquids and PLG). In addition to the commonly applied and used accident scenarios involving small punctures of full bore ruptures in vessels and pipes/pipelines, ESTM1 also comprises a simplified approach for

more complex piping systems, commonly forgotten in extensively used models/software packages.

The well-established equation developed for choked and unchoked flows [Mannan, 2005] is used to estimate the hazmat gas mass flow rate, q_s , in case of small holes/punctures in a vessel wall:

$$q_s = C_D \times A_h \times \psi \times \sqrt{\rho_v \times P \times \gamma \times \left(\frac{2}{\gamma+1}\right)^{\frac{\gamma+1}{\gamma-1}}} \quad \text{Eq. 3-22}$$

where C_D is the discharge coefficient for the hole, A_h is the cross-sectional area of the hole, ψ is the outflow coefficient (Eq. 3-23), ρ_v is the gas density, P is the upstream pressure of the gas inside the vessel and $\gamma = C_{pV}/C_{vV}$ is the specific heat capacity ratio. Gas specific heat capacity at constant pressure, C_{pV} , and volume, C_{vV} , are internally determined by EFRHA chemical properties database as a function of the gas temperature T [Yaws, 1999].

$$\left\{ \begin{array}{l} \psi = \sqrt{\frac{2}{\gamma-1} \times \left(\frac{\gamma+1}{2}\right)^{\frac{\gamma+1}{\gamma-1}} \times 1 - \left(\frac{P_a}{P}\right)^{\frac{\gamma-1}{\gamma}}} \quad P/P_a \geq ((\gamma+1)/2)^{\gamma/(\gamma-1)} \quad (\text{choked}) \\ \psi = 1 \quad P/P_a < ((\gamma+1)/2)^{\gamma/(\gamma-1)} \quad (\text{unchoked}) \end{array} \right. \quad \text{Eq. 3-23}$$

The density, ρ_g , is estimated as a function of the gas pressure, P , and temperature, T [Green and Perry, 2008] as:

$$\rho_g = z \frac{P \times M}{R \times T} \quad \text{Eq. 3-24}$$

In which $R=8.314 \text{ J.mol}^{-1}.\text{K}^{-1}$ is the gas constant and M is the molar mass of the hazmat is input directly from the chemical properties database. Considering that for compressible gases, the ideal gas approach can be used, the compressibility factor, z , is assumed to be equal to unit [Green and Perry, 2008].

In case of gas releases through a vessel piping, the mass flow rate at the pipe opening, $q_{s,hr}$, is estimated based on the principle that, total pressure drop between the vessel and the ambient (ΔP), is equal to the pressure drop over the pipe (ΔP_p), and the pressure drop over the downstream opening in the pipe (ΔP_h) [VROM, 2005a] stated in Eq. 3-25. The mass flow rate through the pipe opening, $q_{s,hr}$, is determined by the overpressure in the vessel and the flow resistance, as a function of the pressure drop over the piping [Fingas, 2002], in order to fulfil the condition of Eq. 3-26:

$$\Delta P = P_0 - P_a = \Delta P_p - \Delta P_h \quad \text{with} \quad \begin{cases} \Delta P_p = P_0 - P_e \\ \Delta P_h = P_e - P_a \end{cases} \quad \text{Eq. 3-25}$$

$$q_{s,p}(\Delta P_p) = q_{s,h}(\Delta P_h) \quad \text{Eq. 3-26}$$

where P_a is ambient pressure, P_0 is the stagnant (initial) pressure at the upstream of the pipe (in the vessel) and P_e is the pressure at the end of the pipe just before the opening to the atmosphere (initially unknown), $q_{s,p}$ is the mass flow rate through the pipe controlled by the ΔP_p , and $q_{s,h}$ is controlled by the ΔP_h .

An iterative process by trial and error is implemented to estimate P_e (between P_0 and P_a) q_{sh} and q_{sp} . Whereas $q_{s,h}$ is estimated through the use of Eq. 3.22, q_{sp} is estimated by Eq. 3-27 until the condition from Eq. 3-26 is satisfied [Mannan, 2005].

$$q_{s,p} = A_p \times \sqrt{\frac{2 \times P_0 \times \rho_{v,0} \times \left(\frac{\gamma}{\gamma+1} \times \left(\left(\frac{P_e}{P_0} \right)^{\frac{1+\gamma}{\gamma}} - 1 \right) \right)}{4 \times f_F \times \frac{l_p}{d_p}}} \quad \text{Eq. 3-27}$$

In this expression A_p is the pipe cross-sectional area, l_p is the pipe length, d_p is the pipe cross-sectional diameter and f_F is the Fanning friction factor calculated by the Colebrook-White expression approach described in CCPS [1999], P_0 is the vessel pressure and ρ_0 is vessel gas density. The iteration continues until Eq. 3-26 reaches a convergence less than 0.1%. Finally, it is assumed an averaged outflow rate $q_s = q_{sh}$. Detailed description of the iterative is available in Mannan [2005] and VROM [2005a].

A near instantaneous release of all gas volume is assumed for the total rupture of a vessel (e.g. total collapse of a vessel), generating a gas cloud with a similar shape of the vessel and no model is implemented. In this case it is assumed that initial cloud shape is similar to the vessel dimensions (e.g. a spherical or a vertical cylindrical cloud).

As regards to accidents involving pipes and pipelines, EFRHA integrates two widely used models, namely the Wilson [1979] and the Weiss [Weiss *et al.*, 1988] models, for full bore ruptured and small holes in the pipe wall, respectively. According to the Wilson model [Wilson, 1979], q_s in case of full bore ruptured pipelines or long pipes scenarios, is given by

$$q_s(t) = \frac{q_{s,0}}{\left(1 + \frac{m_0}{t_B \times q_{s,0}}\right) \times \left(\frac{m_0}{t_B \times q_{s,0}} \times e^{-t/t_B} + e^{-t \times t_B \times (q_{s,0}/m_0)^2}\right)} \quad \text{Eq. 3-28}$$

In this expression $q_{s,0}$ is the initial gas release rate (from Eq. 3-21 with P_0 , T_0 and $C_D=1$), m_0 is the initial total gas mass contained in the pipe, t is the time after the start of the release and t_B is a time constant (from Eq. 3-29).

$$t_B = \frac{2}{3} \times \frac{l_p}{u_s} \times \sqrt{\frac{\gamma \times f_D \times l_p}{d_p}} \quad \text{Eq. 3-29}$$

where u_s is the sonic velocity in the gas and f_D is the Darcy friction factor calculated by the Colebrook-White expression approach described in CCPS [1999]. Assuming adiabatic expansion and non-ideal gas behaviour, u_s is given by:

$$u_s = \sqrt{(\gamma \times R \times T)/M} \quad \text{Eq. 3-30}$$

According to Hanna and Drivas [1987], the Wilson model compares quite well with the more detailed numerical calculations, however it is only valid while the pressure wave travelling upstream didn't reach the opposite side of the pipeline. Thus, it is necessary to estimate the maximum time after the start of the release, until the model is valid (t_E) as:

$$t_E = l_p / u_s \quad \text{Eq. 3-31}$$

In fact, when $t \geq t_E$, the iterative process stops. Additionally, if the rupture occurs near the pipe's half length q_s is multiplied by two to consider the release from both ruptured sections [VROM, 2005a].

On the other hand, in case of small holes in pipe wall, an adaptation of the Weiss model [Weiss *et al.*, 1988] is implemented in ESTM1 to estimate q_s by Eq. 3-32 as:

$$q_s = \rho_V \times V_p / t_{bd} \quad \text{Eq. 3-32}$$

In which V_p is the total volume of gas in the pipe/pipeline and t_{bd} is the blow-down time (Eq. 3.32), *i.e.* the duration of the outflow from a small hole in the pipe wall [Weiss *et al.*, 1988].

$$t_{bd} = (\tau_{cr} + \tau_s) \times \tau_v \times C_b \quad \text{Eq. 3-33}$$

where τ_{cr} is the dimensionless sonic blow time (Eq. 3-34), τ_s is the dimensionless subsonic blow time (from Eq. 3-35), τ_v is the time constant (from Eq. 3-36) and C_b is the blow-down correction factor (from Eq. 3-37).

$$\tau_{cr} = \ln\left(\frac{P_0}{P_a}\right) - \left(\frac{\gamma}{\gamma-1}\right) \times \ln\left(\frac{\gamma+1}{2}\right) \quad \text{Eq. 3-34}$$

$$\tau_s = -0.0792 \times \gamma^2 + 0.6952 \times \gamma + 0.0602 \quad \text{Eq. 3-35}$$

$$\tau_v = V_p \times \frac{(\gamma+1/2)^{\gamma+1/2 \times (\gamma-1)}}{u_s \times A_h \times C_D} \quad \text{Eq. 3-36}$$

$$C_b = a_1 + a_2 \times \log\left(f_D \times \frac{l_p}{d_p}\right) + a_3 \times \left(\log\left(f_D \times \frac{l_p}{d_p}\right)\right)^2 + a_4 \times \left(\log\left(f_D \times \frac{l_p}{d_p}\right)\right)^3 \quad \text{Eq. 3-37}$$

A conservative approach is implemented to estimate an averaged hypothetical finite duration q_s , assuming a constant emission based on initial conditions in the pipe/pipeline and estimated t_{bd} , as previously considered in Eq. 3-32 (replacing τ_s by t_{bd}).

Unlike most CA models, scenarios involving gas release from piping systems are also considered in EFRHA model. According to Crane [1986], it is possible to estimate q_s (for both choked and unchoked conditions) in piping systems, considering the influence of piping fittings like elbows, valves of pumps influence, as follows:

$$q_s = Y \times A_h \sqrt{(2 \times g \times \rho_v \times (P - P_a)) / \sum K_f} \quad \text{Eq. 3-38}$$

where Y is the expansion factor and $\sum K_f$ is the sum of the individual excess head loss terms. The Y and $\sum K_f$ are estimated as detailed recommended in CCPS [1999].

3.4.2 ESTM2 – Non-boiling liquid

With the exception of accident scenarios involving the total rupture of vessels, the spilled liquid mass outflow rate (q_{sL}), is only estimated if (and while) the opening point is located below the liquid height inside the container. In any case, the Bernoulli principle is the theoretical basis for the estimation of q_{sL} , independently of the type of failure and equipment [Hanna and Drivas, 1987].

As regards to small holes in vessel wall, the q_{sL} is estimated by modified expression of Bernoulli equation principle, to account friction loss and characteristics of the hole, as follows:

$$q_{sL} = C_D \times A_h \times \sqrt{2(P_L - P_a) \times \rho_L} \quad \text{Eq. 3-39}$$

where ρ_L is the liquid density and P_L is the total pressure at opening (Eq. 3-40).

$$P_L = \rho_L \times g \times h_L + P_a \quad \text{Eq. 3-40}$$

In which the h_L corresponds to the relative liquid height above the failure opening in the vessel.

Accident scenarios considering the total rupture of vessels can be seen as a special case, in which no model is used to estimate the amount of liquid spilled. Instead, a near instantaneous spill of the total liquid volume is assumed just after the release leading to the formation of a liquid pool at the ground level.

In case of full bore ruptured pipelines and pipes connected to vessels, the assumption that q_{sL} can be estimated from the flow inside the pipe [Fingas, 2002] is used. Thus, q_{sL} is estimated by Eq. 3.41 as follows:

$$q_{sL} = \rho_L \times A_p \times u_L = \rho_L \times A_p \sqrt{\frac{\Delta P \times d_p}{2f_F \times \rho_L \times l_p}} \quad \text{Eq. 3-41}$$

where u_L is the (average) liquid flow velocity inside the pipe (Eq. 3-42) and ΔP_L is the pressure drop over the pipe (Eq. 3-43).

$$u_L = \sqrt{\frac{\Delta P \times d_p}{2 \times f_F \times \rho_L \times l_p}} \quad \text{Eq. 3-42}$$

$$\Delta P_L = f_D \times \frac{\rho_L}{2} \times u_L^2 \times \frac{l_p}{d_p} \quad \text{Eq. 3-43}$$

The f_F and f_D are functions of the Reynolds number (Re) which depends on the liquid flow in the pipe u_L as described in [CCPS, 2000; Green and Perry, 2008]. Thus, to account the interdependency of the variables, q_{sL} is estimated by an iteration procedure based on the trial-and-error method described in Mannan [2005].

In general, liquid spill scenarios include the formation of liquid pools on the ground. Even not observed in all cases (*e.g.* non-boiling liquids at ambient temperature), evaporation phenomena may take place, and must be considered, especially for the formation of hazmat gas clouds. Thus, ESTM2 is linked to the ESTM4 enabling the estimation of the hazmat gas evaporation rate required for subsequent modules. If no evaporation phenomena are observed, the modelling process stops, since no hazmat gas source rate is estimated.

3.4.3 ESTM3 – Pressurized liquefied gas

PLG source term models are rather more complex than single phase models as a result of the need to consider the two-phase ‘champagne effect’ (*i.e.* expansion of the liquid volume due to

bubble formation in the liquid and the expansion of the boiling liquid) observed inside the container during the release [see DIERS, 1986; Fingas, 2002; Manna, 2005]. Therefore, in addition to the previously observed single phase regimes (pure vapour or liquid), ESTM3 must comprise modelling approaches able to numerically describe two-phase outflow conditions (mixture gas-liquid) regimes, depending on the location of the orifice and liquid surface level locations [Mannan, 2005].

In view of maintaining the relative straightforwardness of modelling algorithm, a set of 'simplified' models specifically developed for the estimation of PLG hazmat outflow conditions is implemented in ESTM3 to account for the more relevant and common accident scenarios analyzed in CA studies.

Unlike single-phase outflow regimes, instantaneous and continuous releases of PLG releases require a more careful analysis. After the instantaneous spill, it is assumed a sudden depressurization causing the flashing of all PLG into a two-phase hazmat cloud. As regards to steady-state outflow rates, the initial physical state is defined, based on the location of the aperture, in relation to the liquid fraction level. If the aperture is located below the liquid level, it is assumed a pure liquid release and subsequent flashing must be determined; otherwise, it is considered a pure gaseous outflow. In any case, if liquid fraction (pure liquid or two-phase liquid droplets) is considered during the release phenomena, it is also calculated the degree of flashing of the spilled material. The description of the flashing and estimation of liquid and vapour fractions, as well as the hazmat gas cloud formation follows the methodologies and recommendations described in Fingas [2002] and VROM [2005a].

Accidents involving transient releases from small holes in the vessel wall, two distinct situations are considered:

- (i) Top venting orifices - (DIERS method),
- (ii) Side or bottom wall holes (Mayinger correlation approach).

Whereas the analytical Design Institute for Emergency Relief Systems (DIERS) method [DIERS, 1986] is implemented to numerically describe the outflow conditions in case of top venting openings; the Mayinger correlation approach [Belore and Buist, 1986] is used to characterize the outflow of hazmat PLG from small holes in vessel side and bottom wall.

In the first case, only two possible outflow regimes are considered along the calculation process - pure vapour and two-phase outflow, depending of the level of the expanded liquid fraction, which is considered as a two-phase regime. As recommended in the literature [see

Melhem and Croce, 1993; Green and Perry, 2008], an initial pure vapour outflow above the liquid surface is assumed, driven out only by the rise of the liquid that acts like a piston.

According to DIERS [1986], the pure vapour outflow regime is assumed during the initial vapour outflow blow-out period (t_v) (Eq. 4.44)

$$t_v = m_{v,0} / q_{s,0} \quad \text{Eq. 3-44}$$

In which $m_{v,0}$ is the initial vapour mass in the vessel (from Eq. 3-45) and $q_{s,0}$ is the initial mass flow rate of pure vapour (from Eq. 3-21), considering saturated conditions (*i.e.* $P_0 = P_0^0$). Initial vapour and liquid mass fractions ($m_{v,0}$, $m_{L,0}$) are known from the hazmat filling degree (ϕ) as follows:

$$m_{v,0} = (1 - \phi) \times V_v \times \rho_{v,0} \quad \text{Eq. 3-45}$$

$$m_{L,0} = \phi \times V_v \times \rho_{L,0} \quad \text{Eq. 3-46}$$

where V_v is the vessel volume, $\rho_{L,0}$ and $\rho_{v,0}$ are the initial liquid and vapour densities, respectively. Contrarily to ESTM1, the compressibility factor (z) must be estimated in ESTM4 to use Eq. 3-23. The Reid *et al.* [1988] approach is used based on the pitzer factor (ω) for the analyzed hazmat, because the ideal gas assumption is not valid for PLG. The rise of the liquid fraction due to the rapid depressurization is a consequence of the formation of bubbles and expansion of the liquid during the vapour outflow t_v period [VROM, 2005a].

Two ways of liquid expansion (rapid flashing) inside the vessel can be considered to occur, namely, the bubbly and the churn boiling regimes [DIERS, 1986]. The bubbly flow is characterized by smooth vaporization and reduced number of small dimension bubbles in the liquid fraction, while the churn flow regime is distinguished by extensive bubble coalescence and the formation of larger dimension bubbles. When liquid level reaches the vessel top wall, two-phase is apparent and a more complex algorithm is used to estimate the q_{sF} , considering the two-phase rapid flashing regimes. DIERS [1986] suggested that q_{sF} can be estimated iteratively based on the following equations:

$$q_s = C_D \times A_h \times \sqrt{(2(P_0 - P_a) \rho_F)} \quad \text{Eq. 3-47}$$

$$\rho_F = 1 / (\Phi_m / \rho_v + (1 - \Phi_m) / \rho_L) \quad \text{Eq. 3-48}$$

where ρ_F is the two-phase mixture density and Φ_v is the vapour mass fraction in the two-phase flow estimated according to the rapid flashing regime [Fingas 2002]. The estimation of

Φ_m follows the methodology described in Green and Perry [2008]. In some cases, after the two-phase regime, a pure vapour outflow is restarted and q_s is estimated as at initial instants of the release. Detailed description of the DIERS method procedure is presented in DIERS [1986] and VROM [2005a].

On the other hand, the Mayinger correlation approach [Belore, 1986; Mayinger, 1990] is implemented for accident scenarios considering small holes in the vessel side or bottom wall. In addition to pure gas and two-phase outflows, it must be also considered pure liquid spills if the aperture is located below the liquid levels, at least in the initial instants of the release. At the initial instant, the standard relations for pure vapour (see Section 3.4.1) or pure liquid (see Section 3.4.2) state can be applied, depending on the location of the orifice relative to the h_L . The rise of the liquid volume and the two-phase regime are estimated according to the Mayinger correlation principles [see Belore and Buist, 1986].

Two-phase regime can be apparent after the initial instant due to the formation of bubbles, while the expanded liquid volume remains above the level of the hole. For this outflow regime, a slightly different procedure from the used in case of top venting is implemented as described by Dinis and Dinis [2002] and Mannan [2005]. The q_{sF} is estimated from Eq. 3-47 with Φ_V calculated using on the Mayinger correlation approach [VROM, 2005a]. A detailed description of the Mayinger correlation approach methodology is described in Green and Perry [2008].

In order to cover accidents in pipes and pipelines, ESTM3 integrates different methods according to initial PLG conditions and dimensions of the equipment.

The modified form of the Homogeneous Non-equilibrium Model [Leung and Grolmes 1987] suggested by Fauske and Epstein [1988] is implemented in ESTM3 for subcooled PLG releases from small pipes ($l_p \leq 0.1$ m), as follows:

$$q_{sF} = A_h \times F \times \sqrt{G_{SUB}^2 + G_{ERM}^2} / N_F \quad \text{Eq. 3-49}$$

where F is the frictional flow reduction factor based on the length-to-diameter ratio, G_{SUB} is the subcooled mass flux (Eq. 3-50), G_{ERM} is the equilibrium mass flux (Eq. 3-51) and N_F is a non-equilibrium dimensionless parameter (Eq. 3-52).

$$G_{sub} = C_D \times \sqrt{2\rho_F(P_0 - P_v^{sat})} \quad \text{Eq. 3-50}$$

$$G_{ERM} = \frac{H_{vap}}{v_{fg}} \times \sqrt{\frac{1}{T_0 \times C_{pL}}} \quad \text{Eq. 3-51}$$

$$N_F = \frac{H_{vap}^2}{2(P_0 - P_v^{sat}) \times \rho_F \times C_D^2 \times v_{fg}^2 \times T \times C_{pL}} + \frac{l_p}{0.1} \quad \text{Eq. 3-52}$$

where v_{fg} (Eq. 3-53) is the change in specific volume from liquid to vapour (Eq. 3-53) and P_v^{sat} is the saturation vapour pressure at T_0 and H_{vap} is the heat of vaporization at T_0 .

$$v_{fg} = 1/\rho_v - 1/\rho_L \quad \text{Eq. 3-53}$$

For longer pipes ($l_p > 0.1$ m), equilibrium conditions are assumed and a simplified form of the Homogeneous Equilibrium Model (HEM) [Fauske and Epstein, 1988] suggested by Leung [1986] and is used to estimate q_{sF} as follows:

$$q_{sF} = F \times C_D \times \sqrt{2\rho_F(P_0 - P_v^{sat})} \quad \text{Eq. 3-54}$$

For PLG in saturated conditions, a simplified form of the Homogeneous Non-Equilibrium Model [Fauske and Epstein, 1988] is implemented to calculate the q_{sF} , by:

$$q_{sF} = F \times \frac{0.1 \times A_h}{v_{fg}} \times \sqrt{\frac{1}{N_F \times T_0 \times C_{pL}}} \quad \text{Eq. 3-55}$$

In this expression N_F and v_{fg} are estimated from Eq. 3-52 and Eq. 3-53, respectively.

While for longer pipes, is possible to assume that flashing conditions are reached and the Homogeneous Non-Equilibrium Model approximately reduces to the Homogeneous Equilibrium Model [Leung, 1986]. According to Fauske and Epstein [1988], the flow is generally choked due to the flashing and equilibrium conditions, then q_{sF} decreases only slightly with increasing l_p and can be considered independent of the vapour quality. Thus, q_{sF} can be simplified to:

$$q_{sF} = F \times \frac{H_{vap}}{v_{fg}} \times \sqrt{\frac{1}{T_0 \times C_{p,L}}} \quad \text{Eq. 3-56}$$

Expelled two-phase mass is often characterized by the presence of aerosol, therefore flashing of released liquid or two-phase mass just outside the orifice is determined for all scenarios presented above to determine the 'final' correspondent liquid and vapour fractions. This last evaluation process aims verifying the physical state of released material and eventual formation of liquid pool on the ground, vapour jet clouds or both at the same time. From the literature [e.g. CCPS, 1999; Mannan, 2005; Green and Perry, 2008], the flashing phenomenon can be characterized by the flash fraction, $\Phi_{V,F}$ of the released mass, estimated through a standard expression suggested by Crowl and Louvar [1990]:

$$\Phi_{V,F} = C_{pL}(T - T_{Boil})/H_{vap} \quad \text{Eq. 3-57}$$

Pure vapour phase is assumed if $\Phi_{V,F} > 0.5$, meaning that no rain-out is considered [VROM, 2005a]; otherwise, rain-out is predicted and both phases (vapour and liquid) are considered, with correspondent fractions estimated. Still, if $\Phi_{V,F}$ approximates to zero, pure liquid spill is considered.

In any case, if liquid (pure liquid or rain-out fraction) spill is predicted, the formation of a liquid pool is assumed and ESTM4 is applied to estimate the 'additional' evaporation phenomenon, by using the most appropriated modelling approach of ESTM4.

3.4.4 ESTM4 – Liquid pool evaporation

Considering that liquid spill of either pure liquid or PLG rain-out fraction, tend to form pools, it is of major importance to describe the subsequent evaporation phenomena and to evaluate its contribution to consequences to human health. For that reason, a set of well-known evaporation models are implemented in ESTM4 to numerically describe the spreading, evaporation rate and duration of hazmat gas emission from the previously formed liquid pools. Considering the applicability of ESTM4, this sub-module is designed to consider two distinct situations: (i) user manually defined input pool dimensions, and (ii) interim characterization of pool dimensions from ESTM2 or ESTM3 liquid spill outputs.

In case of manual definition of evaporation scenario consists of the definitions of an already formed liquid pool within bunds is defined by the user for the estimation of subsequent evaporation rate. Alternatively, depending on previous estimations of liquid spills, instantaneous, continuous or transient liquid spills, with or without bunds scenarios can be analyzed without any control of the user.

Unlike previous ESTM sub-models, pool evaporation models also require a detailed characterization of the surface environmental conditions, such as characteristics of subsoil and dimensions of bunds (if present). For convenience and main purpose of application of the developed modelling system, classic and simple methods based on boiling and non-boiling liquids are implemented in EFRHA source term module to determine the evaporation rate. Nevertheless, despite the gaps/limitations of this type of models [Kootstrat *et al.*, 2004], the complexity of advanced models, like GASP model [Webber, 1993], still require substantial computational efforts [Kootstra, 2004]. Moreover, the selected simple models are currently implemented in similar CA software packages [Britten, 1990; Reynolds, 1992; TNO, 2007] and recommended in the literature [*e.g.* VROM, 2005a; Casal, 2008].

The overall mass balance ($dM_{pl}(t)/dt$) for an evaporating pool and further characterization of dimensions is given by Eq. 3.58 as :

$$\frac{dM_{pl}}{dt} = -q_{sVP} + q'_{rel} \quad \text{Eq. 3-58}$$

In which q_{sVP} is the evaporation rate and q'_{rel} is the liquid spill rate flowing into the pool (neglected in case of instantaneous liquid releases).

The selection of the most appropriated model depends on the 'type of liquid' - boiling or non-boiling liquid, commonly determined by heat and mass balances for boiling and non boiling liquids [see Hanna *et al.*, 1996; Kootstra *et al.*, 2004]. For instance, a non-boiling liquid is assumed if its T_B is higher than the ambient subsoil temperature ($T_{a,s}$); otherwise it is assumed as a boiling liquid [Fingas, 2002].

For non-boiling liquids, the MacKay and Matsugu model [Kawamura and MacKay, 1987] is implemented for the estimation of q_{sVP} , as follows:

$$q_{sVP} = \frac{k_m(t) \times P_v(T_{pl}(t)) \times M}{R \times T_{pl}(t)} \times A_{pl} \quad \text{Eq. 3-59}$$

In this expression $k_m(t)$ is the mass transfer coefficient (Eq. 3-60), P_v is the vapour pressure at pool temperature, T_{pl} and A_{pl} is the pool surface area. The $k_m(t)$ is influenced by the u_{ref} , the pool surface average radius ($r_p(t)$) and the Schmidt number (S_c).

$$k_m(t) = 0.004785 \times u_{ref}^{0.78} \times (2 \times r_p(t))^{-0.11} \times S_c^{-0.67} \quad \text{Eq. 3-60}$$

The evaporation of a (initially) non-boiling liquid pool causes a decrease of the liquid temperature (T_{pl}) during the evaporation (assuming that the surface temperature of the pool is equal to the temperature of the bulk of the liquid in the pool), which will influence the estimated q_{sVP} . Variation of the pool temperature (dT_{pl}/dt) is estimated from the heat balance suggested in VROM [2005a]:

$$\frac{dT_{pl}}{dt} = \frac{\sum H - (q_{sVP}/A_{pl}) \times H_{vap}(T_{pl})}{h_{pl} \times \rho_L \times C_p} \quad \text{Eq. 3-61}$$

where $\sum H$ is the sum of the surrounding environment heat fluxes, from soil, air, solar radiation, long wave radiation and mass flowing into the pool estimated as detailed described in VROM and the references therein [2005a], h_{pl} is the depth of the pool and $H_{vap}(T_{pl})$ is the heat

of evaporation at pool temperature estimated by EFRHA chemical properties database. Pool depth depends on pool surface dimensions and subsoil conditions.

Alternatively, in case of boiling liquid pools, it is possible to assume that T_{pl} is constant and equal to T_B during the evaporation process [VROM, 2005a]. According to Kootstra *et al.* [2004] the evaporation rate can be determined by the amount of heat supplied to the boiling pool from environment:

$$q_{svp} = \frac{\sum H(t)}{H_{vap}(T_{pl})} \times A_{pl} \quad \text{Eq. 3-62}$$

The estimation of $\sum H(t)$ for a boiling liquid pool, is slightly different from non-boiling liquids as suggested in CCPS [1999].

When sufficient heat is available and supplied to a non-boiling liquid pool it may reach its boiling point and start boiling. The other way around is also possible when heat transfer to the liquid pool is insufficient, temperature drops and evaporation decreases [Trijssenaar-Buhre *et al.*, 2008]. As recommended by Kootstra *et al.* [2004], the transition between evaporation mechanisms is based on the T_{pl} relative to T_B .

As regards to the liquid pool dimensions, ESTM4 is designed to consider the presence of bunds or other similar passive retention barriers, in which is assumed that pool dimensions are lower or equal to the bund; otherwise it is considered an evaporation pool without bunds which may significantly spread at the ground surface. This option affects the estimated dimensions, namely A_p , h_p and r_p . The estimation of the variation of the pool dimensions during the release follows the expressions and methods detailed described by Trijssenaar-Buhre *et al.* [2008].

Determined the variation of the hazmat gas outflow conditions it is possible to predict the atmospheric dispersion during and after the release process.

3.5 EDM – EFRHA Dispersion module

Considered the ‘main core’ of EFRHRA model, the EDM comprises an up-to-date Class II shallow layer (Type V) modelling approach to quantitatively describe the hazmat gas transport and dispersion phenomena. Following the philosophy of continuous data transfer along the calculation process, this module takes the main output data from the ‘pre-processors’ EMM, ETM and ESTM (see Figure 3.1) and predicts the hazmat gas concentration fields as a function of time, according to the structure presented in Figure 3.7.

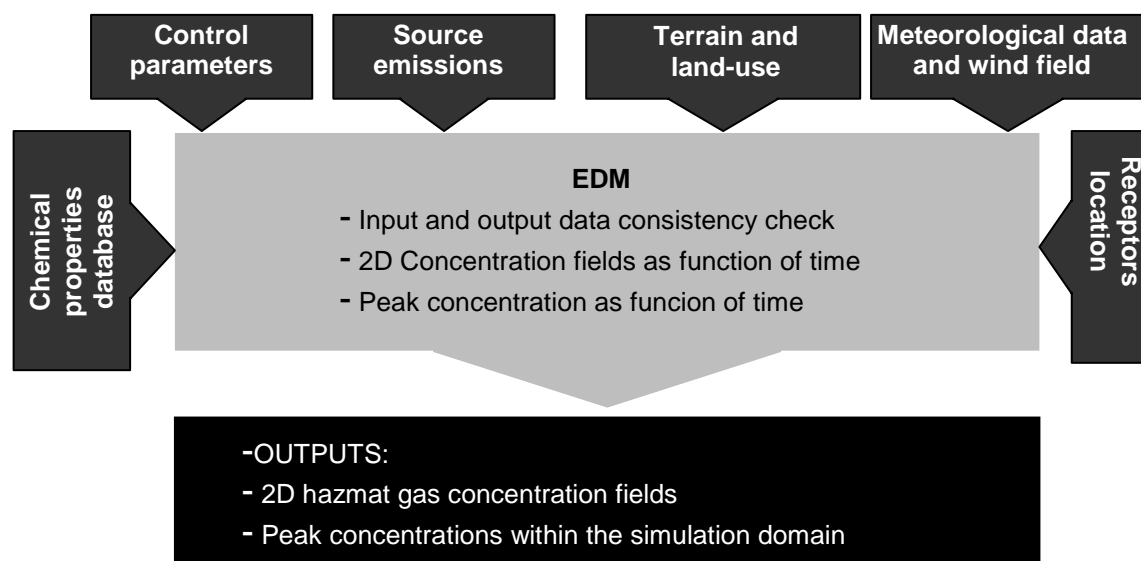


Figure 3.7 – EDM basic structure with the different stages of process.

Taking into account the variety and amount of input information required to properly estimate the hazmat concentration fields, a preliminary consistency check test of source term, meteorological, terrain, obstacles and receptors data completeness and validity is processed.

Aiming to maintain a compromise between the complexity of Class III and the simplicity of Class II models, EDM integrates an atmospheric dispersion shallow layer modelling approach to produce the concentration fields as a function of time. The EDM modelling approach and structure is mainly based on the TWODEE model [Hankin, 1997; Hankin and Britter, 1999a,b,c], recently upgraded by the TWODEE-2 model [Folch *et al.*, 2009]. This model was developed to simulate large scale instantaneous and continuous release and dispersion of dense gas on complex topography. In addition to the main features of the original code, the development of EDM considered a set of relevant modifications in order to consider the more appropriated ‘conditions’ and scenarios for CA studies of hazmat gas accidental releases in industrial and built-up areas.

Considering the large effort in implementing the set of source term models (to describe the variation of the outflow conditions), a multi-puff approach was implemented in EDM modelling algorithm to enable simulating transient releases, in addition to the ‘traditional’ instantaneous and continuous release conditions. The model is also prepared to use fine grid resolutions, to be able to account for the influence of obstacles in the dispersion in a more realistic way. The capability of defining both regular and discrete receptors grids enables counterbalancing the increased efforts associated to the higher grid resolution, particularly for locations of interest or event for the definition of the obstacles. Chemical properties

parameters are continuously corrected as a function of temperature and available information, instead of defining a constant value for the entire period of simulation.

The implemented modelling approach is based on depth-averaged equations of density ($\bar{\rho}$) and horizontal velocity (\bar{u}, \bar{v}) through the integration of conservation equations over the fluid depth, from the bottom up to the free surface ($z=0 \rightarrow h$). Hazmat gas cloud behaviour is described in terms of cloud height (Eq. 3-63), depth-averaged cloud density (Eq. 3-65), two depth-averaged horizontal velocities (Eq. 3-66 and Eq. 3-67) and depth-averaged concentration (Eq. 6-68). It is assumed that h is the height below which a fraction α of 0.95 of the hazmat gas buoyancy $g(\bar{\rho} - \rho_a)$ of the hazmat gas is located (*i.e.*, the cloud height) [Folch *et al.*, 2009]:

$$\int_{z=0}^h (\rho(z) - \rho_a) dz \equiv \alpha \int_{z=0}^{\infty} (\rho(z) - \rho_a) dz \quad \text{Eq. 3-63}$$

The $\rho(z)$ is the vertical distribution of density ρ estimated from its depth-value similarly to Hankin and Britter [1999c] (Eq. 3-64), ρ_a is the ambient air density, u and v are the horizontal mean velocities previously determined in ETM, and z is the vertical coordinate.

$$\rho(z) = \rho_a + \frac{2}{S_1} (\rho(z) - \rho_a) \exp\left(-\frac{2}{S_1} \frac{z}{h}\right) \quad \text{Eq. 3-64}$$

where $S_1=0.5$ is a shape parameter. In a similar way, depth-averaged hazmat gas density ($\bar{\rho}$) and the two horizontal velocities (\bar{u}, \bar{v}) are defined based on the following equations:

$$h(\bar{\rho} - \rho_a) \equiv \int_{z=0}^{\infty} (\rho(z) - \rho_a) dz \quad \text{Eq. 3-65}$$

$$h(\bar{\rho} - \rho_a)\bar{u} \equiv \int_{z=0}^{\infty} (\rho(z) - \rho_a)u(z) dz \quad \text{Eq. 3-66}$$

$$h(\bar{\rho} - \rho_a)\bar{v} \equiv \int_{z=0}^{\infty} (\rho(z) - \rho_a)v(z) dz \quad \text{Eq. 3-67}$$

The concentration vertical profile, $c(z)$, is characterized by an exponential decay [Hankin and Britter, 1999a] and is given by Eq. 3-68 in ($\mu\text{g}\cdot\text{m}^{-3}$)

$$c(z) = 10^9 \times \left(\frac{\rho(z) - \rho_a}{\rho_g - \rho_a}\right) \times \left(\frac{M}{24.45}\right) \quad \text{Eq. 3-68}$$

Shallow water equations are adapted in order to predict the hazmat gas cloud behaviour during the dispersion phenomena. Assuming an incompressible homogeneous fluid behaviour and a hydrostatic pressure distribution, the shallow water equations are adapted to hazmat gases having a non-uniform vertical profile and therefore given by [Hankin, 1997; Hankin and Britter, 1999a]

$$\frac{\partial h}{\partial t} + \frac{\partial h\bar{u}}{\partial x} + \frac{\partial h\bar{v}}{\partial y} = u_{entr} + u_{inf} \quad \text{Eq. 3-69}$$

$$\frac{\partial h(\bar{\rho} - \rho_a)}{\partial t} + \frac{\partial h(\bar{\rho} - \rho_a)\bar{u}}{\partial x} + \frac{\partial h(\bar{\rho} - \rho_a)\bar{v}}{\partial y} = u_{entr}\rho_a + u_{inf}\rho_g \quad \text{Eq. 3-70}$$

$$\begin{aligned} & \frac{\partial h\bar{\rho}u}{\partial t} + \frac{\partial h\bar{\rho}u^2}{\partial x} + \frac{\partial h\bar{\rho}uv}{\partial y} + \frac{1}{2}S_1 \frac{\partial g(\bar{\rho} - \rho_a)h^2}{\partial x} + S_1g(\bar{\rho} - \rho_a)h \frac{\partial e_{sf}}{\partial x} + \frac{1}{2}\bar{\rho}C_D\bar{u}|u_{uv}| + V_x + \\ & + k_i\rho_a \left[\frac{\partial}{\partial t} + u_a \frac{\partial}{\partial x} + v_a \frac{\partial}{\partial y} \right] [h(\bar{u} - u_a)] = u_{entr}\rho_a u_a \quad \text{Eq. 3-71} \end{aligned}$$

$$\begin{aligned} & \frac{\partial h\bar{\rho}v}{\partial t} + \frac{\partial h\bar{\rho}v^2}{\partial y} + \frac{\partial h\bar{\rho}uv}{\partial x} + \frac{1}{2}S_1 \frac{\partial g(\bar{\rho} - \rho_a)h^2}{\partial y} + S_1g(\bar{\rho} - \rho_a)h \frac{\partial e_{sf}}{\partial y} + \frac{1}{2}\bar{\rho}C_D\bar{v}|u_{uv}| + V_y + \\ & + k_i\rho_a \left[\frac{\partial}{\partial t} + u_a \frac{\partial}{\partial x} + v_a \frac{\partial}{\partial y} \right] [h(\bar{v} - v_a)] = u_{entr}\rho_a u_a \quad \text{Eq. 3-72} \end{aligned}$$

In which u_{entr} and u_{inf} are the air entrainment (Eq. 3-76) and dense gas inflow velocities, respectively, e_{sf} is the terrain surface elevation, t it the time after starting the simulation, x and y are the horizontal spatial coordinates, ρ_g is the hazmat gas density, u_a and v_a are the ambient air horizontal velocities along x and y , respectively, k_i is an semi-empirical coefficient (Eq. 3-73), C_D is the drag coefficient (Eq. 3-74), V_x and V_y (Eq. 3-75) are the turbulent shear stress forces along x and y , respectively.

As mentioned in Folch *et al.* [2009] Eq. 3-69 to 3-72 express, respectively, the balances of volume, mass and components of momentum. Left-hand side terms of Eq. 3-71 and Eq. 3-72 include time evolution, the effect of convection, the pressure gradient for the case of hydrostatic but non-uniform density profile, the effect of the ground, the surface shear stress (proportional to C_D), the force per unit area applied by turbulent shear stress and the leading edge terms that consider the interaction among dense gas and ambient air. The last one provides a correction of the shallow water equations that may produce erroneous results for the leading edge, as they assume that the pressure distribution is hydrostatic, which is also

proportional to k_i . The k_i is estimated based on the front Froude number, Fr , usually set to 1 [Hankin and Britter, 1999a]:

$$k_i = \frac{2}{S_1 Fr^2} \quad \text{Eq. 3-73}$$

Additionally, C_D , V_x and V_y are estimated based on Eq. 3-74 and Eq. 3-75:

$$C_D = \max\left(\min\left(\frac{2u_*^2}{u_{auv}}; 10^{-2}\right); 10^{-4}\right) \quad \text{Eq. 3-74}$$

$$(V_x, V_y) = \zeta h \bar{\rho} \nabla |u_{uv}| \nabla u_{uv} \quad \text{Eq. 3-75}$$

The constant of proportionality of turbulent shear stress, ζ , is commonly set to 0 [Folch *et al.*, 2009]. The u_{entr} is estimated by empirical formulations as described by Hankin and Britter, [1999a].

$$u_{entr} = \frac{k}{1 + 0.11 Ri} \times \sqrt{u_*^2 + (\alpha_2 w_*)^2} + \frac{1}{2} C_D \alpha_3^2 |u_{uv}|^2 + \alpha_7^2 |u_{uv} - u_{auv}|^2 \quad \text{Eq. 3-76}$$

In which $\alpha_2=0.7$, $\alpha_3=1.3$ and $\alpha_7=0.45$ are empirical constants. This equation describes the top entrainment of ambient air into the dense gas cloud. In the present modelling approach, edge entrainment is not considered.

Hazmat gas concentration is calculated through Eq. 3-69 to Eq. 3-72, together with the closure relationships Eq. 3-73 to Eq. 3.75 [Hankin and Britter, 1999b]. Moreover, the flux corrected transport scheme suggested by Zalesak [1979] is implemented to maintain a certain simplicity and fast run for the estimation of concentration fields as a function of time. Similarly to Folch *et al.* [2009], incoming flux concentrations at boundaries are null (*i.e.* $h=0$, $\bar{\rho} = \rho_a = a$, $\bar{u} = 0$ and $\bar{v} = 0$) and zero derivative conditions are assumed for the outgoing flux.

Even detected a somewhat longer simulation time requirements than 'traditional' CA Class II models (Type II - IV models), it is counter-balanced by the increased capability to account the influence of obstruction on the released hazmat gas, allowing considering variations of meteorological conditions along the period of simulation highlights the higher complexity of the developed EDM.

Predicted the 2D concentration fields as a function of time, it is possible to determine the potential consequences on human health from the exposure to levels of concern for the released hazmat gas. With the intention to prepare the information in a way that facilitates

their interpretation, EDM main outputs are processed in EEM, according to user defined control and post-processing options and purposes.

3.6 EEM – EFRHA Effects Module

The EEM is designed to post-process the main outputs of EDM based on the comparison of estimated concentrations fields with reference safety threshold limits. Following the same design of previous modules, EEM is structured to initially verify the consistency of input data and quantify the consequences and effects according to user defined formats, as schematized in Figure 3.8.

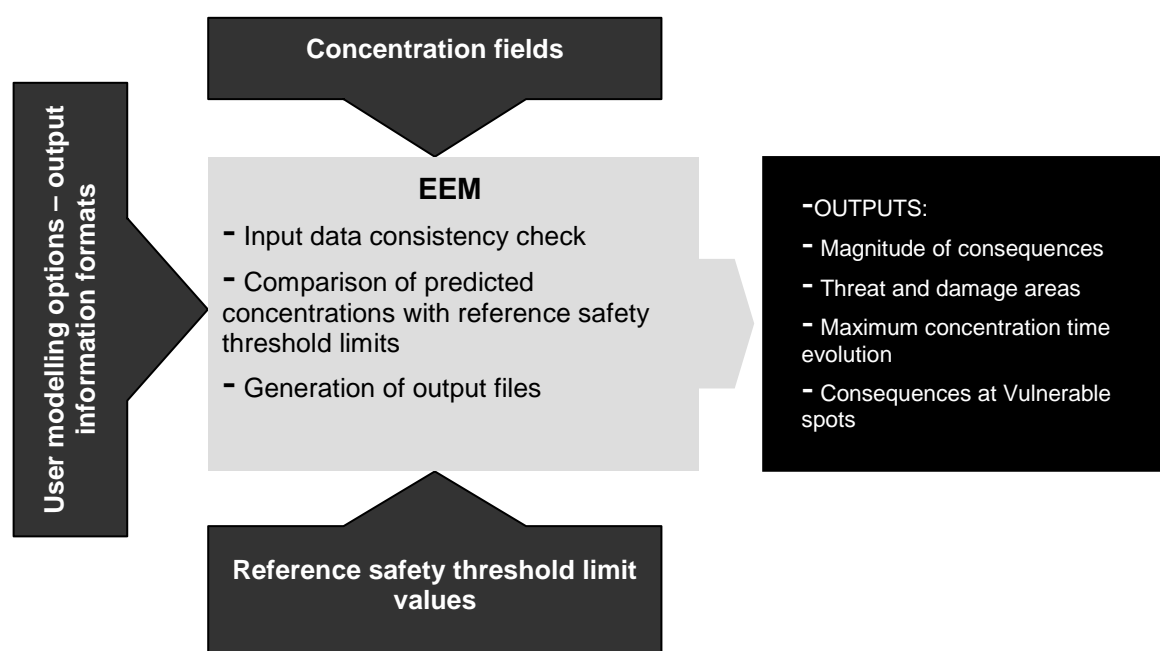


Figure 3.8 – EEM basic structure with the different stages of process.

A preliminary consistency check of this module's input data intends verifying if hazmat gas concentrations fields are effectively produced, but also if the selected/defined safety threshold limits are appropriated for further comparison with estimated concentrations. In spite of using the *Emergency Response and Planning Guideline* (ERPG) values compiled in EFRHA chemical properties database by default, the user can manually define different threshold values concerning toxicological and/or flammability limits. Therefore, the analysis of selected threshold limit values assures the use of acceptable data. Although modelled concentration fields encompass both regular and discrete receptors grids, a special attention is taken to discrete receptors information (if included).

Depending on user modelling options, the main outputs of this module may be presented in different formats, from summary text files to table information, as a function of time and/or spatially distributed. Nonetheless, main output information is formatted to be used in visualization and plotting tools to generate maps and graphical data. With the purpose of determining threat and damage temporal and spatial distribution, direct comparisons between modelled concentration fields and safety threshold limits are performed. In this analysis, both regular and discrete receptors points are covered. Hence, points in which concentrations are higher than reference limit values are identified as potentially affected spots. In case of spatial distribution analysis, consequence contours maps are generated at different periods of time after the accident. Alternatively, time evolution of concentrations can be analyzed for a specific spot of interest (*e.g.* vulnerable spot') and graphically plotted.

If spatial distribution of population is available, the direct overlap of information allows estimating the total number of people (potentially or effectively) exposed to certain levels of hazmat gas concentrations after the accident event. This capability represents an enhanced tool to determine threat and damage areas and therefore evacuate the population in case of real accident scenarios.

The integration of this module intends to produce EFRHA main outputs in formats able to be easily evaluated by analysts and unspecialised users, in particular decision and emergency response operators.

3.7 Main input and output data of EFRHA model

Apart from the amount of information required for a proper estimation of short-term pollution episodes and consequences in case of accidents involving the release of hazmat gases, EFRHA model is designed in a way that main outputs from one module are used as inputs in the subsequent. This structure enables defining a minimum list of strict mandatory parameters that must be provided by the user, independently of the degree of completeness of input datasets. Moreover it is assured a constant data consistency evaluation. Main inputs and outputs can be categorized as control options; meteorological conditions; terrain characteristics; source term conditions; and effects threshold limits (see Table B.1 in Appendix B).

Control parameters specify the selected modelling options for the simulation and the correspondent input/output data links. Meteorological conditions comprise surface and upper air meteorological and ABL parameters during the period of analysis. Terrain

characteristics include information concerning geographic location, topography, source location and buildings distribution within the study domain. Source term conditions characterize hazmat storage/transportation conditions and leakage phenomena. Finally, the effects threshold limits inputs consist of sets of relevant limit values to estimate potential human exposure effects to hazmat gaseous concentrations distribution.

Notwithstanding the definition of the minimum list of strict mandatory parameters, the user may also provide all available input and interim information. If all input parameters are available, EDM, through the continuous consistency check test verifies the validity and quality of the introduced information. The same procedure is also performed if bypass option is selected. In this case, control parameters can be defined manually or internally as a function of initial consistency tests. Additionally, specific control parameters are also considered in each module to assure an appropriated estimation of interim and main output information.

The main outputs of the EFRHA model are generated in text and table data formats to make the format compatible with other software. Overall, main output data comprises the hazmat gas concentration fields given as temporal and spatial distributions for the receptor grids. Concentration values are expressed as micrograms per cubic meter of air ($\mu\text{g}\cdot\text{m}^{-3}$). The spatial concentration distribution output data can then be represented with any 2D surface visualization and data treatment software. Table B.2 (Appendix B) summarizes the principal output parameters generated during the simulation.

As for input data, main outputs can be divided in accordance to the model phase and type of data. Moreover with the exception of the EEM, most outputs from previous modules can be considered to be main inputs for, at least, one of the EFRHA modules. Aiming to enables post-processing of main output parameters, all outputs are generated in separated files depending on the module along the simulation. This option allows verifying the main features and performance of individual modules but above all, the entire model set up. Additional control messages are generated in case of errors or missing data detected during the calculation process.

3.8 Synthesis

This chapter presented the structure of the developed model, describing the various modules and modelling approaches implemented. Unlike most modelling systems currently applied in CA studies, EFRHA integrates a set of numerical approaches, usually separated, in an attempt to reduce well-known constrains and limitations frequently linked to the unavailability of

relevant information or specialized knowledge. Moreover, EFRHA attempts contributing for the application of alternative Class II modelling systems suitable to predict, as realistic as possible, the consequences of hazmat dispersion in industrial and built-up areas and to be applied in CA studies. The set of five main modules encompass the variety of information required to reliably perform a CA study. Nevertheless, as shown, the development, integration or even adaptation of available and developed modelling approaches and tools may result in a somewhat complex algorithm, which may require multiple information types and process techniques.

As described in this chapter, the developed tool comprises several modelling approaches and/or numerical methods, in an attempt to enable a broader application to different study scenarios and/or sets of available input data. However, it is necessary to evaluate if the sequential data flow is consistent, but most of all, if implemented atmospheric dispersion modelling approach and assumptions provide reliable results. For that reason, a set of validation exercises was performed, comprising the various modules and particularly the implemented modelling approaches and assumptions. With this purpose, Chapter 4 presents the set of performed validation exercises and main findings.

CHAPTER 4

4. VALIDATION OF EFRHA MODEL

This chapter contains the EFRHA model validation. An overview of the methodology, quality indicators and stages is provided. Next, quality analyses of modelled results based on four independent stages of evaluation are addressed. Finally, main findings from the validation study are discussed, emphasizing its reliability to predict hazmat gas accidental release and atmospheric dispersion in industrial and build-up areas.

4.1 Overview of the methodology

Models of whatever type are only of use if their quality (fitness-for-purpose) has been quantified, documented, and communicated to potential users. In this sense, evaluation plays a key role to assure quality and demonstrate that a model can provide reliable results for a desirable purpose. According to Britter and Schatzmann [2007a], model evaluation is a six steps process comprising the scientific evaluation, code verification, model validation with data, and user oriented operational assessment. Notwithstanding the relevance of scientific evaluation and code verification, model validation can be considered the mandatory requirement to assess the capability to numerically describe the various conditions and/or phenomena experimentally observed, and to have confidence on modelled results. Considering that scientific evaluation and model verification have been tested along the development process, the present evaluation methodology will focus on model validation, in order to demonstrate EFRHA reliable application and further user-oriented assessment.

Despite the lack of a generally accepted simple technique to determine whether a model is good or bad, there is an extensive experience and scientific background on Class II models validation methods, as discussed by Britter and Schatzmann [2007a,b]. Significant research has been conducted, over the last years, into devising structured methods for assessing model quality, based on direct comparisons of modelled outputs with reference experimental observations or results from models that have themselves undergone formal validation [Hanna *et al.*, 1991]. Although experimental observations are recommended to be used as reference data, modelled results can also be used in case of unavailable or limited measurements. Still, given their intrinsic uncertainties, modelled outputs should be used as

guidance to test consistency and similarity between modelled outputs [Hanna and Chang, 2001].

In view of EFRHA model Class, as well as main purpose of application, the model validation methodology suggested by Britter and Schatzmann [2007b] in the 'Model Evaluation Guidance Protocol Document' (MEGPD), was adopted. The MEGPD was developed in the frame of the COST Action 732 [URL4.1] compiling guidance, qualitative and quantitative analyses validation techniques, and quality indicators (metrics). It is based on preceding research initiatives, such as the work conducted by Hanna *et al.* [1991; 1993, 2004], European Research Community on Flow, Turbulence and Combustion (ERCOFTAC) [Casey and Wintergerste, 2000], Oberkampf *et al.* [2004], Chang and Hanna [2005], as well as, guidance documents, such as the German Association of Engineers (VDI) guidelines [VDI, 2005], the Model Evaluation Group (MEG) Guidelines [1994a,b] or the Scientific Model Evaluation of Dense Gas Dispersion models (SMEDIS) Protocol [Carissimo *et al.*, 2001].

Qualitative analysis can be considered a preliminary exploratory data evaluation based on visual inspection of modelled results graphical representations, like scatter, quantile-quantile or time/space evolution plots. This is a well suited approach to highlight observable features in predictions and reveal model shortcomings. Scatter plots show the degree of correlation between paired point-by-point modelled and reference values, their trends and offsets. Quantile-quantile (q-q) plots permit direct comparison of modelled and reference ranges of values, removing the pairing aspect of comparison. These plots are deduced by ranking both datasets from the highest to the lowest value and plotting ranked modelled against reference data pairs. According to Schatzmann *et al.* [2010] q-q plots are adequate to assess Class II models concentration outputs quality (more than scatter plots), because the user has to be sure that especially the highest values or high percentiles are reliably calculated; allowing the judgement of whether hazmat risk thresholds will be violated or not. Additionally, time/space evolution plots show the degree of agreement between modelled and reference data trends and ranges of values during a period of time or distance.

Quantitative analysis can be considered a more accurate and detailed study, based on the direct comparison of modelled results against reference data, in the form of statistical (quality) metrics, such as the ones defined by the American Society for Testing and Materials [ASTM, 2005]. The set of paired and unpaired quality metrics used in EFRHA validation study were: fractional bias (*FB*), geometric fraction within a factor of 2 (*FAC2*), correlation coefficient (*r*), normalised mean square error (*NMSE*), geometric mean bias (*MG*), geometric variance (*VG*),

squared bias (SB) and the difference between the standard deviations of modelled results and observations ($SDSD$). The expressions for the calculation of each of these metrics are summarized in Table 4.1, along with acceptability limits and 'perfect model' guidance values suggested for research-grade experiments, as given in the literature [Chang and Hanna, 2004].

Table 4.1 - Statistical parameters for the assessment of modelling performance. S_i is the i^{th} simulated value, M_i is the i^{th} measured value, and x is the quantity under analysis [Abramowitz and Stegun, 1972; ASTM International, 2005; Chang and Hanna, 2005].

Statistical parameters	Equation	Model acceptance criteria ¹	Ideal value	Units
Fractional bias	$FB = \frac{\sum_i (M_i - S_i)}{0.5 \sum_i (M_i + S_i)}$	$ FB < 0.3$	0.0	-
FAC2: fraction of data that satisfy				
Factor of two	$0.5 \leq \frac{S_i}{M_i} \leq 2.0$	$FAC2 > 0.5$	1.0	-
Pearson correlation coefficient	$r = \frac{\sum (M_i - \bar{M})(S_i - \bar{S})}{\left[\sum (M_i - \bar{M})^2 \times \sum (S_i - \bar{S})^2 \right]^{1/2}}$	Undefined	1.0	-
Normalized mean squared error	$NMSE = \frac{\overline{(M_i - S_i)^2}}{MS}$	$NMSE < 1.5$	0.0	-
Geometric mean bias	$MG = \exp(\ln \bar{M}_i - \ln \bar{S}_i)$	$0.7 < MG < 1.3$	1.0	[x]
Geometric variance	$VG = \exp\left[\overline{(\ln M_i + \ln S_i)^2}\right]$	$VG < 4$	1.0	[x ²]
Squared bias	$SB = (\bar{M}_i - \bar{S}_i)^2$	Undefined	.	[x ²]
Standard deviation of modelled results and observations	$SDSD = \left(\sqrt{\frac{1}{n} \sum_{i=1}^n (S_i - \bar{S}_i)^2} - \sqrt{\frac{1}{n} \sum_{i=1}^n (M_i - \bar{M}_i)^2} \right)^2$	Undefined	.	[x ²]

¹ The limit values for all the criteria represent typical thresholds on air quality modelling studies [Chang and Hanna, 2005].

While $NMSE$ and VG reflect both systematic and unsystematic (random) errors; FB and MG only indicate systematic errors. The FB is a symmetrical and bounded metric, with values ranging between -2.0 and +2.0 for, respectively, extreme over- and underestimation [Britter and Schatzmann, 2007b]. The r describes the correlation between the two datasets. The range

of modelled results levels can also be assessed by the unpaired-points *SB* and *SDSD* metrics. The *SB* describes the differences between modelled and reference mean values; while *SDSD* indicates possible failures on predicting the magnitude of fluctuations of reference data. Given their nature, *SB* and *SDSD* are mainly used in evaluation of concentrations datasets. Each metric has intrinsic characteristics that make it more or less proper for a desirable application; yet no single quantified metric is generally applicable to all conditions. Hence, simultaneous analysis of multiple metrics is recommended to verify model performance quality. Whilst *FB* and *NMSE* are deeply influenced by extremely high and low values, *MG* and *VG* guarantee a balanced treatment. Moreover, *FB* and *NMSE* make no sense for data that take both positive and negative values [Schatzmann *et al.*, 2010]. Even so, when both reference and modelled values vary significantly along the datasets, *FAC2* becomes the most robust indicator since it is not strongly affected by the deviations on the magnitude of the parameters [Chang and Hanna, 2005].

With the purpose of demonstrating the EFRHA aptness to produce quality assured results, but also identify its main features and weaknesses, a validation exercise comprising four independent stages was performed, as schematized in Figure 4.1. Performance quality and consistency of the EFRHA's modelled parameters (outputs and/or interim variables) was validated through its application to typifying test cases and direct comparisons of modelled results against reference data.

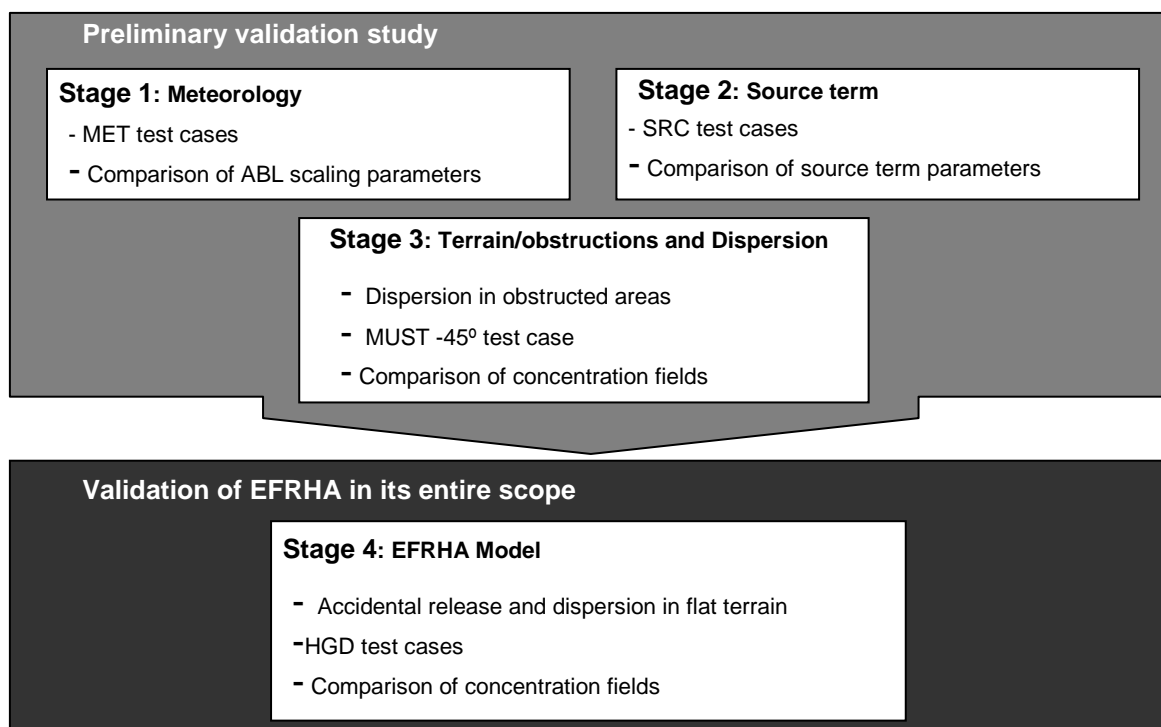


Figure 4.1 – Schematic summary of stages of EFRHA model validation exercise.

Preliminary analysis comprises the individual validation of EMM, ESTM and ETM+EDM (stages 1 to 3); whereas the last stage is the validation of the developed model in its entire scope. First, EMM and ESTM consistency to produce 'interim data' required for subsequent modules is analyzed individually in the first two stages. Next, the suitability of implemented modelling approaches in ETM and EDM to account the influence of obstructions in hazmat gas dispersion are jointly evaluated in the third stage. Finally, EFRHA aptness to reproduce quality assured short-term pollution episodes in case of hazmat gases accidental release and atmospheric dispersion is demonstrated in the last stage.

Direct comparisons of EFRHA's modelled outputs against extensively validated and used experimental observations or modelled results were carried out following the MEGPD validation techniques recommendations. EEM was not validated due to the nature of the implemented modelling and data processing approach.

4.2 Stage 1: Meteorology

In view of the influence of meteorological conditions in ESTM and EDM modelled outputs, the first stage of the validation consisted of the analysis of EMM performance quality. In view of this module's main purpose – input meteorological data treatment and estimation of ABL scaling parameters – direct comparisons between EMM modelled outputs and reference data were conducted. Test cases were defined and the following estimated ABL scaling parameters analyzed: Monin-Obukhov length (L), surface friction velocity (u^*), convective velocity scale (w^*), sensible heat flux (H), convective (z_{ic}) and mechanical mixing heights (z_{im}).

Considering that examined parameters are not commonly measured in routine monitoring stations, results from models that satisfy Hanna *et al.* [1991] recommendations can be alternatively used as reference data. Hence, in the lack of measured data, the AERMOD meteorological pre-processor AERMET [USEPA, 2004a,b; URL4.2] modelled outputs were used as reference data to assess EMM performance. This is a well-established and extensively validated meteorological pre-processor [Cimorelli *et al.*, 2004], developed to process input meteorological data for the atmospheric dispersion AERMOD model [USEPA, 2004a]. Both EMM and AERMET follow similar MOST principles, which make possible direct comparisons of modelled ABL scaling parameters results. Moreover, different assumptions and modelling approaches, in particular for missing or over-ranged data records, can be compared.

Aiming to cover a broad range of meteorological conditions and input content completeness, two distinct test cases were defined for the application of EMM and comparison with

AERMET outputs. The test cases summarized in Table 4.2 are based on extensively validated hourly surface and twice-daily upper air measured meteorological datasets recommended by USEPA for ‘exemplifying’ AERMET runs [URL4.2].

Table 4.2 – Summary of MET test cases used in EFRHA validation Stage 1.

Run ID	Location	Period of time	# records [h]	# missing data [h]
MET1	Albany County, NY	01/03/1988 – 04/03/1988	96	0
MET2	Houston, Texas	01/07/1996 – 31/12/1996	4,416	1,520

The MET1 test case can be considered a short-term complete input dataset, based on surface and upper air profiles meteorological observations measured in Albany County, New York (USA) between March 1st and 4th, 1988 (96 recorded hours). On the other hand, MET2 illustrates a long-term period comprising input surface and upper air datasets with limited (missing) contents. It consists of surface and upper air meteorological data measured in Houston, Texas (USA), between the 1st July and 31st December 1996 (4,416 recorded hours), with a total of 1,520 missing records, including surface and upper air records ($\approx 34\%$ of the total number of recorded hours). Whereas MET1 aims demonstrating EMM consistency with theoretical MOST approach principles and therefore, its aptness to estimate ABL scaling parameters; the application to MET2 intends verifying the suitability of implemented modelling algorithms and assumptions to deal with missing input meteorological data.

In any case, the same surface observations datasets were directly used by both models, but distinct upper air databases were required, due to various constrains on data availability and formats. Whilst data from the Meteorological Resource Centre database [URL4.3] was directly used in AERMET runs, data from the Department of Atmospheric Science of the University of Wyoming database [URL4.4] was processed for EMM runs. Anyway, detected differences between databases are only related to storage formats and number of parameters compiled.

With the purpose of demonstrating EMM consistency and performance quality, but also the reliability of implemented modelling assumptions, direct qualitative and quantitative comparisons of EMM and AERMET modelled results were conducted for the defined test cases. Visual inspection of scatter plots intends examining the level of correlation between modelled results. Additionally, quality metrics were estimated and results analyzed to check the degree of agreement between modelled outputs.

Figure 4.2 and Figure 4.3 present the comparison between EMM and AERMET modelled ABL scaling parameters in the form of scatter plots for MET1 and MET2, respectively.

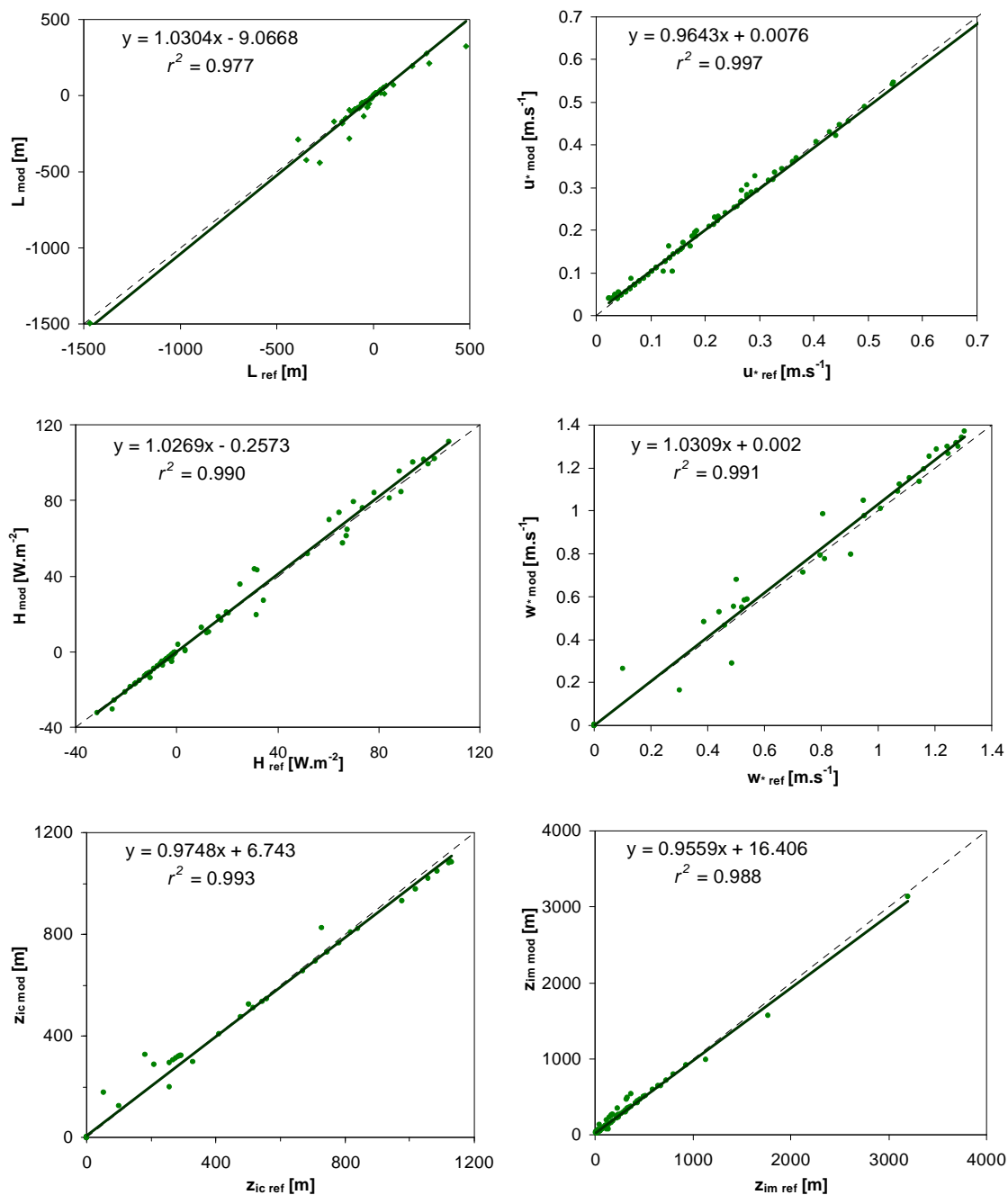


Figure 4.2 - Scatter plots of EMM modelled ABL scaling parameters for the MET1 test case period.

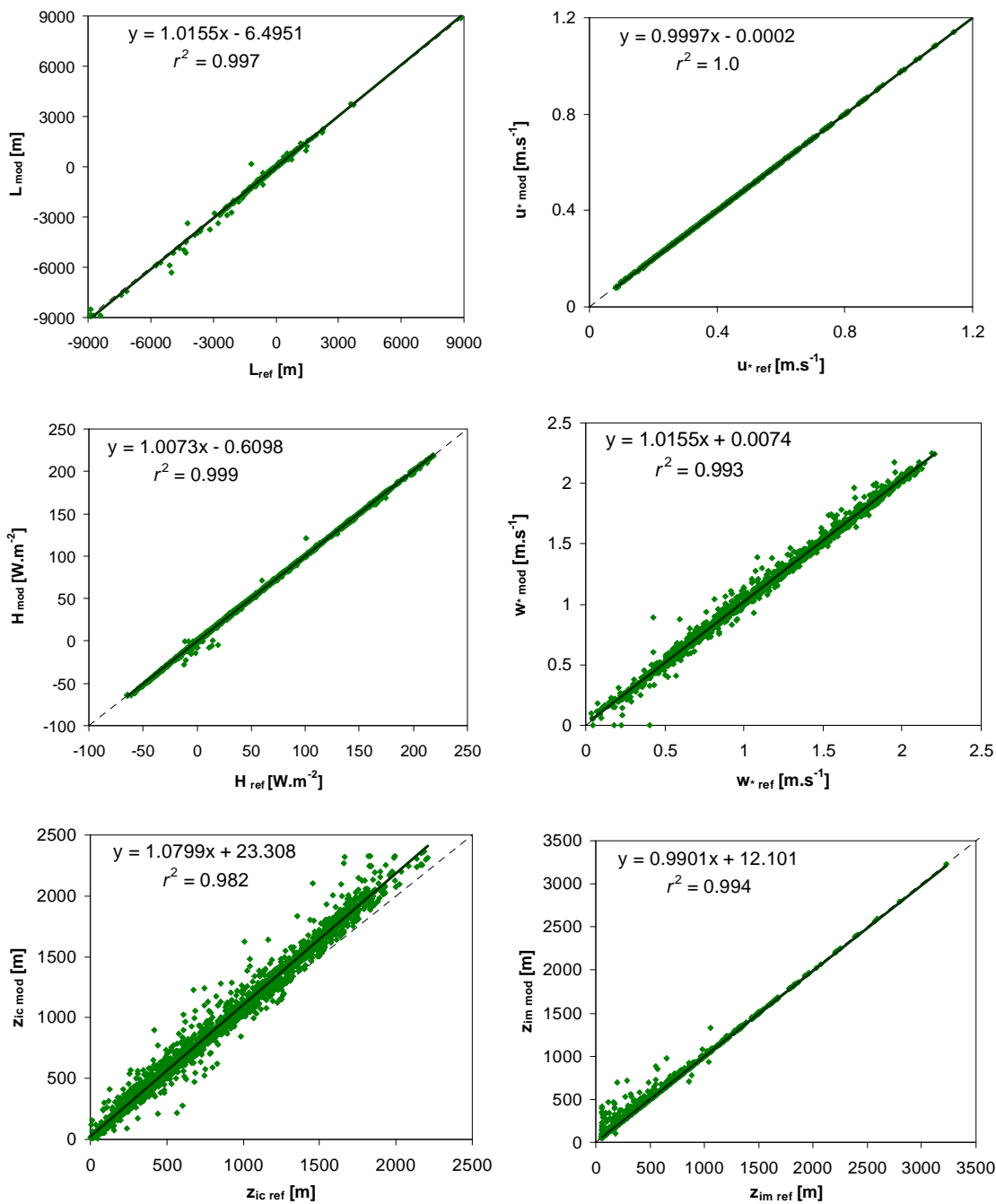


Figure 4.3 – Scatter plots of EMM modelled ABL scaling parameters for the MET2 test cases period.

Overall, Figure 4.2 and Figure 4.3 illustrate the strong approximation and high levels of correlation between EMM and AERMET modelled values, evidenced by the estimated linear trend lines ($r^2 \geq 0.977$ in MET1 and $r^2 \geq 0.982$ in MET2). Nonetheless, some positive and negative deviations from reference values can be observed in both test cases, particularly for L , w^* , z_{ic} and z_{im} parameters scatter plots. In general, the results indicate that EMM tends to present a somewhat increased degree of variation from AERMET outputs under neutral ($|L| > 150$ m) and convective ($|L| < 0$ m) conditions. Supported by the analysis of time evolution plots presented in Figure C.1 and Figure C.2 (Appendix C), it is noted the larger differences between modelled results during daytime and the transition periods, apart from the resemblances (in some cases near overlapping) in terms of temporal variation and ranges of values. In spite of the detected increased sensitivity of modelling algorithm for neutral and convective conditions, it is evident the consistency between modelled datasets.

The results show the strong influence of implemented algorithm, assumptions and calculation techniques, considering that the numerical methods follow the same theoretical approach. As expected, differences between calculation approaches, especially in the iterative procedures for the estimation of L , u^* and H can be detected on their own deviations, but also in a 'cumulative' way in w^* , z_{ic} and z_{im} results (see Figure 3.3). Moreover, in the case of z_{im} , despite the strong resemblances with u^* trend, it is also noted the influence of the smoothing technique, particularly for lower z_{im} values ($z_{im} < 1000$ m). Even so, it is visible the good correlation between modelled datasets, illustrating the reliable performance of EMM.

The analysis of MET2 modelled results evidences the reasonability of implemented modelling assumptions for missing data. Although presenting higher deviations in w^* and z_{ic} modelled results, it is also highlighted the good correlation between modelled datasets (through the analysis of estimated linear trend line r^2). Therefore, it is possible to mention that, despite punctual deviations, EMM reasonably reproduces meteorological and ABL conditions even in case of missing data, in particular during daytime periods.

Notwithstanding the visually demonstrated high degree of correlation between EMM and AERMET modelled datasets and consistency of implemented modelling approach, the set of quality metrics summarized in Table 4.3 was estimated for the modelled ABL scaling parameters, for each MET test cases, and compared with guidance model acceptance criteria (listed in Table 4.1) assuming AERMET modelled outputs the reference databases. Bearing in mind the use of AERMET datasets as reference data, it would be expected that estimated quality metrics concur with theoretical ideal values. Nonetheless, it was observed that the

values of *FAC2* for *L* and *H* do not fit so well with the expected 'ideal value' and acceptance criteria (see footnote of Table 4.3) These results indicate that, even the AERMET results for these parameters are not within a factor of 2. Such results must be taken into account during the analysis of EMM outputs.

Table 4.3 – Summary of quality metrics for modelled ABL scaling parameters for MET test cases (parameters not satisfying guidance acceptability limits are in bold).

Parameter	MET	FB	FAC2	r	NMSE	MG	VG
<i>L (m)</i>	1	-0.007	0.302 ^(a)	0.989	0.078	0.89	1.09
	2	-0.049	0.511 ^(b)	0.998	3.900	0.99	1.01
<i>u* (m.s⁻¹)</i>	1	0.021	1.000	0.994	0.040	0.95	1.02
	2	0.001	1.000	1.000	0.0	1.00	1.00
<i>H (W.m⁻²)</i>	1	0.017	0.333 ^(a)	0.995	0.0	0.93	1.04
	2	0.010	0.551 ^(b)	1.000	0.0	1.0	1.12
<i>w* (m.s⁻¹)</i>	1	-0.029	1.000	0.995	0.0	0.97	1.00
	2	-0.023	0.997	0.996	0.0	0.97	1.01
<i>z_{ic} (m)</i>	1	-0.126	1.000	0.994	0.020	0.88	1.03
	2	-0.103	0.988	0.991	0.020	0.88	1.05
<i>z_{im} (m)</i>	1	0.014	0.969	0.994	0.150	0.93	1.05
	2	-0.015	0.987	0.997	0.010	0.97	1.04

^(a) AERMET model L – *FAC2*=**0.333**, H – *FAC2*=**0.333**
^(b) AERMET model L – *FAC2*=0.511, H – *FAC2*=0.559

Despite the slender deviation tendencies previously observed in some modelled parameters, the analysis of quality metrics listed in Table 4.3 indicates that estimated quality metrics are overly within acceptance criteria, replicating the good correlation between EMM and AERMET modelled results. Additionally, the closeness of EMM results to reference guidance values for some parameters also demonstrates its good performance in both applications.

The *FB* between -0.126 and 0.017 reflects the mixed under- (*u**, *H* and *z_{im}* (MET1)) and overestimation (*FB*<0 - *L*, *w**, *z_{ic}* and *z_{im}* (MET2)) of EMM modelled outputs in relation to reference AERMET data. With the exception of *L* for MET1, the estimated *FAC2* values satisfy the recommended acceptance criteria with a noticeable nearness to reference ideal values, particularly for *u**, *w** and *z_{ic}*. Bearing in mind the exceptionality of AERMET reference *FAC2* for *L* and *H* parameters (see footnote of Table 4.3), it is also visible the substantial resemblance between AERMET and EMM estimated metrics, demonstrating the overall good correlation between modelled results. As expected, *r* values are markedly close to 1.0, supporting

previous visual inspections main findings. As regards to NMSE, only L (MET2) does not satisfy the acceptance criteria. However, following Schatzmann *et al.* [2010] indication that this metric does not make sense for datasets that take negative values (*e.g.* L and H), it is possible to mention that this result is not be considered in the overall analysis. Furthermore, supporting quality of modelled outcomes, the analysis of FB , $NMSE$, MG and VG results as a whole, illustrates that, no obvious influence of systematic or random deviations from reference data are detected in EMM outputs when applied to both test cases.

Overall, both qualitative and quantitative analyses demonstrate EMM aptness to process meteorological and ABL scaling parameters, even with large fractions of missing surface and/or upper air meteorological input data. Known the influence of L , u^* and H on $w^* z_{ic}$ and z_{im} values, related quality metric indicate that EMM modelling approaches and assumptions for missing data make possible the estimation of reasonable values. Additionally, the use of different upper air input databases did not visibly affected EMM modelled results quality, in spite of the fairly overestimation trend. Quality metrics also show that EMM modelling assumptions to extrapolate missing records and smoothing technique can produce reasonable z_{im} values, especially during the transition between night and daytime periods (and vice-versa).

Therefore, based on EMM application to both test cases and performance quality analyses, it is possible to state that this module is reliable to internally process meteorological information and estimate ABL scaling parameter required in subsequent modules. Its integration in EFRHA model not only reduces the number of strict mandatory input meteorological information, but also allows considering datasets with missing records, which are frequently considered/available in emergency response or planning studies.

4.3 Stage 2: Source term

An accurate description of hazmat gas outflow behaviour is crucial for a realistic prediction of atmospheric dispersion, particularly in accidental release scenarios. Although ESTM is designed to process instantaneous, continuous and transient release scenarios, the greater challenges and uncertainties are related to transient outflow conditions modelling, which require a special attention. Thus, assuming the effortlessness of instantaneous and continuous release scenarios data processes, this stage focuses on evaluating ESTM reliability to properly describe hazmat gas transient release scenarios. Moreover, known that ESTM incorporates well-established and validated models in the various sub-modules, in addition to the internal

chemical properties database (see Section 3.3), its performance quality strongly depends on the implemented modelling approaches and assumptions, as well as on the interaction between models and chemical properties database. For that reason, the main purpose of this stage is not to verify the performance quality of any specific model(s), but to assess the consistency of modelling approaches, assumptions, and interaction between the various components of ESTM, based on its application to the set of release scenarios summarized in Table 4.4.

Table 4.4 – Summary of test case scenarios defined for the ESTM validation study.

Run ID	Sub-Module	Release scenario
SRC1	ESTM1	- Transient release scenario of 95 m ³ of compressed hydrogen gas, initially stored at 50 bars and 15 °C, through a small hole in the vessel side-wall.
SRC2	ESTM2	- Transient release scenario of 5,280 m ³ of liquid acrylonitrile through a small hole in the vessel side-wall close to the bottom base surface.
SRC3	ESTM3	- ‘Champagne release’ from a safety relief valve of pressurized liquefied propane initially stored at 10.8 bars and 30 °C, through a small hole in a 4.7 m ³ vessel top side-wall.
SRC4	ESTM4	- Evaporation of an already formed liquid gasoline pool of about 1,500 m ³ at ambient temperature and pressure.

The set of SRCs is based on typifying outflow scenarios commonly used in exemplifying applications of theoretical methodologies or source term models [VROM, 2005a; TNO, 2007]. Information used for the definition of the SRC accident scenarios is summarized in Tables C.1 to C.4 (Appendix C).

Direct comparisons of ESTM modelled results and outputs from the well-established EFFECTS 7.5 model [TNO, 2007; URL4.5] were performed for the various outflow scenarios. This software tool is specifically designed to support CA studies and predict accidental release and atmospheric dispersion of hazmat gases. It also incorporates a set of extensively validated and used modelling approaches/models to estimate outflow conditions for typifying accident scenarios considered in CA studies. Because ESTM and EFFECTS 7.5 [TNO, 2007] integrate similar theoretical modelling methods, it is possible to carry out direct comparisons of modelled outputs and therefore verify the consistency of ESTM modelling approaches and assumptions, in particular for the reduction of the number of minimum mandatory input parameters in ESTM. A clear difference between models is the chemical properties databases used. Whereas ESTM uses the principles of Yaws [1999], EFFECTS 7.5 integrates the DIPPR database [URL4.6].

In spite of the number and variety of parameters estimated, this chapter presents the analysis of three parameters for each SRC scenario that can be considered relevant for demonstrating ESTM consistency and aptness to predict the accident scenarios. For SRC1, the evaluation of ESTM performance is based on direct comparison of mass outflow rate (q_s), gas temperature (T) and orifice pressure (P). In case of SRC2, direct comparisons of modelled and reference values were performed for liquid mass flow rate (q_{sL}), liquid filling degree (ϕ_L) and total liquid mass released (M_L). Given the complexity of the theoretical methodology developed for SRC3, the validation exercise comprises the comparison of gas mass flow rate (q_{sV}), ϕ_L and vapour fraction released (Φ_m). Finally, in SRC4 direct comparisons between ESTM4 modelled outputs and reference data were carried out based on the analysis of the following parameters: gas mass flow rate (q_{sVp}), liquid temperature (T) and liquid pool depth (h_L). Additional parameters could have been included in the comparison study; nonetheless, taking into account the implemented methodologies and correlations, the results would present significant resemblances on overall variations, replicating the analysis of the selected illustrative parameters.

A preliminary qualitative analysis of ESTM consistency and performance was carried out based on visual inspection of time evolution plots of the modelled parameters presented in Figure 4.4. At a first analysis, time evolution plots highlight the overall resemblances between ESTM and EFFECTS 7.5 modelled outputs for the set of SRC test cases. Nonetheless, some differences can also be detected on ESTM outputs, particularly in SRC3 and SRC4 tested parameters.

As regards to SRC1 modelled outputs (Figure 4.4. a), almost imperceptible overestimation of q_s and T values are obtained with ESTM1, in contrast to the small underestimation trend of P values. Given the apparent overlapping of corresponding datasets, mentioned deviations from reference data can be considered negligible. Therefore, it is possible to state that implemented modelling approaches and assumptions and the chemical properties database are consistent with reference EFFECTS 7.5 outputs, in case of initially compressed gas.

Visual inspection of Figure 4.4b indicates that ESTM2 modelled spill phenomenon stops earlier than reference EFFECTS 7.5 values. Such difference is mainly caused by the slight, but still relevant, overestimation trend of q_{sL} values. Consequently, this deviation generates the overestimation of M_L and underestimation of ϕ_L . Nonetheless, overall analysis of modelled results time evolution plots shows that ESTM2 modelled parameters follow the same variation and ranges of reference values, demonstrating the good correlation between datasets.

The time evolution plots of ESTM3 main outputs (Figure 4.4c) show that, even with perceptible deviations from reference data, the results tend to follow the overall behaviour of EFFECTS 7.5 model values. A general overestimation of q_{sV} and Φ_m is observed along the simulation period, in particular during the initial instants of the release, opposing the underestimation of ϕ_L modelled values.

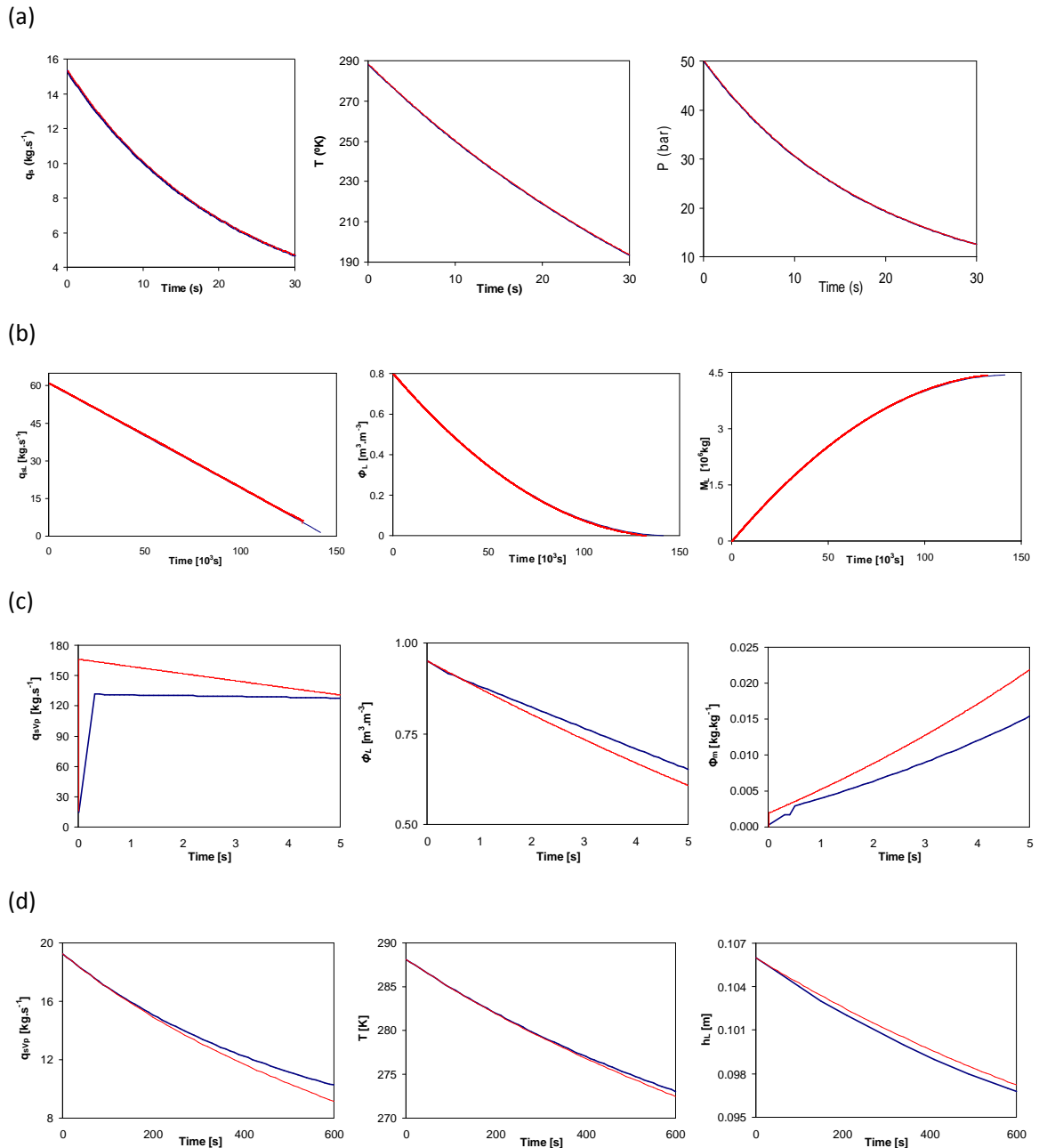


Figure 4.4 - Time evolution of source term parameters of EFRHA (red) and EFFECTS 7.5 (blue) models for: (a) SRC1, (b) SRC2, (c) SRC3 and (d) SRC4 test cases.

Since input data and mathematical principles are identical in both approaches, the main cause of the estimated differences is the implemented code algorithm, modelling assumptions and chemical properties parameters used along the numerical procedure (e.g. ρ_L , vapour saturation pressure (P_v^o) or liquid and vapour heat capacities (C_{pL} , C_{pv})). Disparities (even just small differences) on chemical properties databases values combined with modelling assumptions will endorse larger deviations along the calculation process, resulting in the observed variation on modelled results. Even with the detected deviations from reference values, the visual inspection of time evolution plots illustrates ESTM reliability to produce reasonable outputs.

Finally, visual inspection of Figure 4.4d enables realizing the consistency of ESTM4 modelling approach. There is a trend of ESTM4 to underestimate q_{svp} , and subsequently overestimate h_L values, mainly due to the direct dependency of remaining liquid fraction in the pool on the degree of evaporation. Although not so visible, especially during the initial instants, a general tendency to underestimate T can also be noted. Once again there is an influence of EFRHA chemical properties database in these results, since near identical mathematical methodologies are implemented in ESTM and EFFECTS 7.5.

Notwithstanding the good correlation and consistency between the ESTM and the EFFECTS 7.5 outputs, a quantitative analysis of quality metrics was also carried out and main results are listed in Table 4.5.

Table 4.5 – Summary of quality metrics of ESTM modelled source term parameters for the set of SRC test cases.

SRC	Parameter	FB	FAC2	r	NMSE	MG	VG
1	q_s ($kg.m^{-3}$)	-0.004	1.0	1.0	0.0	1.00	1.00
	T (K)	-0.004	1.0	1.0	0.0	1.00	1.00
	P (bar)	0.005	1.0	1.0	0.003	1.03	1.02
2	q_{sl} ($kg.m^{-3}$)	-0.007	1.00	1.00	0.00	0.99	1.00
	ϕ ($m^3.m^{-3}$)	0.013	0.98	1.00	0.00	1.05	1.09
	M_L (kg)	-0.005	1.00	1.00	0.00	1.00	1.00
3	q_s ($kg.m^{-3}$)	-0.114	1.00	0.92	0.02	0.90	1.02
	ϕ ($m^3.m^{-3}$)	0.030	1.00	1.00	0.00	1.03	1.00
	Φ_m ($kg.kg^{-1}$)	-0.217	0.94	0.99	0.22	0.79	1.27
4	q_{svp} ($kg.m^{-3}$)	0.029	1.00	0.99	0.00	1.00	1.00
	T (K)	0.001	1.00	1.00	0.00	1.00	1.00
	h_L (m)	-0.020	1.00	0.99	0.00	1.00	1.00

As expected, all estimated metrics are within acceptability limits and remarkably close to recommended guidance perfect model thresholds. The *FB* values between -0.217 and 0.03 reveals the slender deviations from EFFECTS 7.5 modelled outputs. The estimated deviations may result from the uncertainties associated with mathematical expressions used along the calculation process, but also from implemented modelling assumptions and divergences on chemical properties databases. With the exception of q_{svp} in SRC4, there is an overall tendency to overestimate mass flow rate (q_s , q_{SL} and q_{svp}). Visually detected differences between ESTM and EFFECTS 7.5 modelled outputs are replicated in *FB* values, in practically all SRC test cases. Furthermore, the values of *FAC2*, *r*, *NMSE*, *MG* and *VG* close to 'ideal values' emphasize the elevated level of agreement (in some cases 'almost perfect') between ESTM and EFFECTS 7.5 datasets.

Overall, the application of ESTM to the set of SRC test case demonstrates its consistency and reliability to generate valid results in case of transient release scenarios. It is also shown that implemented modelling approaches and assumptions respect theoretical/mathematical methodologies principles. Apart from slender deviations, especially in liquid or PLG source term modelling outputs, the main advantages of the chemical properties database integration to estimate valid interim data, in an attempt of reducing the number of required user defined input parameters, don't causes significant errors or critical deviations from reference values.

4.4 Stage 3: Dispersion in obstructed areas

In order to demonstrate EFRHA aptness to include the influence of obstructions, in particular obstacles, on modelled concentration fields and provide reasonable results, the third stage of EFRHA validation exercise focuses on the evaluation of ETM and EDM modelling approaches. With this purpose, a joint application of both modules to the Mock Urban Setting Test (MUST) -45° wind inflow experimental set up was carried out. Direct comparisons of modelled and measured values of mean concentrations were conducted in the form of exploratory data graphical representations (qualitative) and quality metrics (quantitative) analyses.

4.4.1 The Mock Urban Setting Test experiment

The MUST experiment was originally a set of full-scale field tests focused on investigating the transport and atmospheric dispersion behaviour of plumes and their detailed concentration structure within an idealized urban atmospheric boundary layer under real atmospheric conditions. The set of tests was conducted at West Desert Test Centre of Dugway Proving

Ground, a US Army test facility in Utah (USA) in September 2001 [Yee and Bilitoft, 2004]. The experimental set up centred in an area of 200 by 200 m long, consisted of a nearly regular array of 12 by 10 aligned obstacles composed by 119 shipping containers (12.2 m long, 2.42 m wide and 2.54 m high), together with the so-called 'VIP car' (6.10 m long, 3.51 m high and 2.44 m wide) located near the centre of the obstacles array, as illustrated in Figure 4.5. The VIP car served as a measuring point for sampled wind and concentration data.

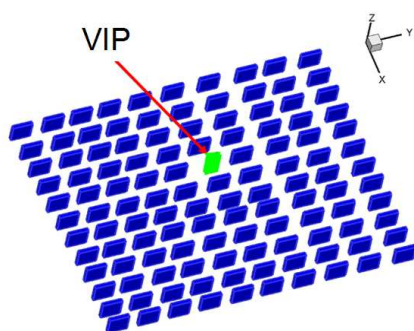


Figure 4.5 - 3D perspective of MUST case obstacles array with identification of VIP car

The test site can be described as flat open terrain homogeneously covered by sparse vegetation [Yee, 2004]. Most of the tests were conducted at the late evening and night under slight to strong stable ABL stratification conditions with prevailing south-easterly and lower than 3 m.s⁻¹ winds (at building height) [Bezpalcova, 2007]. Short (quasi-instantaneous) and long (quasi-steady state) duration point sources with varying locations were tested and flow and dispersion measurements performed; however in the scope of EFRHA validation study only long duration point sources were taken into account. Several meteorological and concentration sensors were placed around, above, and throughout the array on various towers [Yee, 2004]. Detailed descriptions of MUST field experiments instrumentation, inflow and dispersion conditions are given in Bilitoft [2001], Yee [2004] and Yee and Bilitoft [2004].

Notwithstanding the relevance of full-scale experiments, small-scale wind-tunnel experiments were also conducted aiming to reproduce the field experiments, obtaining more accurate and complete information of flow and dispersion [Schatzmann *et al.*, 2010]. For that reason, measured data from the -45° MUST test case wind-tunnel experiment reported by Bezpalcova and Harms [2005] and Bezpalcova [2007] was used in this stage of the EFRHA validation. The experiments were carried out in the large boundary layer wind tunnel facility 'WOTAN' at the Environmental Wind Tunnel Laboratory (EWTL) of Hamburg University, shown in Figure 4.6.



Figure 4.6 -The MUST wind tunnel model set up in WOTAN facility [Bezpalcova and Harms, 2005].

The scaled 1:75 model set up of field test containers array, including slight irregularities in the obstacles placement, was placed on the wind tunnel's turn table (see Figure 4.6), modelled in a stably stratified boundary layer flow [Bezpalcova, 2007]. To assure the consistency of wind tunnel measurements, the experimental coordinate system was subsequently converted into real scale coordinates, enabling further comparisons and data analysis based in a unified coordinate system as schematized in Figure 4.7.

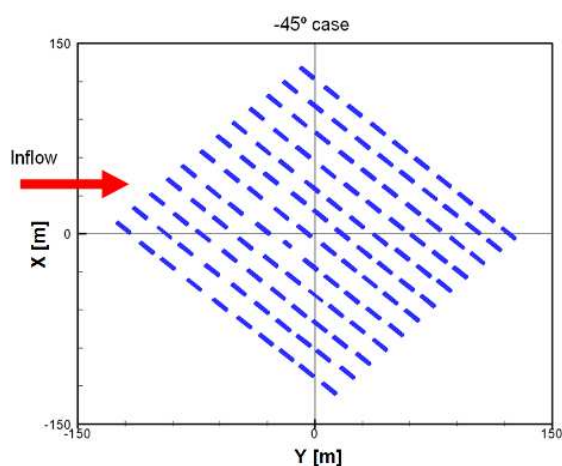


Figure 4.7 - MUST test set-up reference coordinate system for the -45° MUST case.

Measurements of flow properties were recorded at different positions and heights within the obstacles array [Bezpalcova and Harms, 2005]. The results of flow observations were non-dimensionalized by an inflow measured wind velocity at a given reference height ($7 \text{ m}\cdot\text{s}^{-1}$ at 9 m height). In terms of dispersion modelling, the point source and concentration measurements locations schematized in Figure 4.8 were used to describe, as detailed as possible, modelled mean concentrations spatial distribution within the obstacles array and the source locates at the point (-102, -7) m according to the 'normalized coordinates system.

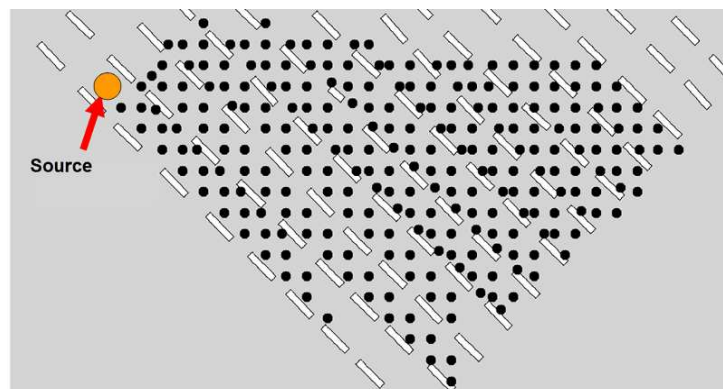


Figure 4.8 - Location of point source (orange spot) and concentration sensors (black spots) considered for the -45° MUST case validation study.

A quasi-stationary ethane outflow emission rate of about 7 g.s⁻¹ was tested in the wind tunnel experiments, to simulate the dispersion of a neutrally buoyant tracer [Bezpalcova, 2007]. Yet, due to technical reasons, wind tunnel modelled point source was located at ground level, with a corresponding diameter of 0.75 m at full scale, instead of the 0.05 m diameter elevated pipe used during the field tests. Mean concentration in the 256 points around the obstacles (Figure 4.8) were measured at a height of 1.275 m [Bezpalcova and Harms, 2005]. To make possible concentration data rescaling adapted for any user or model specific needs, measurements of mean concentrations were normalized and estimated in the form of dimensionless concentrations (C^*) [Schatzmann *et al.*, 2010] as follows:

$$C^* = \frac{Cu_{ref}H_{bd}^2}{q_s} \quad \text{Eq. 4-1}$$

In which C is the measured volume concentration (background-corrected), u_{ref} is the reference wind velocity (measured at 9 m), H_{bd} is the container height (2.54 m) and q_s is the source mass outflow rate [Schatzmann *et al.*, 2010].

4.4.2 EFRHA modelling set up and validation for the -45° MUST case

With the purpose of accounting the presence of obstructions, EFRHA model is designed to use surface base elevation and buildings spatial characterization based on the combination of their top elevation/height and surface roughness height (z_0) description (see Section 3.3). Bearing in mind that different combinations of input data can be used to numerically describe the presence of obstacles, it is of major importance to demonstrate the most appropriate Input Obstructions Configurations (IOMC) to predict, hazmat dispersion in industrial and urban areas. For that reason, the set of six different IOMCs listed in Table 4.6 was defined, based on

ETM buildings description techniques and z_0 values applied to the -45° MUST case buildings configuration.

Table 4.6 – Overview of the IOMC runs and input parameters for the -45° MUST case.

Run ID	Obstacles	z_0 [m]	Comment on z_0 definition
IOMC1	Buildings heights	0.300	Wind profile in the middle of the building array.
IOMC2	Buildings heights	$0.1 \cdot H_{bd}$	Recommended in MEGPD.
IOMC3	Buildings heights	0.035	Wind profile above the source location.
IOMC4	No	0.300	Wind profile in the middle of the building array.
IOMC5	No	$0.1 \cdot H_{bd}$	Recommended in MEGPD.
IOMC6	No	0.035	Wind profile above the source location.

Simple and complex ways to include the obstructions were examined using the joint ETM-EDM modules system. The most complex ways to integrate buildings were used in IOMC1 to IOMC3, considering the 120 individual buildings spatial distribution based on their top height variation in relation to the ground level, independently of the z_0 value. On the other hand, in IOMC4 to IOMC6 assume a flat terrain without any kind of physical obstruction.

Additionally, the influence of surface roughness characterization was tested by defining different values for z_0 in both sub-sets of IOMCs. Both guidance (theoretical) and experimental (from the wind-tunnel tests) based data were considered and representative values input in the various IOMC configurations (with and without obstacles). In IOMC1 (with), and IOMC4 (without) a value of $z_0 = 0.300$ m derived from wind profile observations measured in the middle of the obstacles array [Bezpalcova and Harms, 2005] was used. Following the MEGPD recommendations, a value around 10% of H_{bd} was provided for z_0 (≈ 0.254 m) in IOMC2 (with) and IOMC5 (without). Whereas in IOMC3 (with) and IOMC6 (without) was employed a $z_0 = 0.035$ m, deduced from wind profile observations at the source location [Schatzmann *et al.*, 2010].

In order to properly apply ETM-EDM to the -45° MUST test case, a simulation domain with 450x450 m with a horizontal grid resolution of 5x5 m was applied, in which concentrations were estimated at a height of 1.275 m from the ground, as experimentally performed. To assure the proper comparison between modelled and measured concentration values, the spatial distribution of the 256 sensors locations was also considered, based on experimental data previously documented in the scope of COST Action 732 [URL4.1].

Taking into consideration that EFRHA modelling parameterizations are not capable to accurately describe the flow behaviour around buildings, like Class III CFD models, the

validation study was conducted based on the analysis of modelled mean concentrations spatial distribution for the set of IOMC runs as recommended in MEGPD for 'non-CFD models' [Britter and Schatzmann, 2007a; Schatzmann *et al.*, 2010]. Therefore, aiming to validate EFRHA performance, q-q and scatter plots, plume features and quality metrics calculated using the 'Excel sheets' [Olesen and Berkowicz, 2008] developed for the evaluation of Class II models in the frame of COST Action 732 work [URL4.1] were analyzed.

To evaluate the degree of correlation between modelled and measured ranges of concentrations visual inspection of q-q plots was performed without considering their coincidence in time and space, avoiding the 'spatial dependence' of scatter plots point-by-point validation as recommended in MEGPD [Britter and Schatzmann, 2007a] and by Schatzmann *et al.* [2010]. Figure 4.9 presents the set of q-q plots obtained for the IOMC modelled data against measured concentrations for the -45° MUST case.

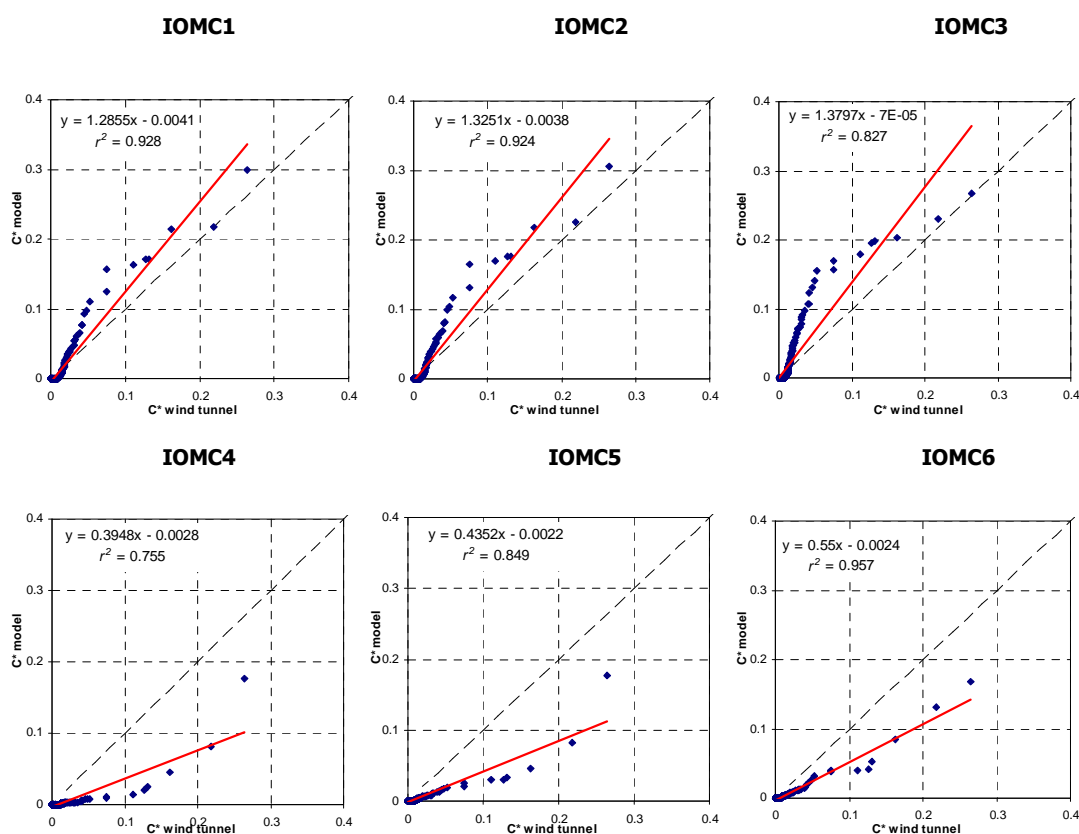


Figure 4.9 - Q-q plots of the IOMC modelled against measured concentrations for the -45° MUST case.

At a first analysis, it is visible an overall better performance for IOMCs with obstacles (IOMC1 to IOMC3), illustrating the added-value of the implemented modelling approach in ETM-EDM. In general, results from IOMCs with obstacles tend to approximate more to reference

observations, evidenced by the estimated linear trend lines and related r^2 values; but at the same a clear overestimation of intermediate values is also detected. On the other hand, IOMCs without any consideration of obstructions (IOMC4 to IOMC6) present a considerable underestimation trend in all ranges of concentration values and less favourable trend lines. As regards to the potential influence of z_0 , it is possible to observe a somewhat opposing behaviour for 'extreme' values (0.035 m and 0.30 m), if obstacles are considered or not. Even hardly noticeable, a somewhat increase of the degree of correlation is observed for higher z_0 values in case of IOMCs with obstacles (IOMC1); in contrast to the worsening trend noted in IOMCs without any obstacle.

Although IOMC1 and IOMC2 show larger overestimations of higher values, as stated by Schatzmann *et al.* [2010], it is preferable a Class II model that produces somewhat overestimated data in order to assure a more credible performance. For that reason, and based on the overall analysis it is possible to mention that, q-q plots clearly demonstrate the increased performance quality when considered the ETM-EDM modelling approaches to account the presence of obstacles.

To support the previous analysis, Appendix C contains the comparison and analysis of data based on scatter plots and conclusions are similar. Even not being over-interpreted, scatter plots also highlight the added-value of implemented modelling approach for the presence of obstacles, as well as, the stronger tendency of overestimation in IOMC1 to IOMC3, when compared with IOMC4 to IOMC6. It also presents the spatial distribution of concentration residuals (ratios between modelled results and measurements), highlighting the somewhat differences between concentration fields with and without obstacles. Moreover, the results evidence the substantial resemblances with similar Class II dispersion models.

Verified the relative consistency of measured values along the trajectory, Schatzmann *et al.* [2010] deduced an approximation of observations to a Gaussian fit, enabling the direct comparison between modelled and measured concentrations in the form of descriptive plume feature parameters. Gaussian fitting of measured concentrations consisted on fitting a Gaussian curve to each measured cross-section along the dispersion trajectory x -axis allowing estimating a representative maximum concentrations (C^*_{max}) in the plume centre line and the correspondent standard deviation of the horizontal distribution (σ_y) along the x -axis trajectory. Similarly to previous q-q (and scatter) plots, the 'Excel sheet' developed by Olesen and Berkowiks [2008] in the frame of COST Action 732 were used to calculate and plot both estimated C^*_{max} and σ_y along trajectory centrelines (x -axis) [Schatzmann *et al.*, 2010] for each

IOMC run outputs. Figure 4.10 shows the estimated C_{max}^* in the plume according to measurements and IOMC runs results. The source was located at the point (-102;-7) m.

Overall, Figure 4.10 shows the typical variability of concentrations spatial distribution previously discussed by Hankin [1997]. Visual inspection of modelled C_{max}^* shows that, even with a clear overestimation tendency, all IOMC modelled results tend to follow the variation trend and ranges of measured observations, especially the ones with the definition of obstacles. Despite the fairly resemblances of IOMCs estimated C_{max}^* at distances near the source (until $x \approx 40$ m), it is perceptible the overall influence of the inclusion (or not) of the obstacles modelling approaches, in particular for $x > 40$ m points. Even presenting a larger variability of C_{max}^* (with varying degrees of magnitude), in particular at farther distances from the source ($x \geq 40$ m), IOMCs with obstacles tend to be closer to measured values than IOMCs without with a smaller variability tendency.

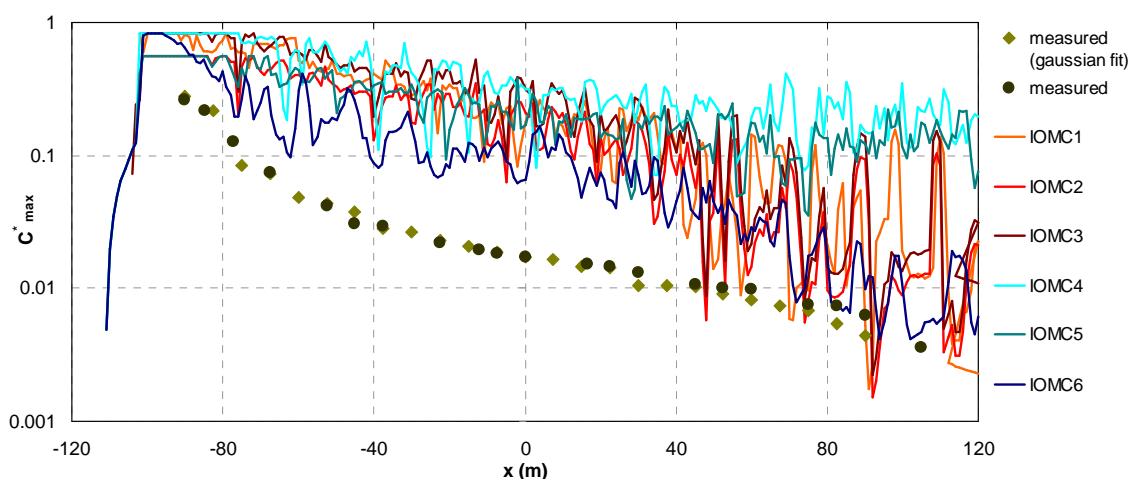


Figure 4.10 – Estimated maximum concentrations using Gaussian fitting, with distance x from the source (with obstacles IOMC1 – IOMC3; without obstacles: IOMC4 – IOMC6).

Corroborating q-q plots visual inspection, it is also noted the influence of z_0 values. Opposing the less favourable performance for IOMC4 and IOMC5, IOMC6 presents a clearly better performance for estimated C_{max}^* values that tend to approximate more to measured data, with ranges of values quite similar to IOMCs with obstacles at farther distances. As regards to IOMCs with obstacles, such differences are not so evidenced along the x distance.

The analysis of C_{max}^* distribution along the x -axis trajectory evidences the overestimation tendency previous detected in q-q plots, but most of all, highlights the reasonability of ETM-EDM modelling approaches to account the presence of obstructions. Contrarily to previous main findings, differences between estimated C_{max}^* from IOMCs with obstacles are hardly

noticeable, even so it is also demonstrated the wider approximation of IOMC1 and IOMC2 results to reference measured and estimated C_{max}^* values.

Aiming to evaluate C_{max}^* lateral consistency along x -axis, correspondent σ_y values were estimated for both measured and modelled concentrations and plotted in Figure 4.11.

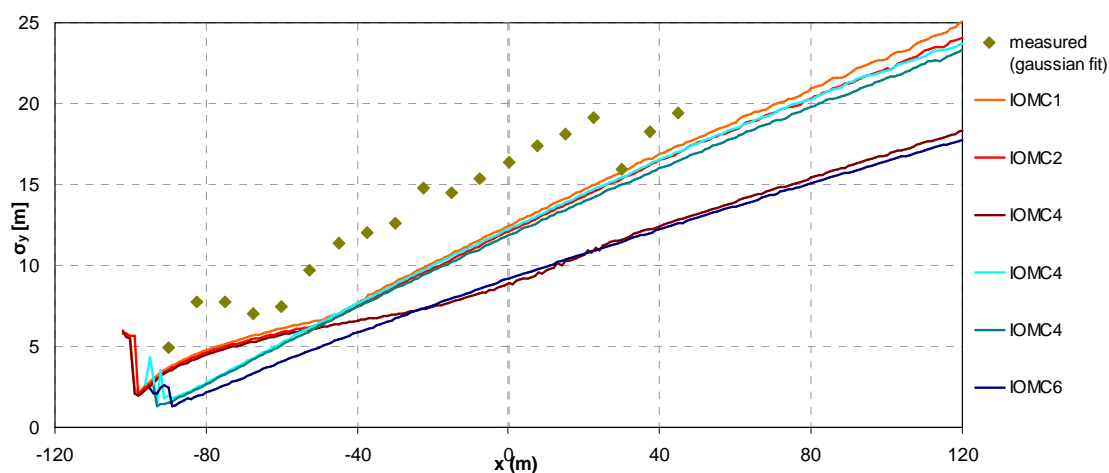


Figure 4.11 - Estimated plume width, using Gaussian fitting, with distance x from the source for the IOMCs.

The analysis of Figure 4.11 shows the general propensity of IOMC modelled results to underestimate measured (Gaussian fitting) σ_y values, regardless the noticed analogous tendency 'shape' along distance x . A pronounced influence of z_0 values is also displayed through the significantly lower values of IOMC3 and IOMC6 ($z_0=0.035$ m), particularly for ($x \geq -40$ m). In general higher z_0 (0.3 m and 0.254 m) values produce a better and consistent agreement with correspondent σ_y measured observations. Contrarily to previous analysis, IOMC6 shows the less favourable results of IOMCs without obstacles, significantly similar to the IOMC4 σ_y values. Such results are mainly due to the strong influence of σ_y values in the cloud lateral dispersion.

Overall, examined σ_y values are consistent to previous C_{max}^* and spatial variation. In contrast to previous main findings from Figure 4.10, variability of EDM modelled results is not as obvious as for C_{max}^* plots. Yet, clear divergences are detected, not only in the closer distances from the source, but also along the plume trajectory.

Regardless Schatzmann *et al.* [2010] stating that the analysis of paired point-by-point quality metrics is not totally recommended and may not make sense for EDM's Class model, both paired and unpaired point-by-point quality metrics were estimated for the set of IOMC runs following MEGPD recommended methodology. Direct comparisons of paired point-by-point

modelled and measured concentrations were considered as in the scatter plots represented in Figure C.3 (Appendix C). Quality metrics were also estimated using the COST Action 732 developed Excel sheet [Britter and Schatzmann, 2007b; Olesen and Berkowicz, 2008]. Table 4.7 summarizes the estimated quality metrics for the set of IOMCs. The best results for each metric are highlighted in bold and the ones that satisfy acceptance limits underlined.

Table 4.7 – Summary of quality metrics estimated for IOMC runs modelled concentrations of -45° MUST case (with: IOMC1 – IOMC3; without: IOMC4-IOMC6).

Run ID	FB	FAC2	NMSE	r	MG	VG	SB	SDSD
IOMC1	<u>0.071</u>	0.254	4.47	0.697	1.41	4.78	7.5E-7	<u>6.4E-5</u>
IOMC2	<u>0.008</u>	0.267	4.54	0.689	1.36	5.00	<u>1.2E-8</u>	8.3E-4
IOMC3	0.343	0.243	5.84	0.533	<u>1.11</u>	7.95	2.7E-5	2.0E-4
IOMC4	1.160	0.335	13.57	0.619	1.98	4.03	8.7E-5	2.0E-4
IOMC5	1.160	0.314	13.54	0.625	1.94	4.11	8.7E-5	2.2E-4
IOMC6	0.933	0.251	9.93	0.579	1.79	4.09	6.5E-5	1.5E-4

The overall analysis of estimated metrics summarized in Table 4.7 shows that, even not fulfilling most of proposed acceptance criteria, IOMCs with obstacles (IOMC1, IOMC2 and IOMC3) have the best results for the set of quality metrics, in contrast with the IOMCs without any obstacle (IOMC4, IOMC5 and IOMC6), with the less favourable results. Therefore, it is 'quantitatively' shown the 'better' performance quality of IOMC test cases with the inclusion of obstacles structures and consequently ETM-EDM modelling approach to account the presence of obstacles when applied to the -45° MUST test case wind-tunnel experimental set up. Moreover, quality metrics replicate previous qualitative analysis main findings, *i.e.* the best results are obtained for IOMC1 and IOMC2 in case of IOMCs with and without obstacles, respectively; whilst the worst results are obtained for IOMC4 and IOMC5 (IOMCs without obstacles).

As regards to the *FB*, the values between 0.008 and 1.16 highlight the underestimation of concentrations tendency, also presented in scatter plots (Figure C.3 of Appendix C). Nonetheless, only IOMC1 and IOMC2 satisfy the acceptance criteria and IOMC4 and IOM5 are the less favourable results, demonstrating the relevance of account the presence of obstacles. None of IOMCs satisfy *FAC2* and *NMSE* acceptance criteria showing the somewhat degree of deviation from measured concentrations that may result from systematic or random errors [Chang and Hanna, 2005]. The better result for *FAC2* is estimated in IOMC4, whereas the worst value is estimated for IOMC3 data. On the other hand, for *NMSE* an opposite result is obtained, in which the better results are estimated for IOMC1 and the worst for IOMC4.

Despite not considering a reference acceptance limit for the r , it is clear the 'better performance' of IOMC1 and IOMC2 corroborating previous observations.

Concerning MG , only IOMC3 satisfies the acceptance criteria, yet the overall estimation of values higher than 1.0 reflect the general tendency to 'systematically underestimate' the observed concentrations as mentioned by Chang and Hanna [2005]. Despite having a better performance when MG values are analyzed, IOMC3 show the lesser favourable results for VG . Contrarily to other metrics, IOMC runs without any obstacles (IOMC4 - IOMC6) show slightly higher performance quality trends. Overall, the results for VG combined with MG , reflect the visually noted systematic tendency to underestimate measured concentrations. As regards to the unpaired in space point-by-points based quality metrics results (SB and $SDSD$ values), the less favourable results are obtained in IOMCs without obstacles, showing the improved degree of correlation in terms of concentration magnitudes 'quality' when obstacles are taken into account. These parameters (SD and $SDSD$) replicate the previously discussed results from the q-q plots (Figure 4.9). Whereas SB shows in general substantially reduced values given the ranges of concentrations, $SDSD$ estimated values are at least one order of magnitude higher, reflecting the deviations of modelled concentrations, but also the influence of the presence of not of obstacles.

Even the analysis of quality metrics should not be over-interpreted [Schatzmann *et al.*, 2010], the overall performance of the various IOMC configurations demonstrates the suitability of ETM-EDM modelling approaches to account the presence of obstacles through the effective description of the obstacles spatial distribution, than just increasing the z_0 values. From the analysis of the various IOMC configurations results it is obvious that the performance of the model is strongly dependent on the chosen input configuration and the selection of input parameters, such as the inclusion of buildings spatial distribution and z_0 values.

When compared the various IOMCs modelled outputs, it is visible the improvement of results if buildings are numerically described, even using simple modelling approaches as in ETM-EDM for IOMC1 and IOMC3 input data configurations. Despite the improvements, z_0 values can also influenced the estimated results. For instance, for IOMC1 and IOMC3 which use the same modelling approach to numerically describe the influence of buildings, but different values for z_0 (0.3 and 0.035 m, respectively) strongly affect the estimated concentration fields. Therefore, in order to predict, atmospheric dispersion of hazmat gas in obstructed areas, or not (given IOMC4 and IOMC6 had comparable dissimilarities), the definition of proper z_0 values is important for the overall performance quality.

On the whole, the third stage of the validation exercise demonstrated EFRHA's aptness to account, even in a relatively simple way, the effects of the presence of obstacles in atmospheric dispersion of hazmat gases in industrial and/or built-up areas. Although the implemented approach is not capable to accurately describe the flow around the obstacles, but considering the main purpose of application, it is demonstrated the suitability to provide 'better' results than 'traditional' Class II models, and therefore be used as an alternative, especially for CA studies in industrial and built-up urban areas. The results highlight the variability and general tendency to overestimate measured concentrations, even so, and if compared with the set of models considered in Schatzmann *et al.* [2010], visual inspection reflects the improved capability to account the presence of obstructions. Nonetheless, in case of dispersion in obstructed areas, it may also underestimate, in particular the lateral concentrations, but also, the accurate flow around the obstacles.

4.5 Stage 4: Dense gas accidental release and dispersion

Taking into consideration that most industrial hazmat when released into the atmosphere can form dense gas clouds during (at least) the early moments of the dispersion, the last stage of the validation study intends demonstrating EFRHA suitability to produce quality assured short-term concentration fields when applied to (heavy) hazmat gas accidental release and dispersion scenarios, in its entire scope. With this purpose, the set of Dense gas Dispersion (DGD) test cases summarized in Table 4.8 was defined to validate the developed model. The set of examined DGD test cases are based on well-established experimental tests from full-scale field trials (Thorney Island, Burro, Desert Tortoise and Lathen field trials), extensively used in model validation exercises. Several release, dispersion, meteorological and obstructions conditions were considered in the applied test cases. As regards to hazmat gas release conditions, instantaneous gaseous (DGD1 and DGD2), liquefied gas spill with subsequent evaporation (DGD3, DGD4) and continuous vapour jet (DGD5, DGD6, DGD7 and DGD8) release scenarios were tested. Different meteorological conditions were also examined, particularly, atmospheric stability, ambient temperature and wind velocity, as summarized in Table 4.8.

Additionally, flat unobstructed (DGD1, DGD3, DGD4, DGD5 and DGD6) and obstructed (DGD2, DGD7 and DGD8) terrain conditions were taken into account based on the information summarized in Table 4.8.

Table 4.8 – Overview of experimental data sets used for the validation of EFRHA model. [Nielsen and Ott, 1996; Mannan, 2005]

Run ID	Project	Release Group	Type of release	Test*	Substance	Spill flow [kg.s ⁻¹]	Duration [s]	Spill conditions	Meteorological conditions	Terrain and Obstruction**
DGD1	Thorney Island	Dense gas instantaneous release	Puff	TI08	Freon-12 – N2	3,967.0	1.0	P ₀ = 17.2 °C	T _a = 17.2 °C; P=1 bar;	F, U
								P ₀ = 1.0 bar	u _{ref} = 2.4 m.s ⁻¹ ; class D	
DGD2	Thorney Island	Dense gas instantaneous release	Puff	TI21	Freon-12 – N2	4,962.0	1.0	P ₀ = 18.0 °C P ₀ = 1.0 bar	T _a = 20.9 °C; P=1 bar; u _{ref} = 3.9 m.s ⁻¹ ; class D	F, O
DGD3	Burro	Dense gas evaporation pool release	Pool	B3	LNG	88.0	167.0	P ₀ = -164.0 °C	T _a = 33.8 °C; P=0.94 bar;	F, U
								P ₀ = 0.95 bar	u _{ref} = 5.4 m.s ⁻¹ ; class B	
DGD4	Burro	Dense gas evaporation pool release	Pool	B9	LNG	136.0	79.0	P ₀ = -164.0 °C	T _a = 35.4 °C; P=0.94 bar;	F, U
								P ₀ = 0.94 bar	u _{ref} = 5.7 m.s ⁻¹ ; class D	
DGD5	Desert Tortoise	Dense gas je release	Jet	D3	Ammonia	133.0	166.0	P ₀ = 21.5 °C	T _a = 17.2 °C; P=1 bar;	F, U
								P ₀ = 11.2 bar	u _{ref} = 2.4 m.s ⁻¹ ; class D	
DGD6	Desert Tortoise	Dense gas je release	Jet	D4	Ammonia	108.0	381.0	P ₀ = 24.1 °C	T _a = 33.5 °C; P=0.95 bar;	F, U
								P ₀ = 11.6 bar	u _{ref} = 7.4 m.s ⁻¹ ; class D	
DGD7	Lathen	Dense gas je release	Jet	EEC63	Propane	3.0	360.0	P ₀ = 13.9 °C	T _a = 16.0 °C; P=1 bar;	F, O
								P ₀ = 10.4 bar	u _{ref} = 1.5 m.s ⁻¹ ; class A	
DGD8	Lathen	Dense gas je release	Jet	EEC64	Propane	3.0	390.0	P ₀ = 14.1 °C P ₀ = 10.4 bar	T _a = 17.0 °C; P=1 bar; u _{ref} = 2.0 m.s ⁻¹ ; class D	F, O

* Code of test based on REDDIPHEM nomenclature [Nielsen and Ott, 1996]

** F – Flat, O – Obstructed, U – Unobstructed.

Reference measured observations and predominant ambient (meteorological and terrain) conditions information were mostly collected from the REview and DISsemination of PHysical Effect Models (REDIPHEM) database [Nielsen and Ott, 1996] and Mannan review [2005].

The REDIPHEM database compiles experimental set up, meteorological and measured concentration fields data for a large number of well-know and extensively studied experimental tests [Duijm *et al.*, 1995; Nielsen and Ott, 1996]. The selection of the test cases was based on the available data, as well as, type of release and dispersion conditions reported from the experiments.

Following a brief description of the various full-scale experimental test trials is provided. Quality performance analysis of the set of defined test cases is provided based on visual inspection of time evolution and q-q plots, in addition to the evaluation of estimated quality metrics based on direct paired point-by-point comparisons of modelled and measured values.

4.5.1 Experimental test trials

To illustrate instantaneous gaseous release scenarios, DGD1 and DGD2 are based on tests 8 and 21 from the 'Thorney Island test trials' [McQuaid and Roebuck 1983]. Dispersion over unobstructed (test 8) and obstructed (test 21) flat terrain is considered. In test 21 a rectangular fence structure with 5 m high, nearly 50 m away from the source was included [Nielsen and Ott, 1995]. A collapsible

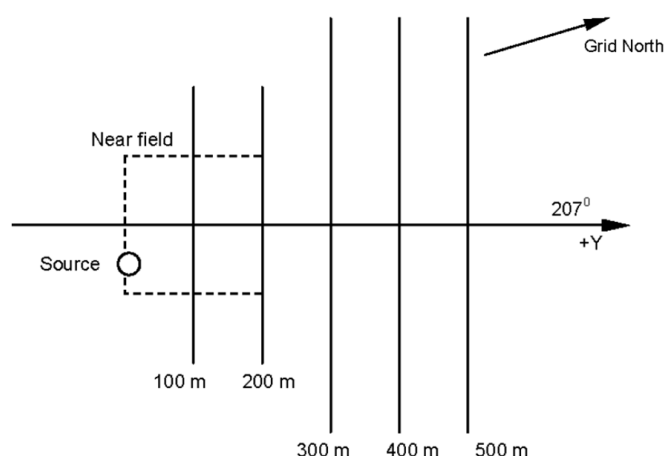


Figure 4.12 – Schematic representations of Thorney Island trials site layout [Hansen *et al.*, 2010].

tent, with 14 m across and 13 m high (see Figure 2.7) was used to discharge the different amounts of mixtures of Freon-12 and nitrogen, in an attempt to illustrate a vessel's total collapse release scenario [McQuaid, 1987].

Around 250 instruments including concentration and meteorological sensors were distributed in the test site [Puttock, 1987a]. Figure 4.12 illustrates a schematic representation of the test trials layout presented by Hansen *et al.* [2010]. A more concentrated array of sensors was used in the near field to enable measuring more accurately the initial stages of the dispersion behaviour. Far-field sensors (over 200 m away from the release) were placed on a uniform grid

spaced 100 m. Concentration sensors were fixed to masts with various levels between 0.4 m and 4.15 m above the ground [Johnson, 1985]. Data from concentration sensors located at the lowest level (0.4 m from the ground) was used for the validation of EFRHA modelled outputs.

The DGD3 and DGD4 were defined based on tests 3 and 9 from the Burro full-scale field trials. This series of experiments were conducted by the Lawrence Livermore National Laboratory (LLNL), at the Naval Weapons Centre, China Lake, California in 1980 [Koopman *et al.*, 1982a,b; Goldwire *et al.*, 1983], to determine the dispersion characteristics of large LNG gas clouds on a flat and unobstructed terrain area. The experiments consisted on varying spillages of LNG onto the centre surface of a 58 m diameter water pond with evaporation and further dispersion into the atmosphere (see Figure 2.6) [Ermak, *et al.*, 1981; Koopman *et al.*, 1982a]. Gas concentration measurements were performed in sensor masts distributed aligned with prevailing wind direction along various arcs downwind from the spill as illustrated in Figure 4.13 [Koopman *et al.*, 1982b; Ermak, *et al.*, 1981].

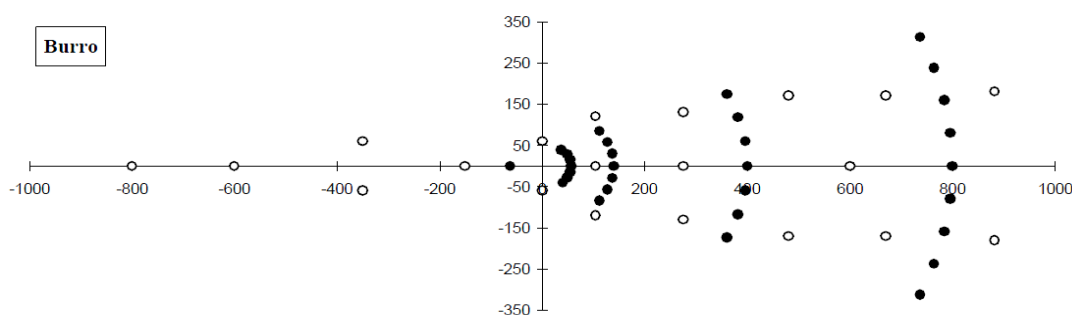


Figure 4.13 – Scheme of Burro test series measurement array. The closed circles represent masts with concentration sensors and the open circles indicate poles with meteorological sensors [Nielsen and Ott, 1996].

The EFRHA model was applied assuming an initial continuous spillage of LNG pure liquid fraction and subsequent vaporization estimated by ESTM4 to predict the various phases of the experiment. Terrain features of China Lake test site were neglected and terrain downwind of the spill pond was assumed as flat and the pool surface considered at terrain level.

Considering the frequency of accidental or deliberated hazmat gases release from small punctures in vessels or pipes, as well as, safety relief valves, the last four test cases are based on tests from the Desert Tortoise [Goldwire *et al.*, 1985] (DGD5 and DGD6) and the Lathen [Buitjes, 1992] (DGD7 and DGD8) full scale experiments.

The DGD5 and DGD6 simulate the set up and ambient conditions from two of the four Desert Tortoise full-scale field trials conducted by the LLNL at the Frenchmans Flat site, Nevada (USA) in 1983 [Goldwire *et al.*, 1985]. This series of tests was designed to measure the

atmospheric dispersion of spilled pressurized liquefied anhydrous ammonia in flat and unobstructed areas [Goldwire *et al.*, 1983]. The liquefied gas was emitted via a two-phase jet directed horizontally downward at 1 m from the ground level. An orifice plate placed at the jet aperture enabled near instantaneous evaporation of the liquid fraction generating a two-phase jet. Due to the reduced liquid fraction deposition observed during the experiments, the released material was considered a vapour jet [Nielsen and Ott, 1996]. Concentration and meteorological measurements were performed in various locations within the test site, as schematized in Figure 4.14.

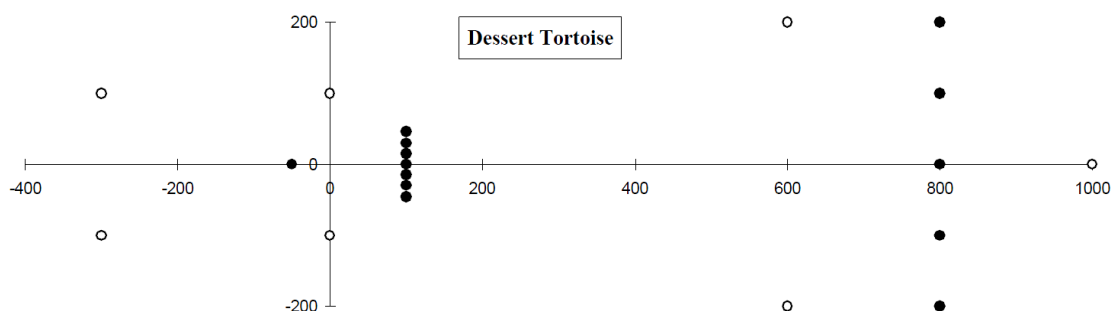


Figure 4.14 - Scheme of Desert Tortoise test series measuring array. The closed circles represent masts with concentration sensors and the open circles indicate poles with concentration sensors [Nielsen and Ott, 1996].

The array of meteorological and concentration sensors was mostly concentrated along the test grid centreline. Ammonia concentrations were obtained from towers placed along arcs at distances 100 and 800 meters downwind at various heights at the test site grid centreline.

Additionally, aiming to evaluate the EFRHA's aptness in case obstructions are taken into account, the DGD7 and DGD8 test cases were defined based on EEC63 and EEC64 tests, respectively, from the EEC experiments series, also known as Lathen Dense gas field experiments [Heinrich and Scherwinski, 1990]. This set of full-scale field experiments comprised continuous two-phase propane releases [Nielsen and Jensen, 1991]. They were carried out in the frame of the EC MTH Project BA 'Research on Instantaneous and continuous dense gas releases' [Bultjes, 1992] by Technischen Überwachungsverein Norddeutschland e. V. (TüV) and Risö at Lathen, Germany in 1988 and 1989 [Nielsen and Ott, 1996]. The examined tests consisted on propane release and dispersion in the presence of a simple fence of 5 m high placed nearly 50 m from the source location (see Figure 4.15).

The horizontal mean gas concentration distribution was measured with an array of up to 36 concentration sensors at various heights. In the specific case of the examined EEC63 and

EEC64 test cases, gas concentration sensors were distributed up- and downwards the obstacle, as schematized in Figure 4.15.

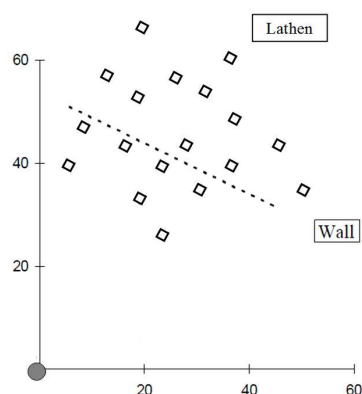


Figure 4.15 - Scheme of Lathen test series measuring array. The open spots represent 2 m poles with concentration sensors and dashed line represents the fence [Nielsen and Ott, 1996].

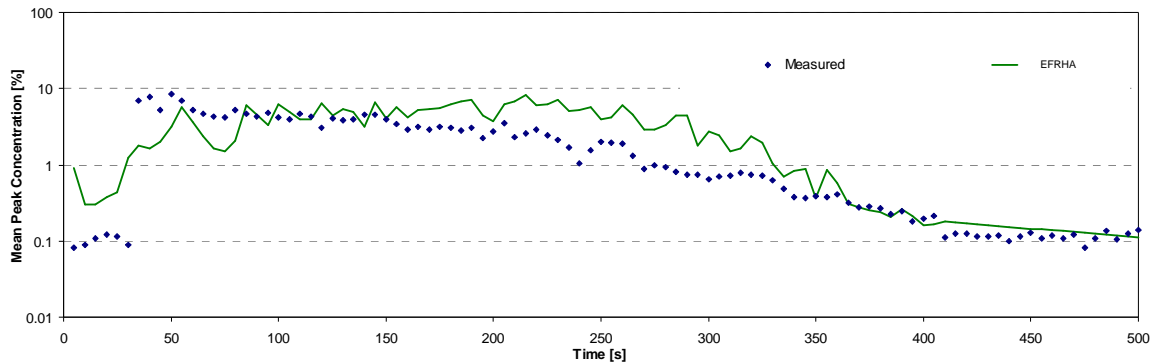
4.5.2 EFRHA modelling set up and validation for the set of DGD test cases

Aiming to evaluate EFRHA performance in its entire scope, the model was applied to the set of DGD test cases and simulated peak concentration values were compared with measurement observations. In each case, concentration fields were estimated at the lowest level of measurements (between 0.4 and 1.5 m high from the ground level) to maintain a somewhat consistency in the analysis, but also, for corresponding to 'normal heights of exposure to hazmat gases'. Depending on the number and spatial distribution of concentration sensors reported in each test case, different dimensions of simulation domains and discrete receptors were considered.

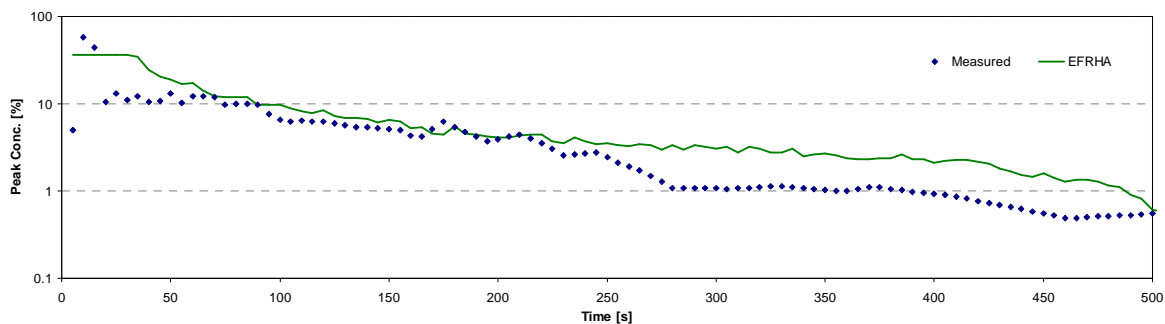
The validation study was conducted based on direct comparisons of modelled against measured peak concentrations at the sensors locations, following the recommendations of MEGPD [Britter and Schatzmann, 2007a]. In order to demonstrate the overall findings, time evolution and q-q plots and quality metrics estimated using the statistical BOOT Software [Chang and Hanna, 2005] were analyzed for the set of test cases. An initial comparison of modelled and observed concentrations is based on visual inspection of EFRHA modelled peak concentrations time evolution and q-q plots. Figure 4.16 presents the time evolution plots of modelled and measured peak concentrations during the initial 500 s after the release start, for the set of defined DGD test cases.

Figure 4.16 -Comparison of the time evolution of measured and modelled peak concentrations [%vol/vol] at plume centreline for (a) DGD1, (b) DGD2 (c) DGD3, (d) DGD4, (e) DGD5, (f) DGD6, (g) DGD7 and (h) DGD8 test cases runs during the initial instants after the release.

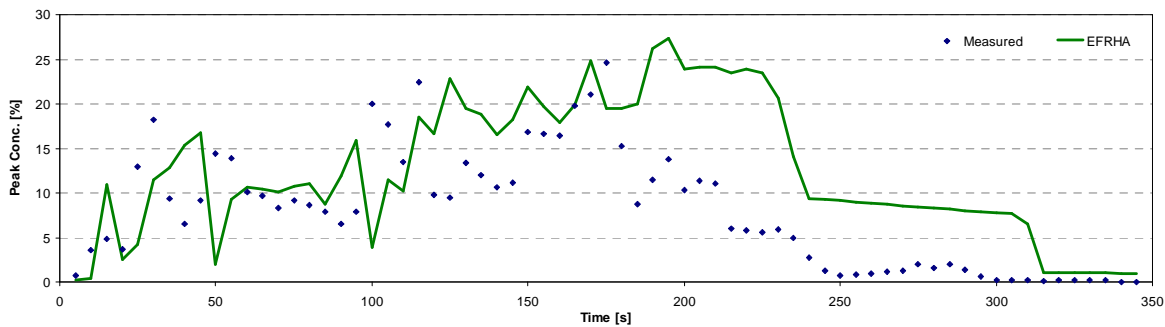
(a) DGD1



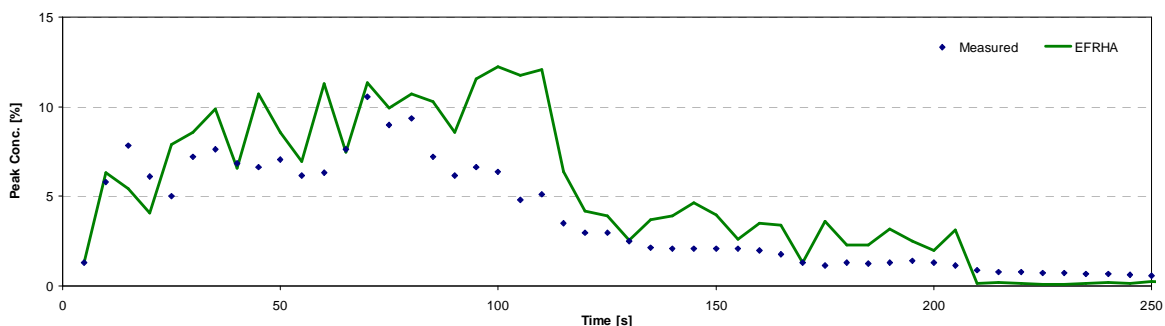
(b) DGD2



(c) DGD3

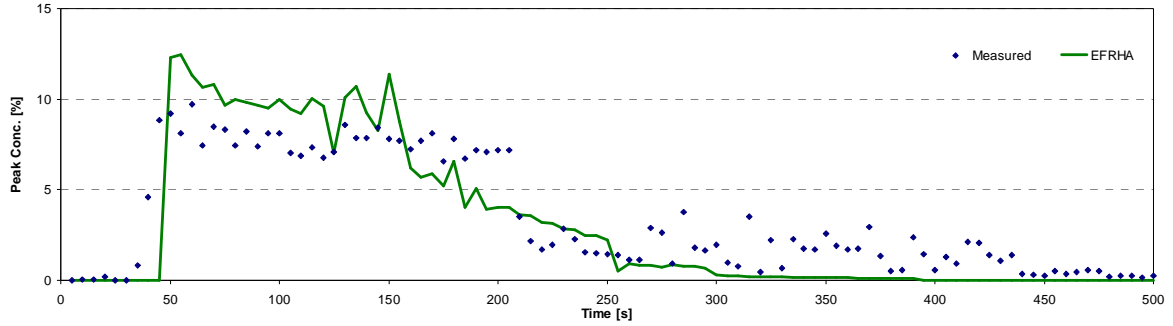


(d) DGD4

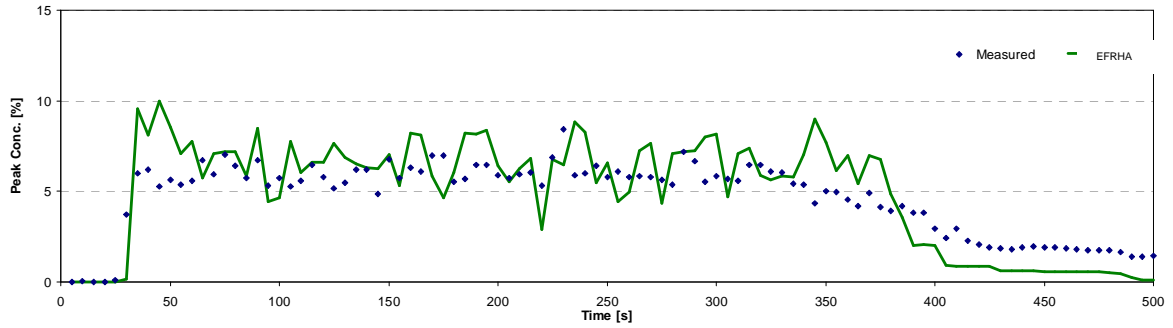


Cont. Figure 4.16

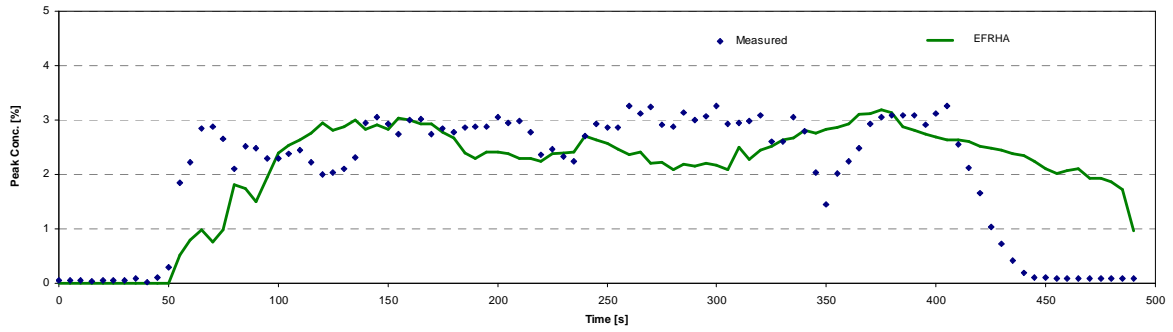
(e) DGD5



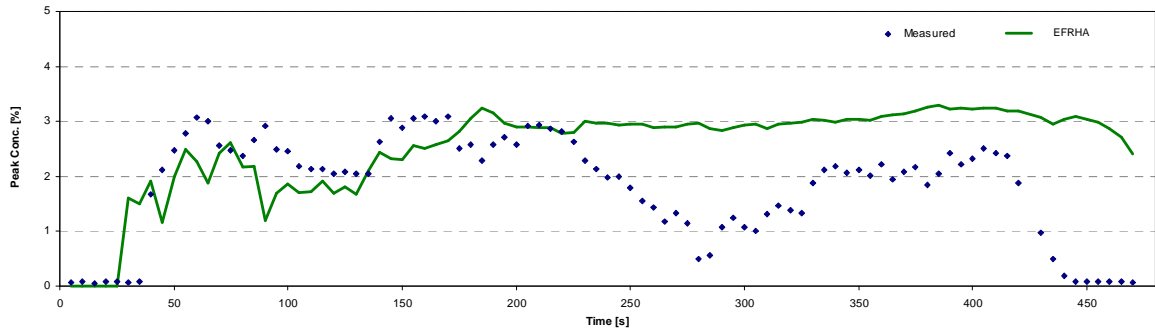
(f) DGD6



(g) DGD7



(h) DGD8



In general, EFRHA simulated peak concentrations follow the behaviour and ranges of measured values. For instance DGD1 (Figure 4.16a) and DGD6 (Figure 4.16f) simulated results tend to substantially approximate to (and in some instants nearly overlap) experimental observations during the analyzed period of time. However, there is a visible overestimation tendency in a large fraction of the simulation periods, in most of DGD test cases, with the exception of DGD5 (Figure 4.16e) and DGD6 (Figure 4.16f). In some cases, the overestimation is linked with a sort of delay in predicting the decrease of concentrations, such as for DGD2 (Figure 4.16b), DGD3 (Figure 4.16c), DGD4 (Figure 4.16d), DGD 7 (Figure 4.16g) and DGD8 (Figure 4.16h). On the other hand, noticeable underestimations, particularly in the final instants of the dispersion period can also be observed for DGD4 (Figure 4.16d), DGD5 (Figure 4.16e) and DGD6 (Figure 4.16f). Notwithstanding the visible deviations, the application of EFRHA model to the set of DGD test cases highlights its capability to predict the different release and dispersion conditions in a reasonable way.

When applied to instantaneous release scenarios (DGD1 and DGD2), it is evident the overestimation during the first 30 s in DGD1 and initial instant for DGD2. This tendency is mainly due to the implemented modelling approach for the definition of hazmat gas instantaneous releases. For this type of accident it is assumed that at the initial instant of the release, a nearly cylindrical cloud is already formed based on the user defined volume and dimensions. This will result in the direct estimation of the 'overlapping' initial peak concentration, even if in reality did not reached the easement sensor. Moreover, simulated values clearly approximate to measurements during a large fraction of time.

Visual inspection of DGD2 and DGD3 outputs evidenced the previously mentioned overestimation of peak concentrations decay. Consequently, it is also observed the underestimation of peak concentration in DGD4 (Figure 4.16d). Such behaviour may result from the estimated evaporation rate and duration of the release gas outflow. The assumption of a continuous release may not be the most correct for further estimation of evaporation rate. Nonetheless, the lack of precise information concerning evaporation rate, duration of the emission and other relevant information disables the evaluation of accuracy and consistency of modelled results.

Finally, when tested vapour jet releases in unobstructed (DGD5 and DGD6) and obstructed (DGD7 and DGD8) areas, simulated concentrations show visibly distinct behaviours. Whilst in DGD5 and DGD6 simulated concentrations tend to nearly overlap measured valued at during a large fraction of the dispersion. Even so, distinct behaviours are observed in DGD5 and

DGD6. In case of DGD5, modelled results tend to underestimate measures after 250 s; whereas in DGD6, the simulated results tend to underestimate measured data after 380 s. On the other hand, a more or less opposite tendency is observed for DGD7 and DGD8 test cases, noticeable by the overestimation during the last instants of the period of simulation. While for unobstructed areas, the degree of dilution of the cloud is modelled faster than it is really observed; the previously mentioned delay is once again detected in both DGD7 and DGD8 time evolution plots. Furthermore, these test cases, also highlight the capability to simulate the release and dispersion, since in all cases, it is simulated the initial increase of peak concentration values with a substantial closeness to measured data.

The analysis of DGD test cases time evolution plots shows the reasonable agreement between simulated and measured peak concentrations for various typifying conditions. Therefore it is evident EFRHA capability to numerically describe the various phases of release and atmospheric dispersion for different release types and meteorological conditions in both obstructed and unobstructed areas.

Regardless the reasonable results of time evolution plots; a more detailed evaluation of the level of correlation between measured and modelled ranges of values was performed based on the analysis of the set of unpaired point-by-point q-q plots presented in Figure 4.17.

On the whole, Figure 4.17 shows that most of modelled results tend to present a relatively good correlation with experimental observations, demonstrating the capability to estimate the ranges of concentration values measured during the examined dispersion period. However, it is also observed the previously identified and discussed overestimation (*e.g.* DGD1, DGD3 or DGD4) and underestimation (*e.g.* DGD5 and DGD6) tendencies. An overall trend to overestimate lower concentrations is also detected in most q-q plots, particularly in DGD3, DGD7 and DGD8 test cases. Regardless the identified deviations, as evidenced by the estimate linear trend lines r_2 , all analyzed test cases present a reasonable correlation degree with measured observation during the period of simulation.

As regards to instantaneous release scenarios (DGD1 and DGD2), it is the reasonable correlation between modelled and measured values. In particular for DGD1, it is also noticeable the acceptable correlation even for lower concentration values, often more sensitive to larger deviations. Hardly noticeable, is the overestimation of a reduced number of concentration values ($C_{modelled} \approx 1\%$ VS $C_{measured} \approx 0.1$), that influences the somewhat overestimation trend for lower concentration values. This discrepancy results from the

previously identified overestimation during the initial instants after the release (see Figure 4.16a).

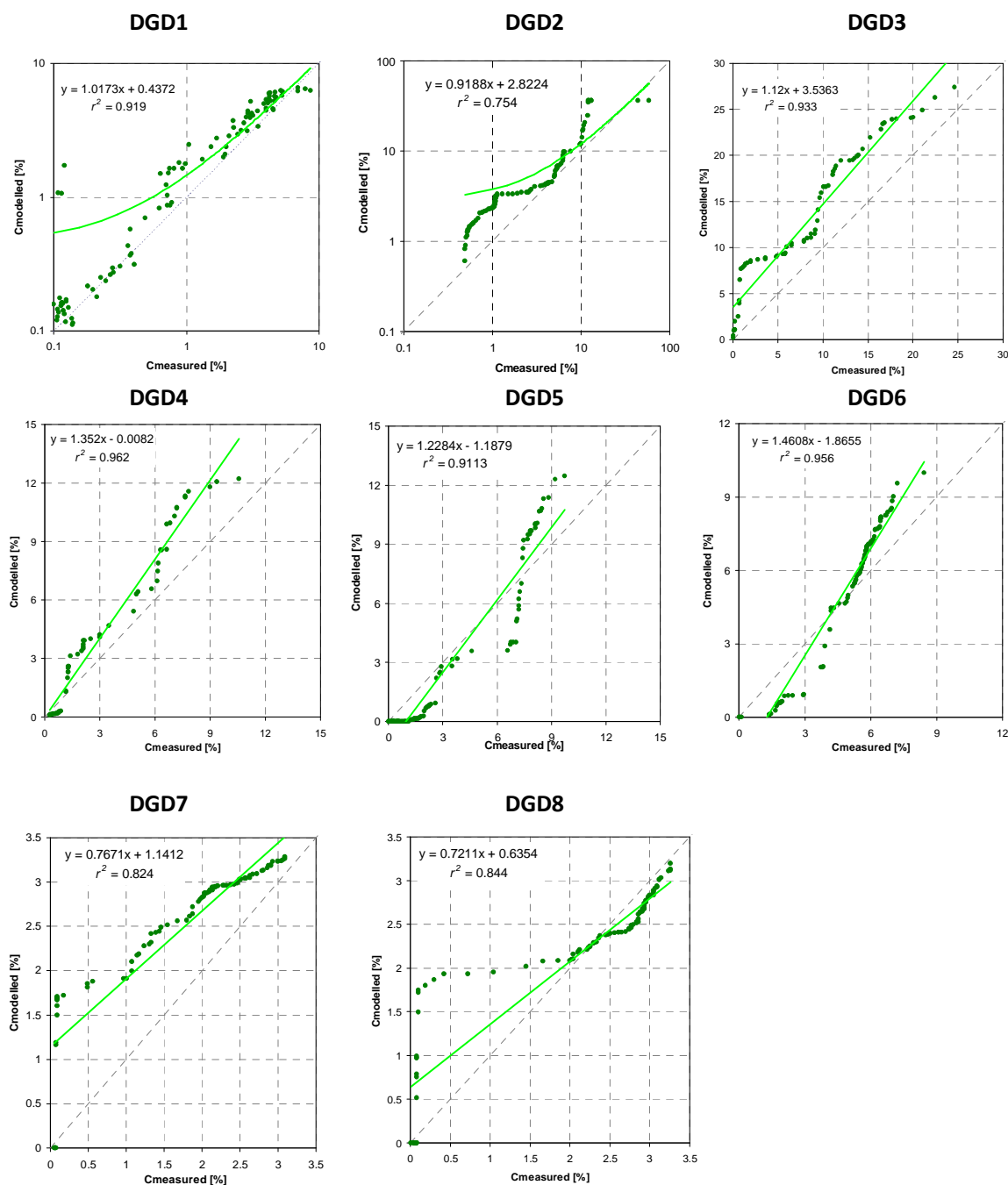


Figure 4.17 - Quantile-quantile plots of modelled results against measurements concentrations [% vol/vol] for set of DGD test cases.

Despite the general tendency to overestimate intermediate and higher concentration values, it is visible the reasonable correlation between modelled and measured concentration datasets. From the set of tests, it is possible to verify that, at a first analysis, DGD2 shows the less

favourable correlation between modelled and measured concentrations. Even the estimated trend line is quite close to the 'ideal trend', in fact the estimated r^2 highlights less favourable correlation between modelled and measured concentrations. Supported by the analysis of Figure 4.6b it is clear that the larger deviations result from the notable overestimation tendency observed especially after 250 s, counter-balanced by the underestimation of the initial peak concentrations. Nonetheless, it can be also observed the stronger correlation at lower and intermediate concentrations. However, opposing results are observed for DGD4 and DGD6 in that tend to present the higher correlations, demonstrating the reasonability of EFRHA model to predict reliable results.

As regards to DGD1, a general good correlation is observed, also evidenced by the estimated r^2 . Still, it can be also observed the punctual strong underestimation of some records, reflecting the strong underestimation observed for the peak measured concentrations resulting from the delayed increase of modelled concentrations, as observed in Figure 4.16a.

Distinct behaviours are observed for DGD3 and DGD4. Whereas in DGD3 it is noticeable a larger overestimation for lower concentration values; such positive deviation is observed in DGD4 for higher concentration values. As expected, the results for jet release scenarios evidence the differences between considering the obstructions or not. In both DGD5 and DGD6 test cases, the noted underestimation results from the previously observed underestimation during the second half of the period of simulation. For instance in DGD5, modelled results reach null concentrations much faster than measured. Nonetheless such result may be caused by some variation on meteorological conditions during the test not considered in the simulation. Contrasting, both DGD7 and DGD8 present the distinguishable overestimation trend of lower concentration values, given the previously observed overestimation tendency during the last instants after the release. Nonetheless, in the four test cases, higher concentrations tend to approximate to reference concentrations, highlighting the reasonability of the EFRHA model.

Nonetheless, as for previous stages of the evaluation, paired and unpaired point-by-point quality metrics were estimated for the set of modelled concentration datasets and results analyzed. Table 4.9 lists the estimated quality metrics for the set of DGD scenarios analyzed in this stage.

Table 4.9 – Summary of quality metrics for the set of DGD test cases.

Run ID	FB	FAC2	NMSE	r	MG	VG	SB	SDSD
<i>DGD1</i>	-1.340	0.570	0.95	0.57	0.70	2.03	0.592	0.130
<i>DGD2</i>	-0.410	0.510	1.30	0.74	0.71	1.71	0.940	0.930
<i>DGD3</i>	-0.240	0.506	0.66	0.56	0.43	8.71	0.170	0.100
<i>DGD4</i>	-0.288	0.673	0.23	0.79	1.03	1.92	0.489	0.010
<i>DGD5</i>	0.121	0.450	0.36	0.84	1.95	2.72	0.160	0.810
<i>DGD6</i>	-0.059	0.730	0.12	0.83	1.50	3.95	0.31	0.980
<i>DGD7</i>	-0.031	0.700	0.20	0.63	1.94	4.90	0.004	0.063
<i>DGD8</i>	-0.298	0.670	0.38	0.36	1.52	1.72	0.514	0.026

The analysis of Table 4.9 shows that, in general EFRHA model satisfies the acceptance criteria or the estimated results are close to them. Therefore, even not ‘over-interpreted’ as recommended by Schatzmann *et al.* [2010], the analysis of EFRHA modelled results, quantitatively demonstrates its reliability to provide acceptable results when applied to accidental release scenarios. From the analysis of Table 4.9 estimated quality metrics it is noted that DGD8 has the less favourable results; yet, estimated quality metrics tend (in general) to approximate to acceptability limits. On the other hand, DGD4 – DGD6 test cases show reasonable (if not possible to mention good) results, given the quality metrics results.

The *FB* results clearly demonstrate and corroborate the previously observed overestimation tendency in the examined test cases with a particular signal in DGD1 and DGD2 resulting from the larger overestimations also observed in previous graphical representations. The only exception is DGD5, for which the positive *FB* values indicate an underestimation trend, strongly influenced by the negative deviations of lower and intermediate concentrations. As regards to *FAC2*, acceptance criteria are satisfied by all test cases, excepting DGD5, which presents a value relatively close to the acceptance limit. If combining *FAC2* with *r* it is possible to mention that, modelled concentrations tend to present a reasonable correlation with reference measured observation, even in DGD5 (given $r = 0.83$). All DGD test cases satisfy *NMSE* acceptance limits, therefore, if combining the correspondent *FB*, *NMSE*, *MG* and *VG* it is possible to mention that, the observed deviations are mainly caused by systematic errors, in particular the overestimation trends in most test cases. In this case, potential occurrence of random errors is small. Since all test cases satisfy *NMSE* and the majority satisfies or is close to acceptance criteria for *FB* and *VG*.

As regards to the unpaired quality metrics it is also possible to observe relatively small values, evidencing the previously good correlation between ranges of modelled and measured values.

Considering that both metrics depend on analyzed concentration ranges, it is possible to verify that once again EFRHA generates reasonable outputs.

Overall, qualitative and quantitative analysis of DGD test cases modelled results shows the reasonable capability to EFRHA reproduce numerically the various phases of release and dispersion of hazmat gases. Moreover, despite some noticeable deviations, it is demonstrated the reliability to account different and typifying release conditions commonly analyzed in the frame of CA studies.

4.6 Synthesis

With the purpose of demonstrating EFRHA skills to provide reasonable information about short-term pollution episodes and consequences from accidents involving the release and dispersion of hazmat gases, a validation exercise consisting of four independent stages of evaluation was performed following the MEGPD recommendations for 'non-CFD' Class II models.

The first stage consisted on the validation of the meteorological component (EMM). Direct comparisons between EMM and AERMET modelled outputs for two distinct test cases were carried out demonstrating its capability to generate valid meteorological and ABL scaling parameters required in subsequent modules, especially in case of input data with large fractions of missing data.

As regards to the source term component, the second stage consisted on direct comparisons between ESTM and EFFECTS 7.5 models results for a set of typifying release scenarios. Given the effortless of instantaneous and continuous release scenarios, only transient release scenarios were tested. Both qualitative and quantitative analyses demonstrate ESTM suitability to produce acceptable results, evidencing its capability to numerically describe transient hazmat gas release source term component for different types of release scenarios, but also the appropriateness of implemented chemical properties database.

EFRHA's increased capability to account the presence of obstructions (complex terrain and/or buildings) was demonstrated through the joint ETM-EDM application to the -45° MUST test case experimental set up. Direct comparison with experimental observations shows its reliability to provide reasonable results for situations involving the dispersion of hazmat gases in obstructed areas. Even, quality metrics do not fully satisfy acceptance criteria, when compared with other Class II models results it is possible to observe a consistent and more

accurate behaviour providing valid results. It is also highlighted the relevance of defining realistic z_0 values.

Demonstrated the suitability of the various modules to produce acceptable results, EFRHA's performance quality was evaluated in its entire scope. Overall, the fourth stage of the validation exercise demonstrates its capability to produce reasonable results, in terms of peak concentrations time evolution, but also ranges of values based on the application to a set of well-know experimental full-scale tests. Direct comparison between modelled and measured peak concentrations was performed demonstrating EFRHA's reliability to produce reasonable and acceptable results. Despite some generalized overestimation tendency and less favourable results when applied to obstructed areas, it is possible to conclude that the developed model is capable to numerically describe the various stages of release and atmospheric dispersion of hazmat dense gases in industrial and built-up areas; and therefore, support CA studies and emergency planning and response measures.

CHAPTER 5

5. APPLICATION OF EFRHA TO A CONSEQUENCE ANALYSIS STUDY

This chapter presents the EFRHA model application in the scope of a demonstrative CA study. The selected case study and defined accident scenarios are described, without forgetting the characteristics of the industrial activity, surrounding built-up area and prevailing ambient conditions. Finally, main findings from the estimation of short-term pollution episodes and consequences at neighbouring population from a set of accident scenarios are discussed illustrating EFRHA's suitability to support decision and emergency planning, training or response actions.

5.1 Selection of the case study

Taking into consideration the present thesis's main purpose and the EFRHA model's core features, the case study area should incorporate both 'hazardous' activity (industrial establishments and/or transportation routes) and potentially affected neighbouring built-up areas, in order to characterize 'realistic' accident scenarios. Bearing in mind these 'requirements', the set of criteria listed in Table 5.1 was used for the definition of the case study.

Table 5.1 – Summary of criteria considered for the selection of the demonstrative case study.

Selection criteria	<ul style="list-style-type: none"> - Presence of 'hazardous' Seveso chemical establishments; - Nature and quantities of hazmat handled (processed, stored and transported); - Geographical location and nearness to built-up areas (residential, services or urban); - Available information of industrial processes, safety and control measures; - Potential most-plausible and worst case accident scenarios; - Relevancy to economical and chemical industrial sectors (local to national levels).
--------------------	--------------------------------------------------------------------------------------------------------------------------------------------------------------------------------------------------------------------------------------------------------------------------------------------------------------------------------------------------------------------------------------------------------------------------------------------------------------------------------------------------------------------------------------------------------------------

The selection of the case study focuses on chemical industrial activities covered by the Seveso Directive, given the requirements on safety, prevention and control of MIA involving hazmat and their consequences, but also, available information. At a first analysis, spatial distribution of Seveso establishments (upper and lower-tier) was checked at European and Portuguese levels (see Figure 1.18 and Figure 1.17).

Portuguese Seveso establishments represent about 1.7% of the total number of EU covered establishments [EEA, 2010] and the majority is heterogeneously distributed in clusters of

establishments, the so-called '*industrial complexes*', generally organized by sectors of activity [Gaspar, 2005]. According to Vieira [2011], most of Portuguese Seveso establishments belong to the chemical and petrochemical sectors of activity, deployed in industrial complexes, like the ones located in Barreiro, Estarreja, or Sines [URL5.1]. Apart from the recognized economical and logistic advantages from this type of set up, when close to built-up areas (either urban, services or residential) technological hazards may generate accentuated risks. As a result, potential consequences to human health and the environment in case of accidents at local (within the complex) and regional (complex and surrounding area) scales must be considered and evaluated in CA studies, decision and emergency planning and response.

In fact, potential for MIA hazards and consequences of Portuguese Seveso establishments clustered in industrial complexes have already been highlighted and discussed within in various European [URL5.2], National [Serviço Nacional de Protecção Cívil (SNPC), 1994; Gaspar, 2005] and Regional [Tavares *et al.*, 2007; Zêzere *et al.*, 2010] scientific studies and research projects. In the frame of the European ESPON project [URL5.2] MIA hazards were estimated and mapped EU-wide, as a function of chemical and petrochemical establishments density per km² per NUT3 [Schmidt-Thomé and Kallio, 2006], as illustrated in Figure 5.1.

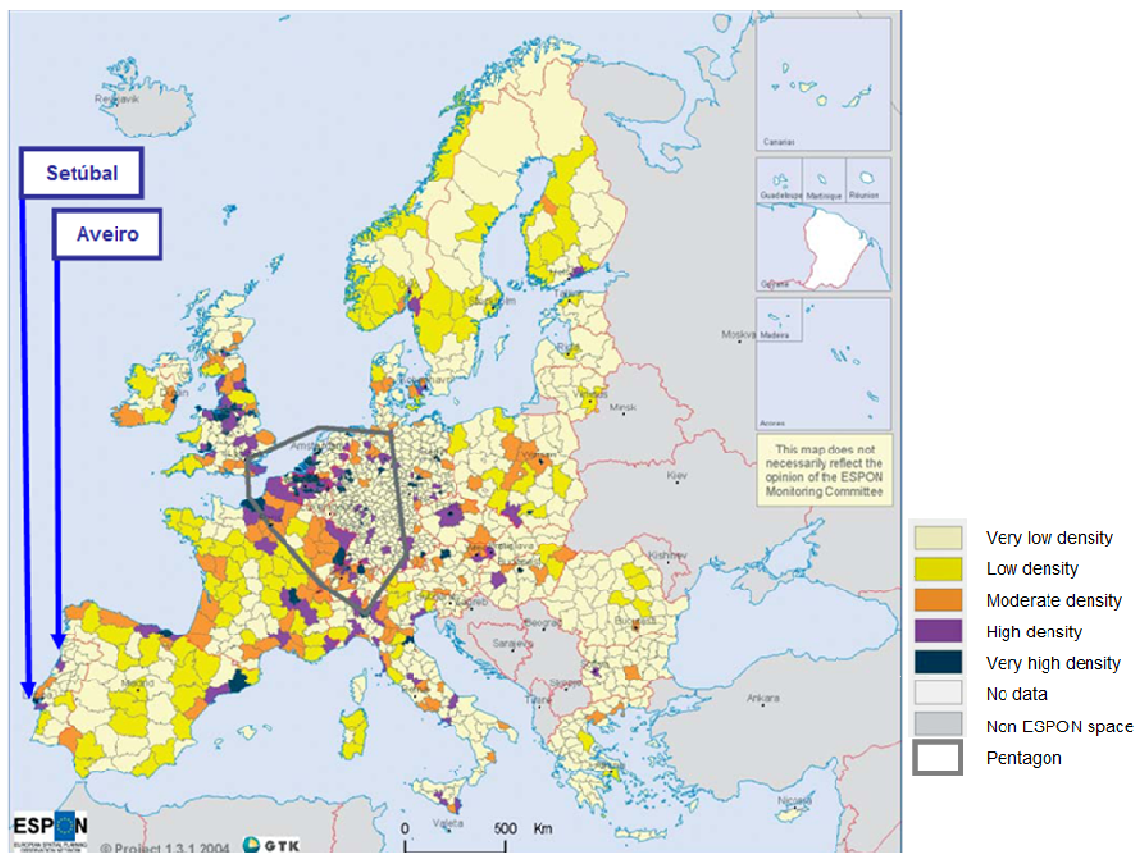


Figure 5.1 - Spatial distribution of MIA hazards estimated based on the density of chemical and petrochemical establishments per km² per NUT3 EU-wide [Schmidt-Thomé and Kallio, 2006].

According to Schmidt-Thomé and Kallio [2006], a sparse distribution of Seveso chemical and petrochemical establishments capable to cause severe MIA hazards can be observed EU-wide, in particular, across central European region (France, UK, Germany, Belgium) within the so-called '*hazardous pentagon*'. At Portuguese level, despite the relatively heterogeneous set up of Seveso establishments [Vieira, 2011], two high density '*spots*' are identified in the districts of Aveiro and Setúbal (see Figure 5.1). This spatial distribution, shows a particular concentration of establishments along Portuguese coastal areas, illustrated with more detail in Figure D.1 (Appendix D), which is influenced by the location of major communication networks (maritime, road and railways) and sea ports usually linked with hazmat transportation routes. The results of ESPON project [URL5.2] and Gaspar [2005] concur with the '*high risk district*' classification of the districts of Aveiro and Setúbal (in addition to Lisbon and Porto), lawfully established by the Portray 1033/95 of 12th August. Furthermore, Gaspar [2005] stated that estimated high density MIA hazard and risk '*spots*' at Aveiro and Setúbal are mainly caused by the presence of some of the most important chemical and petrochemical industrial complexes (Estarreja and Ílhavo in Aveiro; Barreiro and Sines in Setúbal) and sea ports (Ílhavo and Sines). The SNPC [1994] also highlighted the very high propensity for MIA hazards at both Estarreja and Barreiro industrial complexes and resulting risks to neighbouring areas. At regional scale, Zêzere *et al.* [2010] and Tavares *et al.* [2007] highlight the very high technological and social hazards and risks susceptibility in the Municipalities of Barreiro and Estarreja, respectively, due to the installed industrial chemical complexes and hazmat transportation routes.

In view of the intended application of the developed model and of the available information from the various studies and regulations, two '*relevant*' Portuguese chemical complexes with major economical significance and impact at local to national levels were selected, namely the Estarreja Chemical Complex (ECC) and the Barreiro Chemical Complex (BCC). Both complexes have in common the nearness to built-up areas and the presence of Seveso chemical establishments (both upper and lower-tier), including a wide variety and large quantities of processed and stored hazmat, also commonly identified as potential sources of risks and consequences to neighbouring areas [Gaspar, 2005; Zêzere *et al.*, 2010].

Notwithstanding the potentially higher risks and consequences from neighbouring closer built-up areas in BCC (in comparison with ECC), the limited access to information regarding industrial activities or hazmat handle and transported disables a proper (and realistic) characterization of this case study area and the definition of reliable accident scenarios. For that reason, the ECC (industrial facilities and neighbouring area) was selected as an

illustrative case study area for the definition of accident scenarios and further application of EFRHA model.

5.2 Estarreja Chemical Complex

Nowadays, the ECC is considered the 3rd largest cluster of Portuguese chemical industry comprising some of the most important industrial facilities of the chemical sector, with an occupied area of 2 km² [Costa and Jesus-Rydin, 2001]. It is installed in the 'Quinta da Indústria', at 3 km N-NW from the geographical and administrative centre of the Municipality (and city) of Estarreja, as illustrated in Figure 5.2.

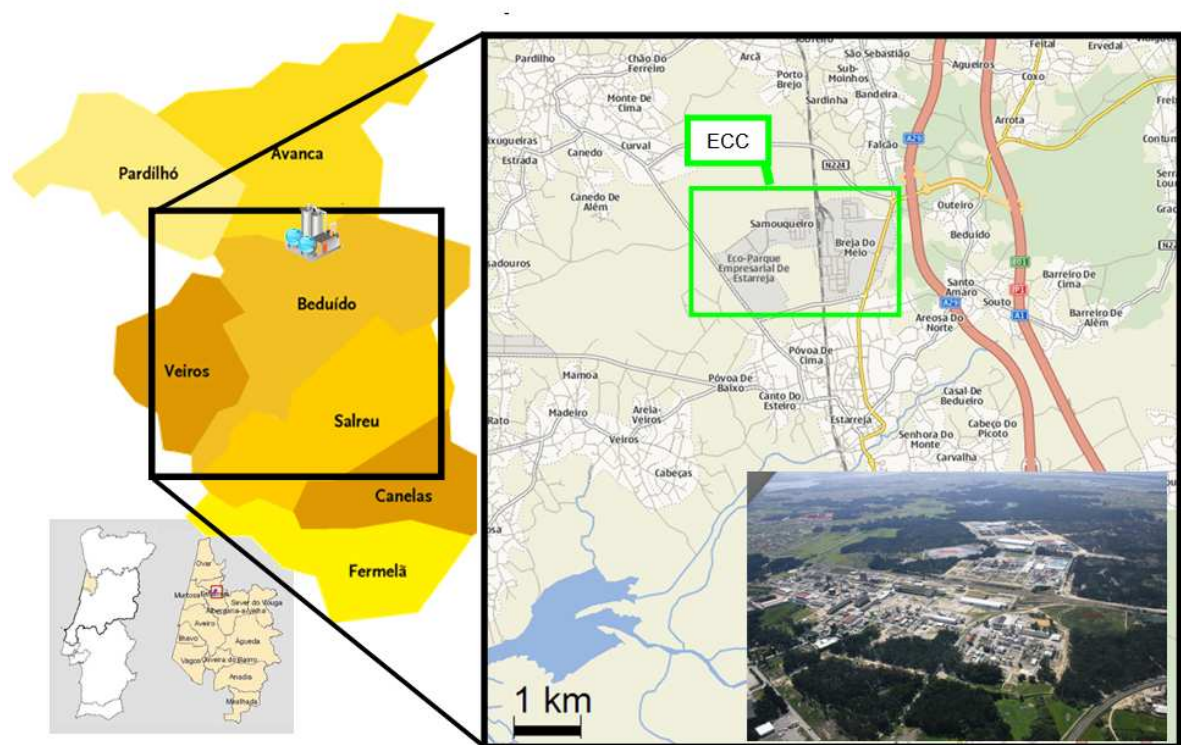


Figure 5.2 - Location of ECC and Estarreja Municipality areas [URL5.3].

5.2.1 Overview of the ECC

Apart from ECC modern set up, numerous and significant modifications have been registered over the last decades with the installation of new industrial establishments, production units or technological upgrades on already installed facilities, as schematized in Figure 5.3.



Figure 5.3 – Chronogram of relevant dates of ECC development.

The first records of ECC industrial activity date back to the 1930s, with the settlement of a chlorine and soda production unit of the Belgian SAPEC Company [Nunes, 2005]. However, the major expansion occurred after the 2nd World War with the beginning of ammoniac production [Atkins Portugal, 1997], turning ECC one of the most important Portuguese chemical clusters. The escalating energy demand during the 1950s and 1960s, particularly at ECC, contributed for the construction of hydropower structures in Douro region (Cávado and Douro), in the frame of the ‘National Hydropower Plan’ and the ‘I and II National Promotion Plans’ [Madureira, 2005]. In 1960, was established the first joint-venture between Portuguese (European) and Japanese industrial companies pioneering the production of polyvinyl chloride (PVC) with the installation of the Companhia Industrial de Resinas Sintéticas (CIRES) industrial facilities [URL5.4]. Later, the first formal Portuguese oil refining and petrochemical cluster was formed in 1979, between the petrochemical complex of Matosinhos and Quimigal [Atkins Portugal, 1997]. In 1982 former ISOPOR starts the production of methyl-di-isocyanate (MDI) and later entirely joins Dow Portugal (the national subsidiary of Dow Chemical Company) in 1989.

In the late 1980s and 1990s a general technological upgrade made possible Dow Portugal (former ISOPOR), Companhia União Fabril – Químicos Industriais (CUF-QI) and Air Liquide establishments to set up a ‘dynamic products chain supply’ of various materials produced internally (*i.e.* in the various ECC units) [Nunes, 2005]. The closeness of the various ECC industrial establishments contributed to the extension of the piping system to all installed facilities improving the raw materials transfer networks inside the complex, but also with other complexes, such as the Port of Aveiro [URL5.5]. This strategic upgrade of the internal transportation system, stirred the strong expansion of the entire production capacity and importance at national and international contexts.

At present, ECC is composed by some of the most important industrial production units of the Portuguese chemical sector, namely Air Liquide (former Oxinorte), Aliada Química Portuguesa (AQP), CIRES, CUF-QI (which includes former Amoníaco de Portugal, Anilina de Portugal, Quimigal and Uniteca units) and Dow Portugal (former ISOPOR) establishments [Nunes, 2005; Vieira, 2010]. Excepting AQP, installed chemical establishments are covered by the Decree-Law 254/2007 (which transposes the Directive 2003/105/CE to the Portuguese legislation), and therefore classified as Seveso establishments given the quantity and nature of handled and transported hazmat. Whereas CIRES, CUF-QI and Dow are classified as upper-tier establishments, Air-Liquide is a lower-tier establishment.

In spite of the continuous modifications observed over the last years, with upward production capacity competitiveness and safety/control measures, Dow, Air Liquide and CUF-QI establishments started, in 2008, a substantial expansion of their production capacity, reinforcing units with up-to-date technological and safety levels [Instituto do Ambiente e Desenvolvimento (IDAD), 2007a,b].

5.2.2 Hazmat production and transportation

The various establishments settled in ECC work in different fields of chemistry, such as the production of organic and inorganic compounds, industrial gases, health and environment appliances, and polyurethanes. In fact, current production in ECC establishments includes mainly: hydrogen, carbon monoxide, carbon dioxide, nitrogen, oxygen, argon and compressed air into liquid air (Air-Liquide); aluminium salts (AQP); PVC resins (CIRES); aniline, ammonia, chlorine, nitrobenzene, sulhpanilic acid (CUF-QI); styrofoam and MDI (Dow), among other products commonly ‘used internally’ [Nunes, 2005].

Strongly influenced by the constant technological upgrade, a complex and dynamic production chain system linking internally the various production units, but also externally connecting the ECC with other (national and international) industrial complexes is installed in ECC, as schematized in Figure 5.4.

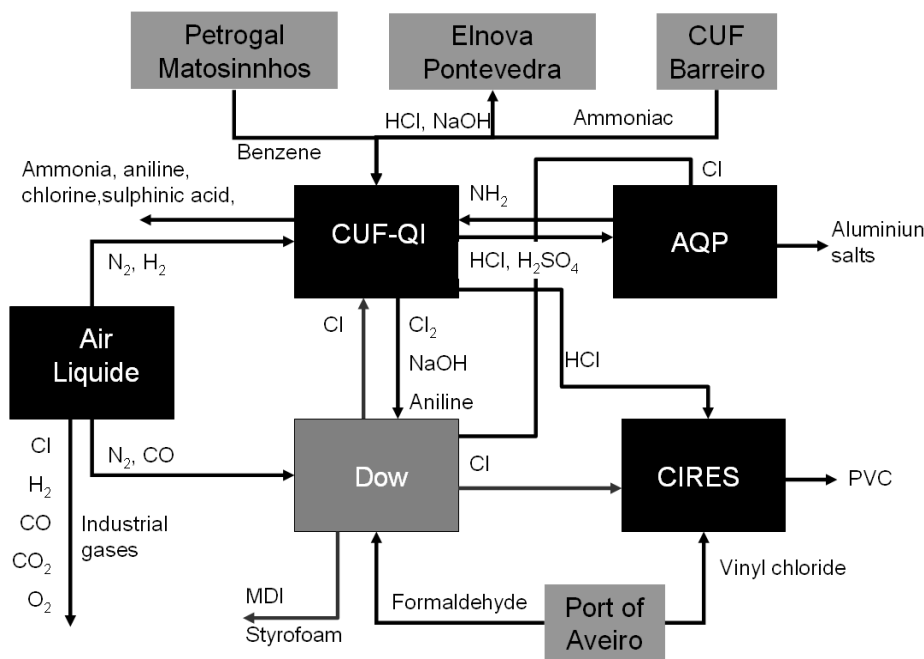


Figure 5.4 - Scheme of relevant products chain in ECC [based on Teixeira, 2010; URL5.6].

Figure 5.4 shows the complex chain of production (including some of the most important/hazardous products), in which materials produced in one establishment are used in others as raw material. This materials network connects the various installations internally, but also link ECC to external complexes, such as the port of Aveiro, the Petrochemical complex of Matosinhos, the CUF-QI unit of BCC [Teixeira, 2010] or even the Spanish Elnosa industrial facilities located in Pontevedra. For instance, Air Liquide produces industrial gases, providing carbon monoxide and nitrogen to Dow, or nitrogen and hydrogen to CUF-QI. Additionally, Dow Chemical receives chlorine from CUF-QI and produces chloridric acid that is used internally and supplied to CIRES [Nunes, 2005].

Notwithstanding the continuous technological and safety upgrade or even the implemented chain of materials in ECC, large quantities of hazmat continue to be processed and stored in fixed installations, as well as, transported or transferred by road and railways and piping (pipes and pipelines) equipments.

A large variety of products is stored and processed in the various establishments [Nunes, 2005; Serviço Municipal de Protecção Cívil (SMPC), 2006a]; including substantial amounts of hazmat in production and/or transportation systems. As regards to fixed installations, Table 5.2 summarizes some of the most relevant hazmat stored and process amount capacities installed in the various ECC establishments that may cause significant risks and consequences in case of accident [SMPC, 2006a].

Table 5.2 – Relevant hazmat storage/process capacity present in ECC in 2004 [SMPC, 2006a].

Product	Company	Existent nominal capacity [ton]	Max. concentrated capacity [ton]
Ammonia	CUF-QI	390.0	130.0
	Dow	12.0	12.0
	Air-Liquide	12.0	9.0
	CIRES	1.7	0.88
Benzene	CUF-QI	1,300	1,300
Chlorine	Dow *	0.5	0.5
	CUF-QI	510.0	100.0
Phosgene	Dow	17.0	5.0 **
Vinyl chloride	CIRES	500.0	200.0

* Pipeline between Dow and CUF-QI.
 ** During 10% of the time stores 5 tonnes; the rest 90%, 2.5 tonnes

The existent nominal capacity refers to the theoretical maximum product storage/process capacity installed (including all types of equipments); whereas the maximum concentrated mass capacity refers to the largest storage/process equipment (including piping) [SMPC, 2006a]. At a first analysis, it is shown that CUF-QI has the largest quantities of hazmat nominal capacity values, illustrated by the 1,300 tonnes storage/process capacity of benzene (in just one structure). Despite some exceptions, it is possible to verify that maximum concentrated capacity is significantly lower than maximum theoretical nominal capacity, but also, that quantities vary significantly (0.5 tonnes of chlorine in Dow to 1,300 tonnes of benzene in CUF-QI). If maximum concentrated capacity equals maximum theoretical nominal capacity it means that such volume is stored or processed in a 'single production or transfer equipment'. For instance, in Dow's listed information, whilst ammonia values refer to a storage vessel; in case of chlorine it corresponds to a transfer pipeline connecting Dow to CUF-QI. Phosgene storage/process capacity is relatively small, given the degree of hazardous, but also as a result of technological upgrade and lesser volumes requirements allied with a 'near real time' transportation capacity from the Port of Aveiro [IDAD, 2007b].

Overall, Table 5.2 illustrates the large volumes of hazmat presently handled in ECC, highlighting the necessity to predict potential consequences in case of accidental release scenarios. Nonetheless, it must be emphasized that information listed in Table 5.2 does not necessarily correspond to the products with the largest values of storage/process capacity installed in ECC, but to the ones considered the more dangerous. A detailed list of the products stored/processed in the various establishments is compiled by SMPC [2006a].

Apart from fixed storage and process installations, the different transportation modes identified in ECC also represent key elements to assure the reliability of products chain production system along the various establishments [SMPC, 2006a; Silva, 2007]. The ECC is served by the 'traditional' road and railway (including a terminal inside the complex) communication accessibilities, in addition to the complex piping systems network (pipes and pipelines) linking the various establishments internally and externally with other complexes. Notwithstanding the benefits, transportation equipments and routes may also contribute to local and regional technological hazards from ECC. For that reason, in view of defining most-plausible and worst-case accident scenarios, most common ways of transportation and quantities were also analyzed and taken into account.

Continuous technological upgrade and implementation of the piping system contributed to the overall drop of road and railway transported hazmat quantities over the last decades [Silva, 2007]. For instance, the pipeline system connecting ECC with the Port of Aveiro enables transferring LNG, phosgene and vinyl chloride [Tavares *et al.*, 2007; ANPC, 2009] substantially reducing stored quantities, as well as, roadway transportation risks. Still, traditional transportations models continue to be largely used, linking the ECC with other Portuguese or international industrial complexes (see Figure 5.4).

Despite ECC comprising an internal railway terminal, only few products are currently transported by train cisterns or in solid form. In addition, 'classical' roadway transportation mode continues active and represents an important fraction of hazmat (either raw material or final product) transfer outside the ECC, mostly by roadway cisterns and containers. Due to database protection measures, it was not possible to characterize piping and pipeline systems and railway transportation mode, yet Table 5.3 summarizes some of the most relevant hazmat transportation modes to and from ECC establishments [SMPC, 2006; Silva, 2007; Tavares *et al.*, 2007].

Table 5.3 shows that, even with the complex piping system, a large amount and variety of products is still transported by road transportation modes, particularly, heavy duty vehicles

with cisterns. Given the location of the railway terminal, CUF-QI is still supplied by this transportation mode. Additionally, most of industrial gases are transported by heavy duty vehicle cisterns from the ECC.

Table 5.3 – Summary of transportation modes and nominal capacity of hazmat in ECC [SMPC, 2006a].

Product	Company	Quantity	Transportation mode
Ammonia	CUF-QI	45 ton	Train – wagon cistern
Aniline	Dow	25 ton	Road – cistern
	CUF-QI - Dow	(unknown)	Piping system
	CUF-QI	25 ton	Road – cistern
		50 ton	Train – cistern
Argon	Air Liquide	28 m ³	Road – cistern
Benzene	CUF-QI	25 ton	Road – cistern
Carbon dioxide	Air Liquide	20 ton	Road – cistern
Chlorine	CUF-QI	18 ton	Road – container
	CUF-QI – Dow	(unknown)	Piping system
Hydrogen	Air Liquide – CUF-QI	(unknown)	Piping system
	CUF-QI – CUF-QI	(unknown)	Piping system
Hydrogen peroxide	CUF-QI	23 ton	Road – container
Isocyanide difenil methane	Dow	25 ton	Road – container
LNG	Port of Aveiro – ECC	(unknown)	Pipeline
Monochlorobenzene	Dow	22 ton	Road – cistern
Monotitrobenzene	CUF-QI	25 ton	Road – cistern
		50 ton	Train – cistern
Nitrogen	Air Liquide	28 m ³	Road – cistern
Oxygen	Air Liquide	28 m ³	Road – cistern
Pentane	Dow	15 ton	Road – cistern
Phosgene	Dow	25 ton	Road – cistern
Vinyl chlorine	Port of Aveiro – CIRES	(unknown)	Pipeline

Reflecting the present dimensions of ECC establishments, CUF-QI has the largest number of cisterns transporting raw or manufactured material, nearly doubling Dow and Air Liquide [SMPC, 2006a].

The inclusion of these transportation equipments in CA studies is crucial, as well as safety and emergency instruments measures taking into account their potential for causing risks and consequences to nearby built-up areas in case of accidental release of hazmat along the transportation routes.

5.2.3 Safety and accident prevention measures

In view of the Decree-Law 254/2007 (that transposes Seveso II Directive and Directive 2003/105/EC) Seveso establishments of the ECC must implement and regularly update internal security control and prevention assessment systems. These measures include the definition of Internal Emergency Plans (IEP), which compile recommendations and procedures to prevent and control potential effects of accidents occurring inside the industrial facilities, as well as information of installed processes, operation and control systems. Additionally, the Estarreja External Emergency Plan (EEEP) is also prepared to assure an integrated emergency response at Estarreja Municipality level (regional scale) in case of accident in ECC. Contrarily to IEP, which is only applied and prepared by the establishment, EEEP is coordinated by the Estarreja Civil Protection Municipal Service (ECPMS) and set up in conjunction with the various ECC establishments and local authorities (administrative, safety and health bodies). This instrument also considers planning and training exercises involving workers and local authorities for emergency response actions in case of accidents. Given the nature of transported material from and to ECC establishments, hazmat transportation modes (road, rail and piping) are also incorporated in prevention and control measures, and consequently in both IEP and EEEP documents at municipal and district levels [SMPC, 2006a].

The various ECC establishments are considered an example, at both national and international context, given the adoption of the Responsible Care Program initiative principles and actions [URL5.6]. For instance, PACOPAR was the winner of Cefic's first pan-European Responsible Care Award in 2005. The main goal of this program is the adoption of a compromise with neighbouring community, in which chemical establishments are voluntarily committed to continuously improve their health, safety and environmental performance within an integrated sustainable development context, and to provide information of their progress [Oliveira, 2008]. The initiative started in 1993 with the incorporation of former Quimigal and Uniteca (CUF-QI), Air Liquide, CIRES and Dow in the local initiative of the Responsible Care Program. Later, the Portuguese Association of Chemical Industries (APEQ) also integrated the group. Aiming to 'make it official', the PACOPAR - Community Advisory Panel of the Responsible Care Programme, was created in January 2001 [URL5.6].

Nowadays, this consolidated and structured organization integrates not only industrial companies, but also administrative, educational, safety, health and social bodies. Such broad organization promotes an active interaction between local community and ECC industrial

companies [URL5.6], but also, the improvement of local and regional safety and prevention measures for emergency response in case of MIA.

5.3 Estarreja municipality characterization

Estarreja municipality and city is located in the coastal zone of Centre Region of Portugal and belongs to the district of Aveiro, integrated in NUT 2 - Centre Region and NUT 3 - Baixo Vouga Sub-Region. The municipality is administratively divided into seven parishes: Avanca and Pardilhó (north), Beduído (administrative and city centre) and Veiros (centre), and Salreu, Canelas and Fermelã (south), as illustrated in Figure 5.2.

The municipality has an approximated area of 108.4 km² mainly used as urban (18%), agricultural (54%) and forested land (27%) [Instituto Nacional de Estatística (INE), 2001]. The larger parishes are Avanca and Beduído, with an area higher than 20 km² each; whilst the smallest are Canelas and Veiros with 10.2 km² and 11.2 km², respectively. Estarreja is confronted by the Municipalities of Ovar (north), Murtoza (west), Aveiro (south) and Oliveira de Azemeis and Albergaria-a-Velha (east) (see Figure 5.2).

Taking into account the relevance and influence of physical, demographic and economical characterization of Estarreja municipality area for a suitable and realistic prediction of hazmat gas accidental release and dispersion in ECC, a brief overview is further presented.

5.3.1 Physical characterization

Geo-morphologically, the municipality of Estarreja can be characterized as a low-lying coastal nearly plane buffer region, flat at west and slightly hilly at east, ranging between 0 and 50 m (in hypsometric terms), divided in three main zones [SMPC, 2006a]. The 'lower zone' (levels < 10 m), includes the most humid and lower areas of Pardilhó, Veiros, Salreu, Canelas and Fermelã parishes close to 'Ria de Aveiro' lagoon. The 'intermediate zone' (levels between 10 and 50 m) comprises agricultural and built-up (residential, industrial and services) areas in all parishes. The 'upper zone' (levels higher than 50 m) binds mostly the eastern areas of Avanca, Beduído, Canelas and Fermelã forest areas, in addition to the upper agricultural and forest areas of Salreu [SMPC, 2006a].

Estarreja is integrated in a temperate climate region with a strong Mediterranean and oceanic influence, characterized by short and dry summers and mild and rainy/wet winters. Figure 5.5 and Figure 5.6 show the monthly temperature and precipitation observations in the region

of Estarreja based on measurements in Aveiro, between 1971 and 2010 [Instituto de Meteorologia and Agencial Estatal de Meteorologia (IM and AEMET), 2010].

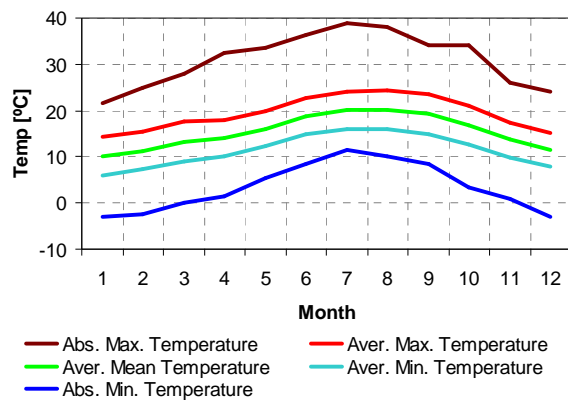


Figure 5.5 - Climate normal values of temperature in Aveiro District (1971-2000) [IM and AEMET, 2010].

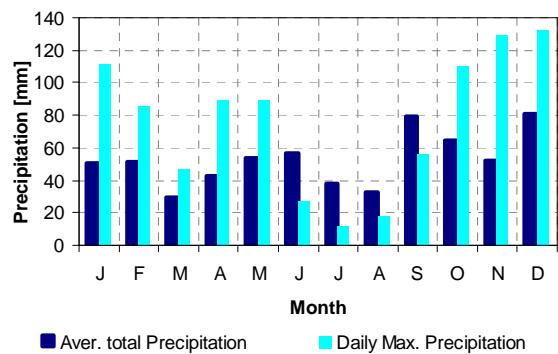


Figure 5.6 - Climate normal values of precipitation in Aveiro (1971-2000) [IM and AEMET, 2010].

Average mean temperatures vary between 10.2 °C (January) and 20.2 °C (August), with an estimated mean value of about 15.4 °C. In general, minimum mean temperatures are observed during winter period (January, February, March, November and December); whilst the maximum mean temperatures are measured in summer period months (between May and September) [SMPC, 2006a]. A nearly regular variation of average minimum and maximum mean temperatures is observed along the year, with amplitude of about 8 °C. Similar temporal evolutions are observed for both absolute maximum and minimum temperatures. Whereas, the lowest absolute minimum temperature of -3 °C was observed in January and December; the highest absolute maximum temperature of 39 °C was recorded in July.

A somewhat 'heterogeneous' variation of mean precipitation values is observed along the year, in addition to perceptible differences between average total precipitation and daily maximum precipitation values. In case of average total precipitation, the highest values are recorded in September (79 mm) and December (81.2 mm), in contrast to the minimum that takes place in March (29.5 mm) and August (32.4 mm); with an estimated mean annual averaged total precipitation value of about 52.6 mm. As regards to daily maximum precipitation, the maximum values are detected in December (131.9 mm) and November (129.2 mm), whilst the minimum are obtained in July (11.8 mm) and August (17.8 mm). A mean annual daily maximum precipitation of about 75.5 mm is mean annual is estimated.

Similarly to precipitation, no general time evolution tendency with traditional differences between winter and summer is observed for both relative humidity and number of days with rain means monthly values summarized in Table 5.4.

Table 5.4 - Averaged monthly relative humidity and number of days with rain in the District of Aveiro [SMPC, 2006a].

Parameter	J	F	M	A	M	J	J	A	S	O	N	D
<i>Rel. humidity [%]</i>	79	78	72	77	80	77	79	80	80	80	79	77
<i>Days with rain</i>	17	11	12	19	16	8	9	7	12	17	14	17

As concerns to relative humidity, an estimated mean annual value of about 78%, with a minimum of 72 % is measured in March, in contrast to the maximum of 80% observed in May, August, September and October. In terms of average number of days with rain, whereas summer months register the lesser values (8, 9 and 7 during June, July and August, respectively); the higher values are detected in April (19 days) and January, October and December with 17 days [SMPC, 2006a]. Even so, no general tendency is observed, in particular during winter months.

Regarding ABL stability conditions, according to Domingos [1980] a prevalence of neutral ($\approx 35\%$) and strong stable ($\approx 25\%$) conditions are estimated for the region of Aveiro, reflecting the closeness to Atlantic Ocean coastal line and the substantial influence of the Atlantic cyclone system and humidity conditions, particularly during winter and night periods.

Concerning wind data, an averaged mean annual value of about 4.25 m.s^{-1} is observed at Aveiro region [Castro, 2010]. Figure 5.7 shows distinct prevailing wind behaviours during winter and summer periods. [SMPC, 2006; Castro, 2010].

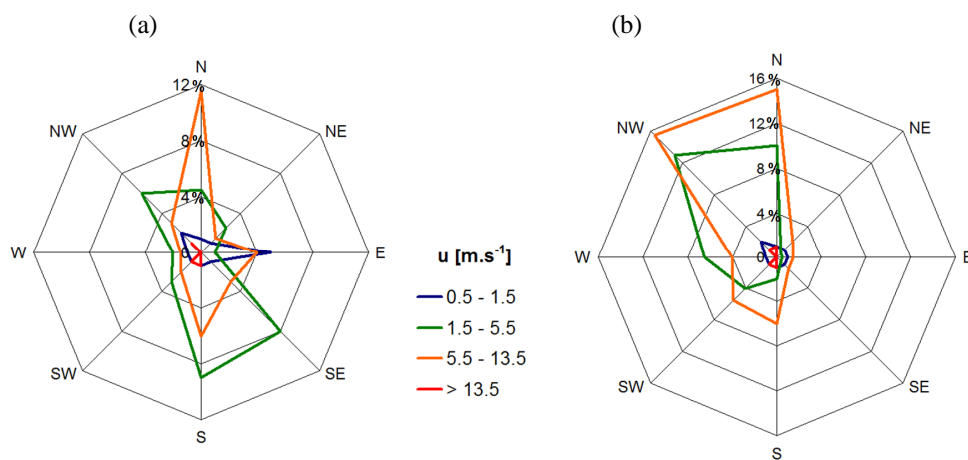


Figure 5.7 - Prevailing wind direction measured in S. Jacinto meteorological station at (a) winter and (b) summer periods (1954-1980) [SMPC, 2006a; Castro, 2010].

In any case, stronger winds ($>13.5 \text{ m.s}^{-1}$) present a somewhat similar behaviour in both periods. For lower wind velocities, distinct behaviours are observed. As regards to winter time, a clear prevalence of N-NW ($5.5 - 13.5 \text{ m.s}^{-1}$) counterbalanced by S-SE ($1.5 - 5.5 \text{ m.s}^{-1}$) wind directions is observed for medium velocity winds, and weaker winds ($< 1.5 \text{ m.s}^{-1}$) are mainly blowing from East. On the other hand, during summer time, a general predominance of N-NW winds is observed in all ranges of wind velocities. Nonetheless, a somewhat frequency of S-SW is also observed at mid-range wind velocities.

5.3.2 Demographic and economical characterization

Based on the most recent census statistics, the total number of resident population in Estarreja municipality is 27,119 inhabitants representing a population density of about $250.6 \text{ inhab.km}^{-2}$ [INE, 2011]. Table 5.5 summarizes demographic statistics in the municipality of Estarreja, by parish, for the most recent census (2001 and 2011).

Table 5.5 - Population distribution in the municipality of Estarreja divided by parish [INE, 2011].

Parish	Area [km ²]	Resident inhabitants		Population density in 2011 [inhab.km ⁻²]
		2001	2011	
<i>Avanca</i>	21.5	6,474	6,213	289.0
<i>Beduído</i>	20.2	7,794	7,657	379.1
<i>Canelas</i>	10.2	1,486	1,438	141.0
<i>Fermelã</i>	13.0	1,482	1,336	102.8
<i>Pardilhó</i>	15.9	4,175	4,163	261.8
<i>Salreu</i>	16.2	4,153	3,825	236.1
<i>Veiros</i>	11.2	2,618	2,487	222.1
Municipality	108.2	28,182	27,119	250.6

Between 2001 and 2011 an overall decrease of 3.8% is observed in the total number of resident inhabitants, more noticeable in Fermelã (-9.9 %) and Salreu (-7.9 %), whereas in Pardilhó is registered a nearly imperceptible variation of -0.3%. Consequently it is estimated a decline of about $9.8 \text{ inhab.km}^{-2}$ in the population density between 2001 ($206.4 \text{ inhab.km}^{-2}$) and 2011 ($205.6 \text{ inhab.km}^{-2}$). A heterogeneous distribution of the population is also observed in the various parishes. The northern parishes (Avanca, Pardilhó and Beduído) constitute around 66.5% of the resident population.

Beduído parish (the administrative city and municipality centre) has the highest number of resident inhabitants (7,657), comprising 28.2% of the total number of inhabitants. On the other

hand, southern and more rural parishes (Salreu, Canelas and Fermelã) represent 19.4 % of the total resident population, showing a decline of about 5.6 % between 2001 and 2011. This distribution is influenced by the location of industrial facilities in Beduído and Avanca, as well as, major communication road and railway accessibilities.

When the distribution per ages is analyzed (see Figure 5.8), between 2001 and 2009 (data from census 2011 is not yet available), it is observed a drop (-5% total) in younger inhabitants (<25 years), counterbalanced by an increase (+5%) of the number of inhabitants older than 25 years [INE, 2010]. This raise is a result of the variation of 4% in adult population (25-65 years) and 1% in elder population (>65 years).

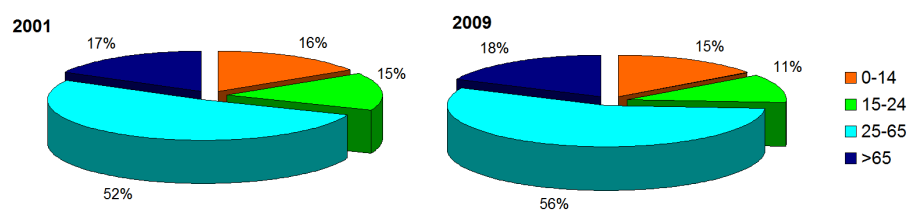


Figure 5.8 - Distribution of resident population of Estarreja municipality by ages in 2001 and 2009 [INE, 2001, 2010].

In general, a large fraction of adult active population works in the secondary (transforming industrial, construction and energy production activities) and tertiary (services) sectors (about 96% in 2001). The primary sector (agriculture) markedly decreased between 2001 and 2009, representing only 4% of the total number of adult workers population [INE, 2010]. These numbers clearly point up the importance of industrial sector in Estarreja region.

Estarreja is served by a dense road and railway networks providing the municipality of good communication accessibilities and transportation routes (see Figure 5.9). The municipality is covered by an extended road net (from local/municipal to highways) with a total length of about 400 km. Four major road transportation routes cross the municipality, namely, the A1 and A29 highways from south to north, connecting Lisbon - Porto and Albergaria - Porto, respectively; and the National Roadways EN109 and EN224 that connect Leiria - Porto and Aveiro - Castelo de Paiva, respectively. Supporting the major roads, a widely spread municipal and inter-municipal road system facilitates local and regional communication accessibilities.

Figure 5.9 shows the spatial distribution of road and railway networks within the municipality of Estarreja, the ECC is also highlight to demonstrate the approximation to main communication accessibilities.

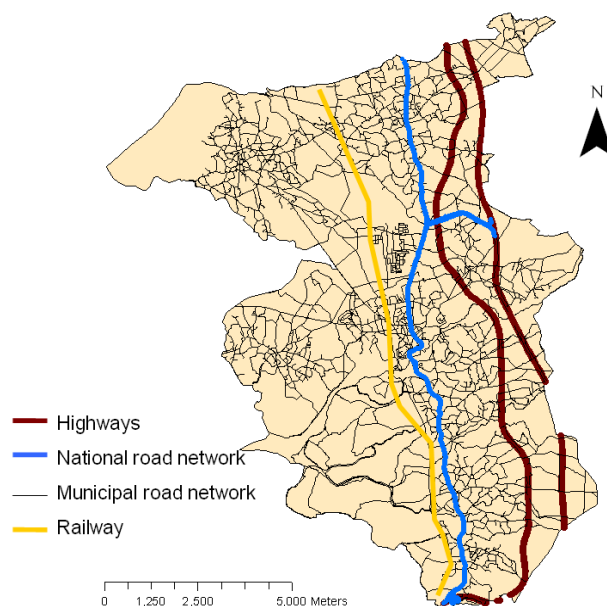


Figure 5.9 – Main road and railway networks in Estarreja municipality area [URL5.3].

Additionally, the Northern line of the Portuguese Rail Network (CP) between Aveiro and Porto, transverses the central area of the municipality from the south to the north, with train stations at Beduído (Estarreja city centre), Avanca, Canelas and Salreu, as well as a terminal inside the ECC administrative area.

In view of the main purpose of CA studies, it is important to identify ‘vulnerable spots’ with particular relevance if potentially affected in case of accident scenarios within the municipality area. Hence, based on up-to-date information [SMPC, 2006; URL5.3] it is possible to identify a total of 99 vulnerable spots listed by the main types of activity and ‘local safety classification’ in Table D.1 (Appendix D), covering a wide variety of types of activity and structures (e.g. administrative services, educational or health centres). As expected, administrative spots (e.g. city hall and parish administrative centres) are generally located at the central area of correspondent parishes. Safety spots (police station and Firefighters headquarter) are mainly concentrated in both Beduído and Avanca parishes. In spite of the variety and nature of identified public places, it is also visible their agglomeration at Beduído area, reflecting the relevance of the municipality central administrative area, relatively close to the ECC. Education and health services are widely spread along the various parishes, in general at parish central areas. Even being considered the most relevant source of MIA hazards, the ECC must be also considered a vulnerable spot, given the degree of potential consequences and effects on workers in case of MIA not, only from the affected establishment but also from the neighbouring installations.

Figure 5.10 shows the spatial distribution of the set of vulnerable spots in the municipality area.

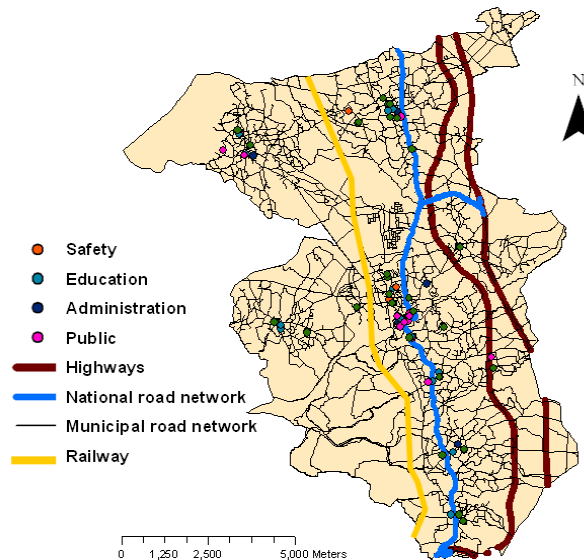


Figure 5.10 - Spatial distribution of vulnerable spots and communication ways in Estarreja Municipality area [URL5.3].

5.4 Accident scenarios

Aiming to demonstrate EFRHA model suitability to be applied in the scope of a CA study based on the ECC, a set of accident scenarios was defined and the predicted short-term pollution episodes and consequences of exposure to the released hazmat gas analyzed. A 'pure DTA approach' was adopted for the definition of potential most-plausible and worst-case accident scenarios. This process took into account the available information concerning the ECC industrial activity (fixed and transportation equipments) and surrounding area (Estarreja municipality).

Plausible and worst-case scenarios were established based on information about the nature and risk of handled hazmat, fixed and transport equipments, prevailing ambient conditions, safety and control guidance, as well as from previous studies main findings [SMPC, 2006; Silva, 2007; Oliveira, 2008; Pereira, 2008], but also, expected outcomes. Notwithstanding the assured existence of proficient safety and control equipment system installed in the various facilities at ECC and emergency response procedures in the context of both IEP and EEEP to reduce or limit the consequences [SMPC, 2006; Pereira, 2008], only the presence of passive retention mechanisms in fixed installations, such as liquid bunds or barriers was assumed.

This approach aims testing EFRHA model with somewhat straightforward, but at the same time, realistic accident scenarios.

Table 5.6 summarizes the set of accident scenarios defined for the demonstrative application of EFRHA model and analysis of short-term pollution episodes and consequences on people.

Table 5.6 - ECC plausible and worst-case scenarios involving the release of hazmat.

Code	Scenario	Type	Location	Substance	Released Mat. [ton]
CE1	Rupture in pipeline	Finite-duration	Near ECC	Chlorine	0.55
CE2	Total collapse of vessel	Instantaneous	Dow	Phosgene	5.0 ¹
CE3	Small hole in vessel wall	Transient	CIRES	Vinyl chloride	200.0
CE4	Road traffic accident	Near-instantaneous	City centre	Benzene	25.0

¹ Despite this amount being registered in 10% of production time (during 90% of process period it is stored 2.5 tonnes of phosgene) [SMPC, 2006a], it is assumed the worst-case accident scenario.

The set of accident scenarios consists on illustrative release conditions for various hazmat that may generate dense gas clouds when accidentally released into the atmosphere. Initial containment conditions include both fixed and transport equipments (pipeline, vessel and cistern). Spatial distribution and quantities considered for the accident scenarios are based on possible equipments location and correspondent hazmat amounts according to Table 5.2 and Table 5.3 listed information [SMPC, 2006a]. Figure 5.11 shows the location of the accident spots considered in the ECC CA study.

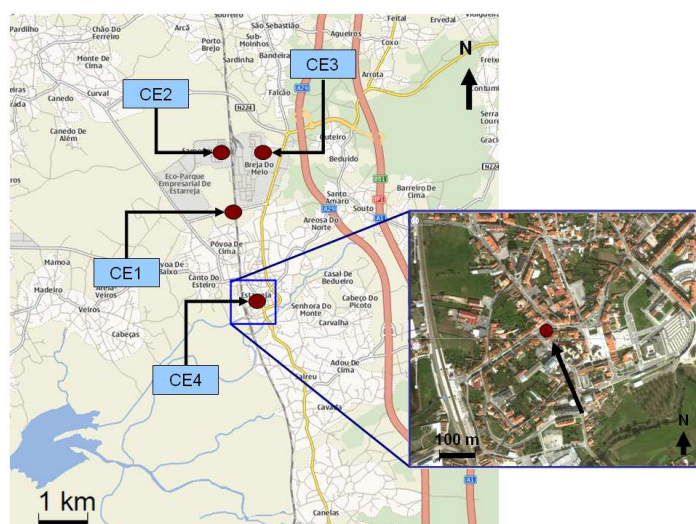


Figure 5.11 - Location of accident points (red spots) considered in the ECC CA study.

Scenario CE1 is based on the theoretical release conditions defined in the frame of the emergency response training exercise carried out in Estarreja on the 22nd November 2006

[SMPC, 2006b] coordinated by ECPMS and, involving the participation of all ECC Seveso-establishments and local entities (*e.g.* administration, communication, education, health, safety bodies and local population). The exercise assumed the occurrence of a 'hypothetical' earthquake causing, among other damages, a rupture of the chlorine pipeline connecting the Port of Aveiro and ECC at the southern frontier of ECC (see Figure 5.11). It was reported the release of gaseous chlorine until the arrival of the emergency response team to repair the failure and 'shut-down of piping system' (about 5 minutes) [SMPC, 2006b]. In view of the lack of detailed technical information regarding the type and conditions of the release, it was considered a continuous chlorine release during a period of about 5 minutes.

Hypothetical plausible and worst case accident scenarios are considered in CE2, CE3 and CE4 in ECC fixed and transportation equipments in accordance with available documentation and previous studies [*e.g.* SMPC, 2006a,b; Silva, 2007; Oliveira, 2008; Tavares *et al.*, 2010]. In case of CE2, it is assumed a worst case scenario, in which is assumed a total rupture/collapse of a vessel storing phosgene (at its full capacity) within the Dow storage production facilities, and subsequent near instantaneous release of the stored volume. As regards to CE3 accident scenario, it is illustrated the transient release of vinyl chloride from a small break in a storage vessel piping valve at CIRES process unit. Finally, with the intention to cover a different transportation equipment, and given the relevance of road transportation mode, the CE4 accident scenario represents a 'near-instantaneous' release of the total content of benzene from a cistern, resulting from a road traffic accident close to Estarreja's administrative and geographic centre (see Figure 5.11).

In addition to the relevance of the first three accident scenarios to represent typifying CA study accidents, the definition of CE4 scenario aims highlighting the need of evaluating this type of accidents and safety and emergency response actions, but also to present EFRHA's increased capability to account the influence of built-up structure on hazmat gas dispersion behaviour and main outputs. Therefore, as illustrated in Figure 5.11, and contrarily to previous accident scenarios sites, in CE4, the crashed cistern truck is located in a central roundabout surrounded by a 'dense' built-up structure of residential and public services buildings.

The selection of two highly toxic and flammability (benzene and vinyl chloride) and two highly toxic (chlorine and phosgene) also intends to analyze the influence of the chemical properties, in particular, in terms of magnitude of consequences and dispersion behaviour. Considering that, most toxic hazmat can disperse faster covering larger areas than flammable

hazmat [CCPS; 2000; Uijt de Haad and Ale, 1999], it is of major relevance to determine analyze the generated hazmat gas cloud footprint along the simulation period, in addition to the magnitude of concentrations estimated [Pontiggia, *et al.*, 2009].

Taking into account the relevance and influence of meteorological conditions on hazmat gas release and atmospheric dispersion behaviour, and subsequently on the predicted consequences, prevailing meteorological conditions at the region of were tested. The set of most representative average meteorological parameters, summarized in Table 5.7, were defined and applied for the prediction of prevailing ambient conditions.

Table 5.7 - Meteorological conditions considered for the ECC accident scenarios EFRHA runs.

Parameter	ME1	ME2	ME3
PG Stability class	A	D	E
Temperature [°C]	20.2	15.1	10.2
Wind direction [°]	N-NW	N-NW	N-NW
Wind velocity [m.s ⁻¹]	1.5	5.0	2.5
Relative humidity [%]	78.5	77.5	77.5
Cloud cover	0.1	0.8	0.4

Three distinct predominant ambient conditions were tested, representing summer (ME1), average annual (ME2) and winter (ME3) mean ABL and meteorological conditions at the region of Estarreja. Reported/compiled data from IM and AEMET [2010] and the surface meteorological station of the University of Aveiro were used according to the input data requirements of EFRHA (EMM). With the purpose of evaluating the influence of meteorological conditions, a common wind direction was defined to be used in all MEs with adapted wind velocities values to properly represent the different ABL stability conditions (convective, neutral and stable). The selection of the N-NW wind direction was mainly due to the potentially affected area - Estarreja municipality centre and most urbanized area. To assure the ABL stability conditions, meteorological parameters were adapted within the measured ranges to properly reproduce the desired ABL conditions.

Aiming to cover both ECC and neighbouring built-up structures/areas, two study area domains were established for this exercise, namely the domains D1 and D2, as illustrated in Figure 5.12.

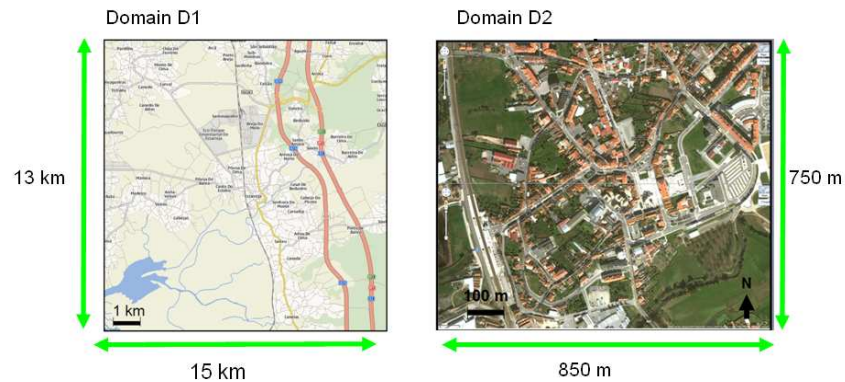


Figure 5.12 – Dimensions of domains D1 and D2 used in CA study of ECC.

The middle point of both simulation domains is the Estarreja's municipality administrative and geographic centre. Whereas the domain D1 was defined for CE1 to CE3 scenarios, covering an area with approximately 15 x 13 km² and a grid resolution of 25 m; the domain D2 was set up for CE4 scenario, consisting of a smaller area of 850 x 750 m² with a finer grid resolution of 5 m, in an attempt to characterize the surrounding built-up area with a superior detail. Furthermore, the definition of D2 resulted from a preliminary application of the EFRHA model using the domain D1, which was not able to accurately describe the built-up spatial distribution and the influence of obstacles because of the coarse grid resolution.

Bearing in mind EFRHA model main purpose and features, land use and built-up structures were characterized for each selected simulation domains. In view of the relatively small variation of surface base elevations within the simulation domain, especially in the area surrounding ECC, dispersion in a nearly flat terrain area was assumed. An averaged and homogeneous z_0 of about 0.604 m was estimated from available up-to-date GIS databases [URL5.3]. Distinct approaches were implemented for built-up structures information, depending of the simulation domain and correspondent grid resolution. Whereas for CE1, CE2 and CE3 only structures close to the accident location (if relevant) were defined; in CE4 a detailed description of the surrounding built-up structure was included. The definition of the equipment (vessel, cistern and pipeline) dimensions was done in accordance to reported information by SMPC [2006a] and the information listed in Table 5.2 and Table 5.3. As regards to the failure dimensions and conditions, recommended information listed in the literature was also considered [see Fingas, 2002; Mannan, 2005; Casal, 2008] for the definition of the information listed in Table D.1 (Appendix D)

In order to analyze the magnitude of potential consequences at 'locations of interest' (e.g. city hall building, schools or health centres), the set of vulnerable spots listed in Table 5.8 and spatially distributed in Figure 5.13 was selected and identified in both simulation domains.

The selection of this set of spots, instead of using all identified was mainly to demonstrate the feasibility of the developed tool to determine the magnitude of potential consequences on specific spots. The selection of these spots was mainly based on the type of accident, location at the downwind area under the already defined meteorological conditions, prevailing ambient conditions and relevance to emergency response actions. Considering the importance of Estarreja central urban area, different types of activities are included in the set, namely, administrative, safety, education and health services, as well as, public spaces located at the southern area (downwind area) of the sources locations. In addition to potentially sensible groups (*e.g.* schools or health centres), the set of listed points also includes spots of crucial importance in case of control and manage of emergency response, such as the city hall building or even the Firefighters and police headquarters. In case of domain D2, a significantly smaller number of spots were defined given the limited dimensions and covered area.

Table 5.8 – Identification of vulnerable spots considered in the application of EFRHA model to ECC accident scenarios.

Type	Vulnerable Spot ID		Covered structures
	Domain D1	Domain D2	
Administrative	P1.1/1	P2.1	- Estarreja city hall
	P1.6/2	P2.2	- Estarreja courthouse
Education	P1.10/3	-	- Padre Donaciano Elementary and High School
	P1.11/4	-	- Estarreja Secondary High School
	P1.15/5	-	- Beduído parish Elementary School
	P1.12/6	-	- Salreu Elementary School
	P1.13/7	-	- Veiros Elementary School
Health	P1.4/8	-	- Hospital Visconde de Salreu
	P1.5/9	-	- Beduído Parish health centre
Safety	P1.3/10	-	- Police station
	P1.2/11	-	- Firefighters headquarter
Public	P1.8/12	P2.3	- Fair park
	P1.7/13	P2.4	- Train station
	P1.9/14	P2.5	- Library
	P1.15/15	-	- Sports hall
Accident	P1.16	P2.6	Accident location

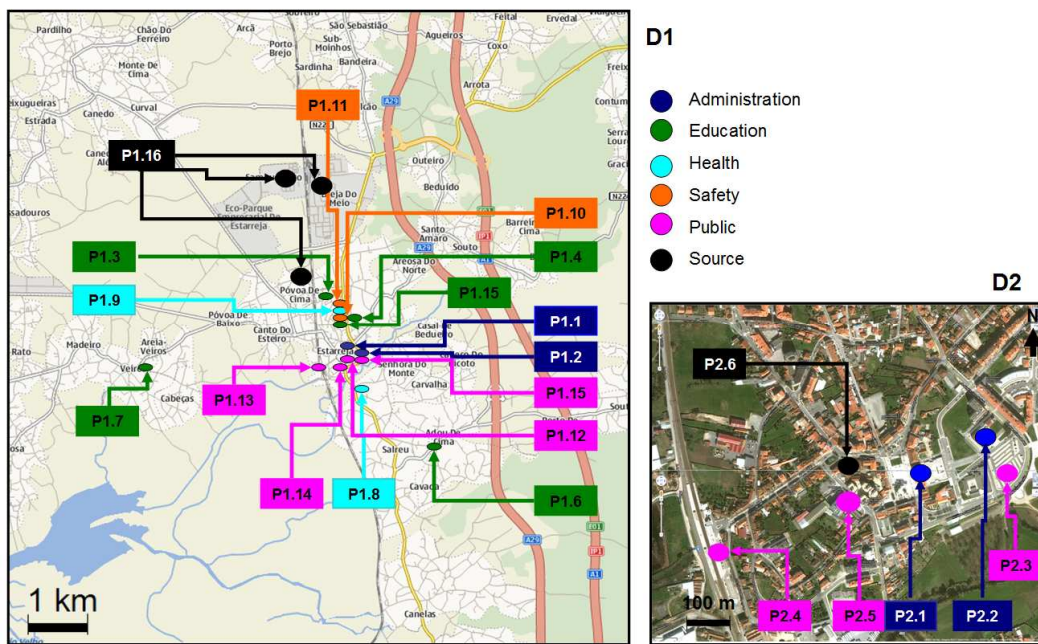


Figure 5.13 – Location of vulnerable spots in domains D1 and D2.

The location of the source is also analyzed as a vulnerable spot (P1.16 in D1 and P2.6 in D2), since it is where, significantly elevated concentration levels are measured, at least while the source remains active. Moreover, it is of substantial importance to verify the local impacts of the released cloud. In this case, covers the industrial facilities (CE1 to CE3) but also the centre of Estarreja municipality area (CE4). Point P1.16 is not identified in domain D1 at Figure 5.13 since it 'overlaps the location of the source for each scenario in Figure 5.11. On the other hand, in domain D2, it is represented point P2.6 because it is only one location. The selection of the source location also allows evaluating the potential level of risk that emergency operators or industrial works would be exposed during the emergency response, within the industrial facilities or just in a central road way. Moreover, the selection of the N-NW wind direction is mainly due to the coverage of the most populated area of the municipality (Beduído central area). Nonetheless, this process was also the result of previous analysis or tests [e.g. SMCP, 2006b; Silva, 2007; Oliveira, 2008; URL5.6].

5.5 Results

With the purpose of estimating the magnitude of consequences on people within the source location and affected surrounding area, direct comparisons of modelled outputs with reference threshold limits were performed for each scenario and hazmat. Despite the wide variety of safety and prevention threshold limits suggested and extensively used in the

literature [e.g. Lees, 1996; Yaws, 1999; CCPS, 2000; VROM, 2005b,c; American Industrial Hygiene Association (AIHA), 2008; Green and Perry, 2008], or even in the legislation, the present analysis considered the toxicological Emergency Response and Planning Guidelines (ERPG) threshold limit values summarized in Table 5.9.

Table 5.9 - Reference ERPG threshold limits considered for the analyzed hazmat [AIHA, 2008]

Product	ERPG [ppm]		
	ERPG1	ERPG2	ERPG3
Chlorine	1	2	3
Phosgene	-	0.2	1
Vinyl chloride	500	5,000	20,000
Benzene	50	150	1,000

The ERPG limits provide estimates of exposure damages based on three distinct concentration ranges that a person may reasonably anticipate observing adverse different ‘degrees’ of effects as a consequence of being exposed for up to one hour to the hazmat in question’ [AIHA, 2008], *i.e.* establishes concentrations of concern that people may suffer certain symptoms from exposure. The ERPGs are three-tiered guidelines for short-term exposures up to one hour (3600 s) of duration of contact to the hazmat in question. The range of symptoms varies between light mild transient adverse health effects (ERPG1) to life-threatening health effects (ERPG3). To simplify the analysis, the EFRHA model concentration values were analyzed in ppm for direct comparisons with standard ERPG threshold limits. Although Portuguese legislation (Decree-Law 254/2007) recommended the preferential use of the Acute Exposure Guideline Limit (AEGL) values, based on levels of concern for various periods of exposure time (from 10 minutes to 1 hour) for the analysis of EFRHA modelled results were considered the correspondent ERPG values. Taking into account the type of acute (peak concentrations) exposure and scenarios considered, the analysis of the maximum observable concentration values can be directly compared with the ERPG since it is mentioned the exposure to levels of concern up-to 1 hour. Additionally, the use of these parameters also facilitates the analysis of instantaneous peak concentrations and therefore, peak/episodic exposure episodes, commonly detected in MIA, strongly felt by the industrial operators during the initial instants after the incident. Detailed definition of the ERPG limits is presented in Appendix D.

Taking into account the nature of the event and generated information, the analysis of the EFRHA modelled outputs is divided in two main steps. The first one comprises the inspection of peak concentrations time evolution and spatial variation at various instants in order to

assess the magnitude of consequences and extent of the affected area. Additionally, a more detailed evaluation of predicted consequences is carried out in the second step, based on the comparison between ERPGs and the 'maximum' concentrations estimated at the vulnerable spots locations during the period of simulation.

Aiming to evaluate the magnitude of estimated concentrations, direct comparisons between modelled and reference ERPG limits were carried out, in the form of the time evolution plots presented in Figures 5.14 to 5.17 for the set of examined accident scenarios. This preliminary analysis enables verifying if harmful 'life-threatening' concentration levels are reached during the period of simulation after the incident.

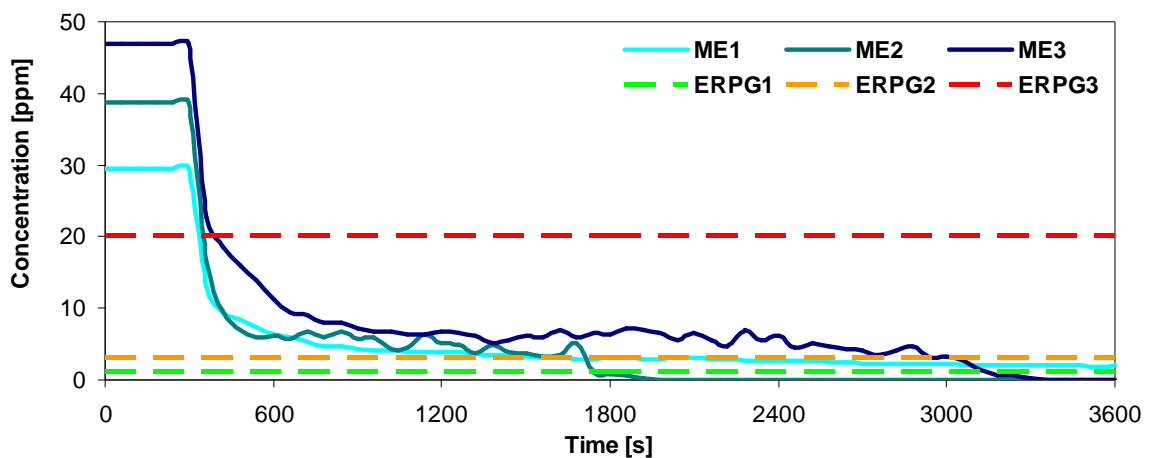


Figure 5.14 - Modelled chlorine maximum concentration time evolution and ERPG limits for CE1 scenario conditions during the initial 3600 s.

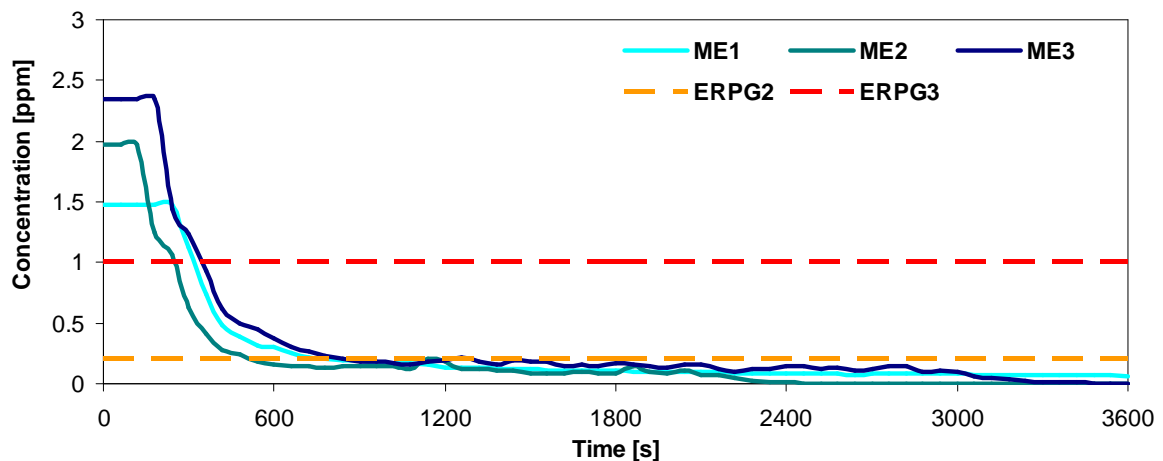


Figure 5.15 - Modelled phosgene maximum concentration time evolution and ERPG limits for CE2 scenario conditions during the initial 3600 s.

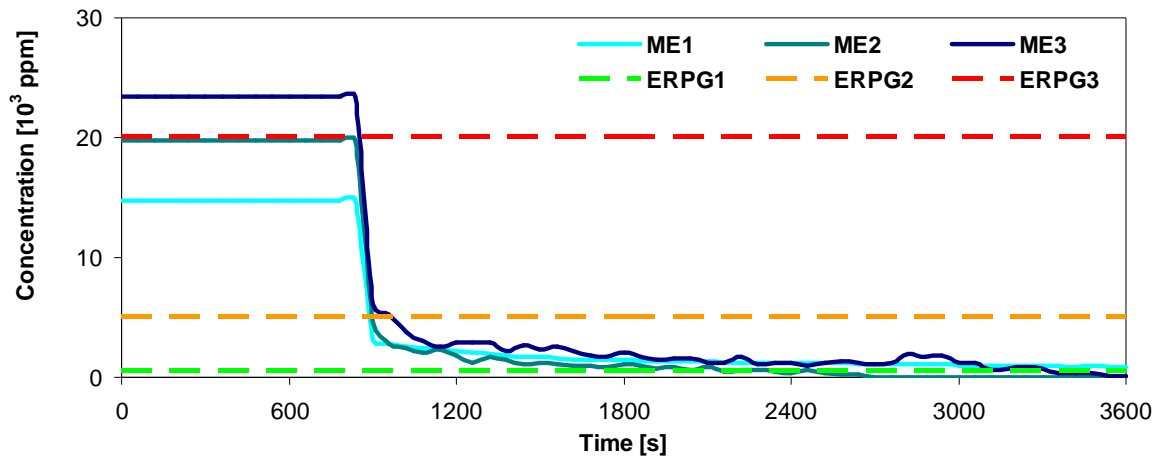


Figure 5.16 – Modelled vinyl chloride maximum concentration time evolution and ERPG limits for CE3 scenario conditions during the initial 3600 s.

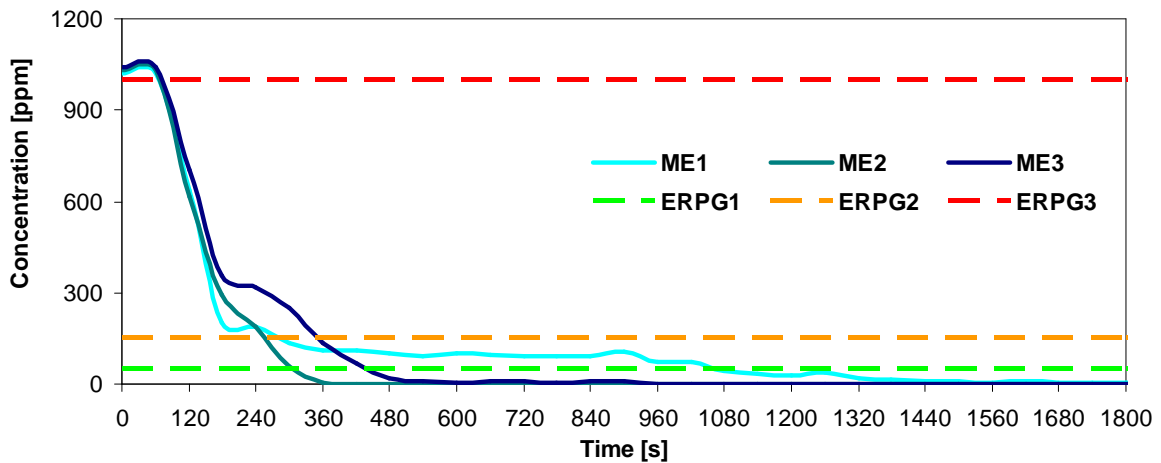


Figure 5.17 – Modelled benzene maximum concentration time evolution and ERPG limits for CE4 scenario conditions during the initial 1800 s.

Overall, Figures 5.14 to 5.17 show that, ERPG3 limits are exceeded by simulated concentrations in all accident scenarios, at least under one ME condition, causing the potential exposure to threatening concentration levels. For instance, while in CE1, CE2 and CE4, estimated concentrations surpass ERPG3 value at least in one moment, under all tested meteorological conditions, in CE3 scenario it is only overtaken for ME3 (stable) conditions. Therefore, in any case, the magnitude of consequences from exposure would require the need to activate the IEP and the EEEP to assure a proper emergency response and safety measured within the affected areas.

Whereas for CE1 (Figure 5.14) and CE2 (Figure 5.15) the magnitude of estimated peak concentrations significantly exceeds the reference ERPG3 limits; in case of CE4 (Figure 5.17) and CE3 under ME2 (Figure 5.16) the difference is somewhat lower. Moreover, the period of

time that the maximum concentrations are observed, is in general proportional to the duration of the active source. This is particularly visible in the case of the continuous and transient releases of chlorine (CE1) and vinyl chloride (CE3), respectively. Eventually, the maximum concentration values correspond to the accident location while the source remains active. On the other hand, considering the dimensions of the container and initially stored amount (see Table 5.7), as well as the range of concentration values estimated, it is possible to check the more or less slender decrease of phosgene and benzene concentrations after the initial peak value (see Figures 5.15 and 5.17). Although CE2 and CE4 have the same type of outflow (near-instantaneous), the range of values 'involved' and the nature/properties of the analyzed hazmat gas generate distinct behaviours. The fall of benzene concentrations is more abrupt than in case of phosgene dispersion. This variation depends on the amount of product released, but also, its intrinsic chemical properties. For instance, whereas phosgene has a molar mass of about 98.92 g.mol⁻¹ and density of 4.35 kg.m⁻³ (gas @ 15 °C and 1 atm); benzene has a molar mass of 78.11 g.mol⁻¹ and density of 3.48 kg.m⁻³ (gas @ 15 °C and 1 atm). Considering the type of accident scenario, but also the thermodynamics presented, under similar conditions, phosgene can be considered denser than benzene and the initial dense gas behaviour/phase will last longer, affecting the cloud dispersion phenomena and the estimated concentration values. On the whole, the results indicate that, during the initial instants if anyone would be 'unexpectedly' exposed to the released hazmat gas, would require emergency and medical assistance, since at least ERPG2 limit (symptoms that could impair individual's to take protection action) is overlapped under any of the tested meteorological conditions.

As regards to meteorological conditions, it is also observed a general and somewhat uniform tendency in CE1, CE2 and CE3 accident scenarios peak concentrations behaviour. From Figures 5.14 to 5.16, it is visible that larger values tend to occur under stable conditions (ME3) during a significant fraction of the analyzed periods, whilst the smaller are observed for convective conditions (ME1). Even so, it can be also noted that, in practically all scenarios (including CE4), concentrations under convective conditions after presenting the significant initial decrease, have the tendency to remain at magnitudes of concern that in general overlap ERPG2 (CE2) or ERPG1 (CE1 and CE3) during longer periods of time (also in CE4). On the other hand, even showing levels of concentrations higher than under convective conditions, during the initial instants of the dispersion, concentrations under neutral conditions (ME2) have the lesser overall 'harmful levels', especially in the second half of the analyzed period of time, where in fact leans to be null earlier than in other meteorological conditions.

As previously mentioned, the CE4 accident scenario presents a distinct temporal variation and overall concentrations behaviour for the various meteorological conditions analyzed. Figure 5.17 shows that initial concentrations are almost identical, independently of the meteorological conditions considered. The clear differences from the general behaviour observed in previous accident scenarios may indicate that, in this case the dispersed cloud behaviour is influenced by other factors in addition to the meteorology, such as the description of the surrounding obstacles. During the initial instants of the dispersion it is visible the strong resemblances of concentrations under the tested meteorological conditions (see Figure 5.17). Only after 180 s, modelled peak concentrations tend to diverge. Furthermore, similarly to the other scenarios, peak concentrations under convective (ME1) conditions tend to overlap ERPG1 during most of the analyzed period of time. In this particular case, concentrations under convective conditions last significantly longer than under neutral (ME2) or stable (ME3) conditions. The results highlight EFRHA's suitability to account the presence of obstacles during the dispersion phase, in order to provide more realistic information.

In general, the analysis of time evolution of hazmat modelled concentrations shows the overall tendency to overlap reference emergency limits, evidencing the need to analyze the extent of potentially affected areas along the dispersion period. Considering the ranges of ERPG values, and modelled concentration, it is possible to mention that, based on this initial analysis, CE2 would represent the less favourable conditions and potentially more affected people and area.

It is also observed the direct influence of meteorological conditions on predicted concentrations. Based on the estimated values it is possible to mention that the most harmful conditions, *i.e.* the higher concentration values, would occur under stable conditions (typical of winter or night time periods), are observed under stable conditions in all examined accident scenarios. On the other hand, it is noted that convective conditions present lower concentration magnitudes, strongly influenced by the wider dispersion and mixing favoured by the atmospheric turbulence, lower wind velocity, but also higher temperatures. Taking into account the influence of temperature on gas density, under higher temperatures, the cloud tends to present less dense gas behaviour during the dispersion [Britter and McQuaid, 1988]. However, 'after a while' it tends to present the higher 'residual' and nearly stable concentrations, that may overlap ERPG1 or ERPG2 limits and cause light mild and/or transient adverse symptoms. Moreover, even concentrations under neutral conditions present concentration values higher than under convective during the initial instants of the dispersion, the estimated levels of harmful concentrations tend to last less time than any other stability condition.

The analysis of peak concentrations time evolution demonstrates the need to evaluate the extent of the affected areas, especially if ERPG2 and ERPG3 levels are overlapped. Hence, in an attempt to analyze the extent of potentially affected areas and cloud behaviour, the set of contour maps presented in Figures 5.18 to 5.21 were examined. Taking into consideration the main differences between CE4 and the other scenarios, Figures 5-18 to 5-20 present instantaneous snapshots of the estimated concentration fields at 5, 15, 30 and 60 minutes after the accident for CE1, to CE3 scenarios; whereas Figure 5.21 includes snapshots of the predicted concentration fields at 2, 5 and 8 minutes after the accident in case of CE4. At a first analysis, Figures 5.18 to 5.20 will be analysed and then the distinct accident scenario conditions considered and predicted for CE4 are discussed next.

The analysis of Figures 5.18 to 5.20 shows that the urban and administrative centre of Estarreja municipality would be strongly affected, at least by concentration levels above ERPG1 limit in all accident scenarios and correspondent meteorological conditions. Moreover, it is visible the larger extensions of affected areas under convective conditions. In a certain way, there results oppose idea that if it is reached the highest peak concentrations, it would directly correspondent to the worst scenario. For instance, even the higher peak concentrations are estimated under stable conditions (ME3), convective conditions tend to show the 'worst accident scenarios', not only in terms of the covered area, but also the duration of the generated cloud. In a certain way, the results replicate the previously observed 'higher' concentrations in the second half of the analyzed period of simulation.

Moreover, contour maps confirm the previous idea that scenario CE2 would generate the 'most harmful' results, not only in terms of magnitude of concentrations, but also the extent of affected areas (see Figure 5.19). Under ME1 and ME3 conditions, it is possible to observe levels of concentrations higher than ERPG3 in certain areas, 15 minutes after the accident, but also concentrations higher than ERPG2 are observed 60 minutes after the accident for the ME1 conditions. If only analyzed the extension of affected areas it is possible to conclude that, in spite of previous idea concerning the possible direct link between the magnitude of concentrations/consequences and dangerousness of a scenario, the most harmful scenario would occur under convective and not stable conditions, given the predicted extension of the affected area during the initial 60 minutes after the accident (see Figure 5.19).

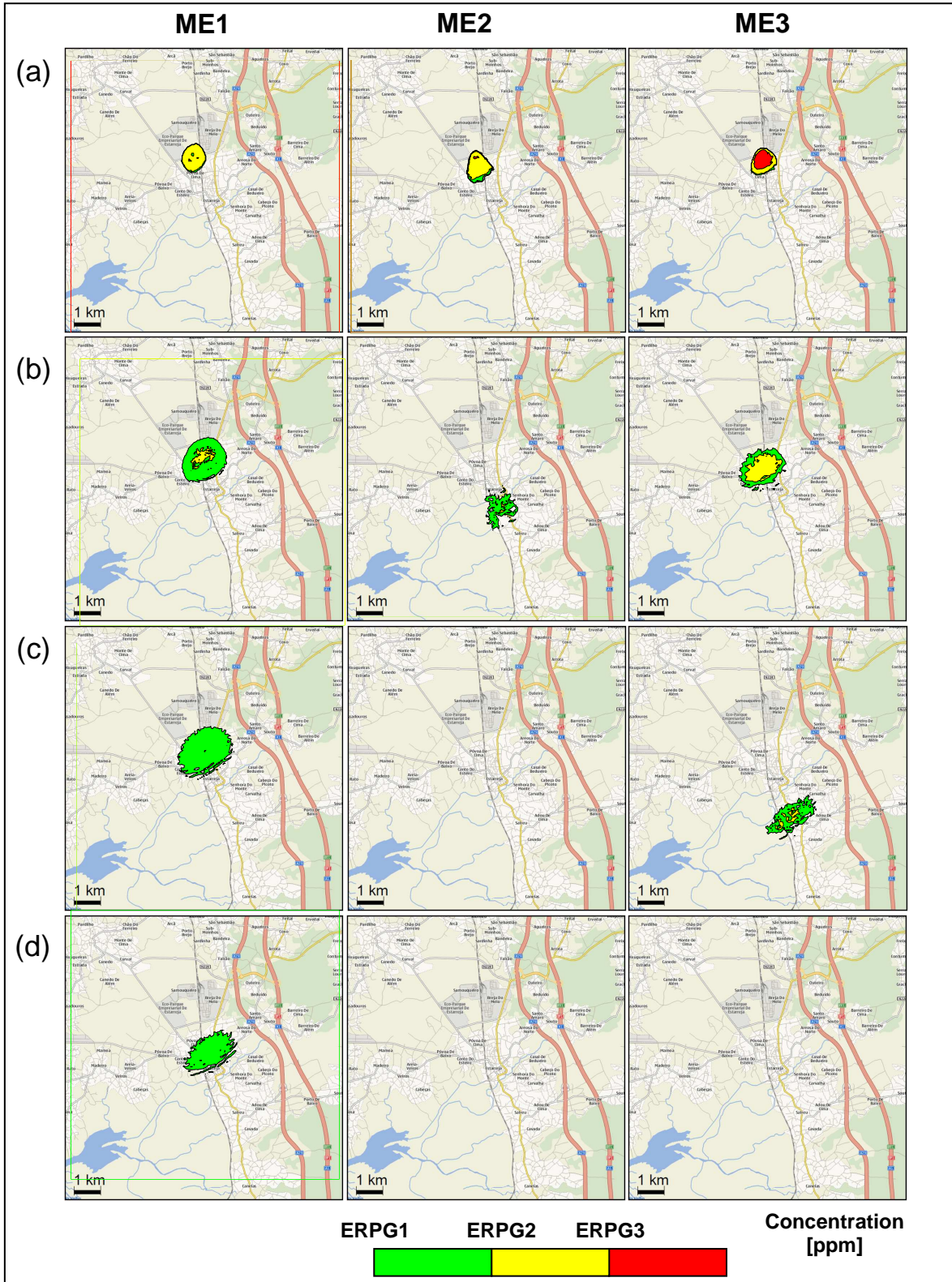


Figure 5.18 – Snapshots of modelled chlorine concentration fields [ppm] at 5 (a), 15 (b), 30 (c) and 60 (d) minutes after the vessel piping rupture for the set of ME of CE1 scenario.

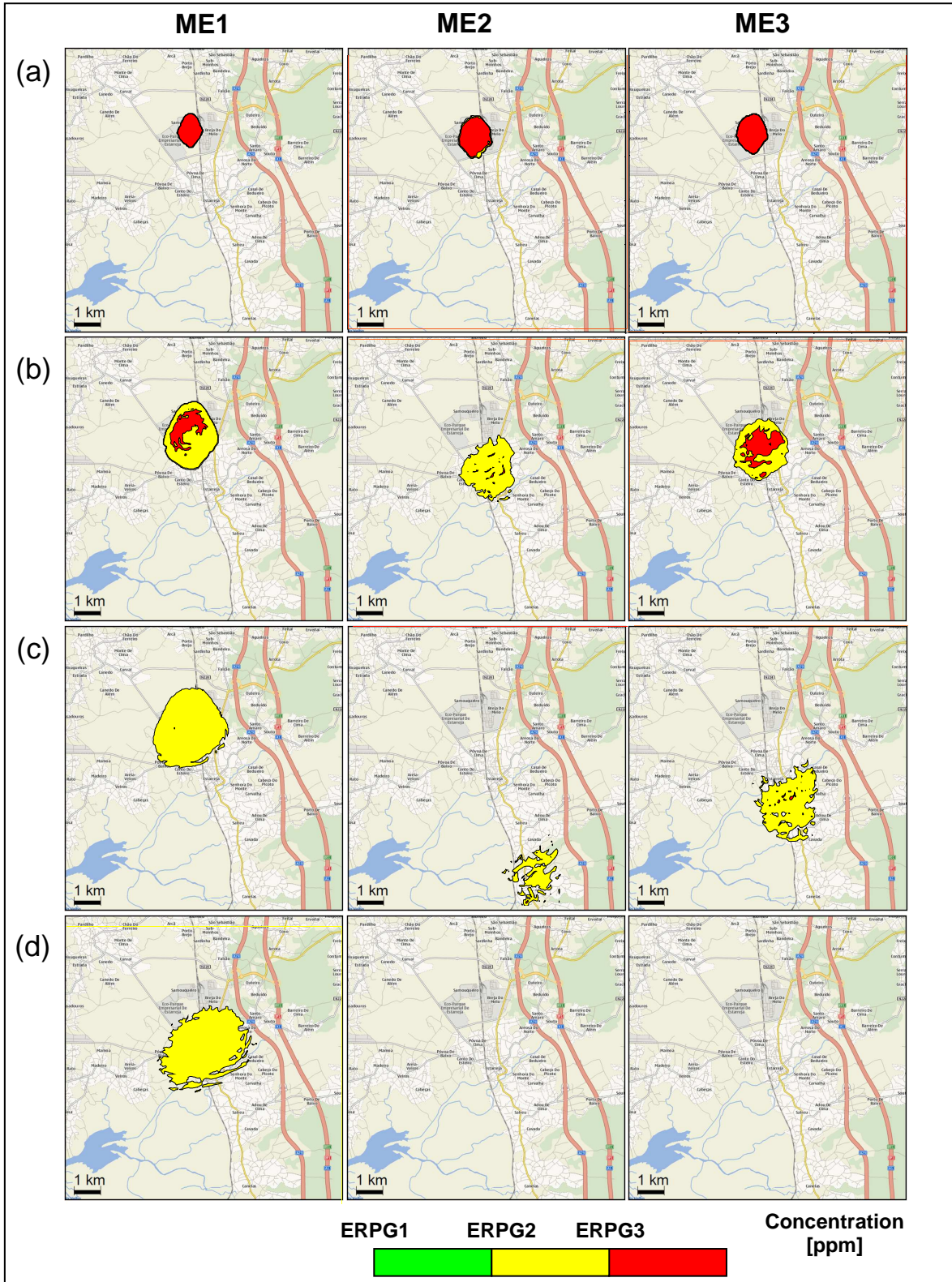


Figure 5.19 – Snapshots of modelled phosgene concentration fields [ppm] at 5 (a), 15 (b), 30 (c) and 60 (d) minutes after the vessel piping rupture for the set of ME of CE2 scenario.

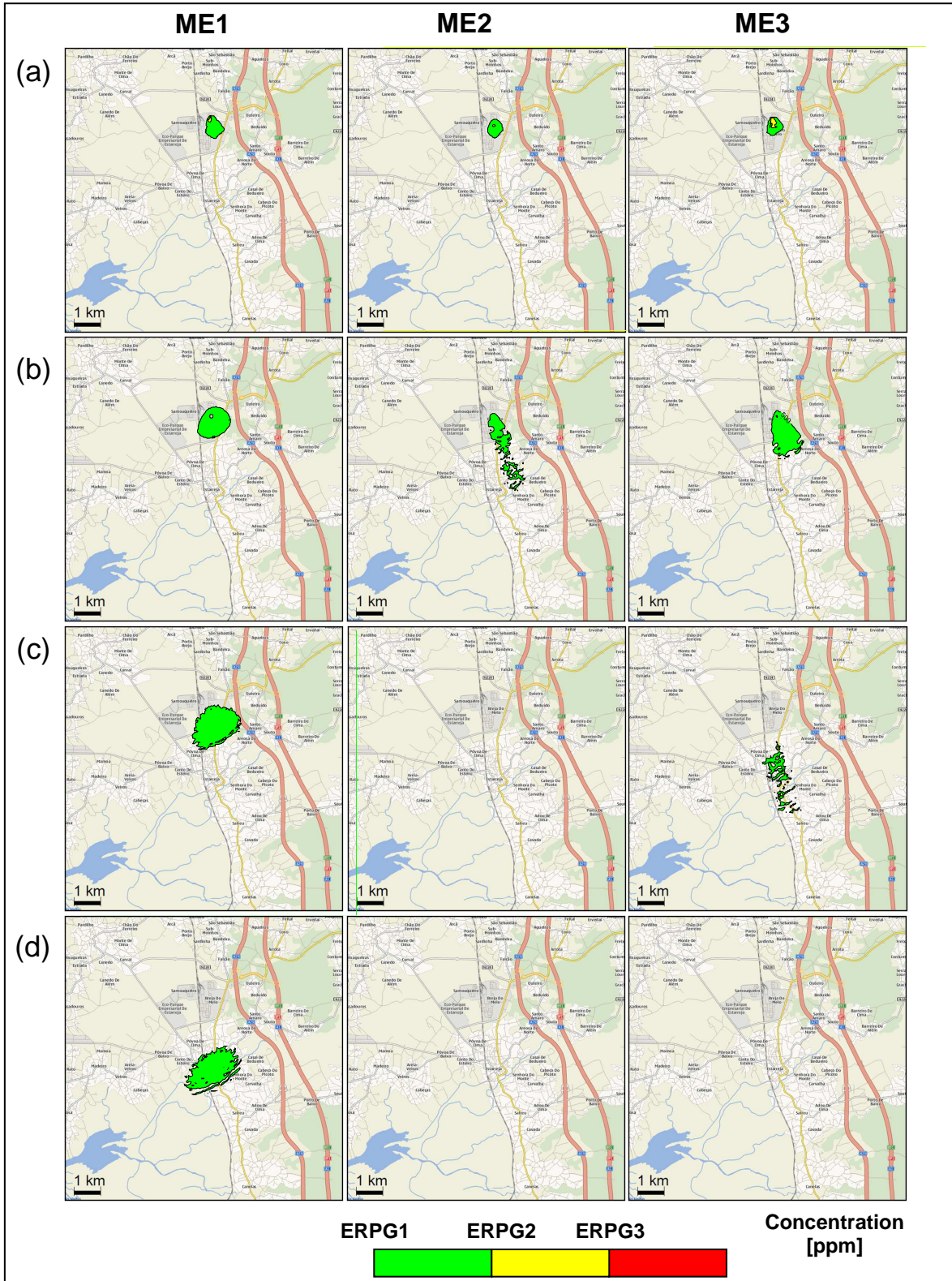


Figure 5.20 – Snapshots of modelled vinyl chloride concentration fields [ppm] at 5 (a), 15 (b), 30 (c) and 60 (d) minutes after the vessel piping rupture for the set of ME of CE3 scenario.

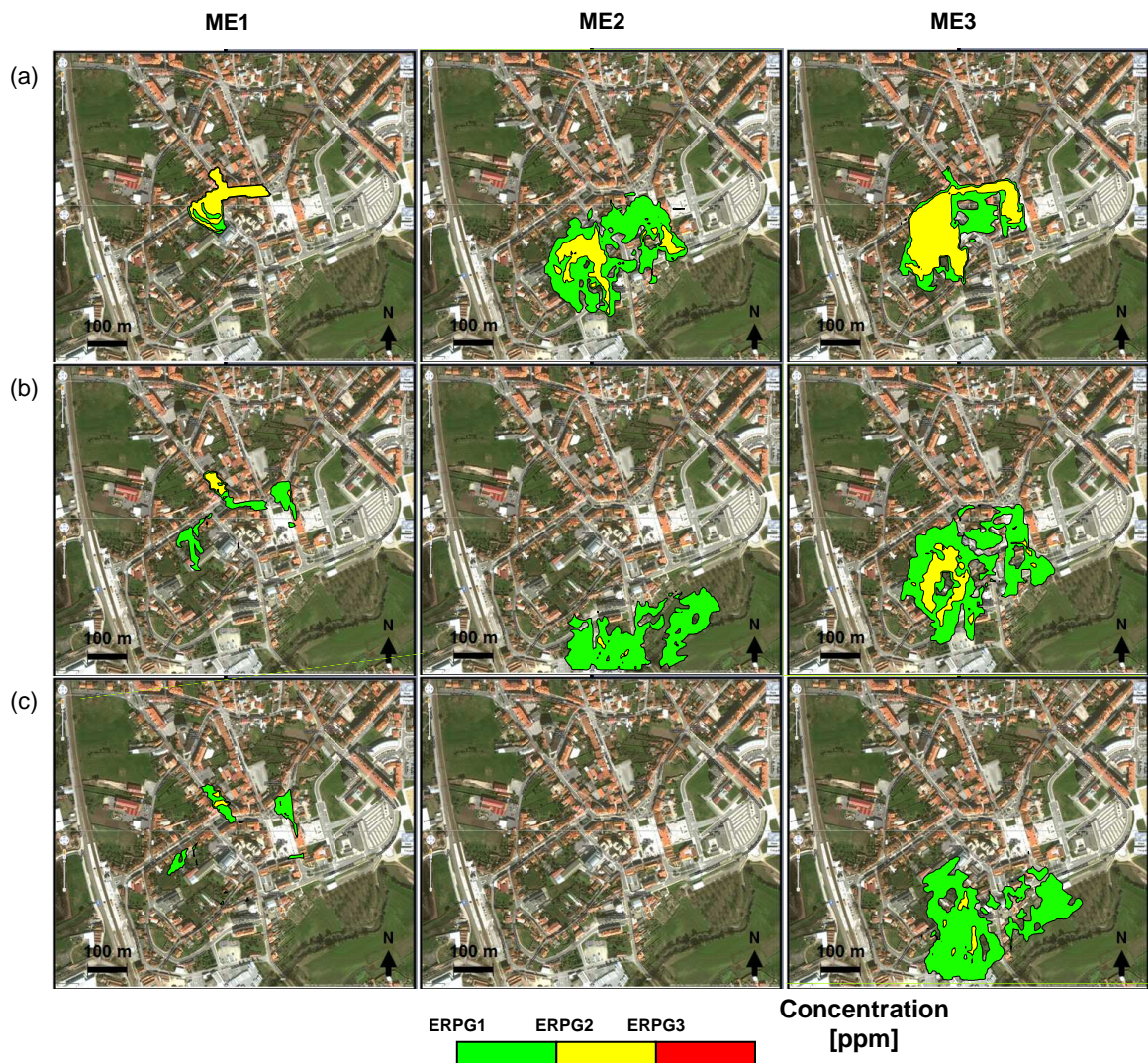


Figure 5.21 - Snapshots of modelled benzene concentration fields [ppm] at 2 (a), 5 (b) and 8 minutes after the cistern truck accident and crash for the set of ME conditions of CE4 scenario.

As regards to CE4 accident scenario, the analysis of Figure 5.21 snapshots clearly indicates the influence of obstacles in the benzene gas dispersion, in addition to the 'traditional' meteorological conditions. Nonetheless, a comparable behaviour to previous accident scenarios main findings is also observed. During the initial instants, the extent of affected area under ME2 and ME3 is substantially higher when compared with the smaller cloud observed under ME1 conditions. This initial expansion may result from the higher wind velocities and the 'intensified' dense gas dispersion behaviour under lower temperatures (for ME2 and ME3). Despite of being less evident for ME2 and ME3 conditions, it can be also observed the influence of the defined obstacles in the general dispersion behaviour. In case of ME1 conditions, the 2 minutes snapshot presents the strong accumulation of benzene in the central open area and narrow streets close to the accident point. Moreover, the influence of obstacles

continues to be visible in the following contour maps, in which it is noted the cloud dispersion in the open spaces around central the obstacles, including Estarreja city hall building. In this case, it would be necessary to assure a fast response of emergency operators. Also, considering that this small area aggregates some of the most relevant administrative and services spots, the analyzed scenario could cause significant consequences in the first instant after the accident.

In general, visual inspection of both peak concentration time evolution and spatial distribution of the generated cloud along the dispersion behaviour highlights the importance of properly defining input meteorological, source term and obstructions data. From the combined analysis of time and spatial evolution of concentrations it is possible to conclude that the less favourable accident scenarios, *i.e.* the scenario that could cause more consequences in the surrounding area, would occur mainly under convective conditions. Even not reaching the same levels of concentrations as estimated for ME3, the extent of affected areas is in general the larger and lasts longer than the ones determined for ME2 or ME3 conditions. Even so, it must be also noted that, distinct behaviour are also observed, that may generate distinct types of consequences. While ME2 and ME3 may generate acute exposure consequences, particularly in the initial instants of the dispersion; ME1 tends to present lower concentrations but during longer periods of time (at least until 60 minutes after the accident) and wider affected areas, especially after 15 min from the accident.

Considering the higher temperature but at the same time lower wind velocity allied with the chemical properties (density), it is possible to mention that the 'dilution' of the cloud is reduced in a certain way during the dispersion process in ME1 conditions. Therefore, an accident occurring during daytime or summer periods would cause more impacts and consequences on local population than under neutral or stable conditions. Moreover, the analysis of CE4 concentrations contour maps shows EFRHA's suitability describe, in a realistic way the dispersion of hazmat gas in obstructed areas, but also the influence of obstacles on hazmat gas atmospheric dispersion.

In addition to the reliable information graphically presented, in case of emergency response, it is also important to evaluate the degree of exposure to hazmat levels of concern at specific spots within the potentially affected area. Aiming to demonstrate EFRHA reliability to generate this type of information, potential consequences on specific vulnerable spots were also analyzed. Tables 5.10- 5.13 summarize the obtained results from the direct comparison

between maximum concentrations modelled at the set of vulnerable spots during the period of simulation (listed in Table 5.9) and reference ERPG limits.

Table 5.10 – Comparison of maximum concentrations estimated in vulnerable spots against reference ERPG values for CE1 accident scenario.

Spot	ERPG limit reached		
	ME1	ME2	ME3
P1.1	Green	Yellow	Yellow
P1.2	Green	Yellow	Yellow
P1.3	Green	Yellow	Red
P1.4	Green	Yellow	Red
P1.5	Green	Yellow	Yellow
P1.6	Green	Green	Green
P1.7	White	White	White
P1.8	Green	Yellow	Red
P1.9	Yellow	Yellow	Yellow
P1.10	Green	Yellow	Yellow
P1.11	Yellow	Yellow	Yellow
P1.12	Green	Yellow	Yellow
P1.13	Green	Yellow	Yellow
P1.14	Green	Yellow	Yellow
P1.15	Green	Yellow	Yellow
P1.16	Red	Red	Red
ERPG	ERP1	ERPG2	ERPG3

Table 5.11 – Comparison of maximum concentrations estimated in vulnerable spots against reference ERPG values for CE2 accident scenario.

Spot	ERPG limit reached		
	ME1	ME2	ME3
P1.1	Yellow	Yellow	Red
P1.2	Yellow	Red	Red
P1.3	Red	Red	Red
P1.4	Red	Red	Red
P1.5	Yellow	Yellow	Red
P1.6	White	Yellow	Yellow
P1.7	White	White	White
P1.8	Yellow	Red	Red
P1.9	Yellow	Red	Red
P1.10	Yellow	Red	Red
P1.11	Yellow	Yellow	Red
P1.12	Yellow	Red	Red
P1.13	Yellow	Yellow	Red
P1.14	Yellow	Yellow	Red
P1.15	Yellow	Yellow	Red
P1.16	Red	Red	Red
ERPG	ERP1	ERPG2	ERPG3

Table 5.12 – Comparison of vinyl chloride maximum concentrations estimated in vulnerable spots against reference ERPG values for CE3 accident scenario.

Spot	ERPG limit reached		
	ME1	ME2	ME3
P1.1			
P1.2			
P1.3			
P1.4			
P1.5			
P1.6			
P1.7			
P1.8			
P1.9			
P1.10			
P1.11			
P1.12			
P1.13			
P1.14			
P1.15			
P1.16			
ERPG	ERPG1	ERPG2	ERPG3

Table 5.13 – Comparison of maximum concentrations estimated in vulnerable spots against reference ERPG values for CE4 accident scenario.

Spot	ERPG limit reached		
	ME1	ME2	ME3
P2.1			
P2.2			
P2.3			
P2.4			
P2.5			
P2.6			
ERPG	ERPG1	ERPG2	ERPG3

Each ERPG is identified by a colour: green (ERPG1), yellow (ERPG2) and finally red (ERPG3). If modelled concentrations in a certain spot do not reach (at least) ERPG1 limit, no colour is defined. In general, the analysis of Tables 5.10 to 5.13 confirms the higher concentration values previously observed under ME2 and ME3 conditions, as well as, that CE2 can be considered the worst accident scenario from the set of accidents analyzed. Taking into consideration the number of spots with concentrations higher than ERPG3 presented in Table 5.12 it is once again observed the magnitude and extension of damage and potential consequences to human health from the total collapse of a phosgene vessel inside the Dow establishment tested in CE2. The extension of the cloud can be also verified through the estimated concentration

levels at farther locations, such as the spot P1.6. Additionally, it is the only case with all spots affected by ERPG3 levels of hazmat gases under neutral and convective conditions, representing potential consequences and life-threatening health effects.

On the other hand, CE3 can be considered the less dangerous accident scenario, when considered the same set of vulnerable spots, in particular at the source location, in which vinyl chloride concentrations only overlap ERPG3 under ME3. In this case, almost all vulnerable spots would suffer ERPG1 light health problems, or transient irritations with reduced health effects or consequences. Transient irritations or more dangerous and irreversible health problems would be observed close to the source, as indicated by the point P1.16 (Table 5.12). In spite of the estimated results, it must be kept in mind that, since the vulnerable spots are mostly located within or close the urban area, for this type of accident, the potentially most exposed persons would be the works and the first response emergency teams. The somewhat reduced level of dangerousness of this scenario is mainly due to the type and nature of the analyzed hazmat (vinyl chloride), the levels of concern established (see Table 5.9) and the correspondent potential consequences to human health, but also the way it is released. Being a transient release from a small valve, the main consequences will be mainly felt within and close to the release point, given the intense mixture and dilution resulting from the jet release. Additionally, it's a fact that estimated consequences from CE4 accident scenario are essentially observed in the surrounding area of the accident. Nonetheless, the degree of resolution, particularly in terms of building structures, demonstrates EFRHA's suitability to provide more realistic information, than commonly applied Class II CA models.

The exercise also demonstrates that the degree of hazardous is not directly dependent on the amount of released material, but most of all their nature and level of concern. For instance, even CE3 considers the transient release of 200 tonnes of vinyl chloride it has been observed that it had the less dangerous 'results. Alternatively, CE1 and CE2 based on the releases of 0.55 tonnes of chlorine and 5 tonnes of phosgene, respectively considered the most dangerous accident scenarios, particularly CE2. Analyzing the ERPGs values it is clear that the degree of dangerousness of phosgene is extremely higher than any of the others. Even so, it has been also demonstrated the importance to analyze eventual failures at the pipeline connecting ECC with the Port of Aveiro and eventual consequences on the surrounding area. Moreover, the relevance of the type of accident and potential consequences must always consider the main purpose of the study and the type of accident and case study area. As observed, even CE4 does not represent a major concern such as CE1 or CE2 scenarios, it is visible that potential

effects on the surrounding area, especially if it is similar to the analyzed, with important public services (*e.g.* banks, offices, restaurants) but also residential spots.

Considering the overall results, it can be observed that, under the defined meteorological conditions, the southern area of the ECC or source location would be affected at least by ERPG1 concentration levels. In general, vulnerable spots would be affected by hazardous concentration levels in case of accident, which could required the evacuation of people inside or close of these structures. Taking into account the results obtained for the set of vulnerable spots, it is clear that, if a MIA does occur under similar meteorological conditions, the entire urban central and administrate area would be affected and exposed to serious hazmat levels. Given the location of safety, education, health and even administrative spots in relation to the ECC, it is required an efficient emergency control and evacuation plan, especially for spots with sensible groups of the local population (*e.g.* schools, hospital). Therefore, the present exercise shows the relevance and applicability of the developed tool to support CA studies, but also emergency planning and response in case of MIA, It is also evidenced that various types of analysis and interpretations from the modelled outputs.

With the exception of CE4 results, it is also possible to determine the maximum distances of risk, and therefore the radius and potential affected area (around the source) along the dispersion under any wind direction and maintaining the other parameters constant. Considering that in the considered domain of simulation the topography or buildings do not present a significant influence on the main results, it is then possible to generalize the results and determine the radius of risk. As regards to CE4, the results cannot be 'generalized' for other wind directions, given the strong influence of the obstacles distribution in the estimated wind fields. In this case it would be necessary to repeat the simulations for different wind directions and verify the main outputs.

5.6 Synthesis

Aiming to demonstrate the main features and capacity to be used in the scope of CA studies, as well as to support decision and emergency response measures/actions, the EFRHA model was applied to a particular case study, based on the Portuguese industrial complex located in Estarreja municipality (the ECC). A set of four accident scenarios was defined: CE1 - leakage of chlorine from a full bore ruptured pipeline; CE2 - total rupture/collapse of a phosgene vessel; the CE3 - transient release of vinyl chloride from a small puncture in a vessel's valve, and finally, CE4 - near instantaneous release of benzene from a crashed cistern in the

municipality central area. Typical convective (ME1), neutral (ME2) and stable (ME3) meteorological conditions were also defined to verify the influence of meteorological conditions on modelled outputs. The magnitude and extension of affected areas were analyzed based on direct comparisons of modelled concentrations and reference ERPG limits, in the form of peak concentrations time evolution plots, contour maps and maximum concentrations at selected vulnerable spots locations.

The application of EFRHA model demonstrates the direct influence of various input 'elements' on the main outputs, in particular the meteorological conditions, release scenario, chemical properties of the studied hazmat gas and the presence (or not) of obstructions (obstacles). The CE1 accident scenario shows that the pipeline system may also represent a source of danger if leakages into to the atmosphere do materialize. The worst case accident scenario CE2 would generate the 'most dramatic' effects in the ECC surrounding area, not only in terms of magnitude, *i.e.* concentrations in relation to correspondent safety threshold limits, but also extension of the affected area, particularly under stable conditions. The accident scenario CE3 would generate the 'less dangerous' effects, even being the scenario involving the higher amount of released material. Finally the CE4 scenario illustrates the added-value of defining the built-up structure, especially at a more detailed scale.

Overall, the application of the EFRHA model to the set of accident scenarios demonstrates its reasonability to produce valid information for the estimation of consequence from the exposure to hazardous levels of hazmat gases accidentally released into the atmosphere. Therefore, it is presented its capability to be used in the scope of CA studies, but also, emergency response and planning.

CHAPTER 6

6. CONCLUSIONS

The production, storage and transportation of hazmat activities are processes of vital economic importance for any advanced and technologically complex society, strongly coupled with an increased number and seriousness of industrial facilities and quantities of hazmat handled. However, as all physical human activities, involve risks to humans and the environment, particularly highlighted by the number of MIAs that continue to occur every year, causing severe consequences on workers and on progressively denser neighbouring populated areas. Subsequently, the increased public and researchers concern on the risks posed by industry and the use of hazmat, enforced regulatory authorities and industrialists to implement new and more complex instruments and measures for the control and prevention of such events. As a result, a series of legislation and regulatory instruments (*e.g.* Seveso Directives), have been published over the last decades, focusing on prevention and control of hazardous industrial activities and their potential consequences. Supported by these measures and constant scientific developments, QRA and CA methodologies became the 'scientific pillar' of regulatory, prevention and control actions and instruments of RA studies, to map and quantify specific consequences and risks in most hazardous industrial activities.

Notwithstanding the wide variety of QRA approaches and techniques, long has been recognized that numerical models can provide valuable information for CA studies and emergency planning and response in case of accidents. Moreover, the need to understand and numerically describe the various stages of accident scenarios involving the release and dispersion of hazmat gases, gave computational models a unique value in CA modelling. Among the various types of models currently applied in CA studies, the dispersion modelling elements are often considered the main core of the entire modelling process, not only due to the complexity associated but also the production of information directly used for the estimation of the consequences from accident scenarios involving the release and dispersion of hazmat gases.

Apart from the large number and variety of dispersion models currently available, the 'Traditional' Class II, particularly Types II-IV models, are almost 'exclusively' applied in CA studies and more recently Class III models started to be also used for more complex environments or studies requiring a higher degree of accuracy. Class II models have been

extensively applied by analysts and emergency planning and response operators in CA studies of accident scenarios, due to their relative effortless and reasonable level of required expertise. Nonetheless, as evidenced in numerous studies, relevant constraints limit their application to broader accident scenarios, but also the quality of main outputs. Among others, the limited application to sets of typifying accident scenarios, their 'simplicity' do not enable considering the influence of obstruction in the dispersion of the accidentally release hazmat gas cloud. On the other hand, although Class III models clearly overcame most of 'well-known' Class II limitations, the level of complexity, expertise and requirements on hardware capability and computational efforts, still limits their broader use, mainly by unspecialized analysts and emergency responders. Therefore, the development of 'intermediate' models, capable to simulate the various phases of the hazmat gas release and dispersion, in a more realistic way, but at the same time maintaining a certain straightforwardness of Class II models can be considered a challenge to current engineering and applied environmental sciences. Moreover, the existence of Class II models, often forgotten by CA modelling prone communities, may also represent alternative ways to overcome the constraints of Class II Types II - IV models.

This important framework determined the main goal of this thesis through the development of an integrated modelling system that incorporates an 'alternative' Class II modelling approach, capable of estimating short-term pollution episodes and consequences from the accidental release and dispersion of hazmat gases in industrial and/or built-up areas. To achieve this purpose, the developed model is designed to simulate the various stages of CA studies and correspondent modelling elements, with particular attention to the source term and dispersion phases, with similar or even less expert or technical requirements of 'Traditional' Class II and Class III models often considered.

To estimate short-term pollution episodes and consequences from accidents involving the release of hazmat gases in industrial and urban areas, the EFRHA model includes a shallow layer dispersion modelling approach, specifically developed for dense gas dispersion in complex environments. The implementation of this 'often forgotten' approach results from the intention to increase the accuracy of modelled results, in particular for hazmat gas accidental release scenarios in complex terrain and/or obstructed areas, but without the need of the Class III CFD models 'complexity'.

Considering the common limitations on accessing the required input information (e.g. chemical properties of the analyzed hazmat or ABL scaling parameter), an additional feature

of EFRHA is the integration of a set of 'pre-processing' modules, to assure the provision of necessary information for the reasonable description of a wide variety of accident scenarios. This procedure enables, not only controlling possible errors or mismatched input or interim information, but also to reduce the minimum strict mandatory input user defined data. Therefore, the integration of EMM, ESTM and ETM modules resulted in a clear easiness on preparing input information, as well as, the definition of accident scenarios and surrounding environment, especially by unspecialized users.

In order to demonstrate the expected better accuracy on overall simulated information and effortless of input data provision through the integrated data flow chain structure, the EFRHA's performance quality was evaluated against measured and/or modelled data from well-established and widely used databases in a series of validation tests. Taking into consideration the various modelling approaches/types implemented, four independent validation exercises were carried out illustrating its performance quality and reliability to be used in CA studies. Taking into account that there is no simple model evaluation guidance approach available for the type of modelling approaches implemented in eFRHA model, the validation exercise was based on the recommendation and quality metrics proposed in the *Model Evaluation Guidelines* (MEG) for 'non-CFD' models.

At a first analysis, the EMM and ESTM pre-processors modelling approaches and assumptions consistency were tested, based on direct comparisons of modelled results with reference data. Given the limited availability of measured information allowing a somewhat broad evaluation, modelled results from extensively validated models was considered. Bearing in mind the intrinsic uncertainties and possible 'errors' from both reference and tested datasets, it is verified the reliability of the implemented modelling algorithm and assumptions with respect to the theoretical principles and provide valid information. The strong approximation to reference data, shown by both qualitative and quantitative analyses, indicates that modelling approaches implemented in both modules respect the main theoretical principles and provide valid data.

As regards to EMM, it is demonstrated the reasonability of implemented modelling assumptions to 'overcome' the main limitations of missing input information available. This feature allows applying the model in more test cases, especially in case of emergency response or planning studies in situations of large amount of missing input data. Additionally, it is highlighted the added-value of integrating the chemical properties database through the quality of ESTM modelled results. Nonetheless, in both cases, it can be observed the influence

of input datasets on modelled outputs. For instance, the 'accumulated' uncertainties and deviations generated along the calculation process of surface ABL scaling parameters, is perceptible on the estimated ABL mixing height variables. Moreover, the slight differences between chemical properties databases considered by EFRHA and EFFECTS 7.5 model, result in 'amplified' deviations in modelled results, especially in case of liquid and PLG release scenarios.

The inclusion of ETM in EFRHA model represented an enhanced capability for reproducing, in a simple way, the influence of complex terrain and/or building in the hazmat gas atmospheric dispersion, and thus, overcoming one of the most known limitations of most of Class II models currently applied in CA studies. Notwithstanding the relative straightforwardness of ETM-EDM approach, it was observed the increase of modelling performance quality if this option is selected when applied to the well-known and widely used experimental set up -45° MUST test case. In this stage, the validation exercise consisted of direct comparisons of modelled against measured mean concentrations. At the same time, it was evaluated the most appropriate and realistic way to input obstructions and complex terrain data through the variation of surface roughness values and inclusion of obstacles or not.

Based on the overall performance analyses, it was observed that, similarly to other 'non-CFD' Class II models (of varied Types) it does not satisfies most of quality paired point-by-point metrics, originally defined for more accurate and complex CFD models. Nevertheless, the results visibly show the added-value reflected on the better correlation when the influence of obstructions is considered in the dispersion simulation. Furthermore, if analyzed the ranges of concentration values and modelled plume features, it is also demonstrated the increased performance if the obstacles are considered. Hence, even considering a simple quasi-steady-state modelling approach, it is highlighted the improved performance quality of including the presence of obstacles. Furthermore, the influence of surface roughness values on final results can be also noted. As presented in both qualitative and quantitative analysis, the selected of the most realistic value for z_0 can also affect the quality of modelled results. Consequently, this preliminary evaluation analysis evidences the added-value of considering realistic input parameters, as well as, describing numerically the presence of obstacles in the simulation domain and their influence on generated concentration fields. The evidenced possibility to account the presence of obstacles and complex terrain is of particular importance, when applied to industrial and urban areas.

Finally, demonstrated the suitability of the various modules to produce valid and reasonable interim and output information (for the dispersion in obstructed areas), the developed model was validated in its entire scope through the simulation of a set of well-established and widely used field experimental. A special attention was given to the analysis of EFRHA's performance quality when the released gases tend to shown dense gas behaviour, under difference outflow, meteorological and presence of obstructions situations.

In general, despite some deviations from measured values, it was demonstrated its capability to model the various phases of the release and atmospheric dispersion phenomena. On the whole, quality criteria acceptability limits were satisfied, with a reasonable accuracy for 'typical' accident scenarios. Noticeable overestimations were predicted in a large fraction of experiments, nonetheless, the overall temporal variation and ranges of values are predicted with an acceptable correlation degree. Moreover, as expected, less favourable correlations were observed for scenarios considering the presence of obstacles, specifically when compared with EFRHA's performance results from comparable tests under similar conditions. Nonetheless, the exercise demonstrates its reliability to predict the various stages of the release and dispersion phenomena.

After its successful validation, EFRHA model was applied to a set of accident scenarios based on the Portuguese ECC located in the Municipality of Estarreja. The concentration of various Seveso-establishments, nature and quantities of hazmat handled and transported, as well as, available technical information enabled the definition of potential accident scenarios, as realistic as possible, for the application of EFRHA model in view of CA purposes. Both fixed and transportation equipments were analysed. A set of four distinct accidents was considered, comprising plausible and worst-case release/leakage scenarios. Corroborating previous studies, it can be also observed the notable differences between highly toxic and highly flammable hazmat. Although flammable hazmat tends to present higher magnitudes/ranges of concentrations, toxic gases tend to disperse faster and therefore cause larger potentially affected areas. Overall the application of EFRHA showed the suitability and consistence of implemented modelling algorithms. The various simulations evidenced the potential use of EFRHA model to support CA studies or emergency decision and planning, given the relative low efforts and computational efforts, when compared with Class III models.

The work developed within the scope of the present thesis intends responding to the need of new and more realistic modelling tools to support CA and emergency planning simultaneously assuring easiness and a relative straightforwardness to be applied by both

experts and unspecialized users. Even not so generalized, the integration of different models in one single modelling tool also represents a practical way to optimize time and work efforts. It is well known that integration of various models in one modelling system may increase potential uncertainties and errors, but if this tool is properly designed, may represent an alternative to existing models as demonstrated in this thesis.

Notwithstanding the presented added-value of the developed tool, some constraints were detected during the application to the various test cases, stressing the need to improve some aspects of model in the future. Current version of the EFRHA model is only designed to simulate accident scenarios involving the release and atmospheric dispersion of hazmat gases, from a single incident event. Taking into account the relevance on considering the occurrence of multiple sources in case of two-phase PLG release scenarios, it is possible to apply the same modelling principle for multiple sources. Such feature will be of major significance, in particular for accident scenarios involving various equipments/structures, or even the potential domino effects.

During the definition of the accident scenarios, it was also highlighted the potential consequences from fires and explosions, which cannot be directly handle by the implemented dispersion modelling approach. This integration will allow applying the model to more accident scenarios, but also, incorporating a more accurate description of the accident scenario, it also increases the accuracy and quality of main outputs.

Meanwhile the model has only been applied in the scope of DTA modelling approaches. Considering the 'expanding' use of PRA approaches, the potential inclusion of probability and vulnerability methods, may also raise the quality of the definition of accident scenarios, as well as, the 'realistic' estimation of main consequences based on both failure type and probability of occurrence. The continuous development of new mathematical and computational methods represents a challenge to integrate more complex effects models, as well as, probabilistic (probit and dose response methods) methodologies. Such modifications/updates represent new challenges and the development of new and innovative products, not only for scientific community, but also, risk assessment and regulation authorities.

Another relevant constrain is the strong dependency on modelled cloud density and difference with ambient air densities. Taking into account that for lower values, the cloud practically is not considered, it is important to apt the model for situations of passive gas dispersion behaviour. Although not considering in the present version of EFRHA model, it is

being tested the potential coupling of EFRHA dispersion model with the 'up-to-dated' new generation Gaussian models, enabling estimating the dispersion until the cloud reaches significantly reduced concentration levels. Even so, recognized the limitations of Class II models, in particular for considering the presence of obstacles, this procedure is still in the starting point. However, several examples have already been presented in similar studies. Among other challenges is the integration of a more accurate wind fields modelling approach in order to account the real flow around the obstacles.

It's a fact that continuous increase and development of computational and hardware capacities, pushes the development of new and more complex modelling tools, however it is important to establish links and compromises between communities promoting the development of new and more usable new tools, but at the same time, assuring a somewhat easiness enabling potential unspecialized end-users to apply and maybe implement these tools in other areas. Therefore, apart from the development of more complex models, it is also a test attempting to improve existing approaches, but maintaining its straightforwardness to endorse and emphasise their use not only in CA studies, but also by emergency response operators. Overall the present thesis demonstrates the possible application of alternative modelling approaches often forgotten with acceptable results, instead of the extensively used and still complex class III CFD models. Moreover, the increased risk of industrial and urban areas to be affected in case of industrial and/or deliberated release of hazmat gases enforces the development and proper application of more accurate and realistic, but at the same time, operational and somewhat fast-run tools.

REFERENCES

REFERENCES

- Abdolhamidzadeh B., Abbasi T., Rashtchian D., Abbasi S.A., 2011. Domino effect in process-industry accidents – An inventory of past events and identification of some patterns. *Journal of Loss Prevention in the Process Industries*, 24(5), 575-593.
- Abramowitz M., Stegun I.A. (Eds.), 1972. *Handbook of mathematical functions with formulas, graphs, and mathematical tables*. National Bureau of Standards-Applied Mathematics Series 55, USA. 1046 pp.
- AIHA, 2008. *Emergency Response Planning Guidelines (ERPG) and Workplace Environmental Exposure Levels (WEEL)*, American Industrial Hygiene Association, Emergency Response Planning (ERP) and Workplace Environmental Exposure Level (WEEL) Committees.
- Ale B., 2009. *Risk: An Introduction The Concepts of Risk, Danger and Chance*, Rutledge.
- Allwine K.J., 2004. Overview of JOINT URBAN 2003 - an atmospheric dispersion study in Oklahoma City, *Proceedings of the AMS Symposium on Planning, Nowcasting, and Forecasting in the Urban Zone*, January 11-15, Seattle, Washington, USA.
- Allwine K.J., Shinn J.H., Streit G.E., Clawson K.L., Brown M., 2002. Overview of URBAN 2000: a multiscale field study of dispersion through an urban environment. *Bulletin of the American Meteorological Society* 3, 521-536.
- Andrews J.D., Moss T.R., 1993. *Reliability and Risk Assessment*. 1st Ed. Longman Group UK.
- ANPC, 2009. *Guia para a caracterização do risco no âmbito da elaboração de planos emergência de protecção civil*. *Cadernos Técnicos PROCIV 9*, ANPC.
- Arcuri A., 2005. *Governing the risks of ultra-hazardous activities: Challenges for contemporary legal systems*. Rotterdam: Erasmus University.
- ASTM International, 2005. *Standard guide for statistical evaluation of atmospheric dispersion model performance*, D 6589 - 05. ASTM International. 17 pp.
- Atkins Portugal, 1997. *Projeto de validação da solução proposta pela ERASE, para recuperação e regeneração de águas e solos contaminados pelos resíduos industriais tóxicos acumulados no parque industrial de Estarreja e envolvente*. Lisboa: Atkins Portugal.
- Attwood D., Khan F.I., Veitch R., 2006. Validation of an offshore occupational accident frequency prediction model – A practical demonstration using case studies. *Process Safety Progress*, 25 (2), 160-171.
- Baechlin W., Theurer W., Plate E.J., 1991. Wind field and dispersion in a built-up area – A comparison between field measurements and wind tunnel data, *Atmospheric*

Environment, 25A(7), 1135-1142.

Bagster D.F., Pitblado R.M., 1991. The estimation of domino incident frequencies—an approach, *Process Safety and Environmental Protection*, 69, 196.

Baik J., Kim J., 2002. On the escape of pollutants from urban street canyons, *Atmospheric Environment* 2002, 36: 527-536.

Baklanov A., Mahura A. 2003. Assessment of possible airborne impact from nuclear risk sites - Part I: Methodology for probabilistic atmospheric studies. *Atmos. Chem. Phys. Discuss.*, 3, 5289-5317.

Baklanov A., Mahura A., 2004. Assessment of possible airborne impact from risk sites: methodology for probabilistic atmospheric studies. *Atmospheric Chemistry and Physics*, 4, 485-495.

Baklanov A., Joffre S.M., Piringer M., Deserti M., Middleton D.R, Tombrou M., Karppinen A., Emeis S., Prior V., Rotach M.W., Bonafè G., Baumann-Stanzer K., Kuchin A., 2006. Towards estimating the mixing height in urban areas. Recent experimental and modelling results from the COST-715 Action and FUMAPEX project. Scientific Report 06-06. Danish Meteorological Institute, Denmark, 41 pp.

Barthelemy F., Hornus H., Roussot J., Hufschmitt J., Raffoux J., 2001. Report of the General Inspectorate for the Environment, Accident on the 21st of September 2001 at a factory belonging to the Grande Paroisse Company in Toulouse, Explosive Inspectorate and INERIS, affair no. IGE/01/034.

Baverstock K., Williams D., 2006. The Chernobyl Accident 20 Years On: An Assessment of the Health Consequences and the International Response. *Environmental Health Perspectives*, 114, 1312-1317.

Belore R., Buist I., 1986. A computer model for predicting leak rates of chemicals from damaged storage and transportation tanks, S.L. Ross Environmental Research Lim. Ottawa, Ontario, Canada.

Bennett B., Repacholi M., Carr Z. (eds), 2006. Health Effects of the Chernobyl Accident and Special Health Care Programmes - Report of the UN Chernobyl Forum Expert Group "Health", WHO, Geneva, Switzerland.

Bernatik A., Zimmerman W., Pitt M., Strizik M., Nevly V. and Zelinger Z., 2008. Modelling accidental releases from mobile sources. *Process Safety and Environment Protection*, 86, 198-207.

Bertazzi P.A, Bernucci I, Brambilla, G, Consonni, D., Pesatori, A.C., 1998. The Seveso Studies on Early and Long-Term Effects of Dioxin Exposure: A Review. *Environmental Health Perspectives Supplements* 106 (S2), 5-20.

Bezpalcova K., 2007. Modelling of Flow and Diffusion in Urban Canopy, Ph.D. thesis, Faculty of Mathematics and Physics, Charles University, Prague, Czech Republic. 193 pp.

- Bezpalcova K., Harms F., 2005. EWTL Data Report / Part I: Summarized Test Description Mock Urban Setting Test. Environmental Wind Tunnel Laboratory, Centre for Marine and Atmospheric Research, University of Hamburg.
- Biltoft C.A., 2001a. Abbreviated Test Plan for Customer Test - Mock Urban Setting Test. Technical Report WDTC-TP-01-028. West Desert Test Centre, U.S. Army Dugway Proving Ground, Dugway, UT.
- Biltoft C.A., 2001b. Customer Report for Mock Urban Setting Test. Technical report, DPG Document No. WDTC-FR-01-121. US Army Dugway Proving Ground, Dugway, Utah.
- Blackmore D.R., Herman M.N., Woodward J.L., 1982. Heavy gas dispersion models. *Journal of Hazardous Materials*, 6, 107-128.
- BMIIB, 2006. Initial Report to the Health and Safety Commission and the Environment Agency of the investigation into the explosions and fires at the Buncefield oil storage and transfer depot, Hemel Hempstead, on 11 December 2005, Buncefield Major Incident Investigation Board, London, U.K..
- BMIIB, 2008a. The Buncefield Incident 11 December 2005, The final report of the Major Incident Investigation Board, Volume I, HSE Books, London, U.K..
- BMIIB, 2008b. The Buncefield Incident 11 December 2005, The final report of the Major Incident Investigation Board, Volume II, HSE Books, London, U.K
- BMIIB, 2008c. Recommendations on land use planning and the control of societal risk around major hazard sites. HSE Books, London, U.K
- Borrego C., Amorim J.H., 2007. Risk and Emergency Modelling for Environmental Security: General Aspects In: Air, Water and Soil Quality Modelling for Risk and Impact Assessment. Adolf Ebel and Teimuraz Davitashvili . (eds) NATO Security through Science Series - C: Environmental Security. Springer. Dordrecht. (1). 365 pp.
- Borrego C., Miranda A.I., Amorim J.H., Santos P., Tavares R., 2009. Sistema integrado para auxílio à tomada de decisão em caso de acidente grave RISCAV. Universidade de Aveiro. AMB - QA - 11/2009, Aveiro, Portugal. 120 pp.
- Borrego C., Tchepel O., Salmim L., Amorim J.H., Costa A.M., Janko J., 2004. Integrated modelling of road traffic emissions: application to Lisbon air quality management. *Cybernetics and Systems: An International journal*. Taylor & Francis, Vol. 35, Numbers 5-6, p. 535-548.
- Brambilla S., Manca D., 2011. Recommended features of an industrial accident simulator for the training of operators. *Journal of Loss Prevention in the Process Industries*, 24(4): 344-355.
- Brambilla, S., Brown, M.J., 2010. Survey on thorney Island trials. 16th Conference on Air Pollution Meteorology at the 90th AMS Annual Meeting, Atlanta, GA, 18-21 Jan.
- Brambilla S., Manca D., Williams M., Gowardhan A., Brown M.J., 2009. A SHALLOW WATER MODEL FOR DENSE GAS SIMULATION IN URBAN AREAS. *Proceeding of*

AMS 8th Symposium on the Urban Environment, Phoenix, AZ January 12-1.

Britter R.E., 1980. The ground level extent of a negatively buoyant plume in a turbulent boundary layer, *Atm. Env.*, 14, 779.

Britter R., Schatzmann M., (eds.), 2007a. Background and Justification Document to Support the Model Evaluation Guidance and Protocol Document, COST, Brussels.

Britter R.E., 1989. The atmospheric dispersion of dense gases *Annual Review of Fluid Mechanics*, 21. 317-344.

Britter R.E., 1990. GASTAR user manual, CERC Cambridge, U.K.

Britter R.E., 1998. Recent research on the dispersion of hazardous materials Office for Official Publications of the European Union, Luxembourg.

Britter R.E., Griffiths R.F., 1982. Dense gas dispersion Elsevier Press, Amsterdam.

Britter R.E., McQuaid J.M., 1988. Workbook on the Dispersion of Dense Gases. HMSO, UK.

Britter R., Schatzmann M., (eds.), 2007b. Model evaluation guidance and protocol document. COST, Brussels.

Britter R.E., Cleaver R.P., Cooper M.G., 1991. Development of a simple model for the dispersion of denser-than-air vapour clouds over real terrain. Technical Report MRS E 622, British Gas, Research and technology, Midlands Research Station, Wharf Lane, Solihull, B91 2JW.

Builtjes P., 1992. Research on continuous and instantaneous heavy gas releases. TNO-ME report 92-135, TNO, Appeldorn, Netherlands.

Cahen B. 2006. Implementation of new legislative measures on industrial risks prevention and control in urban areas. *Journal of Hazardous Materials*, 130(3): 293-299.

Cardis, E, Kesminiene, A, Ivanov, V, Malakhova, I, Shibata, Y, Khrouch, V., Drozdovitch, V, Maceika, E, Zvonova, I, Vlassov, O. *et al.*, 2005. Risk of thyroid cancer after exposure to 131I in childhood *J Natl Cancer Inst* 97:724-732.

Carissimo B., Jagger S.F., Daish N.C., Halford A., Selmer-Olsen S., Riikonen K., Perroux J.M., Wuertz J., Bartzis J.G., Duijm N.J., Ham K., Schatzmann M., Hall R., 2001. The SMEDIS Database and Validation Exercise. *Int. Journal of Environment and Pollution*, 16, pp. 614-629.

Carol S, Vilchez J.A., Casal J., 2002. Study of the severity of industrial accidents with hazardous substances by historical analysis. *Journal of Loss Prevention in the Process Industries*, 15 (6), 517-524.

- Carson D.J., 1973. The development of a dry inversion-capped convectively unstable boundary layer. *Quarterly. Journal of the Royal Meteorology Society*, 99, 450-467.
- Casal J., 2008. Evaluation of the effects and consequences of major accidents in industrial plants. Elsevier, Amsterdam.
- Casey M., Wintergerste T., (eds.), 2000. ERCOFTAC SIG "Quality and Trust in Industrial CFD": Best Practice Guidelines.
- CCPS 1999. Guidelines for consequence analysis of chemical releases. Center for Chemical Process Safety/AIChE, New York, USA.
- CCPS 2000. Guidelines for Chemical Process Quantitative Risk Analysis, 2nd Ed., CCPS/AIChE, New York, USA.
- CERC, 002. GASTAR model Version 3. Cambridge Environmental Consultants Ltd. Cambridge, U.K..
- Chang J.C., Hanna S.R., 2004. Air quality model performance evaluation. *Meteorology and Atmospheric Physics*, 87, 167-196.
- Chang J.C., Hanna S.R., 2005. Technical descriptions and user's guide for the BOOT statistical model evaluation software package, version 2.0. 66 pp.
- Christensen F.M., Andersen O., Duijm N.J., Harremoës P., 2003. Risk Terminology-A platform for common understanding and better communication. *Journal of Hazardous Materials*, A103, 181-203.
- Christou M.D., Kirchsteiger C., Papadakis, G.A., 1998. Risk Assessment & Management in the context of the Seveso II Directive, *Industrial Safety*, Volume 6. Elsevier, Amsterdam, Netherlands.
- Cimorelli A.J., Perry S.G., Venkatram A., Weil J.C., Paine R.J., Wilson R.B., Lee R.F., Peters W.D., Brode R.W., Paumier J.O., 2004. AERMOD: Description of model formulation, US Environmental Protection Agency, EPA Report No. 454/R-03-002d, 85pp.
- Cimorelli A.J., Perry S.G., Venkatram A., Weil J.C., Paine R.J., Wilson R.B., Lee R.F., Peters W.D., Brode R.W., 2005. AERMOD: A Dispersion Model for Industrial Source Applications. Part I: General Model Formulation and Boundary Layer Characterization. *J. of Applied Meteorology*, 44, 682-693.
- Cleaver R.P., Cooper M.C., Halford A.R., 1994. Further development of a model for dense gas dispersion over real terrain. *J. of Haz. Mater.*, 40, 85-108.
- CMOEP, 2005. Plano de emergência externo de Estarreja. Estarreja: CMOEP-Centro Municipal de Operações de Emergência de Protecção Civil.
- Colenbrander G.W., 1980. A mathematical Model for the Transient Behavior of Dense Vapor Clouds, 3rd International Symposium on Loss Prevention and Safety Promotion in the Process Industries, Basel, Switzerland.

- Colenbrander G.W., Evans A., Puttock J.S., 1984. Spill tests of LNG and refrigerated liquid propane on the sea, Maplin Sands 1980: Dispersion Data Digests. Thornton Research Centre, Shell Research Limited, Thornton, U.K.
- Cormier, B.R., Qi, R., Yun, G.W., Zhang, Y., Mannan, M.S., 2009. Application of computational fluid dynamics for LNG vapor dispersion modeling: A study of key parameters, *J. Loss Prev. Process Ind.*, Vol. 22, pp. 332-352.
- COST 715, 2002. Mixing height and inversions in urban areas. Piringer, M., Kukkonen, J., (Eds.), *Proceedings of the Workshop, 3-4 October, 2001, Toulouse, France*. COST Action 715, EUR 20451, European Communities, Luxembourg, 113 pp.
- Costa A.M., 2008. Microscale modelling of exposure to atmospheric pollutants in urban areas. PhD thesis, University of Aveiro.
- Costa, C, Jesus-Rydin, Cláudia, 2001. Site investigation on heavy metals contaminated ground, *Engineering Geology*, 60, 39-47.
- Covello V., 1983. The perception of technological next term risks: A literature review. *Technological Forecasting and Social Change* Vol. 23 (4), pp. 285-297.
- Cox R.A. and Carpenter R.J., 1980. Further development of a dense vapour cloud dispersion model for hazard analysis, In Hartwig, S.(Ed), *1st Battelle Institute Symposium on Heavy gas and Risk Assessment*, D Reidel, Dordrecht, 55-87.
- Cozzani V., Salzano E., 2006. The quantitative assessment of domino effects caused by overpressure. Part I. Probit models, *Journal of Hazardous Materials* 107, 67-80.
- Cozzani V, Gubinelli G., Salzano E., 2006. Escalation thresholds in the assessment of domino accidental events. *Journal of Hazardous Materials*, A129:1-21.
- Crane Co., 1986, *Flow of fluids through valves, fittings, and pipe*, Technical Paper No. 410, New York, NY
- Crowl D.A., Louvar, J. F., 1990. *Chemical process safety: fundamentals with applications*, 157-192. New Jersey, USA.
- Darbra R.M., Casal J., 2004. Historical analysis of accidents in seaports. *Safety Science*, 42, 2, 85-98.
- Darbra R.M, Palacios A., Casal J., 2010. Domino effect in chemical accidents: Main features and accident sequences. *Journal of Hazardous Materials*, 183 (1-3), 565-573.
- Davidson M.J., Mylne K.R., Jones C.D., Phillips J.C., Perkins R.J., Fung J.C.H., Hunt J.C.R., *Plume dispersion through large groups of obstacles - A field investigation*, *Atmospheric Environment*, 29(22), 3245-3256, 1995.
- Dechy N., Dien Y., Funnemark E., Roed-Larsen S., Stoop J., Valvisto T., Arellano A.L.V., 2009. Results and lessons learned from the ESReDA's Accident Investigation Working Group: Introducing article to "Safety Science" special issue on "Industrial Events Investigation". *Safety Science*, in press.

- Dechy T., Bourdeaux N., Ayrault M.A., Kordek, Le Coze J.-C., 2004. First lessons of the Toulouse ammonium nitrate disaster, 21st September 2001, AZF plant, France. *J. of Haz. Mater.*, 111,131-138.
- Dellacasa E., 2009. *Corriere della Sera* (Italian newspaper) 1-Jul-2009, p. 3.
- Delvosalle C., Levert J. M., Benjelloun F., Schayes G., Moyaux B., Runday F., Everbecq E., Bourouag T., Dzisiak J. P., 1993. Major industrial hazards: The SEVEX project: source terms and dispersion calculation in complex terrain.
- Díaz-Ovalle C., Vázquez-Román R., Mannan M., 2010. An approach to solve the facility layout problem based on the worst-case scenario. *J. of Loss Prevention in the Process Industries*, 23, 385-392.
- DIERS, 1986. Technology Summary Emergency Relief Systems for Runaway Chemical Reactions and Storage Vessels: A Summary of Multiphase Flow Models AIChE/DIERS Publication, New York, 1986.
- Dinis P., Dinis R., 2002. Cálculo das consequências de acidentes industriais graves - Projecto de Termodinâmica Aplicada. Instituto de Engenharia Mecânica. Universidade Técnica de Lisboa, Lisboa. 117 pp.
- Douglas S., Kessler R., 1990. User's Manual for the Diagnostic Wind Model. Eed. Carr, L. Volume III, EPA-450/4-90-007C, San Rafael, CA.
- Drogaris G., 1993. Major accident reporting system—lessons learnt from accidents notified, CEC-JRC Ispra, ISBN-0-444-81665-8. Elsevier, Amsterdam.
- Dudhia J, Gill D, Guo Y, Manning K, Wang W., Chiszar J. 2001. Mesoscale Modeling System Tutorial Class Notes and User's Guide: MM5 Modeling System Version 3, PSU/NCAR.
- Duijm N. J., Ott S., Nielsen M., 1996. An evaluation of validation procedures and test parameters for dense gas dispersion models. *Journal of Loss Prevention in the Process Industries*, 9, 323-338.
- Duijm N.J., 1994. Research on the dispersion of two-phase flashing releases – FLADIS. Fladis final report R94-451, TNO Environmental and Energy Research, Appeldorn, Netherlands.
- Duijm N.J., Stork B., Nielsen M., Ott S., 1994. An overview of the REDIPHEM project. *International Journal of Environment and Pollution* 1995 - Vol. 5, No.4/5/6 pp. 635 - 644
- Durham K., 2003. Treating the risks in Cairns, *Natural Hazards*, 30, 251- 261.
- EEA, 2003. Europe's environment: the third assessment. Environmental Assessment Report No 10. European Environment Agency, Copenhagen, Denmark, 213-229.
- EEA, 2010. Mapping the impacts of natural hazards and technological accidents in Europe - An overview of the last decade. EEA Technical report No 13/2010. ISSN 1725-2237.

- Eidsvik K.J., 1980. A model for heavy gas dispersion in the atmosphere. *Atmospheric Environment*, 14, 769-777
- Elliott M, Wang Y, Lowe R., Kleindorfer P., 2004. Environmental justice: Frequency and severity of US chemical industry accidents and the socioeconomic status of surrounding communities. *Journal of Epidemiology and Community Health*, 58(1), 24-30.
- Ellis J., 2011. Analysis of accidents and incidents occurring during transport of packaged danderous goods by sea. *Safety Science*, 49 (8-9), 1231-1237.
- Emmott N. 1999. IPPC and beyond - developing a strategic approach to industry for European environmental policy. *Journal of Environmental Policy and Planning*, 1: 77-92.
- EPA, 2004a: User's Guide for the AMS/EPA Regulatory Model - AERMOD. EPA-454/B-03-001. U.S. Environmental Protection Agency, Research Triangle Park, NC. 216 pp.
- Ermak D.L., 1990. User's Manual for SLAB: An Atmospheric Dispersion Model for Denser-Than-Air Releases, ACRL-MA-105607, Lawrence Livermore National Laboratory, Livermore, CA 94550.
- Ermak D.L., Chan S.T., Morgan D.L., Morris L.K., 1981. A comparison of dense gas dispersion model simulations with Burro series LNG spill tests results, UCRL - 86713 . Lawrence Livermore National Laboratory , Livermore, CA.
- Ermak D.L., Chan S.T., Morgan D.L., Morris L.K., 1982. A comparison of dense gas dispersion model simulations with Burro Series LNG spill test results, *J. of Haz. Mater.*, 6 (1-2), 43-84.
- Fang D.P., Xie F., Huang X.Y., Li H., 2004. Factor analysis-based studies on construction workplace safety management in China, *International Journal of Project Management* 22, 43-49.
- Fauske H., Epstein M., 1988. Source Term Considerations in Connection with Chemical Accidents and Vapour Cloud Modelling. *Proc. Intl. Conf. On Vapour Cloud Modeling*. New York: Center for Chemical Process Safety, Amer. Inst. Chem. Engrs., 251-2
- Fay J.A., Ranck D.A., 1982. Comparison of experiements on dense gas cloud dispersion. *Atmospheric Environment*, 17, 239-248.
- Fay J.A., Zemba S.G., 1985. Dispersion of initially compact dense gas clouds, *Atmospheric Environment*, 19, 1257-1261.
- Fay J.A., Zemba S.G., 1986. Integral Model of Dense Gas Plume Dispersion, *Atmospheric Environment*, 20, 1347-1354.
- Feldbauer G.F., May W.G., Heigl J.J., McQueen W., Whipp R.H., 1972. Spills of LNG on water - vaporization and downwind drift of combustible mixtures, ESSO-API Report EE61E-72, 1972.
- Fingas M., 2002. *The handbook of hazardous materials spills technology*. McGraw-Hill, New York. ISBN 007135171-X.

- Folch A., Costa A., Hankin R., 2009. TWODEE-2: A shallow layer model for dense gas dispersion on complex topography, *Computer and Geosciences*, 35(3), 667-674.
- Gailis R.M., Hill A., 2006. A wind-tunnel simulation of plume dispersion within a large array of obstacles. *Boundary-Layer and Meteorology*, 119:289-338.
- Gaspar J. (coord.), 2005. Programa Nacional da Política de Ordenamento do Território, Relatório. 2ª Versão, Fevereiro 2005, MAOT, DGOTDU, Lisboa.
- Gavelli F., Bullister E., Kytomaa H., 2006. Validation of FLUENT predictions for LNG spills into an impoundment. Mary Kay O'Connor Process Safety Centre 2006 International Symposium, College Station, TX.
- Gilham S., Deaves D.M. and Woodburn P., 2000. Mitigation of dense gas releases within buildings: validation of CFD modelling, *J. of Haz. Mater*, 71: 193-218.
- Golder D., 1972. Relations among stability parameters in the surface layer. *Boundary Layer Meteor.*, 3, 47-58.
- Goldwire H.C. Jr., Rodean H.C, Cederwall R.T., Kansa E.J., Koopman R.P., McClure J.W., McRea T.G., Morris L.K., Kamppinen L, Klefer R.D., Urtlew P.A., Lind C.D., 1983. Coyote Series data report, LLNL/NWC 1981 LNG Spill Tests: dispersion, vapour burn, and rapid phase transition, UCID-199953, Lawrence Livermore National Laboratory, Livermore, California.
- Goldwire Jr., H.C., McRae T.G., Johnson G.W., Hipple D.L., Koopman R.P., McLure J.W., Morris, L.K., Cedarwall R.T., 1985. Desert Tortoise Series Data Report – 1983 Pressurized Ammonia Spills, Lawrence Livermore National Laboratories Report UCID-20562, Livermore, CA.
- Green D.W., Perry R.H., 2008. Perry's Chemical Engineers' Handbook, 8th Ed. McGraw-Hill, New-York.
- Greenberg H.R., Cramer J.J., 1991. Risk Assessment and Management for the Chemical Process Industry (Stone and Webster Engineering Corporation). Van Nostrand Reinhold. ISBN 0 4422 3438 4.
- Gresho P.M., Chan S.T., Upson C.D., Lee R.L., 1983. A Modified Finite Element Method for Solving the Time-Dependent, Incompressible Navier-Stokes Equations, UCRL-88937. LLNL.
- Grioret F., Lieto J., St-Georges M., Buchlin J.-M., Riethmuller M.L., Astarita G., Costa M.-J., Barros N., Borrego C., 1995. Mitigation of accidental releases of toxic clouds by reactive fluid curtain, *Loss Prev. Saf. Prom. Proc. Ind.*, 1.
- Guedes C.S., Jacinto C., Teixeira A.P., Antão P., (Eds), 2009. Riscos Industriais e Emergentes. Volumes 1&2, Edições Salamandra, Lisboa, 2009, ISBN 978-972-689-233-5.
- Gunn A.M., 2008. Encyclopaedia of Disasters: Environmental Catastrophes and Human Tragedies Volumes I & II, Greenwood Press, Westport, USA.

- Hadad, Y, Laslo, Z., Ben-Yair, A. 2007. Safety improvements by eliminating hazardous combinations, *Technological and Economic Development of Economy* 13(2), 114-119.
- Haddow G.D., Bullock J.A., Coppola D.P., 2008. *Introduction to emergency management*. 3rd Ed. Elsevier.
- Hald K., Buchlin J. M., Dandrieux A. and Dusserre G., 2005. Heavy Gas Dispersion by Water Spray Curtains: A Research Methodology, *J. of Loss Prev. in the Process Industries*, 18, 506-511.
- Hall D.J., 1991. Repeat variability in instantaneous released heavy gas clouds – some wind tunnel experiments. Report No. LR 804, (PA), Warren Spring Laboratory, UK.
- Hankin R., 1997. Heavy gas dispersion over complex terrain. Ph.D. Thesis, Cambridge University, Cambridge.
- Hankin R., 2003. Heavy gas dispersion: integral models and shallow layer models. *Journal of Hazardous materials*, A103:1-10.
- Hankin R., Britter R.E., 1994. The shallow water approximations in dense gas dispersion over complex terrain. In I. P. Castro and N. J. Rockliff, editors, *Proceedings of the 4th IMA Conference on stably stratified flows: flow and dispersion over topography*, pages 223-245. Clarendon Press, Oxford.
- Hankin R., Britter R.E., 1999a. TWODEE: the health and safety laboratory's shallow layer model for dense gas dispersion. Part 1. Mathematical basis and physical assumptions, *J. Hazard. Mater.* 66 (3), 211-226.
- Hankin R., Britter R.E., 1999b. TWODEE: the health and safety laboratory's shallow layer model for dense gas dispersion. Part 2. Outline and validation of the computational scheme, *J. Hazard. Mater.* 66 (3), 227-237.
- Hankin R., Britter R.E., 1999c. TWODEE: the health and safety laboratory's shallow layer model for dense gas dispersion. Part 3. Experimental validation (Thorney Island), *J. Hazard. Mater.* 66 (3), 239-261.
- Hanna S.R., Chang J.C., 1992. Boundary-layer parameterizations for applied dispersion modelling over urban areas. *Boundary-Layer Meteorology* 58, 229-259.
- Hanna S.R., Chang J.C., Strimaitis D.G., 1993. Hazardous gas model evaluation with field observations. *Atmos Environ*, 27A, 2265-2285
- Hanna S.R., Dharmavaram S., Zhang J., Sykes I., Witlox H., Khajehnajafi S., Koslan K., 2008. Comparison of six widely-used dense gas dispersion models for three recent chlorine railcar accidents, *Process Safety Prog.* 27, 248-259.
- Hanna S.R., Drivas P.J., 1987: *Guidelines for the Use of Vapor Cloud Dispersion Models*. Published by CCPS/AIChE, 345 East 47th St., New York, NY 10017, 178 pp.
- Hanna S.R., Drivas D.G., 1996. *Guidelines for Use of Vapor Cloud Dispersion Models*, 2nd Edition. Wiley-American Institute of Chemical Engineers. ISBN 0-8169-0702-1.

- Hanna S.R., Hansen O.R., Dharmavaram S., 2004. FLACS CFD air quality model performance evaluation with Kit Fox, MUST, Prairie Grass, and EMU observations. *Atmospheric Environment*, 38, 4675-4687.
- Hanna S.R., Hansen O.R., Ichard M., Strimaitis D.G., 2009. CFD model simulation of dispersion from chlorine railcar releases in industrial and urban areas. *Atmos. Environ.* 43, 262-270.
- Hanna S.R., Strimaitis D.G., 1989. *Workbook of Test Cases for Vapor Cloud Source Dispersion Models*, 1st Edition. Center for Chemical Process Safety, American Institute of Chemical Engineers. ISBN 0-8169-0455-3.
- Hanna S.R., Strimaitis D.G., Chang J.C., 1991. In: *Hazard response modelling Uncertainty (A Quantitative Method)*, Vol. II; Evaluation of commonly-used hazardous gas dispersion models, Sigma Research Corporation, Westford, U.S.A. (1991).
- Hanna, S.R. and R.E. Britter, 2008: *Conclusions and Recommendations from Workshop on Toxic Industrial Chemical (TIC) Source Emissions Model Improvements (25-26 March 2008)*. Report P098-3 by Hanna Consultants, Kennebunkport, ME., prepared for DTRA, Ft. Belvoir, VA.
- Hanna, S.R., J. Chang, 2001. Use of the Kit Fox field data to analyze dense gas modelling issues. *Atmos. Environ.* 35, 2231-2242.
- Hanna, S.R., J.S. Chang, 1993: Hybrid Plume Dispersion Model (HPDM), improvements and testing at three field sites. *Atmos. Environ.*, 27A, 1491-1508.
- Hansen O., Gavelli F., Ichard M., Davis S., 2010. Validation of FLACS against experimental data sets from the model evaluation database for LNG vapor dispersion. *Journal of Loss Prevention in the Process Industries*, 23(6): 857-877.
- Havens J., 1988. A dispersion model for elevated dense gas jet chemical releases. Volumes I and II, EPA-450/4-88-06, U.S.. Environmental Protection Agency.
- Havens J.A., 1982. A Review of Mathematical Models for Prediction of Heavy Gas Atmospheric Dispersion, Institute of Chemical Engineers Symposium Series, 71, 1982.
- Havens J.A., Spicer T.O., 1985. Development of an Atmospheric Dispersion Model for Heavier-than-Air Gas Mixtures. Report No. CG-D22-85 for the U.S. Coast Guard, Univ. of Arkansas,
- He, G, Zhang, L, Lu, Y., Mol, A.P., 2011. Managing major chemical accidents in China: Towards effective risk information. *Journal of Hazardous Materials*, 187, 171-181.
- Heinrich M., Scherwinski, R., 1990. Research on propane releases under realistic conditions. Determination of gas concentrations considering obstacles, Report 123U1000780, TUV report, TUV, Germany.
- Hewitt C.N., Jackson A.V., 2003. *Handbook of Atmospheric Science - Principles and Applications*. Blackwell Publishing Science Ltd. Oxford, UK.

- HMSO, 1975. Report of the Court of Inquiry, The Flixborough Disaster, Department of Employment, HMSO, London.
- Hofmann, D.A, Jacobs, R., Landy, F., 1995. High reliability process industries: individual, micro and macro organizational influences on safety performance. *J. of Safety Research*, 26, 131-149.
- Hofmann, D.A., Stetzer, A., 1996. A cross-level investigation of factors influencing unsafe behaviors and accidents. *Personnel Psychology*, 49: 307-339.
- Högström U., 1996. Review of some basic characteristics of the atmospheric surface layer. *Boundary-Layer Meteorology*, 78, 215-246.
- Høiset, S.; Hjertager, B.H.; Solberg, T., Malo, K., 2000. Flixborough revisited – an explosion simulation approach. *J. Of Haz. Mater.*, A77, 1-9.
- Hola B., 2007. General model of accident rate growth in the construction industry, *Journal of Civil Engineering and Management* 13(4): 255–264.
- Holtslag A.A.M., van Ulden A.P., 1983. A simple scheme for daytime estimates of the surface fluxes from routine weather data, *J. Clim. Appl. Meteorol.* 22:517.
- Hoot T.G, Meroney R.N., Peterka J.A., 1973. Wind tunnel tests of negatively buoyant plumes, Report No. EPA-650/3-74-003, Environmental Protection Agency, Research Triangle Park, NC 27711, USA.
- Hopkins, A. 2005. *Safety, Culture and Risk: The Organisational Causes of Disasters*. Sydney, CCH.
- Hou, Y., Zhang, T.-Z., 2009. Evaluation of major polluting accidents in China – results and perspectives, *Journal of Hazardous Materials* 168, 670–673.
- HSE, 1984. Heavy gas dispersion trials Thorney Island 1982 - 3: Data for trials . Research and Laboratory Services Division, Sheffield.
- HSE, 2009. Safety and environmental standards for fuel storage sites Process Safety Leadership Group, Final report, HSE Books, U.K., ISBN 9780717663866.
- Hughes, G., Kornowa-Weichel M., 2004. Whose fault is it anyway? A practical illustration of human factors in process safety, *Journal of Hazardous Materials* 115, 127-132
- Hunt J.C.R., Rottman J.E., Britter R.E., 1984. Some physical processes involved in the dispersion of dense gases. In Ooms G. and Tennekes H. (eds.) *Atmospheric Dispersion of Heavy Gases and Small Particles*, 361-396. Springer-Verlag, Berlin.
- IAEA, 2006. Environmental consequences of the Chernobyl accident and their remediation: Twenty years of experience – Report of the Chernobyl Forum Expert Group ‘Environment’. Radiological assessment reports series, IAEA Vienna, Austria, ISBN 9201147058.

- ICE/ISO, 2009. 31010 Risk Management – Risk assessment techniques. Geneva Switzerland.
- IDAD, 2007a. Estudo de Impacte Ambiental Projecto de Ampliação do CQE, CUF-QI, Universidade de Aveiro, Aveiro.
- IDAD, 2007b. Estudo de Impacte Ambiental Projecto de Ampliação do CQE, DOW, Universidade de Aveiro, Aveiro.
- IM, AEMET, 2010. Iberian Climate Atlas, AIR TEMPERATURE AND PRECIPITATION (1971-2000). Instituto de Meteorologia Português and Agencia Estatal de Meteorologia Española. 80 pp. ISBN 978847837079-5
- IMPEL, 1998. Interrelationship between IPPC, EIA and Seveso directives and EMAS Regulation. Final Report, December 1998. IMPEL, Brussels.
- INE, 2001. CENSOS - 2001. Lisboa: Instituto Nacional de Estatística.
- INE, 2010. Anuário Estatístico da Região Centro - 2009. Lisboa: Instituto Nacional de Estatística.
- Jacobsson A, Sales S., Mushtaq F., 2010. Underlying causes and level of learning from accidents reported to the MARS database, *J. of Loss Prev. in the Process Industries*, 23 (1), 39-45.
- Jager T., Vermeire T.G., Rikken M.G.J. van der Poel P. 2001. Opportunities for a probabilistic risk assessment of chemicals in the European Union. *Chemosphere*, 43, 257-264.
- Jager P., Kuhnreich K., 1998. Approach to a systematic determination and evaluation of risk potential. In *Proceeding from ninth international symposium loss prevention and safety promotion in the process industries* (pp. 393-403).
- Jensen N.O., 1981. On the calculus of heavy gas dispersion. Riso-R-439, Riso National Laboratory, DK-4000 Roskilde, Denmark.
- Jezler W., 1998. Earthquake safety of structures and installations in chemical industry in the context of risk analysis. In *Proceeding from ninth international symposium loss prevention and safety promotion in the process industries* (pp. 414-421).
- Johnson R.D., 1985. Thorney Island trials: Systems development and operational procedures. *J. of Haz. Mater.*, 11, 35-64.
- Jones, D., 1992. Nomenclature for hazard and risk assessment in the process industries. 2nd edition, Institution of Chemical Engineers U.K.
- Kaiser G.D., Walker B.C., 1978. Releases of anhydrous ammonia from pressurised containers – the importance of denser than air mixtures. *Atmospheric Environment*, 12, 2289-2300.

- Karppinen, 2001. Meteorological Pre-Processing and Atmospheric Dispersion Modelling of Urban Air Quality and Applications in the Helsinki Metropolitan Area. PhD Thesis. Helsinki University of Technology, Finland. ISBN 9516975526.
- Kasten F., Czeplak G., 1980. Solar and terrestrial radiation dependent on the amount and type of cloud. *Solar Energy*, 24, 177-189.
- Kawamura, MacKay D., 1987. The Evaporation of volatile liquids, *J. of Hazardous Materials*, 15, 365-376.
- Kennedy R., Kirwan B., 1998. Development of a hazard and operability-based method for identifying safety management vulnerabilities in high risk systems. *Safety Sciences*, 30, 249-274.
- Kentel E., Aral M.M., 2007. Risk tolerance measure for decision-making in fuzzy analysis: A health risk assessment perspective. *Stochastic Environmental Research and Risk Assessment* 21(4) (2007) 405.
- Khan F.I., Abbasi S.A., 1995. Risk analysis: a systematic method of hazard assessment and control. *Journal of Industrial Pollution Control*, 11(2), 89-98
- Khan F.I., Abbasi S.A., 1996. Major accident case studies in chemical process industries. *Chemical Engineering World*.
- Khan F.I. and Abbasi S.A., 1998. MAXCRED - a new software package for rapid risk assessment in chemical process industries. *Environmental Modelling and Software*, 14(1), 11-25.
- Khan F.I., Abbasi S.A., 1999a. Major accidents in process industries and an analysis of causes and consequences. *Journal of Loss Prevention in the Process Industries*, 12, 5, 361-378.
- Khan F.I., Abbasi S.A., 1999b. Modelling and simulation of heavy gas dispersion on the basis of modifications in plume path theory. *J. of Haz. Mater.*, A80, 15-30.
- Khan K.I., Abassi S.A., 2001. An assessment of the likelihood of occurrence, and the damage potential of domino effect (chain of accidents) in a typical cluster of industries, *Journal of Loss Prevention in the Process Industries*, 14, 283-306.
- Kim Y.H., Baik, J.J. 2003: Effects of inflow turbulence intensity on flow and pollutant dispersion in an urban street canyon. *Journal of Wind Engineering and Industrial Aerodynamics* 91, 309-29.
- Kirchsteiger C., 1998. Major accident reporting system (MARS), *Industrial Safety Series*, 6, 367-403.
- Kirchsteiger C., 1999. On the use of probabilistic and deterministic methods in risk analysis. *Journal of Loss Prevention in the Process Industries*, 12 (5), 399-419.
- Kirchsteiger C., 2001. How frequent are major industrial accidents in Europe?. *Process Safety and Environmental Protection*, 79, 4, 206-210.

- Kirchsteiger, C., 2002. Review of International Industrial Safety Management Frameworks. *Process Safety and Environmental Protection*, 80(5) 235-244.
- Kirchsteiger, C., 2003. Industrial risk management and international agreements, *International Journal of Emergency Management*, 1(3), 247 - 267.
- Kirchsteiger C., Christou M.D. and Papadakis G.A., 1998. Risk assessment and management in the context of the Seveso II Directive. *Industrial Safety Series*, Vol. 6. Elsevier, Amsterdam, The Netherlands.
- Kiša M., Jelemenský L., 2009. CFD dispersion modelling for emergency preparedness. *L. of Loss Prev. in the Process Industries*, 22 (1), 97-104.
- Kishawy H., Gabbar, H., 2010. Review of pipeline next term integrity management practices. *International Journal of Pressure Vessels and Piping*, 87(7), 373-380.
- Kleindorfer P.R., Lowe R.A., Rosenthal I., Fu R., Belke J.C., Elliott M.R., Wang Y., 2007. Accident Epidemiology and the RMP Rule: Learning from a Decade of Accident History Data for the U. S. Chemical Industry. Working Paper, Wharton Center for Risk Management and Decision Processes.
- Kletz T., 1988. *Learning from accidents in industry*. London, Butterworth.
- Kletz T., 1993. *Lessons from disaster*. , IChemE, Rugby, UK.
- Kolluru, R, Bartell, S, Pitblado, R., Stricoff, S., 1996. *Risk assessment and management handbook for environmental, health and safety professionals*. McGraw - Hill , New York .
- Koopman R.P., Ermak D.L., 2007. Review: Lessons learned from LNG safety research. *J. Hazard. Mater.* 140, 412 - 428 .
- Koopman R.P., Ermak D.L., Chan S.T., 1989. A review of recent field test and mathematical modelling of atmospheric dispersion of large spills of denser-than-air gases. *Atmospheric Environment* 23, 731-745.
- Koopman R.P., Cederwall R.T., Ermak D.L., Goldwire H.C.Jr., Hogan W.J., McClure J.W., McCrae T.G., Morgan D.L., Rodean H.C., Shinn J.H., 1982b. Analysis of Burro series 40 m3 LNG Spill experiments. *J. Hazard. Mater.* 6 , 43 - 83
- Koopman R.P., R.T. Cederwall, D.L. Ermak, H.C. Goldwire Jr., J.W. McLure, T.G. McCrae, D.L. Morgan, H.C. Rodean, J.H. Shinn, 1981. *Description and Analysis of Burro Series 40-m3 LNG Spill Experiments*”, UCRL-53186, Lawrence Livermore National Laboratory.
- Koopman R.P., Baker J., Cederwall R.T., Goldwire H.C.Jr., Hogan W.J., Kamppinen L.M., Kiefer R.D., McClure J.W., McCrae T.G., Morgan D.L., Morris L.K., Spann M.W.Jr., Lind C.D., 1982a. *Burro Series Data Report, LLNL/NWC 1980 LNG Spill Tests*, UCID - 19075, Lawrence Livermore Laboratory, Livermore, CA.
- Kootstra F., van het Veld B.F.B., Opschoor G., 2004., A complete description of an advanced evaporation model for accidentally released hazardous liquids from land. Part IA-Theoretical background, AICHE 2004 Spring National Meeting, 38th Annual Loss

Prevention Symposium.

Kourniotis, S.P; Kiranoudis, C.T., Markatos N.C., 2000. Statistical analysis of dominó chemical accidents. *Journal of Hazardous Materials*, 71(1-3), 239-252.

Kunsch J.P. and Webber D.M., 2000. Simple box model for dense gas dispersion in straight sloping channel, *J. of Haz. Mater.*, 157-177.

Kunsch J.P., Fannelop T.K., 1995. Unsteady heat transfer effects on the spreading and dilution of dense cold clouds. *J. of Haz. Mater.*, 169-193

Kwon H., 2006. The effectiveness of process safety management (PSM) regulation for chemical industry in Korea, *Journal of Loss Prevention in the Process Industries* 19, 13-16.

Lagadec, P., 1997. Learning Processes for Crisis Management in Complex Organizations. *Journal of Contingencies and Crisis Management*, 5 (1), 24-31.

Landucci, G, Tugnoli, A, Busini, V, Derudi, M, Rota, R., Cozzani, V., 2011. The viarregio LPG accident: Lessons learnt. *Journal of Loss Prevention in the Process Industries*, 24 (24), 466-476.

Lapin A., Foster R.H., 1967. Oxygen diffusion in the atmosphere from liquid oxygen pools, *Adv. Cryo. Eng.*, 13, 555.

Lari S., Frattini P., Crosta G.B., 2009. Integration of natural and technological risks in Lombardy, Italy. *Nat. Hazards Earth Syst. Sci.*, 9, 2085-2106.

Larson N., Kusiak A., 1996. Managing design processes: A risk assessment approach. *IEEE Transactions on Systems, Man, and Cybernetics—Part A: Systems and Humans*, 26(6), 749-759.

Laubach J., McNaughton K. G., 2009. Scaling properties of temperature spectra and heat flux cospectra in the surface friction layer beneath an unstable outer layer. *Bound.-Layer Meteor.*, 133, 219-252.

Lees F., 1996. *Loss prevention in the process industries*, 2nd. Ed., Butterworth-Heinemann, Boston, Massachusetts.

Legget D.J., 2004. Process safety in the future - a view from the chemistry. *Process Safety Progress*, 23 (2), 163-169.

Leitl B, Pascheke F., Schatzmann M., Kastner-Klein P., 2003. Wind tunnel experiments within the scope of the Oklahoma City tracer experiments. *Proc. Int. Workshop on Physical Modelling of Flow and Dispersion Phenomena PHYSMOD2003*, Prato, Italy, September 3-5, ISBN 88-8453-095-4.

Leung J.C., 1986. A generalized correlation for one-component homogeneous equilibrium flashing choked flow. *AIChE Journal*, Vol. 32, No. 10, pp. 1743-1746

Leung J.C., Grolmes M.A., 1988. A Generalized Correlation for Flashing Choked Flow of Initially Subcooled Liquid. *AIChE Journal*, Vol. 31, No. 4 , pp. 688-691.

- Lindberg A., Hansson S.O., Rollenhagen C., 2010. Learning from accidents - what more do we need to know?, *Safety Science*, 48 (6), 714-721.
- LLNL, 1983. Coyote series data report. UCID: 19953 V. 1, 2, LLNL/NWC, Livermore.
- Luketa-Hanlin A., 2006. A review of large-scale LNG spills: experiments and modelling, *J. Haz. Mats.*, Vol. A132, pp 119 - 140.
- Luketa-Hanlin A., Koopman R.P., Ermak D.L., 2007. On the application of computational fluid dynamics codes for liquefied natural gas dispersion. *J. of Haz. Mater.*, 140, 504-517.
- M&M Protection Consultants, 1997. Large Property Damage Losses in the Hydrocarbon-Chemical Industries A Thirty-year Review. AcuSafe
- Macdonald, R.W., Griffiths, R.F., Cheah, S.C., 1997. Field experiments of dispersion through regular arrays of cubic structures, *Atmospheric Environment*, 31(6), 783-795.
- Madureira N., 2005. História da Energia Portugal 1890-1980. Livros Horizonte, Lisboa.
- Manca D., Brambilla S., Totaro R., 2010. A Quantitative Assessment of the Viareggio Railway Accident. In: 20th European Symposium on Computer Aided Process Engineering - ESCAPE20 S. Pierucci and G. Buzzi Ferraris (Editors), Elsevier.
- Mannan, S. (Ed.) 2005. Lees' Loss Prevention in the Process Industries. Hazard Identification, Assessment and Control, 3rd Edition, Vol. 1 - 3, Elsevier Butterworth-Heinemann, Oxford, ISBN 0750675551.
- Marhavidas P.K., Koulouriotis D., Gemeni V., 2011. Risk analysis and assessment methodologies in the work sites: On a review, classification and comparative study of the scientific literature of the period 2000-2009. *Journal of Loss Prevention in the Process Industries*, 24(5), 477-523.
- Markiewicz, M., 2006. Mathematic Modeling of the Heavy Gas Dispersion, Models and Techniques for Health and Environmental Hazard Assessment and Management. Center of excellence management of health and environmental hazard, Otwock, Swierk.
- Martins J.M.M., 1998. Dispersão de poluentes atmosféricos na esteira de um obstáculo em condições de vento fraco. Dissertação de Doutoramento em Ciências Aplicadas ao Ambiente; Universidade de Aveiro, Departamento de Ambiente e Ordenamento. Aveiro - Portugal. 196 pp..
- Marshall, V.C., 1987. Major Chemical Hazards, Chemical Engineering Series, Ellis Horwood, Chichester, England.
- May W.G., McQueen W., Whipp R.H., 1973. Spills of LNG on water, American Gas Association, Operation Section Proceedings, Paper 73-D-9.
- McNaughton K., 2009. The rise and fall of Monin-Obukhov theory. *AsiaFlux Newsletter* No 30. September, pp 1-4.

- McQuaid J., 1979. Dispersion of Heavier-than-air gases in the atmosphere: review of research and progress report on HSE activities. HSL Tech. paper 8, Health and Safety Executive, Sheffield.
- McQuaid J., 1984. The box model of heavy gas dispersion: A useful and practical tool. *Journal of Occupational Accidents*, 6: 253-261.
- McQuaid J., 1987. Design of the Thorney Island continuous release trials. *J. Haz. Mater.*, 16, 1-8.
- McQuaid J., B. Roebuck, 1985. Large Scale Field Trials on Dense Vapour Dispersion, Final Report to Sponsors on the Heavy Gas Dispersion Trials at Thorney Island 1982-94, Health and Safety Executive, UK.
- MEG, 1994a. Guidelines for Model Developers. European Communities Directorate General XII Science Research and Development.
- MEG, 1994b. Model Evaluation Protocol. European Communities Directorate General XII Science Research and Development.
- Melhem G.A., Croce P.A., 1993. Advanced Consequence Modelling Emission, Dispersion, Fires, and Explosions, second draft, A.D. Little.
- Meroney R., 1982. Wind-tunnel experiments on dense gas dispersion. *Dense Gas Dispersion*, Britter and Griffiths, Eds., Elsevier Scientific Pub. Co., Amsterdam.
- Meroney R., 1984a, Transient Characteristics of Dense Gas Dispersion, Part I: A Depth-averaged Numerical Model, *J. Haz. Mats.*, 9, 139-157.
- Meroney R., 1984b, Transient Characteristics of Dense Gas Dispersion, Part II: Numerical Experiments on Dense Cloud Physics, *J. Haz. Mats.*, 9, 159-170.
- Meroney R., 1987, Validation of Fluid Modeling Techniques for Assessing Hazards of Dense Gas Cloud Dispersion, *Journal of Hazardous Materials*, 15, 377-417.
- Meroney R., 2010. CFD prediction of dense gas clouds spreading in a mock urban environment. The Fifth International Symposium on Computational Wind Engineering (CWE2010) Chapel Hill, North Carolina, USA May 23-27, 2010
- Meroney R.N., Pavageau M., Rafailidis S. and Schatzmann M., 1996. Study of line source characteristics for 2-D physical modelling of pollutant dispersion in street canyons. *Journal of Wind Engineering and Industrial Aerodynamics* 62, 37-56.
- Michalakes, J., Dudhia J., Gill D., Henderson T., Klemp J., Skamarock W., Wang W., 2004: "The Weather Research and Forecast Model: Software Architecture and Performance. In Proceedings of the 11th ECMWF Workshop on the Use of High Performance Computing In Meteorology, 25-29 October 2004, Reading U.K. Ed. George Mozdzynski.
- Mills M.T., Paine R.J., 1990. A survey modelling techniques for consequence analysis of accidental chemical releases to the atmosphere. *Reliability Engineering and System Safety* 29, 69-102.

- Ministry of Environmental Protection of China, 2006. Measures on the Reporting of Environmental Emergency Accidents (Trial), MEP Document No. 50, implemented on 31 March 2006.
- Mitchison N., 1999. The Seveso II directive: guidance and fine-tuning. *Journal of Hazardous Materials* 65, 23–36.
- Mohan M., Panwar, T.S., Singh, P.M., 1995. Development of dense gas dispersion model for emergency preparedness, *Atmospheric Environment*, 29, 2075-2087.
- Monache L.D., Weil J., Simpson M., Leach M., 2009. A new urban boundary layer and dispersion parameterization for an emergency response modelling system: Tests with the Joint Urban 2003 data set. *Atmospheric Environment*, 43 (36), 5807-5821.
- Monin A.S., Yaglom A.M., 1971. *Statistical Fluid Mechanics: Mechanisms of Turbulence*. Vol. 1. The Massachusetts institute of Technology (MIT) Press, Massachusetts, US. 769 pp.
- Monin, A.S., Obukhov, A.M., 1954. Osnovnye zakonomernosti turbulentnogo peremeshivaniya v prizemnom sloe atmosfery. *Trudy Inst. Theor. Geofiz. AN SSSR*, 24: 163-187.
- Morgan D.L.Jr., Morris L.K., Ermak D.L., 1983. SLAB: a time-dependent computer model for the dispersion of heavy gases released in the atmosphere. Technical Report UCRL-53383, Lawrence Livermore National Laboratory, University of California, Livermore, California, 94550.
- Muhlbauer W.K. 2004. Pipeline risk management manual, ideas, techniques, and resources (3rd ed.). Elsevier, New York.
- Muralidhar R., Jersey G.R., Krambeck F.J., Sundaresan S., 1995. A two-phase release model for quantifying risk reduction for modified HF alkylation catalyst. *J. of Haz. Mater.*, 44, 141-183.
- Nicolet-Monnier M., 1996. Integrated regional risk assessment: The situation in Switzerland. *International Journal of Environment and Pollution*, 6(4-6), 441–461.
- Nielsen M., 1994. Comment on: A model of the motion of a heavy gas cloud release on a uniform slope. *J. of Haz. Mater.*, 48, 251-258.
- Nielsen M., 1996. Surface concentrations in the FLADIS field experiments, Risø National Laboratory, Roskilde.
- Nielsen M., 1998: Dense gas dispersion in the atmosphere, Risø National Laboratory, Denmark.
- Nielsen, M., Jensen N.O., 1991: Continuous Release, Dense Gas, Field Experiments with Obstacles Final Report on Project BA.X2, Risø National Laboratory, Roskilde, Denmark, February 1991, 26 S.
- Nielsen M., Ott S., 1996. A collection of data from dense gas experiments, RISO Report R-845(EN) RISO, Roskilde.

- Nielsen M., Bengtsson R., Jones C., Nyren K., Ott S., Ride D., 1994. Design of the Fladis field experiments with dispersion of liquified ammonia, Risø-R-755(EN), Risø National Laboratory.
- Nielsen, M, Ott, S, Jorgensen, H.E, Bengtsson, R, Nyren, K, Winter, S, Ride, D., Jones, C., 1997. Field Experiments with Dispersion of Pressure Liquefied Ammonia. *Journal of Hazardous Materials*, 56, 59-105.
- Nikmo J., Kukkonen J., 1991. Modelling Heavy Gas Cloud Transport in Sloping Terrain, Report 2-91, Technical Inspection Centre of Finland, Helsinki
- Nivolianitou Z.S, Leopoulos V.N., Konstantinidou M., 2004. Comparison of techniques for accident scenario analysis in hazardous systems, *Journal of Loss Prevention in the Process Industries* 17 (6), 467-475.
- Nivolianitou Z.S., Konstandinidou M, Michalis C., 2006. Statistical analysis of major accidents in petrochemical industry notified to the major accident reporting system (MARS). *J. of Haz. Mater.*, 137 (1), 1-7.
- Nunes C., 2005. O Complexo Químico de Estarreja - A conquista da competitividade global, *Ingenium* 87, 28-31.
- Nussey C., Davies J.K.W., Mercer A., 1985. The Effect of Averaging Time on the Statistical Properties of Sensor Records, *Journal of Hazardous Materials*, 11, 125-153.
- Nussey C., Pantony M., Smallwood R. 1992. HSE's risk assessment tool, RISKAT. In *Major Hazards: Onshore and Offshore*.
- Oberkampf W.L., Trucano T.G., Hirsch C., 2004. Verification, validation, and predictive capability in computational engineering and physics. *Appl. Mech. Rev.*, 57(5):345 - 384.
- Oggero A. Dabra R. M. Munoz M., Planas E., Casal J., 2006. A survey of accidents occurring during the transport of hazardous substances by road and rail. *Journal of Hazardous Materials*, A133 (1-3): 1-7.
- Oke T.R., 1978. *Boundary Layer Climates*. John Wiley and Sons, New York, New York, 372pp.
- Olesen H.R. and Berkowicz R., 2008. Guide to Excel sheets for MUST experiment <http://www2.dmu.dk/atmosphericenvironment/Docs/SpreadsheetInfo.pdf>
- Oliveira J.P., 2007. Avaliação de riscos para o Complexo Químico de Estarreja. Msc. Thesis. Universidade de Aveiro, Aveiro, Portugal. 116 pp.
- Ooms G., 1972. A new method for the calculation of the plume path of gases emitted by a stack, *Atmospheric Environment* 6, 899.
- Oot S., 1990. GReAT jet model, A short description of the Gas Release Analysis Tool for continuous releases of either pure or liquefied gas, Riso National Laboratory.

- Ott O., Nielsen M., 1996. Shallow layer modeling of dense gas clouds, Risoe-R-901, Risoe National Laboratory, Roskilde, Denmark.
- Paine R. J., Egan B.A., 1987. User's guide to the Rough Terrain Diffusion Model (RTDM) - Rev. 3.20. ERT Document PD-535-585, ENSR, Acton, MA, 260pp.
- Palau J.L., Pérez-Landa G., Diéguez J.J., Monter C., Millán M.M., 2005. The importance of meteorological scales to forecast air pollution scenarios on coastal complex terrain. *Atmos. Chem. Phys.*, 5, 2771–2785.
- Papazoglou I. A., Noivolianitou Z., Aneziris O., Christou M., 1990. Probabilistic safety analysis in chemical installation. *Journal of Loss Prevention in the Process Industries*, 5(3), 181–191.
- Panofsky H.A., Dutton J.A., 1984. *Atmospheric Turbulence: Models and Methods for Engineering Applications*. John Wiley and Sons, New York, 417pp.
- Pereira V.X., 2008. *Percepção social do risco de acidente industrial grave*. Msc Thesis, Universidade de Aveiro, Aveiro, Portugal. 193 pp.
- Perrow, C., 1999. *Normal Accidents: Living with High-Risk Technologies* ((Revised edition), Princeton University Press, Basic Books, Princeton, NJ, USA. ISBN 9780691004129.
- Perry R.H., Green D.W., 2008. *Perry's Chemical Handbook*, 8th Ed., McGraw-Hill, New York.
- Pesatori, A.C, Consonni, D, Rubagotti, M, Grillo, P., Bertazzi, P.A., 2009. Cancer incidence in the population exposed to dioxin after the "Seveso accident": twenty years of follow-up. *Environ Health* 8:39-49.
- Picknett, R.G., 1981. Dispersion of dense gas puffs released in the atmosphere at ground level, *Atmospheric Environment*, 15, 509-525.
- Pintarič Z.N., 2007. Assessment of the Consequences of Accident Scenarios Involving Dangerous Substances. *Process Safety and Environmental Protection*, 85(1), 23-38.
- Poling B., Prausnitz, J., O'Connell, J. 2001. *Properties of Gases and Liquids*, 5th Edition. McGraw-Hill, . ISBN: 0071499997
- Pontiggia M., Derudi M., Busini V., Rota R., 2009. Hazardous gas dispersion: A CFD model accounting for atmospheric stability classes. *J of Haz. Mater.*, 171 (1-3), 739-747.
- Pontiggia M., Derudi M., Alba M., Scaioni M., Rota R., 2010. Hazardous gas releases in urban areas: Assessment of consequences through CFD modelling. *J. of Haz. Mater.*, 176 (1-3), 589-596.
- Puttock J.S., 1987a. Analysis of meteorological data for the Thorney Island phase trials, *Journal of Hazardous Materials* 16, 43–74.
- Puttock J.S., 1987b. Comparison of Thorney Island data with predictions of Hegabox/Hegadas, *Journal of Hazardous Materials* 16, 439–455.

- Puttock J.S., Blackmore D.R. and Colenbrander G.W., 1982. Field experiments on dense gas dispersion. *J. Haz. Mater.* 6, 13-41.
- Puttock J.S., Blackmore D.R., Colenbrander G.W., Davies P.T., Evans A., Homer J.B., Redfearn J.J., Vand 't Sant W.C., Wilson R.P., 1984. Spill tests of LNG and refrigerated liquid propane on the sea, Maplin Sands, 1980: experimental details of the dispersion tests, TNER.84.046, Shell Research Ltd., Thornton Research Centre, Combustion Division.
- Puttock J.S., Macfarlane K., Prothero A., Rees F.J., Roberts P.T., Witlox H.W., Blewitt D.N., 1991. *J. of Loss Prev. Proc. Ind.*, 4,16.
- Qin T.X., Guo Y.C., Lin W.Y., 2009. Large Eddy Simulation of Heavy Gas Dispersion around an Obstacle. *New Trends in Fluid Mechanics Research, Part 3*, 107-110
- Rasmussen K., 1996. The Experience with the Major Accident Reporting System from 1984 to 1993. CEC, EUR 16341 EN
- Reason J., 1997. *Managing the Risks of Organizational Accidents*. Ashgate Publishing Limited, England.
- Reid, Robert C., Prausnitz, John M., Poling, Bruce E., 1988. *The properties of gases & Liquids*; 4^a edição; McGraw-Hill.
- Reniers G.L.L., Dullaert W., Ale B.J.M., Soudan K., 2005. The use of current risk analysis tools for preventing external domino accidents, *Journal of Loss Prevention in the Process Industries*, 18(3),119-126.
- Reynolds R.M., 1992: ALOHATM 5.0 Theoretical Description, National Oceanic and Atmospheric Administration (NOAA), Seattle.
- Ricciardi L., Prévost C., Bouilloux L., Sestier-Carlin R., 2008. Experimental next term and numerical study of previous term heavy gas next term dispersion in a ventilated room. *Journal of Hazardous Materials*, 152(2): 493-505.
- Rice A.P., 1982. Seveso accident: Dioxin. Chapter in *Hazardous Materials Spills Handbook*. McGraw-Hill, New York, pp. 11-44.
- Robins A., Castro I., Hayden P., Steggel N., Contini D., Heist D., 2001. A wind tunnel study of dense gas dispersion next term in a neutral boundary layer over a rough surface. *Atmospheric Environment*, 35(13): 2243-2252.
- Rogers R.L., 2000. The RASE Project risk assessment of unit operations and equipment, 1-50.
- Ronza A., 2007. *Contributions To The Risk Assessment Of Major Accidents In Port Areas*; Ph.D. Thesis; CERTEC - Centre d'Estudis del Risc Tecnològic; Departament d'Enginyeria Química; Escola Tècnica Superior d'Enginyers Industrials de Barcelona; Universitat Politècnica de Catalunya, Spain.
- Rundmo T., 1996. Associations between risk perception and safety. *Safety Science*, Vol. 24(3), 197-209.

- Schatzmann M., Leitl B., 2002. Validation and application of obstacle-resolving urban dispersion models, *Atmospheric Environment*, 2002, 36: 4811-4821
- Schatzmann M., Leitl B., 2011. Issues with validation of urban flow and dispersion CFD models. *Journal of Wind Engineering and Industrial Aerodynamics*, 99(4), 169-186.
- Schatzmann M., Marotzke K., Donat J., 1991. Research on continuous and instantaneous heavy gas clouds. Contribution to project EV 4T-0021-D to the final report of the joint CEC project. University of Hamburg, Hamburg, Germany.
- Schatzmann M., William H., Snyder R.E., Lawson Jr., 1993. Experiments with heavy gas jets in laminar and turbulent cross flows. *Atmospheric Environment*, 27, 1105-1116.
- Schatzmann M., Olesen H., Franke J., (eds.), 2010. COST 732 model evaluation case studies: approach and results. COST, Brussels.
- Schlechter W. P., 1996. Facility risk review as a mean to addressing existing risks during the life cycle of a process unit, operation or facility. *International Journal of Pressure Vessels and Piping*, 66(1-3), 387-402.
- Schmidt-Thomé P. (eds.), 2005. *The Spatial Effects and Management of Natural and Technological Hazards in Europe*. Final report of the ESPON 1.3.1 project. Espoo, Luxembourg: ESPON. 193 pp.
- Schmidt-Thomé P., Kallio H., 2006. Natural and technological hazard maps of Europe. *Natural and Technological Hazards and Risks Affecting the Spatial Development of European Regions*, Geological Survey of Finland, Special Paper 42, 17-63.
- Seibert P., Beyrich F., Gryning S.-E., Joffre S., Rasmussen A., P. Tercier 1998. Mixing height determination for dispersion modelling. Report of Working Group 2. In: *Harmonisation in the pre-processing of meteorological data for atmospheric dispersion models*, COST Action 710, CEC Publication EUR 18195, pp.145-265.
- Seinfeld J.H., Pandis, Spyros N., 2006. *Atmospheric Chemistry and Physics - From Air Pollution to Climate Change* 2nd Ed. John Wiley & Sons.
- Sergeant R.J., Robinett F.E., 1968. An experimental investigation of the atmospheric diffusion and ignition of boil-off vapors associated with a spillage of liquefied natural gas. TRW Systems Inc. Report no. 08072-7 for American Gas Ass., New York.
- Shaluf I.M., Ahmadun F., Shariff A.R., 2003. Technological disasters. *Journal of Loss Prevention in the Process Industries* Vol. 16 (6), pp. 513-521.
- Sherif Y., 1990. Environmental and technological risks and hazards. *Microelectronics Reliability*. Vol. 30 (5). pp. 915-950.
- Shrivastava P., 1992. *Bhopal: Anatomy of a crisis* (2nd Ed.), Paul Chapman Publishing Ltd, London, UK.
- Silva F., 2007. Avaliação do risco associado a actividades industriais e de transporte de substâncias perigosas. Departamento de Ambiente e Ordenamento. Universidade de

- Aveiro. Aveiro. Mestrado. 137pp.
- Sklavounos S., Rigas F., 2006. Simulation of coyote series trials – Part I: CFD estimation of non-isothermal LNG releases and comparison with box-model predictions, *Chem. Eng. Sci.* 61, 1434-1443.
- Slovic P., 2000. Perception of risk. London: Earthscan. Earthscan Risk in Society Series. Taylor and Francis, Inc. London, U.K.. ISBN 1853835277.
- Smith K., 1996. Environmental Hazards: Assessing Risk and Reducing Disaster, Routledge, London, Taylor and Francis Group, ISBN: 0415012171.
- SMPC, 2006a. Plano Municipal de Emergência de Estarreja. Estarreja: Serviço Municipal de Protecção Civil.
- SMPC, 2006b. Relatório final do exercício de simulação de activação do PMEE e do PEEE. Estarreja: Serviço Municipal de Protecção Civil.
- SNPC, 1994. Plano Nacional de Emergência. Presidência do Conselho de Ministros, Lisboa.
- Snyder WH., 1981. Guideline for fluid modeling of atmospheric diffusion. EPA-600/8-81-009.
- Sonnemans P., Körvers P., 2006. Accidents in chemical industry: are they foreseeable?, *Journal of Loss Prevention in the Process Industries* 19 (1), 1-12.
- Sonnemans P. J. M., Korvers P. M. W., Brombacher A. C., van Beek P. C., Reinders J. E. A., 2003. Accidents, often the result of an 'uncontrolled business process' – a study in the (Dutch) chemical industry. *Quality and Reliability Engineering International*, 19(3), 183-196.
- Sorensen P.B., Thomsen M., Assmuth T., Grieger K., Baun A. 2010. Conscious worst case definition for risk assessment, part I: A knowledge mapping approach for defining most critical risk factors in integrative risk management of chemicals and nanomaterials, *Science of the Total Environment*, 408, 3852-3859.
- Stephens H., 1993. The Texas City Disaster: A re-examination. *Industrial and Environmental Crisis Quarterly*, 7(3), 189-190.
- Stull R., 1997. An Introduction to Boundary Layer Meteorology. Kluwer Academic Publishers, London.
- Tavares R., 2007. CO₂ concentration measurements in VKI wind gallery on urban dispersion modelling test case CEDVAL B-1.1, Stagiare Report 2007-30, Von Karman Institute, Belgium.
- Tavares R., Sara J., Lopes M., Miranda A.I., 2010. Potential effects on population due to an accidental release of vinyl chloride in a sea port. ESREL Annual Meeting 2010. 5-9 September, Rhodes, Greece.

- Tavares R., Santos P., Costa A.M., Amorim J.H., Miranda A.I., Borrego C., 2008. Modelling system for accidental release of atmospheric contaminants in a sea port. 2nd International Conference on Harbours Air Quality & Climate Changes. 29-30 May, Rotterdam, the Netherlands.
- Tavares J., Quintela D., Viegas X., Góis J., Baranda J., Mendes J., Cunha L., Neves L., Figueiredo R., Patrício J, Ribeiro L., Silva N., Freiria S., 2007. Riscos Naturais e Tecnológicos Contributo para a Síntese de Diagnóstico e Visão Estratégica. PROT Centro. CCDRC.
- Te Riele, P., 1977. The atmospheric dispersion of heavy gases emitted at or near ground level. *Loss Prevention and Safety Promotion*, 2, 347.
- Teixeira D., 2010. Análise Estratégia do Cluster Petrolífero/Petroquímico Português, O Passado, o Presente, e o Futuro. Msc Thesis, Instituto Superior Técnico, Universidade Técnica de Lisboa, Lisboa, 104pp.
- Tixier J, Dusserre G, Salvi O., Gaston D., 2002. Review of 62 risk analysis methodologies of industrial plants. *Journal of Loss Prevention in the Process Industries* 15, 291–303.
- TNO, 2007. TNO Safety Software EFFECTS Version 7.5 – User and reference manual. TNO Built Environment & Geosciences, Department of Industrial and External Safety, Apeldoorn, Netherlands.
- Trijssenaar-Buhre I.J.M., Sterkenburg R.P., Wijnant-Timmerman S.I., 2008. An advanced model for spreading and evaporation of accidentally released hazardous liquids on land. *Safety, Reliability and Risk Analysis*. CRC Press.
- Troutt M., Elsaid, H., 1996. The potential value of SAATY's eigenvector scaling method for short-term forecasting of currency exchanges rates. *Siam Review*, 38, 650–654.
- Turner D.B., 1964. A diffusion model for an urban area. *Journal of Applied Meteorology*, 3, 83-91.
- Tyagunov S., Heneka P., Zschau J., Ruck B., Kottmeier C., 2005. CEDIM: From Multi-Hazards to Multi-Risks, paper presented at Amonia Conference.
- UNISDR, 2009 UNISDR terminology on disaster risk reduction. United Nations International Strategy for Disaster Reduction Secretariat, Geneva, Switzerland.
- UNSCEAR, 2009. Effects of Ionizing Radiation: United Nations Scientific Committee on the Effects of Atomic Radiation - UNSCEAR 2006 Report to the General Assembly, Vol II, UN, New York, USA. ISBN 13: 9789211422702.
- UNSCEAR, 2008. Effects of Ionizing Radiation: United Nations Scientific Committee on the Effects of Atomic Radiation - UNSCEAR 2006 Report to the General Assembly, Vol I, UN, Vienna, Austria. ISBN 13: 9789211422634,
- USDOD, 1984. Procedures for Performing a Failure Mode, Effects and Criticality Analysis, MIL-STD-1629A. Washington D.C..

- USEPA, 1989. Emergency Response Notification System Report EPA/DF/MT-94/107. Environmental Protection Agency, Washington, DC. Office of Emergency and Remedial Response.
- USEPA, 1994. An Evaluation of a Solar Radiation Delta-T Method for Estimating Pasquill-Gifford (P-G) Stability Categories, EPA-454/R-93-055, U.S. Environmental Protection Agency, Research Triangle Park, NC.
- USEPA, 1995. User's Guide for the Industrial Source Complex (ISCST3) Dispersion Models; Volume II - Description of Model Algorithms. EPA-454/B-95-003b.
- USEPA, 1999. User's guide for the AERMOD meteorological pre-processor (AERMET) - Revised draft. US environmental protection Agency (USEPA), Office of Air Quality Planning and Standards. Research Triangle Park, north Carolina, US. 273 pp.
- USEPA, 2000. Meteorological monitoring guidance for regulatory modelling applications. U.S. Environmental Protection Agency, Office of Air and Radiation, Office of Air Quality Planning and Standards, Research Triangle Park, NC 27711 EPA-454/R-99-005.
- USEPA, 2004a. User's Guide for the AERMOD Model, EPA-454/B-03-002 Office of Air Quality Planning and Standards, Emissions, Monitoring, and Analysis Division. 252 pp.
- USEPA, 2004b. User's Guide for the AERMOD Meteorological Preprocessor (AERMET), EPA-454/B-03-002 Office of Air Quality Planning and Standards, Emissions, Monitoring, and Analysis Division. 252 pp.
- USEPA, 2009. General guidance on Risk Management Programs for chemical accident prevention (40 CFR PART 68). EPA 555-B-04-001. Available on www.epa.gov/emergencies
- Uth H.J., 1999. Trends in major industrial accidents in Germany, *Journal of Loss Prevention in the Process Industries* 12, 69-73.
- Uth H.J., Wiese N., 2004. Central collecting and evaluating of major accidents and near-miss-events in the Federal Republic of Germany – results, experiences, perspectives. *Journal of Hazardous Materials*, 111(1-3), 139-145.
- van Oort H., Builtjes P.J.H., 1991. Research on continuous and instantaneous heavy gas clouds. MT-TNO wind tunnel experiments, TNO report 91-026, TNO Division of Technology for Society, TNO, Apeldorn, Netherlands.
- Van Ulden A.P., 1974. On the spreading of a heavy gas released near the ground, *Proc. 1st Int. Symp. on Loss Prevention and Safety promotion in the Process Industries*, Delft, Netherlands, 221-226.
- Van Ulden A.P. 1987. The heavy gas mixing process in still air at Thorney Island and in the laboratory. *J. Haz. Mat.* 16, 411-425.
- van Ulden A. P., Holtslag A.A.M., 1985. Estimation of atmospheric boundary layer parameters for diffusion applications. *J. Climate Appl. Meteor.*, 24, 1196-1207.

- Van Ulden A.P., 1986. The spreading and mixing of a dense cloud in still air. In: J.S. Puttock, Editor, Proc. Stably Stratified Flow and Dense Gas Dispersion Chester, England. Clarendon Press, Oxford.
- VDI, 2005. Environmental meteorology - Prognostic microscale windfield models - Evaluation for flow around buildings and obstacles. VDI guideline 3783, Part 9. Beuth, Berlin.
- Venetsanos A.G., Bartzisa J.G., Würtz J., Papailiou D.D., 2003. DISPLAY-2: a Two-Dimensional Shallow Layer Model for Dense Gas Dispersion Including Complex Features, J. of Haz. Mater., 99, 111-144.
- Venkatram A., 1980. Estimating the Monin-Obukhov length in the stable boundary layer for dispersion calculations. Bound. Layer Meteor., 19, 481-485.
- Venkatram A., 1982. A semi-empirical method to compute concentration associated with surface releases in the stable boundary layer. Atmos. Environ., 16, 245-248.
- Venkatram A., 2004. The role of meteorological inputs in estimating dispersion from surface releases. Atmospheric Environment, 38, 2439-2446.
- Ventura, João; Segurança Industrial - Teoria; Secção de Folhas, Associação de Estudantes do Instituto Superior Técnico, 1994/95.
- Vieira F., 2011. Guia para a integração da prevenção de acidentes graves na avaliação ambiental estratégica dos planos municipais de ordenamento do território., Agência Portuguesa do Ambiente, Lisboa. ISBN 978-972-8577-53-7.
- Vierendeels G, Reniers G.L.L., Ale B.J., 2011. Modeling the major accident prevention legislation change process within Europe . Safety Science, 49(3), 513-521.
- Vílchez J.A, Sevilla S., Montiel H., Casal J., 1995. Historical analysis of accidents in chemical plants and in the transportation of hazardous materials. Journal of Loss Prevention in the Process Industries, 8 (2), 87-96.
- Vose D., 2008. Risk Analysis: A Quantitative Guide, 3rd Edition. Wiley, John & Sons, Incorporated, Chichester, England. ISBN 9780470512845.
- VROM, 2005a. Methods for the calculation of Physical Effects Due to releases of hazardous materials (liquids and gases), Publication Series on Dangerous Substances, PGS 2 (formerly CPR14, "Yellow Book"), Ministerie van Volkshuis-vesting, Ruimtelijke Ordening en Milieubeheer,
- VROM, 2005b. Methods for Determining of Possible Damage to People and Objects Resulting from Releases of Hazardous Materials , Publication Series on Dangerous Substances, PGS 2 (formerly CPR16, "Green Book"), Ministerie van Volkshuis-vesting, Ruimtelijke Ordening en Milieubeheer
- VROM, 2005c. Guidelines for quantitative risk assessment, Publication Series on Dangerous Substances, PGS 3 (formerly CPR18, "Purple Book"), Ministerie van Volkshuis-vesting, Ruimtelijke Ordening en Milieubeheer

- Wald A., 1945. Statistical decision functions which minimize the maximum risk. *Ann. Math.*, 46(2), 265-280.
- Walker G.P., 1995. Land use planning, industrial hazards and the 'COMAH' Directive. *Land Use Policy*, 12 (3), 187-192.
- Webber D.M., 1993. A model of the motion of a heavy gas cloud released on a uniform slope. *J. of Haz. Mater.*, 33, 101-122.
- Weil J.C., Brower R.P., 1983. Estimating convective boundary layer parameters for diffusion applications. PPS-48, Maryland Power Plant Siting Program, Maryland Department of Natural Resources, Baltimore, MD, 45pp.
- Weiss M.N., Botros K.K., Jungowski W.M., 1988. Simple method predicts gas-line blowdown times, *Oil&Gas Journal*, Dec. 12, 1988.
- Wetting J., Porter P. 1999. The Seveso II Directive. DG Environment.
- Wettig, J, Porter, S., Kirchsteiger, C., 1999. Major industrial accident regulation in the European Union. *Journal of Loss Prevention in the Process Industries*, 12, 19-28.
- Wheatley C.J., Webber D.M., 1985. Aspects of the dispersion of heavier-than-air vapours that are of relevance to gas cloud explosions. Report n°. EUR 9592 en, Commission of the European Communities, Brussels.
- WHO, 2004. IPCS Risk Assessment Terminology, Harmonization Project Document No. 1, WHO, Geneva, Switzerland.
- WHO, 2005. Chernobyl: The True Scale of the Accident; 20 Years Later a UN Report Provides Definitive Answers and Ways to Repair Lives [Press Release].
- Willey R.J., 1998. The Bhopal Disaster - a Case History, AIChE-CCPS, New York, New York.
- Willey R.J, Crowl D.A., Lepkowski W., 2005. The Bhopal tragedy: Its influence on process and community safety as practiced in the United States, *Journal of Loss Prevention in the Process Industries* 18, 365-374.
- Wilson D.J., 1979. The release and dispersion of gas from pipeline ruptures. Prepared for Alberta Environment.
- Witlox H.W.M., 1994a. The HEGADAS model for ground level heavy gas dispersion. Part I. Steady state model. *Atmospheric Environment*, 28, 2917-2932.
- Witlox H.W.M., 1994b. The HEGADAS model for ground level heavy gas dispersion. Part II. Time dependent state model. *Atmospheric Environment*, 28, 2933-2946.
- Witlox H.W.M., McFarlane K., 1994. Interfacing dispersion models in the HGSYSTEM hazard-assessment package. *Atmospheric Environment*, 28, 2933-2946.
- Witlox H.W.M., Bowen P.J., 2002. Flashing liquid jets and two-phase dispersion - A review. Contract research report 403/2001. DNV.

- Würtz J., Bartzis J., Venetsanos A., Andronopoulos S., Statharas J., Nijsing R., 1996, A dense vapour dispersion code package for applications in the chemical and process industry, *Journal of Hazardous Materials*, 46: 273-284.
- Wyngaard J.C., 1988. Structure of the PBL. Lectures on Air Pollution Modeling. Venkatram A. and Wyngaard J.C., American Meteorological Society, 9-57pp.
- Yaws C.L. 1999. Chemical properties handbook physical, thermodynamic, environmental, transport, safety, and health related properties for organic and inorganic chemicals. New York: McGraw-Hill.
- Yee A, 2004: Concentration Fluctuation Measurements in a Plume Dispersing Through a Regular Array of Obstacles. *Boundary Layer and Meteorology*, 111: 363-415.
- Yee E., Biltoft C.A., 2004. Concentration fluctuation measurements in a plume dispersing through a regular array of obstacles. *Boundary-Layer Meteorol.* 111, 363-415.
- Zalesak S., 1979. Fully multidimensional flux-corrected method transport for fluid. *J. Comp. Phys.* 31, 335-362.
- Zannetti P., 1990. Air pollution modeling : theories, computational methods, and available software. Van Nostrand Reinhold. ISBN 0-442-30805-1.
- Zêzere J.L., Ramos C., Reis E., 2010. Riscos e Protecção Civil - Diagnóstico Estratégico Final, Lisboa, CCDR-LVT, PROTAML, 31 pp.
- Zhang B.-K, Lu B.-N., Ma X., 2008. Establishment and inquiry of chemical accident database, *Comput. Appl. Chem.* 25, 1303-1306.
- Zilitinkevich S.S., 1972. Boundary layer in the atmosphere. GARP Publications Series, No. 8 (Appendix A), A.1-A.10.
- Zilitinkevich S.S., Elperin T., Kleerorin N., Rogachevskii I., 2007. Energy- and fluxbudget (EFB) turbulence closure model for stably stratified flows. Part I: steady state, homogeneous regimes. *Bound.-Layer Meteorol.*, 125, 167-191.

Legal documents consulted

- EC, 1982. Council Directive 82/501/EEC of 24 June 1982 on the major accident hazards of certain industrial activities. Official Journal of the European.
- EC, 1987. Council Directive 87/216 of 19 March 1987 amending Directive 82/501/EEC on the major accident hazards of certain industrial activities (87/216/EEC). Official Journal of the European Communities.
- EC, 1988. Council Directive 88/610 of 24 November 1988 amending Directive 82/501/EEC on the major accident hazards of certain industrial activities (88/610/EEC). Official Journal of the European Communities.
- EC, 1992. Council Directive 91/692/EEC of 23 December 1992, standardising and rationalising reports on the implementation of certain directives relating to the environment. Official Journal of the European Communities.
- EC, 1993. Council Regulation (EEC) no. 1836/93 allowing voluntary participation by companies in the industrial sector in a Community ecomanagement and audit scheme. Official Journal of the European Communities.
- EC, 1996. Council Directive 96/61/EC of 24 September 1996 concerning integrated pollution prevention and control. Official Journal of the European Communities.
- EC, 1997. Council Directive 96/82/EC of 9 December 1996 on the control of major accident hazards involving dangerous substances. Official Journal of the European Communities, Luxembourg.
- EC, 1998. Council Decision of 23 March 1998 concerning the conclusion of the Convention on the Transboundary Effects of Industrial Accidents; OJ L326 of 03/12/1998.
- EC, 2003. Council Directive 2003/105/EC of the European Parliament and of the Council of 16 December 2003 Amending Council Directive 96/82/EC on the Control of Major-accident hazards involving dangerous substances, Official Journal of the European Union, L 345/97 Brussels.
- EC, 2006. Regulation (EC) No 1907/2006 also called REACH (Registration, Authorisation and Restriction of Chemicals)
- Decree-Law 254/2007 (which transposes the Directive 2003/105/CE to the Portuguese legislation).
- EC, 2008. Directive 2008/1/EC of the European Parliament and of the Council of 15 January 2008 concerning integrated pollution prevention and control.
- EC, 2008. Regulation (EC) No 1272/2008 (2008)
- EC, 2009. Council Regulation (EC) No 1221/2009 of the European Parliament and of the Council of 25 November 2009 on the voluntary participation by organisations in a Community eco-management and audit scheme (EMAS), Official Journal of the European Union, L 342 of 22.12.2009, pages 1-45.

EC, 2010. Commission staff working paper Impact Assessment, Accompanying document to the Proposal for a DIRECTIVE OF THE EUROPEAN PARLIAMENT AND OF THE COUNCIL on the control of major-accident hazards involving dangerous substances COM(2010) 781 final SEC(2010) 1591 final.

Web pages (consulted between 2006 and 2011):

- URL1.1 - <http://www.espon.eu/main/>
- URL1.2 – <http://www.emdat.be/>
- URL1.3 – <http://www.texascity-library.org/TCDisasterExhibit/index.html>
- URL1.4 - <http://philosophyofscienceportal.blogspot.com/2009/12/bhopal-disaster25-year-anniversary.html>
- URL1.5 – <http://toxipedia.org/display/toxipedia/Bhopal+Disaster>
- URL1.6 - <http://www.unscear.org/unscear/en/chernobyl.html>
- URL1.7 – <http://patriciahysell.wordpress.com/2010/04/26/chernobyl-2/>
- URL1.8 – http://www-ns.iaea.org/meetings/rw-summaries/chernobyl_forum.asp
- URL1.9 – http://www.lexpress.fr/actualite/societe/justice/au-proces-azf-une-filiale-de-total-risque-la-peine-maximale_770024.html
- URL1.10 – <http://www.lefigaro.fr/actualite-france/2009/02/21/01016-20090221ARTFIG00140-azf-quatre-mois-de-proces-pour-un-etrange-accident-.php>
- URL1.11 – <http://www.buncefieldinvestigation.gov.uk/index.htm>
- URL1.12 – http://www.msnbc.msn.com/id/31638526/ns/world_news-europe/
- URL1.13 – <http://emars.jrc.ec.europa.eu/>
- URL1.14 – <http://www.factsonline.nl/>
- URL1.15 – http://www.aria.developpement-durable.gouv.fr/index_en.html
- URL1.16 - <http://www.epa.gov/oem/content/rmp/#preparing>
- URL1.17 - <http://www.nrc.uscg.mil/nrcback.html>
- URL1.18 - http://threadic.com/sora/translate.cgi/riodb.ibase.aist.go.jp/riscad/PHP_EN/index.php
- URL1.19 - <http://ec.europa.eu/environment/seveso/review.htm>
- URL2.1– <http://www.epa.gov/oem/content/cameo/aloha.htm>
- URL2.2 - <http://ansys.com/>
- URL2.3 - <http://gexconus.com/>
- URL2.4 - <http://www.mmm.ucar.edu/mm5/>
- URL2.5 - <http://www.wrf-model.org/index.php>
- URL3.1 – http://www.ess.co.at/AIR-EIA/def_mix.html
- URL4.1 - <http://www.mi.uni-hamburg.de/COST-732-in-Brief.470.0.html>
- URL4.2 - http://www.epa.gov/scram001/dispersion_prefrec.htm
- URL4.3 - <http://www.webmet.com/metguide.html>
- URL4.4 - <http://weather.uwyo.edu/upperair/sounding.html>
- URL4.5 - <http://www.tno.nl/index.cfm>
- URL4.6 - <http://www.aiche.org/DIPPR/products/productdescription.aspx>

URL5.1 - <http://www.apambiente.pt/politicasambiente/prevencaoacidentes/Paginas/SevesoII.aspx>

URL5.2 - http://www.espon.eu/main/Menu_Projects/

URL5.3 - <http://sig.cm-estorreja.pt/sig/>

URL5.4 - <http://www.cires.pt/>

URL5.5 - <http://www.portodeaveiro.pt/>

URL5.6 - <http://www.pacopar.org/>

URL5.7 – <http://viajar.clix.pt/geo.php?c=77>

URL5.8 - <http://www.cp.pt/>

APPENDIXES

Appendix A: Major Industrial Accidents

A.1 – Time evolution of reported technological accidents worldwide since 1900 from EM-DAT database.

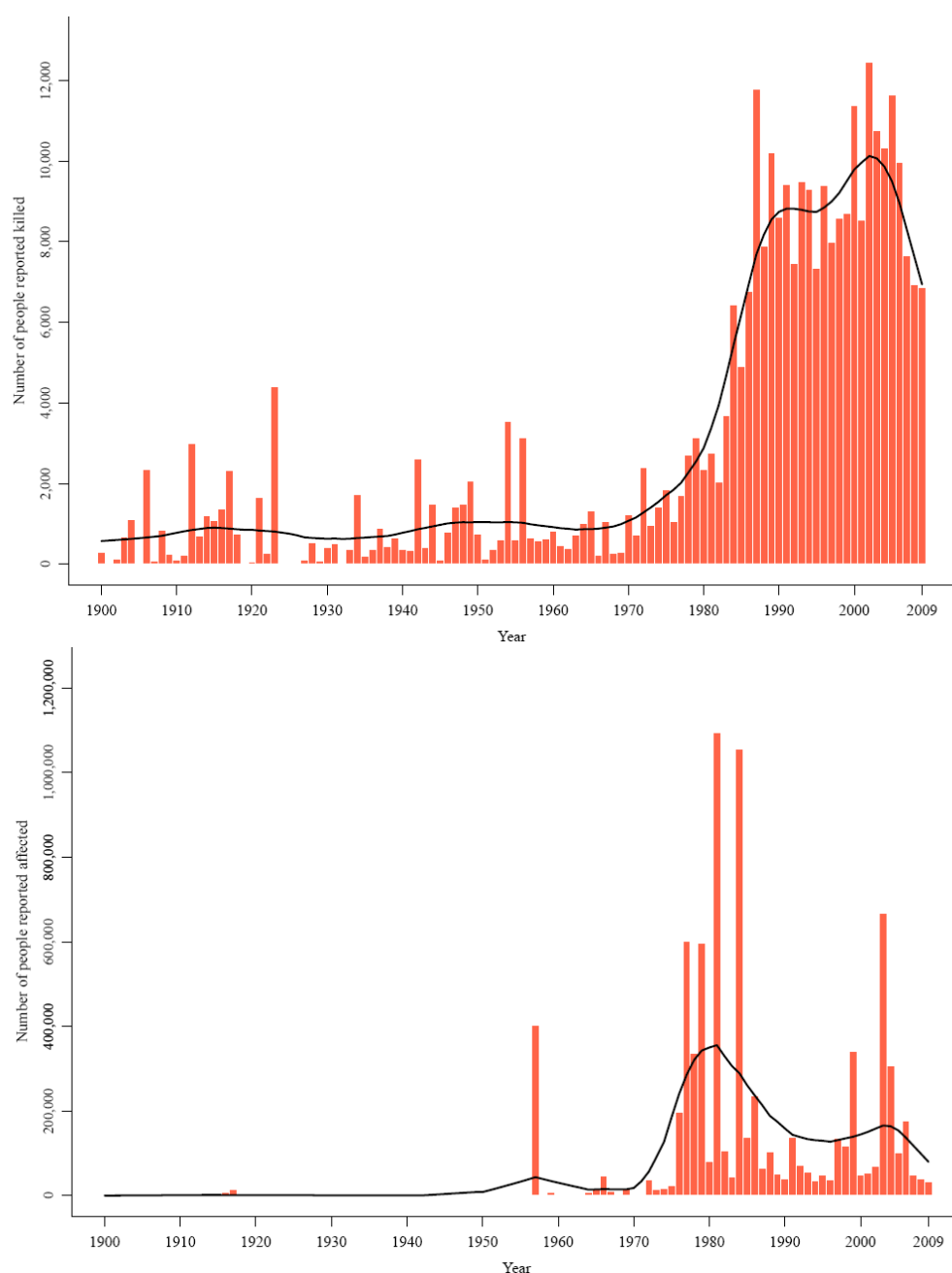


Figure A.1 – Number of people reported (a) killed and (b) affected by technological disasters 1900 – 2009 [URL1.1].

A.2 – Industrial establishments covered by the two-tiers regime of Seveso II Directive

Time

Table A. 1. Number of 'Seveso establishments by Member State [EEA, 2010].

Country	Total number of plants	Upper Tier	Lower Tier	Not known/ not applicable
<i>Germany</i>	2119	1071	1048	
<i>UK</i>	1147	411	736	
<i>Italy</i>	1117	519	598	
<i>France</i>	1106	553	553	
<i>Spain</i>	673	267	406	
<i>Netherlands</i>	384	221	163	
<i>Sweden</i>	379	199	180	
<i>Poland</i>	366	158	208	
<i>Belgium</i>	365	174	191	
<i>Romania</i>	277	115	162	
<i>Finland</i>	264	128	136	
<i>Czech Republic</i>	190	115	75	
<i>Greece</i>	189	83	106	
<i>Portugal</i>	164	57	107	
<i>Austria</i>	146	80	64	2
<i>Hungary</i>	144	64	80	
<i>Bulgaria</i>	135	54	81	
<i>Denmark</i>	121	31	90	
<i>Ireland</i>	88	34	54	
<i>Slovakia</i>	78	41	37	
<i>Latvia</i>	63	30	33	
<i>Slovenia</i>	60	23	37	
<i>Lithuania</i>	53	19	34	
<i>Estonia</i>	50	25	25	
<i>Luxembourg</i>	21	8	13	
<i>Cyprus</i>	16	10	6	
<i>Malta</i>	10	6	4	
TOTAL	9725	4496	5227	2

Table A. 2. Distribution of Number of ‘Seveso establishments by activity [EEA, 2010].

IndustryType	Percentage
Fuel storage (including heating, retail sale, etc.)	10.92%
Wholesale and retail storage and distribution (excluding LPG)	10.36%
General chemicals manufacture (not included above)	7.41%
Power generation, supply and distribution	7.12%
LPG storage	5.53%
Production of basic organic chemicals	5.01%
Production, destruction and storage of explosives	4.36%
Processing of metals using electrolytic or chemical processes	4.30%
Chemical installations - other fine chemicals	3.82%
Chemical installations – Industrial gases	3.52%
Other activity (not included above)	3.39%
LPG production, bottling and bulk distribution	3.30%
Plastic and rubber manufacture	3.10%
Production and storage of pesticides, biocides, fungicides	2.95%
Petrochemical / Oil Refineries	2.55%
Production and storage of fertilizers	2.50%
Manufacture of food products and beverages	2.38%
Waste storage, treatment and disposal	1.90%
Handling and transportation centres	1.80%
Production of pharmaceuticals	1.53%
General engineering, manufacturing and assembly	1.29%
Production and storage of fireworks	1.15%
Processing of ferrous metals (foundries, smelting, etc.)	1.08%
LNG storage and distribution	1.02%
Production and manufacturing of pulp and paper	0.97%
Processing of non-ferrous metals (foundries, smelting, etc.)	0.91%
Agriculture	0.73%
Electronics & electrical engineering	0.72%
Water and sewage (collection, supply, treatment)	0.61%
Ceramics (bricks, pottery, glass, cement, etc.)	0.54%
Manufacture of glass	0.54%
Processing of metals	0.45%
Chemical installations - chlorine	0.36%
Medical, research, education (including hospitals, universities, etc.)	0.33%
Mining activities (tailings & physicochemical processes)	0.24%
Wood treatment and furniture	0.24%
Chemical installations - ammonia	0.21%
Shipbuilding, shipbreaking, ship repair	0.18%
Chemical installations - inorganic acids	0.15%
Manufacture of cement, lime and plaster	0.13%
Chemical installations - fluorine or hydrogen fluoride	0.09%
Chemical installations - hydrogen	0.06%
Building & works of engineering construction	0.04%
Textiles manufacturing and treatment	0.04%
Leisure and sport activities (e.g. ice rink)	0.03%
Chemical installations – carbon oxides	0.01%
Chemical installations - nitrogen oxides	0.01%
Chemical installations - sulphur oxides, oleum	0.01%
Total	100.00%

Appendix B: EFFECTS OF RELEASED HAZARDOUS GAS MODEL DEVELOPMENT

B-1 – EFRHA fluxogram showing the different modules and the main input data, data transferred between modules and output data.

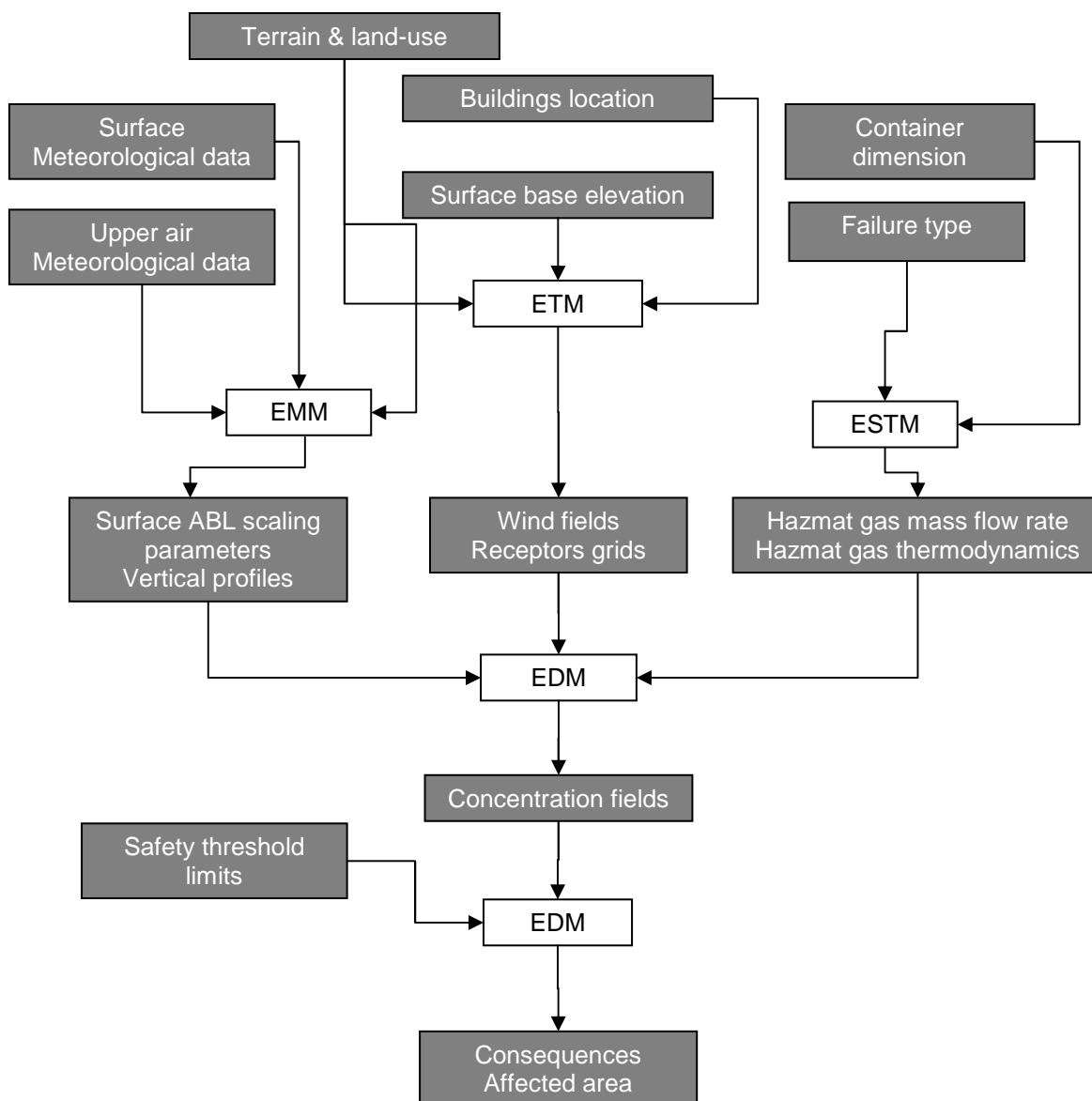


Figure A.1 - Basic fluxogram of EFRHA model data transfer and modelled outputs.

B-2: EFRHA model input/output data

Table B.1 – Input parameters used by the EFRHA model.

Symbol	Input parameters	Units
EFRHA Control parameters		
T_{sim}	Simulation period	s
N_t	Number of time steps	–
Lat	Latitude	°
$Long$	Longitude	°
H_{zone}	Time Zone	h
Meteorological module		
H_m	Measurement height	m
T_m	Measured ambient temperature	°C
U_m	Measured wind velocity	m.s ⁻¹
ϑ_m	Measured wind direction	°
P_m	Measured atmospheric pressure	Pa
Hr_m	Measured relative humidity	%
R	Measured solar radiation	W.m ⁻²
N	Fractional cloud cover	-
$r\{\varphi\}$	Albedo	-
Bo	Bowen ratio	-
ϑ_K	Measured upper air temperature vertical profile	K
Terrain module		
z_0	Surface roughness length	m
z_{hill}	Surface height	m
H_{src}	Source height	m
X_{src}, Y_{src}	Source centre location	m
z_{obld}	Building base height	m
H_{bld}	Building roof height	m
N_{tier}	Number of tiers of the building	–
X_{tier}, Y_{tier}	Building tiers location	m
Source term module		
h_v	Container height	m
l_v	Container length	m
l_w	Container width	m
T_0	Product Temperature	°C
P_0	Product Pressure	Pa
–	Product physical state	–

Symbol	Input parameters	Units
Φ	Filling degree	%
h_h	Leak height	m
d_h	Leak size	m
C_d	Discharge coefficient	–
Dispersion module		
–	2D Receptor grid	–
z_{conc}	Height from the ground	m
C_{thld}	Concentration threshold limits	$\mu\text{g.m}^{-3}$

Table B.2 – Interpretation of the L with respect to PG Stability Class [Seinfeld and Pandis, 2006].

L	(range)	PG
Small negative	$-100 \text{ m} < L < 0$	A
Large negative	$-105 \text{ m} \leq L < -100 \text{ m}$	B-C
Very large (positive or negative)	$ L > 105 \text{ m}$	D
Large positive	$10 \text{ m} \leq L \leq 105 \text{ m}$	E
Small positive	$0 < L < 10 \text{ m}$	F

Table B.3 – Output parameters estimated by theEFRHA model.

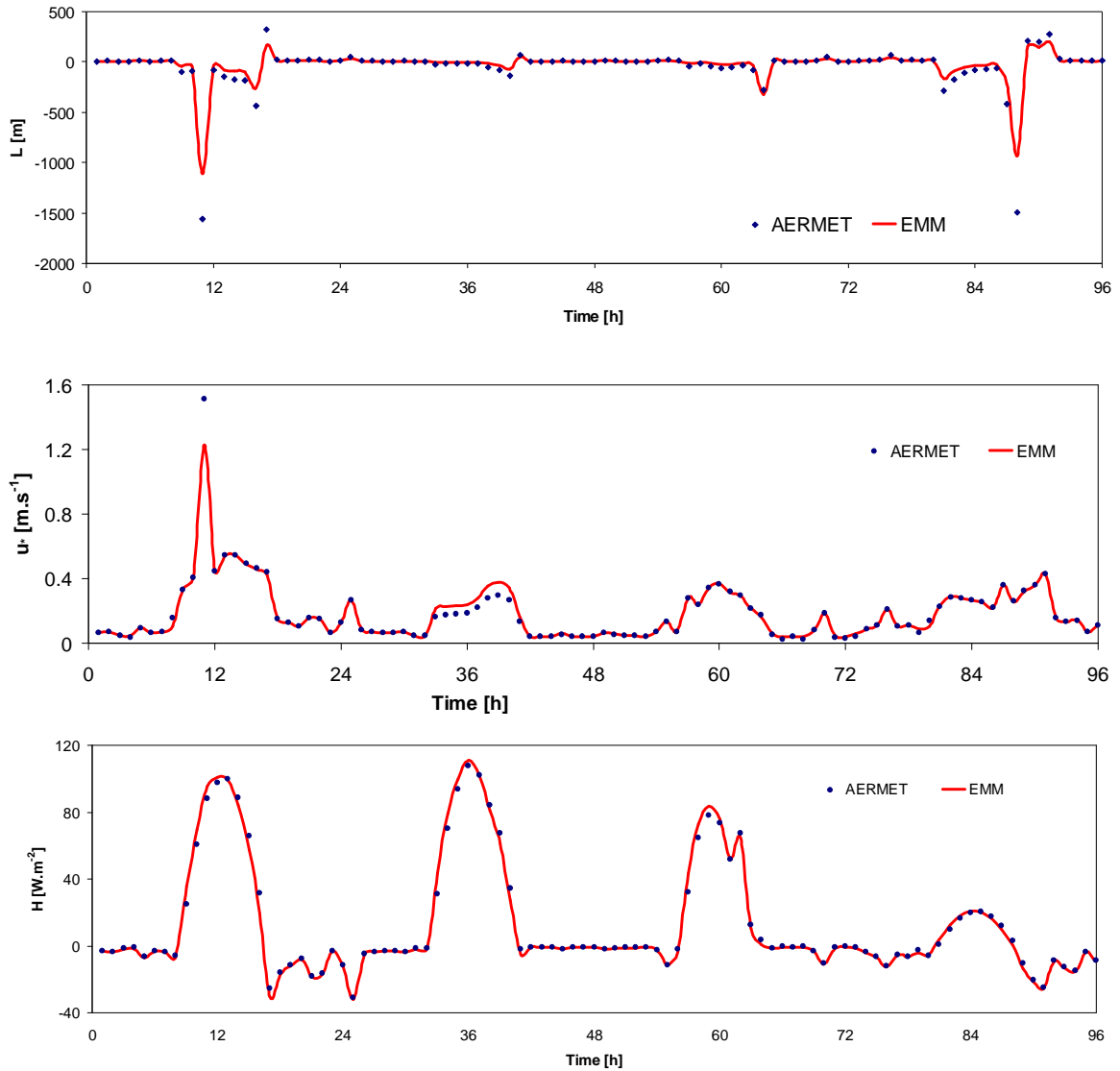
Symbol	Output parameters	Units
Meteorology module		
L	Monin-Obukhov length	m
R_i	Richardson number	–
H_0	Sensible heat flux	$\text{J.m}^{-2}.\text{s}^{-1}$
u^*	Surface friction velocity	m.s^{-1}
w^*	Convective scaling velocity	m.s^{-1}
θ^*	Temperature scale	K
z_i	Mixed layer height	m
z_{ic}	Convective mixed layer height	m
z_{im}	Mechanical mixed layer height	m
–	Atmospheric stability class	–
Source term module		
h_{sc}	Source height	m
q_s	Gas mass flow rate	kg.s^{-1}
u_{sc}	Gas outflow velocity	m.s^{-1}
ρ_{sc}	Gas density	kg.m^{-3}
T_{sc}	Gas temperature	K
P_{sc}	Gas pressure	Pa
A_{sc}	Source cross-sectional area	m^2
-	Physical state	-

Symbol	Output parameters	Units
Source term module		
z_0	Surface roughness length	m
$r_a(\varphi)$	Surface albedo	-
Bo	Surface Bowen ratio	-
nX_r	Number of receptor points in X direction	-
nY_r	Number of receptor points in Y direction	-
ΔX_r	Distance between consecutive receptor point in X direction	m
ΔY_r	Distance between consecutive receptor point in Y direction	m
z_r	Receptor elevation from the terrain base	m
	Receptor hill height scale elevations	m
H_{src}	Source height	m
X_{src}, Y_{src}	Source centre location	m
z_{obl}	Projected building base height	m
H_{bl}	Projected building roof height	m
N_{tier}	Number of tiers of the building	-
X_{tier}, Y_{tier}	Building tiers location	m
Dispersion module		
C	Hazmat concentration	$\mu\text{g}\cdot\text{m}^{-3}$

Appendix C: VALIDATION OF EFRHA MODEL

C.1 – Stage 1: EMM module

Figure C.1 - Time evolution plots of AERMET (green) and EMM (red) estimated ABL scaling parameters for MET1 test case



Cont. Figure C.1

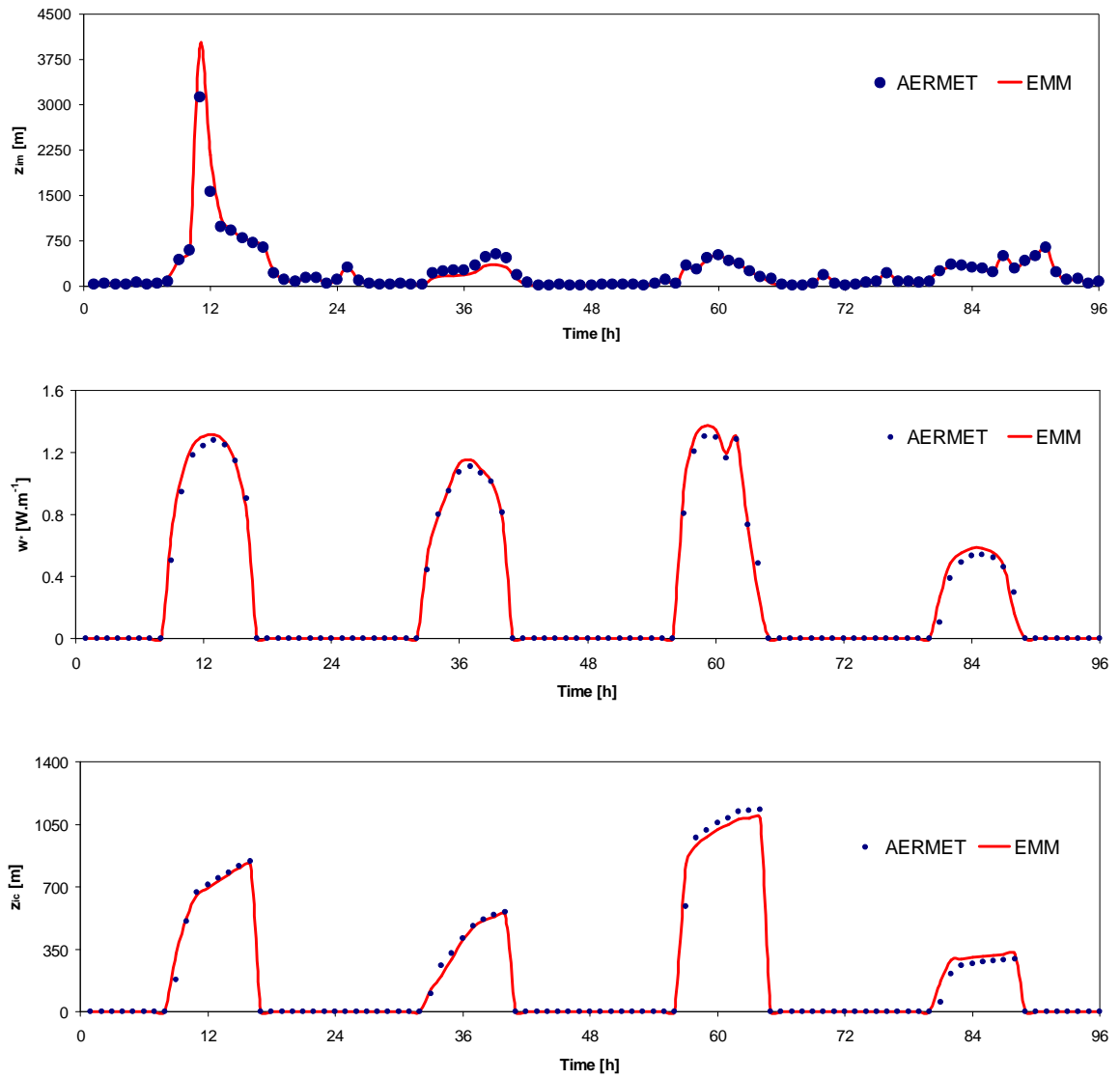
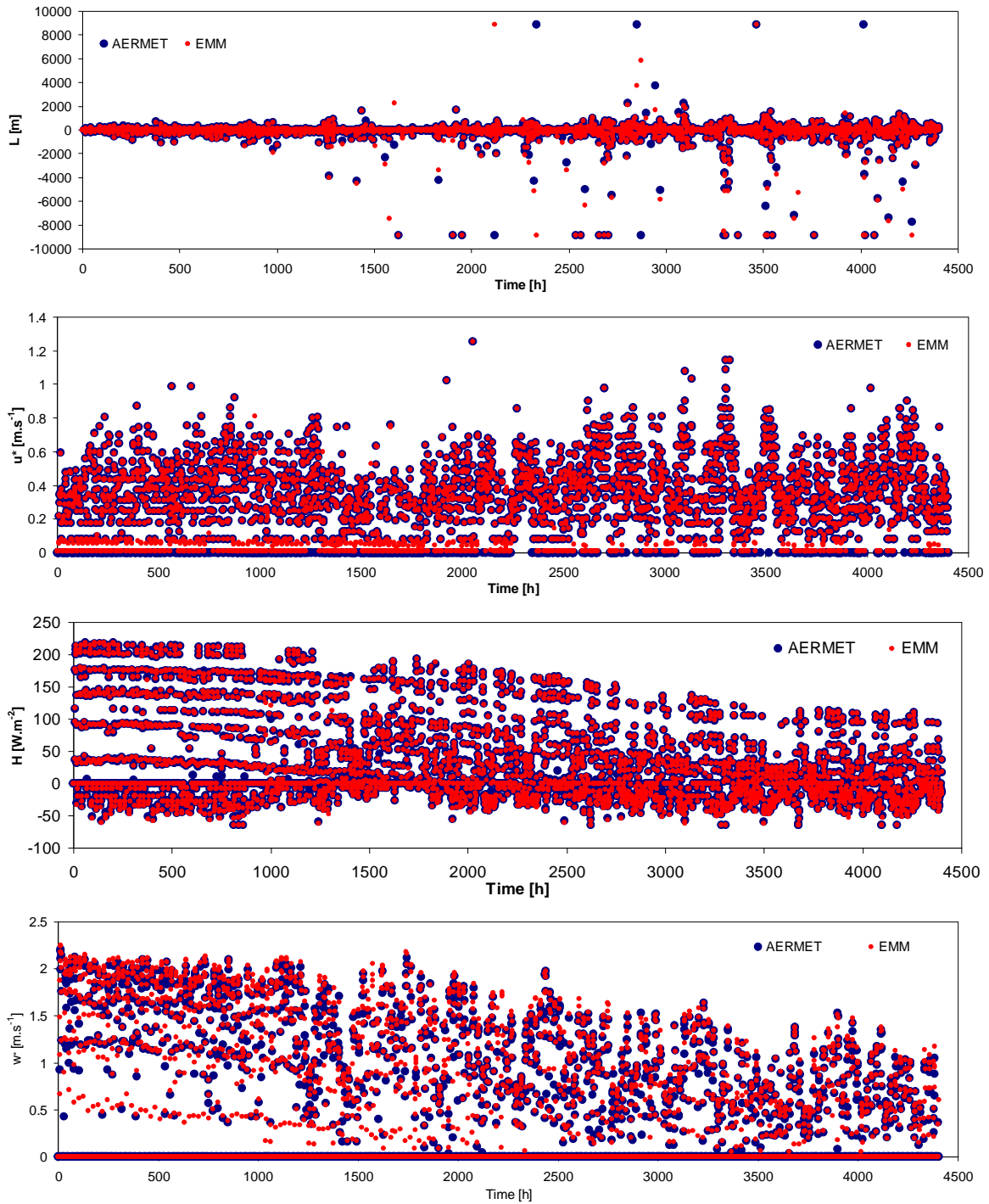
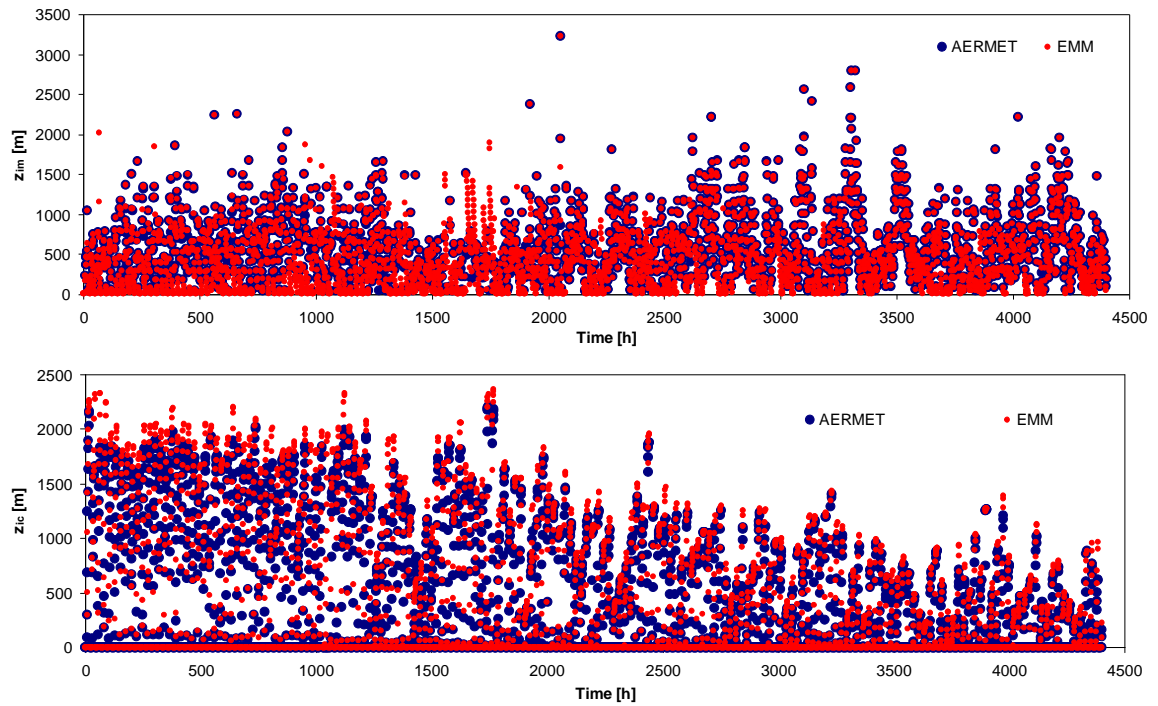


Figure C.2 - Time evolution plots of AERMET (green) and EMM (red) estimated ABL scaling parameters for MET2 test case



Cont. Figure C.2



C.2 – EFRHA model validation Stage 2: ESTM module

Table C.1 – Summary of input parameters of SRC1 test case [VROM,2005a].

Parameter	Inputs	Units
Chemical product	Hydrogen	-
Filling degree	95	%
Vessel volume	100	m ³
Vessel heigh	5.0	m
Vessel diameter	4.1	m
Type of leak	Sharp edge orifice	-
Diameter of leak	0.1	m
Height of leak from vessel's base	3.0	m
Initial temperature	15.0	°C
Initial pressure above liquid	50.0	bar

Table C.2 – Summary of input parameters of SRC2 test case [VROM,2005a].

Parameter	Inputs	Units
Chemical product	Acrylonitrile	-
Filling degree	80.0	%
Vessel type	Vertical cylinder	
Vessel volume	6600.0	M ³
Vessel heigh	14.0	m
Vessel diameter	24.5	m
Type of hole	Sharp edge orifice	-
Diameter of hole	0.1	m
Height of hole from vessel's base	0.0	m
Initial temperature	15.0	°C
Initial pressure	1.0	bar

Table C.3 – Summary of input parameters of SRC9 test case [VROM,2005a].

Parameter		Units
Chemical product	Propane	-
Filling degree	95.0	%
Vessel type	Vertical cylinder	
Vessel volume	4.7	m ³
Vessel heigh	2.00	m
Vessel diameter	24.5	m
Type of hole	Sharp edge orifice	-
Diameter of hole	0.1	m
Height of hole from vessel's base	1.95	m
Initial temperature	303.15	K
Initial pressure	10.79	bar

Table C.4 – Summary of input parameters of SRC4 test case [VROM,2005a].

Parameter		Units
Chemical product	Gasoline	-
Total mass released	100,000	kg
Initial liquid temperature	15.0	°C
Fixed pool surface	1500	m ²
Initial temperature subsoil	15.0	°C
Bund surface material	Isolation concrete	-
Thermal conductivity	0.207	J.m ⁻¹ .s ⁻¹ .K ⁻¹
Thermal diffusivity	2.5x10 ⁻⁷	m ² .s ⁻¹
Ambient temperature	288.15	K
Thermal conductivity air	0.0257	J.m ⁻¹ .s ⁻¹ .K ⁻¹
Prandlt number air	0.786	-
Viscosity air	1.65x10 ⁻⁵	N.s.m ⁻²

C.3 – EFRHA validation stage 3: Dispersión in obstructed areas

Analysis of estimated scatter plots for the set of defined IOMC runs

In spite of Schatzmann *et al.* [2010] recommendation, the comparison of paired point-by-point mean concentrations between wind tunnel and IOMC modelled results in the form of scatter plots is nevertheless presented for information in Figure C.1. The analysis of scatter plots highlights the divergences between IOMC runs with and without the definition of obstacles.

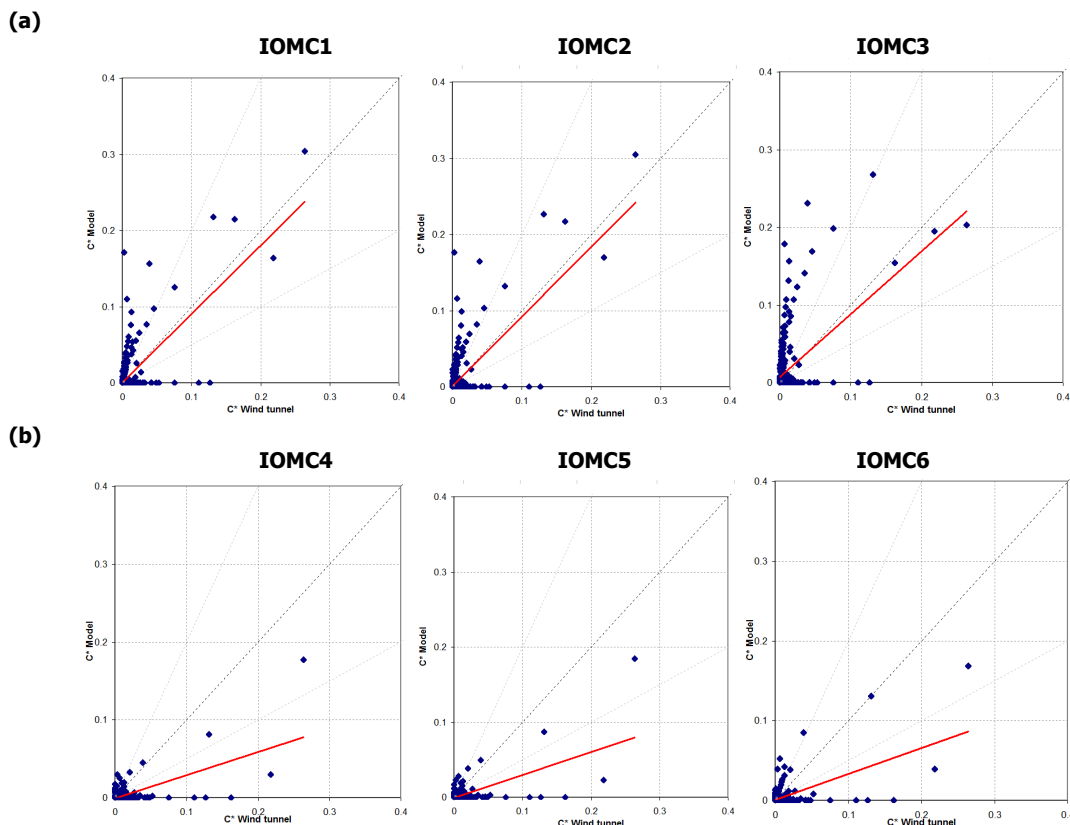


Figure C.3 – Scatter plots of IOMCs modelled results against wind tunnel mean concentration measurements for the -45° MUST case – IOMC runs (a) with and (b) without obstacles definition.

Visual inspection of Figure C.1 shows the underestimation trend lines for IOMC runs without any consideration of obstacles; in case of IOMC runs with the incorporation of obstructions estimated trend lines tend to approximate to the correspondent perfect model trend lines.

In general, IOMC runs with obstacles (IOMC1- IOMC3) present an evident better agreement with observations, in contrast with the perceptible lesser correlation observed for IOMC runs without any consideration of obstacles (IOMC4 – IOMC6). This difference is clearly visible by

the number of overestimated points, but also, by the number of points close to perfect correlation trend line.

As regards to potential influence of z_0 values, exploratory analysis of Figure C.1 demonstrates that concentrations estimated using IOMC1 and IOMC4 ($z_0 = 0.3 \text{ m}$) and IOMC2 and IOMC5 ($z_0 = 0.1 * H_{bd} \text{ m}$) are quite similar. Therefore, it is possible to mention that the definition of more realistic values for z_0 (0.3 m) estimated from the experimental wind profile value observations within obstacles array do not generates noticeable enhancements when compared with the MEGPD guidance value. Nonetheless there is a slight improvement with IOMC3 and IOMC6 ($z_0 = 0.1 \text{ m}$).

Although the analysis of scatter plots results shows a 'poor behaviour' of all IOMC configurations, it is to a great extent analogous to modelled results from a set of Class II models reported by Schatzmann *et al.* [2010] in the frame of COST Action 732 as presented in Figure C.2. Regardless the majority of runs do not consider the presence of effective buildings, as in IOMC1 - IOMC3 runs, their comparison with ETM-EDM modelled results illustrates the typical results and 'limitations' of Class II models. A special attention should be given to ADMSa runs, because these are the only ones in which buildings spatial distribution are considered. Detailed description of input configurations and results from the application of the various 'non-CFD models', in the frame of COST Action 732 is presented in Schatzmann *et al.* [2010].

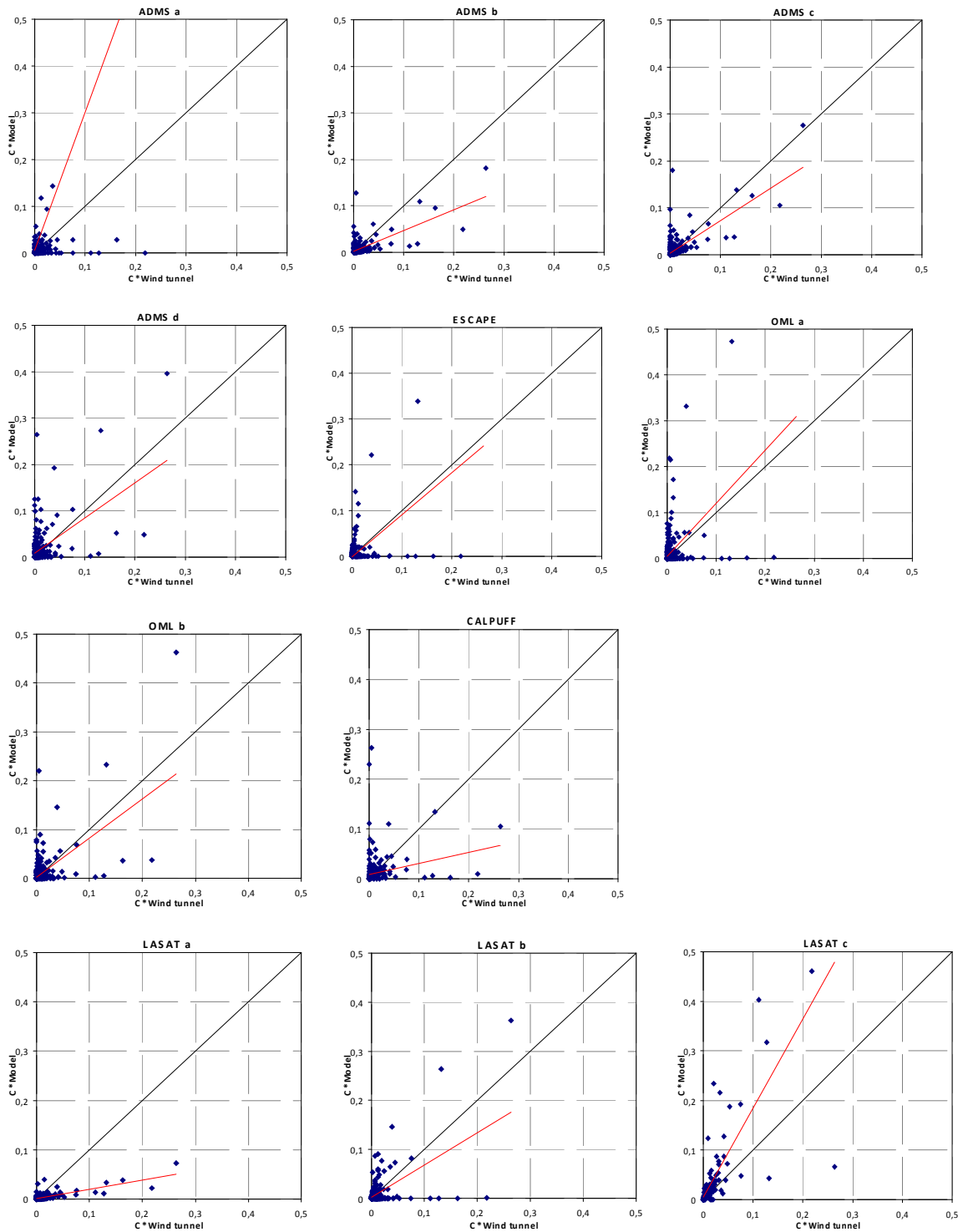


Figure C.4 – Scatter plots: non-CFD model results against wind tunnel measurements for the -45° MUST case [Schatzmann *et al.*, 2010].

Considering the resemblances with equivalent Class II models results it is possible to conclude that, EFRHA modelled concentrations from ETM-EDM results can be assumed consistent and

quite similar to equivalent Class II models and configurations outputs. Taking into account the more 'realistic' configuration of ADMSa and Lasatc runs [Schatzmann *et al.*, 2010], it is also visible that IOMC1 and IOMC2 modelled results show a comparable variability from run to run. Moreover, the inclusion of buildings shows the most severe overestimations as observed in the results of ADMSa and Lasatc [Schatzmann *et al.*, 2010]. Therefore, it is clear that the most complex and 'realistic' way to define the presence of obstacles generates better results, than just varying the value of z_0 .

Aiming to evaluate the consistency between observations and the modelled results previously presented, in terms of spatial distribution, the residuals (ratios between modelled results and observations) were estimated for the set of measured points and presented in Figure C.5.

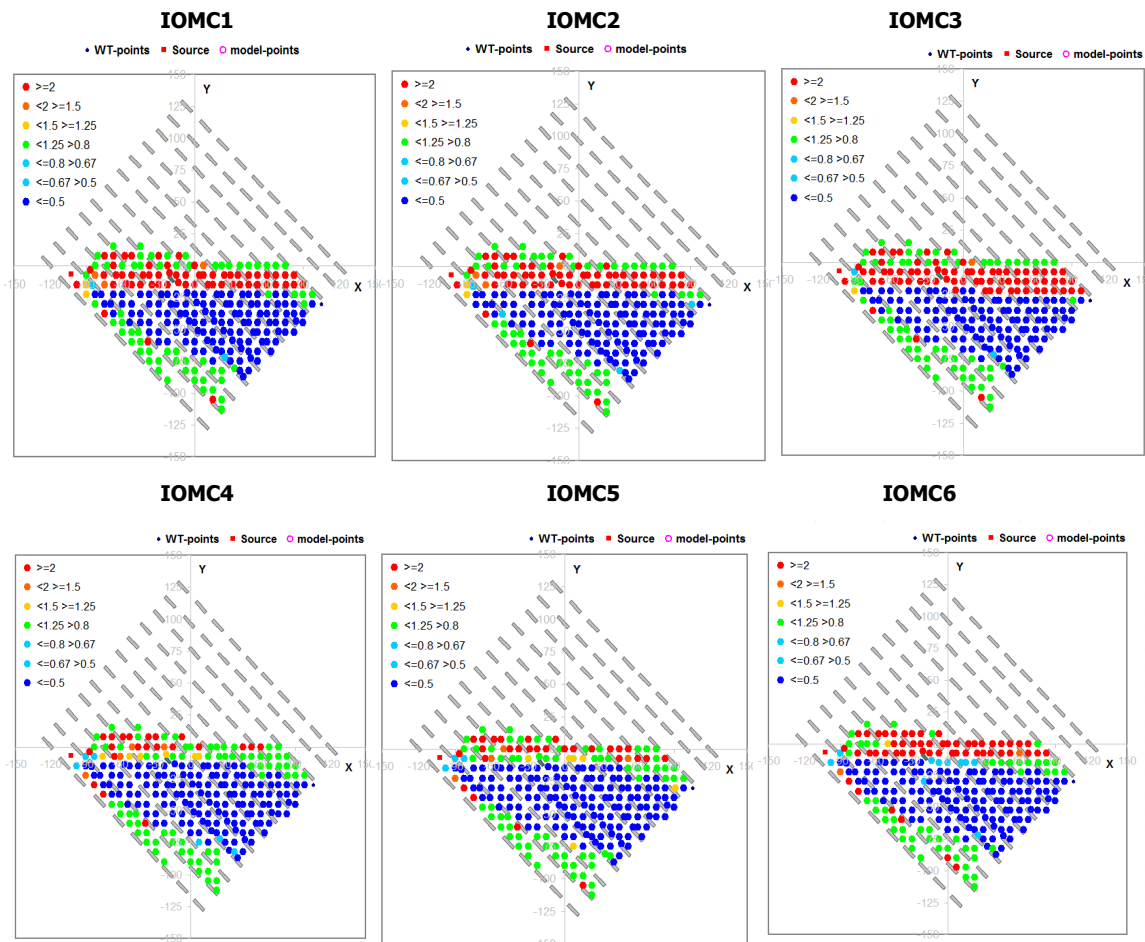


Figure C.5 - Comparison of plume shape based on residuals concentrations modelled/measurements for the -45° MUST test case (with obstacles: IOMC1-3; without obstacles: IOMC4-6).

Dark red points show areas of overestimation, dark blue points identify areas of underestimation and green points correspond to the best agreements between IOMC runs results and observations. In general, IOMC runs show a strong overestimation of

concentrations along the x -axis and a strong underestimation south-east of the source, where the plume really is. This spatial distribution of residuals reflects the typical Class II models near straight-line plume propagation behaviour. Clear divergences are observed in IOMC runs with and without obstacles. These results corroborate previously observed scatter plots.

As regards to potential effects of z_0 values on modelled results, it is possible to detect different trends on results from IOMC runs with and without obstacles. In case of IOMC runs with obstacles, a minor augment of the number of points with larger deviations is observed for higher z_0 values, with the uppermost deviations observed in IOMC3. In contrast, IOMC runs without any obstacles show a more prominent reduction of concentration deviations for higher z_0 values, with the wider number of points with slight to strong overestimations observed in IOMC6 and the lowest in IOMC2. As expected, the most obvious deviations occur between IOMC runs with 'extreme' values for z_0 (0.3 m and 0.035 m). This is mainly due to the combined influence of obstacles integration technique and z_0 values.

Appendix D. CASE STUDY: ESTARREJA

F.1 – Definition of ERPG limits

The Emergency Response Planning Guidelines (ERPGs) are Toxic Levels of Concern (LOCs) generally used to predict the area where a toxic gas concentration might be high enough to harm people. The ERPGs were developed by the ERPG committee of the American Industrial Hygiene Association. The ERPGs were developed as planning guidelines, to anticipate human adverse health effects caused by exposure to toxic chemicals. The ERPGs are three-tiered guidelines for exposure up to 60 minutes of duration of contact.

ERPG 1: The maximum airborne concentration below which it is believed that nearly all individuals could be exposed for up to 1 hour without experiencing other than mild transient adverse health effects or perceiving a clearly defined, objectionable odour.

ERPG 2: The maximum airborne concentration below which it is believed that nearly all individuals could be exposed for up to 1 hour without experiencing or developing irreversible or other serious health effects or symptoms which could impair an individual's ability to take protective action.

ERPG 3: The maximum airborne concentration below which it is believed that nearly all individuals could be exposed for up to 1 hour without experiencing or developing life-threatening health effects.

F.1 – Spatial distribution of Portuguese Seveso-establishments

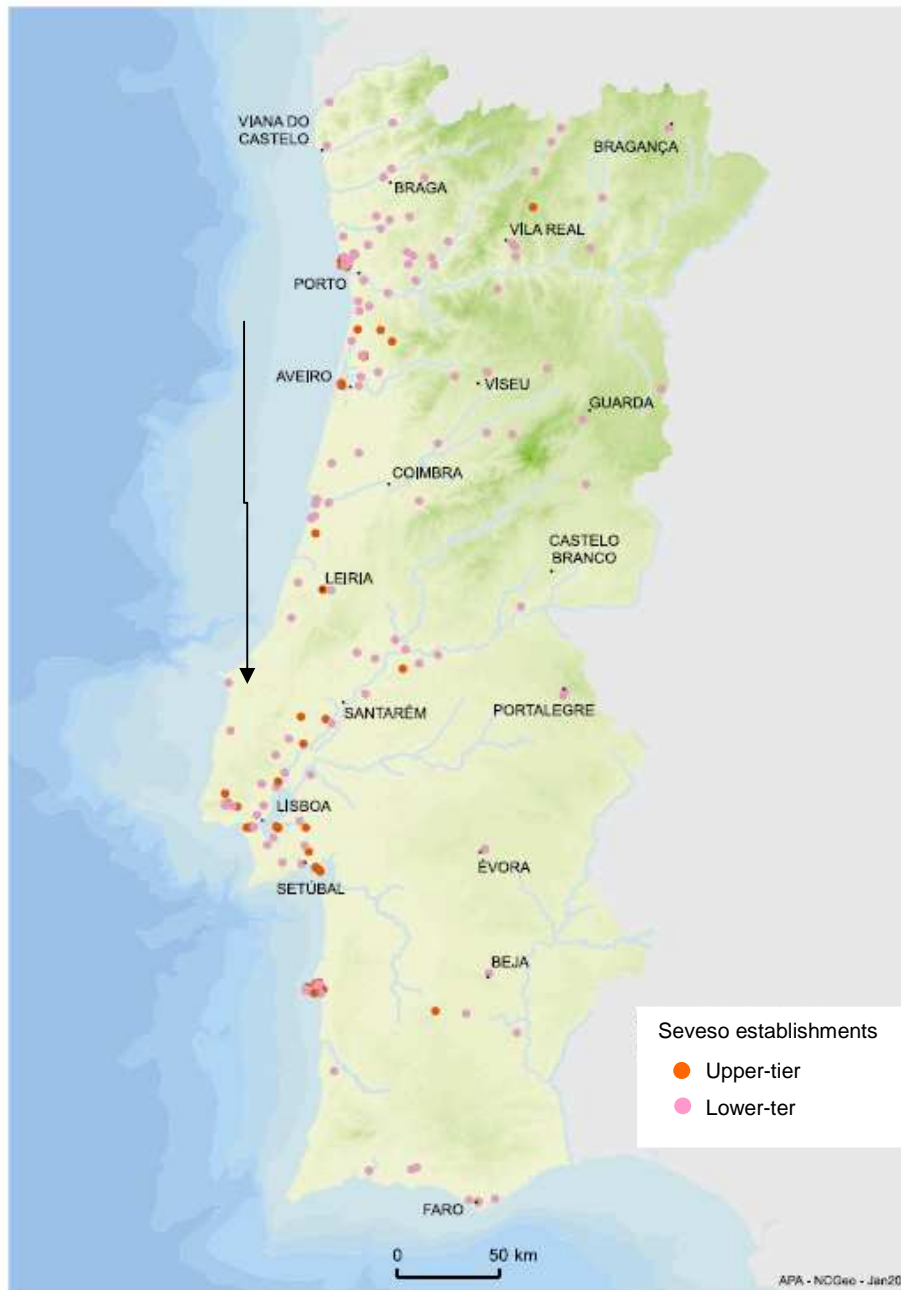


Figure D.1 – Spatial distribution of natural and technological risk at Portuguese national level [Gaspar, 2005]

F.1 – Estarreja Municipality

Table D.1 – Types of vulnerable spots considered in the municipality of Estarreja [SMPC, 2006; URL5.3].

Code	Type	Covered structures
VS1	Administrative services	Estarreja city hall - Courthouse - Parish administrative centres
VS2	Education	- Kinder gardens - 1 st cycle schools - High school
VS3	Health	- Hospital - Parishes health centres
VS4	Safety	- Police station - Firefighters headquarter
VS5	Social & Public	- Elder retirement centres - Social and occupational activities centres - Fair park - Cinema - Library - Sports hall - Swimming pool - Soccer and athletics camps - Public parks - Train station
VS6	Industrial	- Industrial establishments

